universität wien

DISSERTATION / DOCTORAL THESIS

Titel der Dissertation / Title of the Doctoral Thesis

„Platinum(IV) complexes conjugated to polymers designed as novel drug delivery systems for preclinical cancer therapy evaluation“

verfasst von / submitted by

Yvonne Lerchbammer-Kreith, BSc MSc

angestrebter akademischer Grad / in partial fulfilment of the requirements for the degree of

Doktorin der Naturwissenschaften (Dr. rer. nat.)

Wien, 2023 / Vienna 2023

Studienkennzahl lt. Studienblatt / degree programme code as it appears on the student record sheet:	UA 796 605 419
Dissertationsgebiet lt. Studienblatt / field of study as it appears on the student record sheet:	Chemie
Betreut von / Supervisor:	ao. Univ.-Prof. Mag. Dr. Mathea Sophia Galanski

Acknowledgement

This thesis could only be written due to the cooperation and support of many dedicated people to whom I would like to express my sincerest gratitude.

First and almost, I would like to thank **ao. Prof. Dr. Mathea Galanski** for her supervision, guidance, help and patience, the countless NMR measurements, scientific discussions and accurate proofreading.

The dean and head of the institute, **o. Univ.-Prof. Dr. Dr. Bernhard K. Keppler**, who encouraged and supported my funding applications and welcomed me as a member of his research group.

Our collaborators at the University College London, in particular **Prof. Ijeoma Uchegbu, PhD** and **Prof. Dr. Andreas Schätzlein**, who intensively broadened my knowledge of polymers and supported my scientific stay at the School of Pharmacy. This further includes my colleagues, namely **Corinna Schlosser, MSc**, **Ryan Mellor, PhD**, **Gang Li, PhD**, **Savvas Dimiou, MSc** and **Rui Manuel Jesus Lopes**, **PhD**, who were responsible for a memorable time in London.

Our research partners at the Medical University of Vienna, **Univ.-Prof. Dr. Walter Berger** and **Petra Vician, MSc** for their engagement, flexibility and patience.

The head of the cell culture facility, **Dr. Michael Jakupec** including his group members **Michaela Hejl** and **Klaudia Cseh, MSc** for performing countless MTT assays as well as for their tireless support, flexibility and patience with my "not so easy-care" substances.

All my (former) colleagues: **Dr. Selin Hizal**, **Dr. Nadine Sommerfeld**, **Thomas Maier, MSc**, **Dr. Hristo Varbanov**, **Dr. Heiko Geisler**, **Dr. Sophia Harringer**, **Dr. Valentin Fuchs**, **Dr. Felix Bacher**, **Dr. Miljan Milunovic**, **Christopher Wittmann, MSc**, **Dr. Irena Paschkunova-Martic**, **Dr. Björn Bielec**, **Dr. Philipp Fronik**, **Alexander Kastner, MSc**, **Dr. Marlene Mathuber**, **Federico Lo Nardo, MSc**, **Dr. Guilherme Rubio** and **Alexia Tialiou, MSc** for creating an amazing and collaborative working environment.

My special thanks go to **Selin**, **Tom**, **Klaudia**, **Gui** and **Philipp** who are not only exceptional chemists and colleagues, but also become amazing friends. The countless hours of discussions, encouragements, moral support, pleasure, memorable moments as well as the tons of chocolate are highly appreciated and will never be forgotten.

All the staff at the University of Vienna including **Mag. Elfriede Limberger**, **Mag. Veronika Knoll**, **Sylwia Kur, BSc**, **Eva Rasch**, **Sabrina Unterburg**, **Mag. Johannes Theiner** and everyone involved in the **NMR centre**, **ICP-MS service, elemental analysis laboratory** and **X-Ray centre**, thank you very much for every measurement, analysis, service and advice.

Last but not least: To my **friends and family**, especially to my beloved husband **Florian Lerchbammer-Kreith**, who has always supported, encouraged and believed in me, especially in challenging times.

Publications

This dissertation is based on the following publications:

Platinum(IV)-Loaded Degraded Glycol Chitosan as Efficient Platinum(IV) Drug Delivery Platform

Yvonne Lerchbammer-Kreith, Nadine S. Sommerfeld, Klaudia Cseh, Xian Weng-Jiang, Uchechukwu Odunze, Andreas G. Schätzlein, Ijeoma F. Uchegbu, Mathea S. Galanski, Michael A. Jakupec and Bernhard K. Keppler

Pharmaceutics **2023**, 15, 1050

Quaternary Ammonium Palmitoyl Glycol Chitosan (GCPQ) Loaded with Platinum-Based Anticancer Agents – A Novel Polymer Formulation for Anticancer Therapy

Yvonne Lerchbammer-Kreith, Michaela Hejl, Nadine S. Sommerfeld, Xian Weng-Jiang, Uchechukwu Odunze, Ryan D. Mellor, David G. Workman, Michael A. Jakupec, Andreas G. Schätzlein, Ijeoma F. Uchegbu, Mathea S. Galanski and Bernhard K. Keppler

Pharmaceuticals **2023**, 16, 1027

Combination of Drug Delivery Properties of PAMAM Dendrimers and Cytotoxicity of Platinum(IV) Complexes – A More Selective Anticancer Treatment?

Yvonne Lerchbammer-Kreith, Michaela Hejl, Petra Vician, Michael A. Jakupec, Walter Berger, Mathea S. Galanski and Bernhard K. Keppler

Pharmaceutics **2023**, 15, 1515

Abstract

Since the discovery of the anticancer activity of cisplatin in the 1960s, platinum(II)-based chemotherapeutics play an essential role in cancer therapy. However, their use is often accompanied by severe adverse effects as well as the occurrence of resistances. The development of kinetically more inert platinum(IV) prodrugs is a promising approach to overcome these drawbacks. Platinum(IV) complexes develop their cytotoxic activity after the reduction to their corresponding platinum(II) counterpart preferentially in the acidic and oxygen-deficient milieu of tumour tissue. The additional ligands in axial position further allow the introduction of targeting moieties, respectively, the attachment to various macromolecules for drug delivery purposes.

Promising polymers in the nanometre range are PAMAM dendrimers as well as chitosans, especially derivatives such as glycol chitosan and quaternary ammonium palmitoyl glycol chitosan, characterised by excellent drug delivery properties by exploiting the EPR effect (enhanced permeability and retention effect) for accumulation in cancerous tissue. The combination with the cytotoxicity of platinum(IV) complexes enables the development of more selective cancer treatment strategies. Consequently, in the present thesis three different classes of conjugates were synthesised, characterised and tested in *in-vitro* and *in-vivo* experiments and compared with conventional platinum(II) complexes.

Firstly, platinum(IV) analogues of cisplatin, carboplatin and oxaliplatin were conjugated to degraded glycol chitosan (dGC) polymers *via* amide bonds. MTT assays in three human cancer cell lines revealed IC_{50} values in the low micro- to nanomolar range and a correlation between platinum(IV) loading rates and cytotoxicity. Biodistribution studies further showed an increased accumulation in the lung of an oxaliplatin-based conjugate in healthy Balb/C mice.

The second project combined platinum(IV) complexes and quaternary ammonium palmitoyl glycol chitosan (GCPQ) polymers with different degrees of palmitoylation and quaternisation. The formed conjugates revealed increased cytotoxicity by up to 286 times in comparison to their platinum(IV) counterparts and mostly outperformed the corresponding platinum(II) complexes. Similar to dGC-based conjugates, increased accumulation in the lung of an oxaliplatin-based-GCPQ conjugate was detected on basis of biodistribution experiments.

Finally, various unsymmetrically carboxylated platinum(IV) compounds were conjugated to PAMAM dendrimers of generation 2 and 4, leading to extremely cytotoxic conjugates with IC_{50} values in the nano- to picomolar range. Biodistribution and activity experiments were performed with one cisplatin-based-G4 PAMAM conjugate resulting in increased survival lifespan compared to cisplatin.

Zusammenfassung

Seit der Entdeckung der Antitumoraktivität von Cisplatin in den 1960er Jahren spielen Platin(II)-basierte Chemotherapeutika eine wesentliche Rolle in der Krebstherapie. Ihr Einsatz ist jedoch oft mit schweren Nebenwirkungen sowie dem Auftreten von Resistenzen verbunden. Die Entwicklung kinetisch inerter Platin(IV)-Prodrugs ist ein vielversprechender Ansatz, um diese Nachteile zu überwinden. Platin(IV)-Komplexe entfalten ihre zytotoxische Aktivität nach der Reduktion zu ihrem entsprechenden Platin(II)-Pendant bevorzugt im sauren und sauerstoffarmen Milieu des Tumorgewebes. Die zusätzlichen Liganden in axialer Position ermöglichen weiters die Einführung von Targeting-Einheiten bzw. die Anlagerung an verschiedene Makromoleküle zur gezielten Pharmakotherapie.

Vielversprechende Polymere im Nanometerbereich sind PAMAM-Dendrimere sowie Chitosane, im Speziellen Derivate wie Glykolchitosan und quaternäres Ammoniumpalmitylglycolchitosan, die sich durch hervorragende Eigenschaften der Wirkstoffabgabe durch Ausnutzung des EPR-Effekts (Enhanced Permeability and Retention Effect) zur Akkumulation im Krebsgewebe auszeichnen. Die Kombination mit der Zytotoxizität von Platin(IV)-Komplexen ermöglicht die Entwicklung selektiverer Krebsbehandlungsstrategien. Folglich wurden in der vorliegenden Arbeit drei verschiedene Klassen von Konjugaten synthetisiert, charakterisiert und in *in-vitro*- und *in-vivo*-Experimenten getestet und mit konventionellen Platin(II)-Komplexen verglichen.

Zunächst wurden Platin(IV)-Analoga von Cisplatin, Carboplatin und Oxaliplatin über Amidbindungen an degradierte Glycolchitosan (dGC)-Polymere konjugiert. MTT-Assays in drei menschlichen Krebszelllinien zeigten IC_{50}-Werte im niedrigen mikro- bis nanomolaren Bereich und eine Korrelation zwischen Platin(IV)-Beladungsraten und Zytotoxizität. Studien zur Bioverteilung zeigten weiters eine erhöhte Akkumulation in der Lunge eines auf Oxaliplatin basierenden Konjugats bei gesunden Balb/C-Mäusen.

Im zweiten Projekt wurden Platin(IV)-Komplexe und quaternäre Ammoniumpalmitylglycolchitosan-Polymere (GCPQ) mit verschiedenen Graden von Palmitoylierung und Quaternisierung kombiniert. Die gebildeten Konjugate offenbarten um bis zu 286-mal erhöhte Zytotoxizität im Vergleich zu ihrem Platin(IV)-Pendant und übertrafen größtenteils auch die entsprechenden Platin(II)-Komplexe. Ähnlich wie bei dem dGC-basierten Konjugat wurde eine erhöhte Akkumulierung eines Oxaliplatin-basierenden-GCPQ-Konjugates
in der Lunge anhand von Bioverteilungsexperimenten gefunden.

Schließlich wurden verschiedene unsymmetrisch carboxylierte Platin(IV)-Verbindungen an PAMAM-Dendrimere der Generation 2 und 4 konjugiert, das zu sehr zytotoxischen Konjugaten mit IC_{50}-Werten im nano- bis pikomolaren Bereich führte. Bioverteilungs- und Aktivitätsexperimente wurden mit

einem Cisplatin-basierenden-G4-PAMAM-Konjugat durchgeführt und führte zu einer verlängerten Überlebensdauer im Vergleich zu Cisplatin.

Table of Content

1. INTRODUCTION

1.1 Cancer

1.1.1 Key facts of cancer

Cancer causes 1 in 6 deaths worldwide, these are around 10 million deaths in absolute numbers for the year 2020. Thus, cancer is the leading cause of mortality all over the world and leads to significant economic impact [1]. The total global costs between 2020 and 2050 caused by cancer was estimated at 25.2 trillion US Dollar [2].

5 principle reasons such as overweight, unhealthy diet, physical inactivity, consumption of tobacco and alcohol are responsible for about one-third of all cancer deaths. Especially, around a quarter of cancer mortality and 70-80% lung cancer deaths are due to tobacco use. Globally, lung cancer leads to 1.8 million deaths followed by colorectum, liver, stomach and breast cancer. Together they are the foremost types for cancer mortality (Figure 1.1.) [1][3].

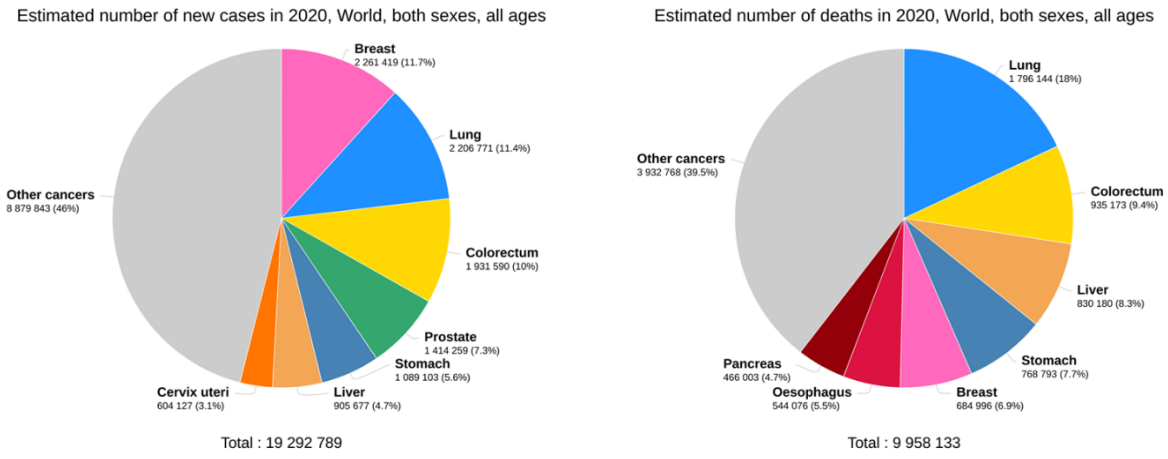

Figure 1.1. Overview of incidence and mortality of different cancer types [4]

1.1.2 Cancer therapy

Up to now, there are different strategies for cancer treatment such as surgery, chemotherapy, radiation therapy, immunotherapy, targeted therapy as well as stem cell or bone marrow transplant and hormone therapy [3]. Especially, for treatment of metastases, chemotherapy is an indispensable part of cancer therapy. Besides different types of drugs like antibiotics, alkylating agents, hormone antagonists, antimetabolites and inhibitors, platinum-based compounds play an essential role in chemotherapy [5][6]. Cisplatin, carboplatin and oxaliplatin are the three platinum(II) complexes in worldwide clinical use and they are alone or together integrated in almost 50% of all chemotherapies [7].

1.2 Platinum(II) complexes

1.2.1 Platinum-based drugs in cancer chemotherapy

In 1965, Barnett Rosenberg investigated the cell reproduction process of Escherichia coli cultures in the presence of an electric field. For his experiment he used platinum electrodes and discovered unintentionally the antiproliferative effect of different generated platinum complexes [8]. The success story of cisplatin was born. The FDA approved cisplatin (Figure 1.2.) as anticancer agent for testicular and metastatic ovarian cancer in 1978. Up to now, cisplatin is used for the treatment of numerous cancer types [9] and belongs to the most profitable anticancer drugs [6].

Although thousands of new platinum(II) complexes were developed and tested, only two further platinum-based compounds, carboplatin and oxaliplatin (Figure 1.2.), were permitted in worldwide clinical use [10].

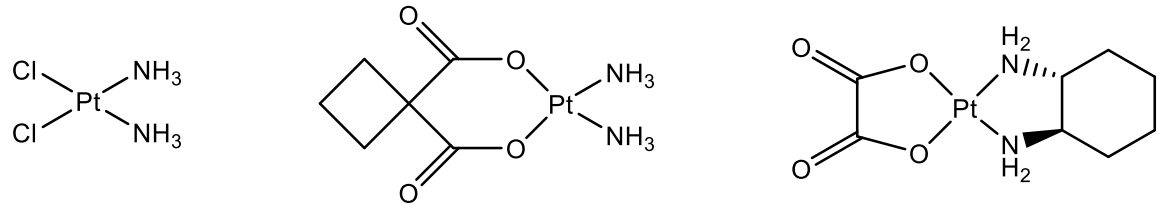

1 **2** **3**

Figure 1.2. Chemical structures of the three platinum(II) compounds used in cancer chemotherapy worldwide: cisplatin **1**, carboplatin **2**, oxaliplatin **3**

1.2.2 Cisplatin

In 1844, Michele Peyrone synthesised cisplatin, calling Peyrone's chloride, for the first-time [11]. Since the discovery of its anticancer activity by Barnett Rosenberg [8] and the approval by the FDA [12], cisplatin, *(SP-4-2)*-diamminedichloridoplatinum(II), has been integrated in the therapy of various tumour types such as testicular, ovarian, head and neck, bladder and small cell lung cancer [13]. Especially, the recovery potential for testicular cancer is impressive. A cure rate of almost 90% can be achieved with cisplatin, whereas only 10% are possible with other therapy methods [9][14].

However, the treatment with cisplatin is accompanied by severe side effects like nephrotoxicity, neurotoxicity, nausea, ototoxicity and myelosuppression [15], whereby nephrotoxicity is the dose-limiting factor [22].

1.2.3 Carboplatin

Replacement of the chloride ligands of cisplatin with the 1,1-cyclobutanedicarboxylato chelator leads to slower aquation to the active aqua species [19]. As a result, lower toxicity with similar cytotoxicity

and application spectrum are observed. This cisplatin-analogue was approved for worldwide cancer therapy in 1989 [16].

Carboplatin, *(SP-4-2)*-diammine(1,1-cyclobutanedicarboxylato)platinum(II), shows dose-limiting myelotoxicity but reduced nephrotoxicity and neurotoxicity [17] and is now the first choice for ovarian cancer treatment [18].

1.2.4 Oxaliplatin

Oxaliplatin, *(SP-4-2)*-(1R,2R)-(cyclohexane-1,2-diamine)oxalatoplatinum(II), was permitted for worldwide clinical practice in 2002 and is the most recent internationally approved platinum(II)-based agent [19].

Due to the introduction of the bulkier 1,2-cyclohexanediamine (DACH) ligand, oxaliplatin is chiral, bearing the most effective R,R-DACH ligand compared with the S,S-isomer or the *meso*-R,S counterpart. This effect is characterised in part by the ability of the R,R isomer to form hydrogen bonds between the pseudo equatorial NH hydrogen atom and the O6 atom of guanine in the d(GpG) cross-link [20].

Therefore, oxaliplatin shows a diverse recognition and processing of formed DNA-adducts in comparison to ciplatin and carboplatin. Consequently, oxaliplatin displays a different spectrum of activity including antiproliferative potential in cisplatin- and carboplatin-resistant tumours such as metastatic colorectal cancer [21][22], the second most common cause of cancer death worldwide [1].

The dose-limiting factor is neurotoxicity [23], occurring as acute hyperexcitability and chronic neuropathy [24].

1.2.5 Mode of action – cisplatin

In general, platinum(II) complexes consist of two different types of ligands. On the one hand, nitrogen donors like monodentate ammines for cisplatin and carboplatin or chelating 1,2-cyclohexanediamine for oxaliplatin form stable bonds with the central platinum ion. These ligands belong to the non-leaving group or so-called carrier ligands. Anionic ligands such as chlorido and bidentate oxalato ligands act, on the other hand, as leaving groups based on their lability [9].

After intravenous application, platinum(II) complexes enter the cell *via* passive diffusion or active transporters like copper transporter CTR1 (Figure 1.3.). Due to the lower chloride concentration in the cytoplasm (~4 mM) in comparison to the bloodstream (~100 mM), cisplatin hydrolyses *via* exchanging chlorido ligands with water molecules inside the cell [25]. The formed active aqua species $[Pt(NH_3)_2Cl(OH_2)]^+$ and $[Pt(NH_3)_2(OH_2)_2]^{2+}$ are able to interact with biological nucleophilic sites of proteins, RNA and DNA, the major target. Especially, these cationic complexes can covalently bind to the N7 atom of adenine and guanine leading to monoadducts, intrastrand and interstrand cross-links

[26]. The most common adducts formed are intrastrand cross-links 1,2-Pt-d(GpG) with a percentage of 60-65% followed by 1,2-Pt-d(ApG) (25%). The geometrical deformations of DNA result in inhibition of transcription and replication mechanism and finally induce apoptosis of tumour cells [21].

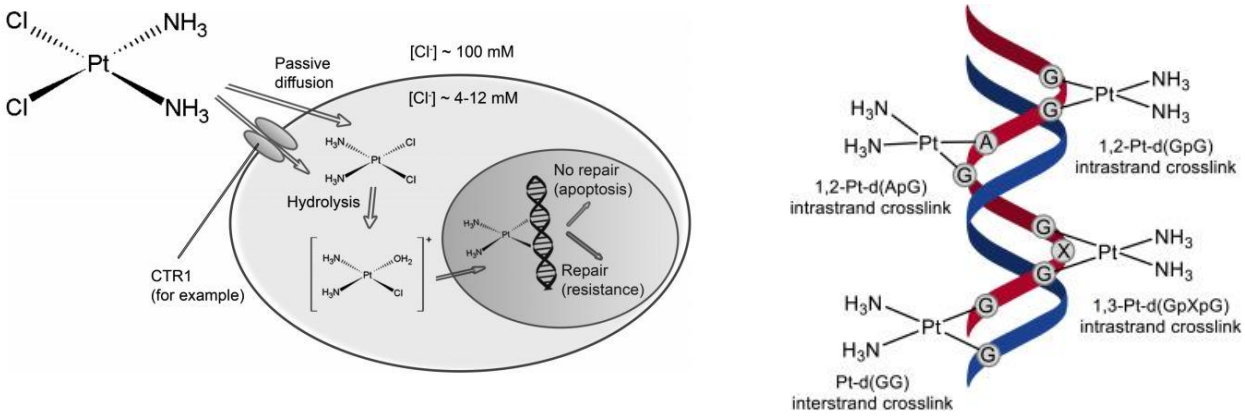

Figure 1.3. Cisplatin's hydrolysis process [27] and formed platinum-DNA adducts [28]

1.2.6 Drawbacks

Although platinum(II) compounds are still an important part of modern cancer treatment strategies, their use is accompanied by several disadvantages.

Based on their instability in the gastrointestinal tract, platinum-based agents have to be administered intravenously, resulting in high therapy costs and patients' inconveniences [29].

In consideration of the HSAB principle, platinum(II) complexes are soft Lewis acids and capable to form stable bonds with sulphur and nitrogen donors [30]. Therefore, their additional kinetical lability and unselectivity towards malignant tissue lead to uncontrolled reactions with biomolecules like amino acids and proteins during residence in the bloodstream from administration until reaching tumour tissue. Consequently, numerous adverse effects, starting from nausea and vomiting to severe nephrotoxicity and neurotoxicity are detected [31][32].

Additionally, resistance of numerous cancer types to platinum-based treatment alias intrinsic resistance point out a major problem. Due to adaptations of cancer cells during repeated drug exposure throughout chemotherapy, resistance can further be developed leading to ineffectiveness. This acquired resistance is related with improved detoxification and degradation as well as decreased cellular drug accumulation [33][34].

1.3 Platinum(IV) complexes

1.3.1 Advantages

In order to reduce side effects and overcome resistances of approved platinum(II) drugs, new strategies were developed. The introduction of two additional axial ligands leads to low-spin d^6 platinum(IV) centres with octahedral coordination sphere (Figure 1.4.). The resulting higher variation and derivatisation possibilities allow fine-tuning of relevant abilities such as stability, reduction behaviour, lipophilicity and bioactivity [20].

Generally, platinum(IV) complexes are kinetically more inert towards ligand substitution compared with their platinum(II) analogues. Enough lipophilicity enables further the absorption by the gastrointestinal tract without degradation, leading to the possibility of oral administration of platinum(IV) compounds [34]. Based on their stability, indiscriminate interactions with biomolecules can be reduced, resulting in lower toxicities and decreased deactivation [35].

Furthermore, platinum(IV) complexes demonstrate an alternative mode of action. They are considered as prodrugs following the "activation by reduction" concept. In order to release their cytotoxic potential, they have to be reduced to their active platinum(II) counterparts [36]. Especially, tumour tissue characterised by an acidic and oxygen-deficient milieu facilitates the reduction of platinum(IV) complexes by releasing their axial ligands [6].

Finally, the octahedral coordination geometry enables the introduction of targeting moieties in axial position for different drug delivery strategies [37].

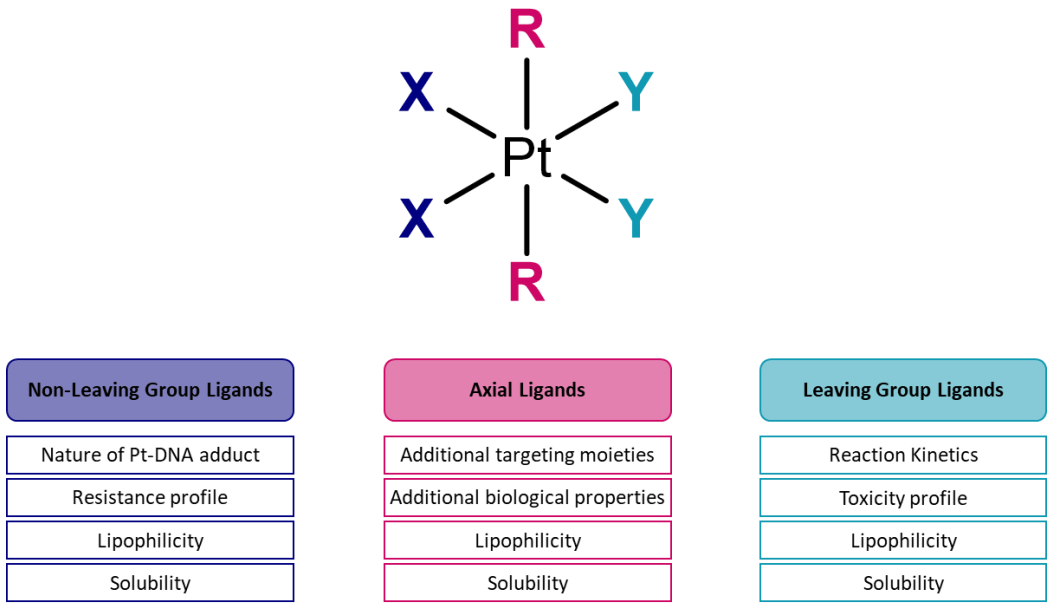

Figure 1.4. General structure of platinum(IV) complexes including the three different ligand types (adapted from [9])

1.3.2 Reduction

Although there are platinum(IV)-DNA species reported [38][39][40], reduction is still a crucial precondition for anticancer activity of platinum(IV) complexes. In general, reduction can occur extracellularly or intracellularly whereby reduction outside the cell leads to deactivation of the compound or toxic side effects (Figure 1.5.). However, the desired intracellular reduction is preferred [41].

Due to the large number of potential reducing biomolecules in blood and cells, the unambiguous identification of all involved reactants is still outstanding. Especially, the influence of biomolecules with high molecular mass such as haemoglobin and myoglobin, metallothioneins as well as diverse sugars or NADH has to be further investigated [32][41]. Nevertheless, it is widely accepted that small molecules like glutathione and ascorbic acid play an essential role in the activation process of platinum(IV) complexes [42].

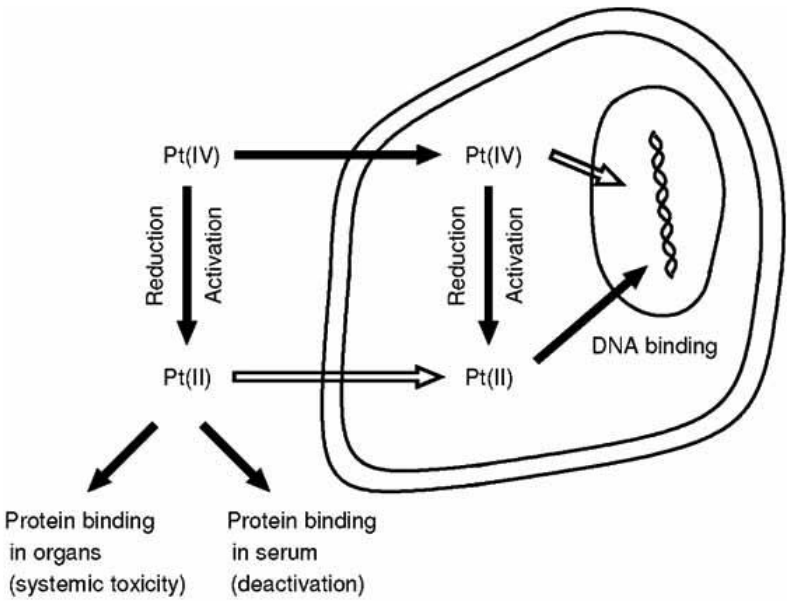

Figure 1.5. Scheme of reduction behaviour of platinum(IV) complexes in biological environment [22]

1.3.3 Reduction potential and rate of reduction

The successful activation of platinum(IV) compounds is decisive for the release of their anticancer activity and associated with their reduction potential. In general, the impact of equatorial ligands on the reduction potential is low especially for the non-leaving amine donors [43]. Nevertheless, chelate or bulkier ligands as well as oxygen donors can stabilise the complex and influence reduction rates based on their electron withdrawing power and steric hindrance [44]. However, the expected and examined correlation between the two parameters reduction potential and rate of reduction [36][45] shows significant deviation for investigated oxaliplatin(IV) analogues [46].

On the contrary, axial ligands exhibit a stronger influence on the reduction behaviour. Higher electronegative ligands in axial position such as chlorides show high reduction potentials, whereas hydroxido ligands lead to low reduction potentials. The reduction potential of compounds with axial carboxylato ligands is in the middle of both [47]. While modifications of their length induce only minimal changes, introduction of electron withdrawing groups leads to significant effects [44].

1.3.4 Platinum(IV) compounds in clinical trials – relationship between reduction potential and cytotoxicity

Although thousands of platinum(IV) complexes were synthesised and some have been investigated in preclinical development in the recent years, no platinum(IV)-based agent was approved for clinical practice. Four platinum(IV) compounds tetraplatin, iproplatin, satraplatin and LA-12 have entered clinical trials so far (Figure 1.6.) [7][48].

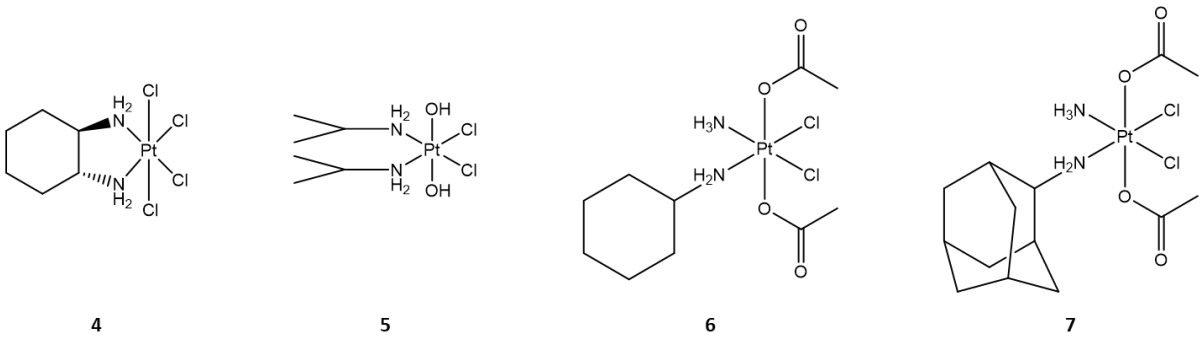

Figure 1.6. Platinum(IV) representatives which entered clinical trials: tetraplatin **4**, iproplatin **5**, satraplatin **6**, LA-12 **7**

The reduction of ormaplatin alias tetraplatin, *(OC-6-22)*-tetrachlorido(transcyclohexane-1,2-diamine)platinum(IV), occurs very fast in the bloodstream based on its chloride ligands in axial position. Therefore, the referring platinum(II) complex has the possibility to react with several biomolecules leading to diverse side effects. After phase I, the clinical trials for therapy of ovarian, breast and myeloma cancer were not continued based on the severe neurotoxicity of tetraplatin.

In contrast, iproplatin, *(OC-6-33)*-dichloridodihydroxidobis(isopropylamine)platinum(IV), was abandoned after phase III for ovarian cancer treatment referring to its lower anticancer activity compared to cisplatin and carboplatin. The lower cytotoxicity accompanied with decreased toxicities resulted from the slow reduction behaviour of axial hydroxido ligands [37][49].

The most promising and first orally administered platinum(IV) representative [50] was JM-216 alias satraplatin, *(OC-6-43)*-bis(acetato)amminedichlorido(cyclohexylamine)platinum(IV). Based on their axial acetato ligands leading to intermediate reduction potentials [34], the toxicity spectrum could be reduced especially neurotoxicity and nephrotoxicity. The effect of satraplatin was evaluated for

several cancer types such as small cell lung cancer and hormone refractory prostate cancer [51]. Although additional improvements in pain progression was observed, no significant survival benefit over conventual therapy could be determined in phase III [52]. However, satraplatin is still investigated in clinical trials phase II in combination with radiotherapy for lung cancer treatment [51]. Finally, the results from clinical trials of the close satraplatin analogue LA-12, *(OC-6−43)*-bis(acetato)(1-adamantylamine)amminedichloridoplatinum(IV) are still missing [5348].

Based on the data of the three platinum(IV) complexes investigated in clinical trials, a correlation between reduction behaviour, anticancer activity and toxicity profile seems to be conceivable and platinum(IV) compounds with carboxylato ligands in axial position are promising candidates for a new generation of anticancer platinum drugs. [34].

1.3.5 Water solubility and lipophilicity

Generally, improved water solubility in combination with higher kinetical inertness avoiding fast aquation is accompanied with a milder toxicological profile. Due to the extended stay in the bloodstream, hydrophilic platinum compounds are primarily excreted *via* the kidneys. Based on their higher stability, metabolisation is impeded and the original platinum complexes is mostly still intact during excretion. However, the resulting lower (nephro)toxicity is further connected with reduced cytotoxic properties [22].

On the contrary, enhanced lipophilicity and higher stability facilitate passive diffusion through the lipophilic cell membranes and thus increase cellular uptake. On the other hand, resistances are associated with reduced drug uptake. Consequently, lipophilic platinum compounds could be a promising approach circumventing resistance. Additionally, the improved cellular uptake is related with higher cytotoxicity and lower renal excretion, resulting in reduced nephrotoxicity.

However, anticancer activity is decreased if platinum compounds are too lipophilic or hydrophilic caused by poor solubility and low absorption through the digestive tract as well as prevented cellular uptake. Therefore, an optimal balance has to be found between both extremes. In this context, water soluble platinum(IV) complexes with axial carboxylato ligands are promising candidates since their lipophilicity can be easily modified by their chain length (CH_2 moieties) [22][54][55].

1.4 Targeting strategies

In order to increase the absent selectivity of conventional platinum-based agents and to reduce resulting side effects, different targeting strategies were developed. Besides a milder toxicity profile, resistances should be circumvent based on the selective accumulation in tumour tissue [56].

1.4.1 Targeting positions

Generally, there are four different approaches to introduce a targeting moiety (Figure 1.7.). Attachment to the leaving group is accompanied with assuring intact arrival to malignant tissue and release during the hydrolysis process. Otherwise, the anticancer activity based on formed platinum-DNA intermediates is compromised.

Linker conjugated to non-leaving am(m)ine groups persist during aquation. Without enzymatic cleavage or severance caused by acidic conditions in tumour tissue, the targeting moiety significantly influences chemical and pharmacological properties of the resulting DNA adduct leading to cytotoxic alterations.

Furthermore, the prodrug strategy of platinum(IV) complexes with releasing axial ligands enables an attractive targeting possibility. Carrier functionalities can be linked to axial ligands without high impact of created DNA-platinum species. An optimised reduction behaviour referring reduction potential and rate of reduction is thereby a crucial parameter.

Finally, drug encapsulation in different macromolecules such as liposomes, (polymeric) micelles or dendrimers is associated with improved solubility and cellular uptake as well as prevented degradation and detoxification. The critical step is thereby the adequate release of the anticancer agent [57][58].

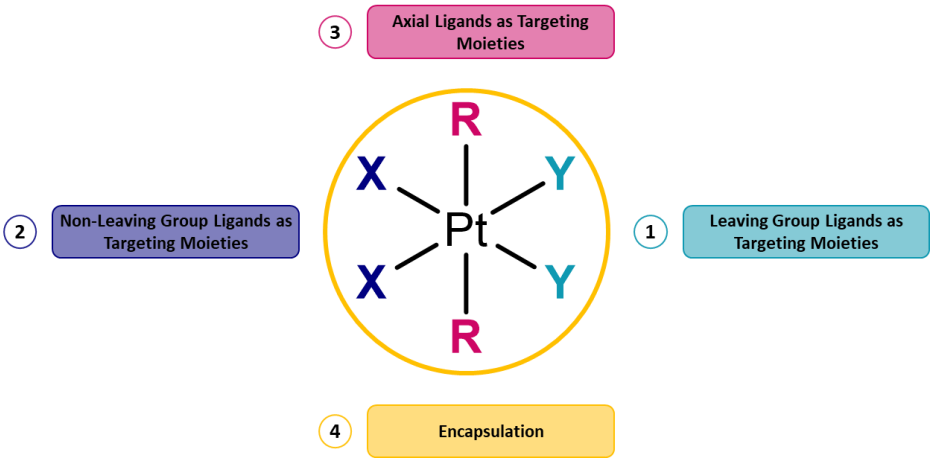

Figure 1.7. The four possibilities to introduce a targeting group (adapted from [58])

1.4.2 EPR-effect and passive tumour targeting

Based on their fast cell division and growth, solid tumours require a huge amount of oxygen and nutrients. Extensive tumour angiogenesis results in chaotic and defective blood vessels characterised by large gaps between their endothelial cells [59] in size range of 10 – 1000 nm. The enhanced vascular permeability enables the penetration of macromolecules in low nanometre range (20-200 nm). The additional dysfunctional lymphatic system leads to ineffective drainage and accumulation of those nanoparticles in tumour tissue [60]. This phenomenon, so-called enhanced permeability and retention

(EPR) effect, was first discovered in 1986 [61]. This vascular abnormality is, besides an oxygen-deficient and acidic milieu with an extracellular pH between 6 – 7, characteristic for cancerous tissue [60]. Consequently, drug targeting approaches to infiltrate and accumulate anticancer agents attached to nanocarriers were devised (Figure 1.8.). ProLindac, a polymer loaded with oxaliplatin, was studied in numerous phase I and II trials and is listed for an ongoing phase III study. Moreover, cisplatin encapsulated in liposomes, so-called lipoplatin, shows improved accumulation in tumour tissue and significantly reduced adverse effects compared with cisplatin. Lipoplatin entered several phase III studies amongst others for advanced ovarian and metastatic pancreas cancer [48].

Besides those passive tumour targeting examples exploiting the EPR-effect, modifications on carrier functionalities such as introducing monoclonal antibodies or peptides are requisite for active targeting. The main targets are thereby receptors overexpressed in cancerous cells and ideally less represented in healthy cells [60].

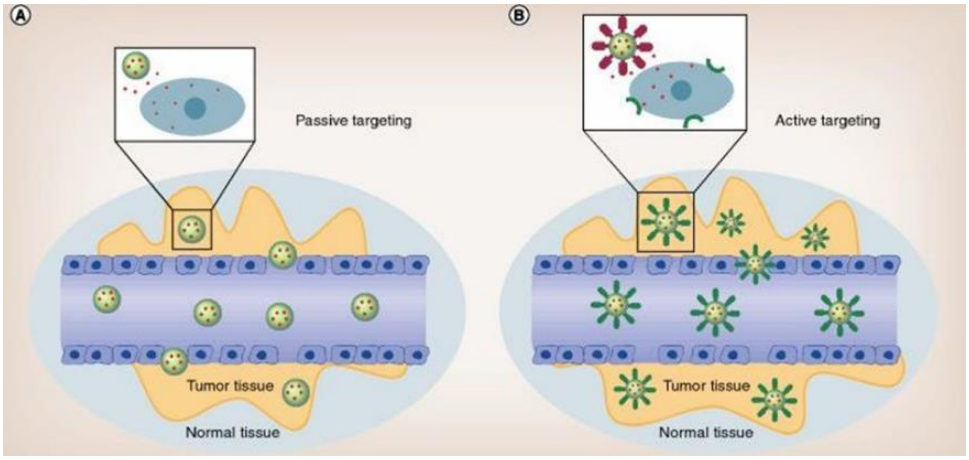

Figure 1.8. Scheme of passive targeting *via* EPR-effect (A) and active targeting involving receptors (B) [62]

1.4.3 Dendrimers

Designing of well-defined nanostructures is of special interest in the field of biotechnology [63] and is expected to play an essential role for the next decades in nanomedicine [64].

Particularly, dendrimers belong to polymeric macromolecules with advantageous properties for chemical, biological and medical applications [65]. Sequences of various monomers, so-called branching units, are constituted radial around a multifunctional core such as a small molecule or a linear polymer. The dendritic structure grows symmetrically controlled step by step around divergent points, whereby each new layer conforms a new generation. The final generation incorporates the terminal groups modified with special functionalities or targeting moieties and influences the physicochemical or biological properties (Figure 1.9.) [64][66].

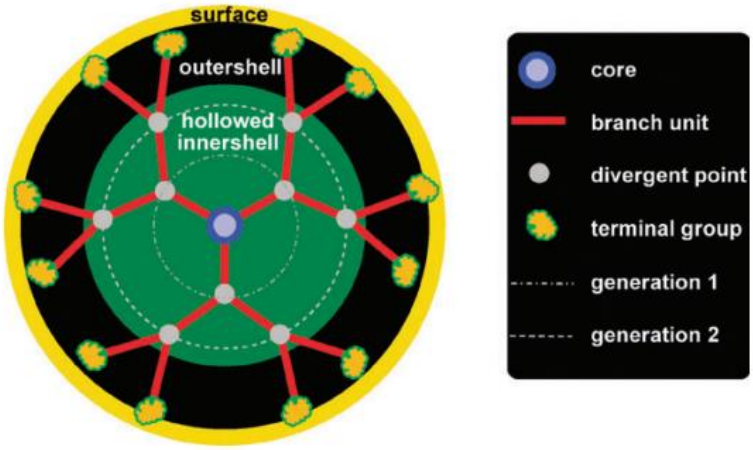

Figure 1.9. Schematic structure of dendrimers [64]

Due to their high architectural control, their size, shape, branching length/density and their surface, functionality can exactly be designed. Therefore, dendrimers are excellent representatives for medical applications such as gene transfection, imaging and drug delivery because of their activity against tumours, bacteria and viruses [67].

In the field of drug delivery, there are two possible ways to conjugate the bioactive agents to dendrimers. On the one hand, the drug can be encapsulated into the interior, whereas on the other hand, it can be bound/coordinated onto the dendrimer's surface. Besides various tuning possibilities of their surface, dendrimers are especially qualified for this application because of their size in the nanometre range, which allows crossing the cell membranes and decreases the undesired clearance through the liver [67]. Their biocompatibility is further improved because of the high porosity of blood vessels typically for inflammation and tumour tissues. Due to the EPR-effect, nano-devices such as dendritic structures accumulate especially in solid tumours [64].

The most extensively studied and first commercially available representatives are poly(amidoamine) (PAMAM) dendrimers [68] or originally called "starburst polymers" by its developer Donald Tomalia in 1985 [69].

Typically starting from an ethylenediamine core [70], PAMAM dendrimers are synthesised through Michael addition of methyl acrylate in a two-step mechanism [71]. A full-generation, synonymous with a complete layer, leads to terminal primary amines, whereas an interrupted one-step cycle results in half-generation PAMAM dendrimers with carboxylic acids as end groups. Depending on the terminal groups and the pH, PAMAM dendrimers are neutral, multiple positively or negatively charged showing a polyelectrolyte character (Figure 1.10.) [72].

Recently, generation 2 and 4 of PAMAM dendrimers were loaded with an oxaliplatin(IV) analogue *via* amide bonds. The cytotoxicity was significantly improved in comparison to the free platinum(IV)

complex. In general, IC_{50} values in nanomolar range were obtained proving the potential of PAMAM polymers for further evaluation in cancer therapy [73].

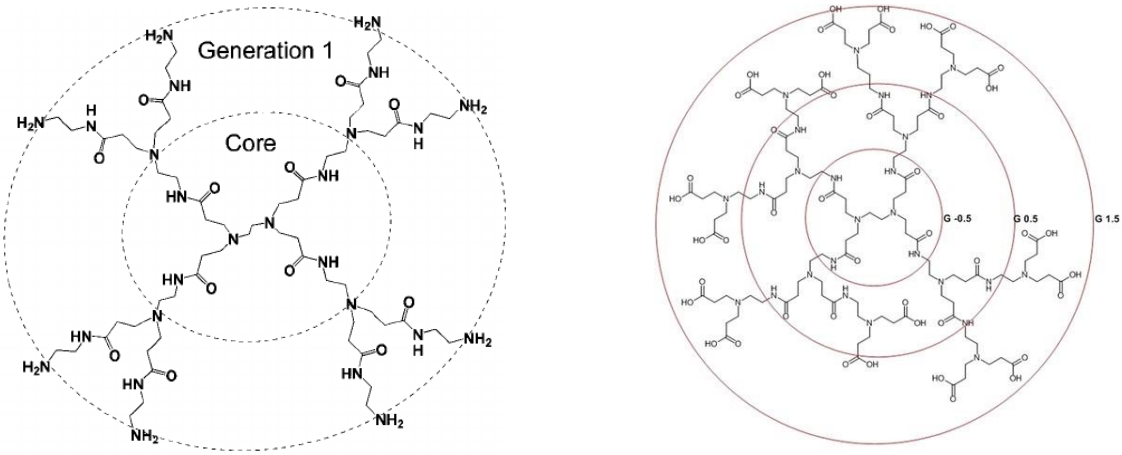

Figure 1.10. Structure of full-generation PAMAM dendrimers with amines as terminal groups [74] and half-generation PAMAM dendrimers containing terminal carboxylic acid functionalities [75]

1.4.4 Chitosans and their representatives dGC and GCPQ

Chitosans are polysaccharides produced from the renewable source chitin, primarily obtained as a waste product of the shellfish industry, via deacetylation [76]. Depending on the desired properties, chitosan polymers of different molecular weights and remaining degrees of acetylation (DA) can be synthesised, which strongly impact solubility. Due to its high DA, chitin is almost insoluble, whereas reduction of the DA to lower than 50 mol% results in chitosan polymers, which are water-soluble under acidic conditions [77]. The solubility can be further improved by modification, leading to good soluble derivatives. Consequently, degraded glycol chitosan (dGC) (Figure 1.11.) and quaternary ammonium palmitoyl glycol chitosan (GCPQ) show good solubility (Figure 1.12) [78][79].

Based on the advantageous properties of chitosan nanoparticles such as their biocompatibility, non-toxicity and adsorption capacities, they are excellent candidates for drug delivery systems [80]. Due to the formation of micelles, the core of chitosan nanoparticles demonstrates good capability for drug encapsulation, whereas their surface can be exploited for targeting purposes [78].

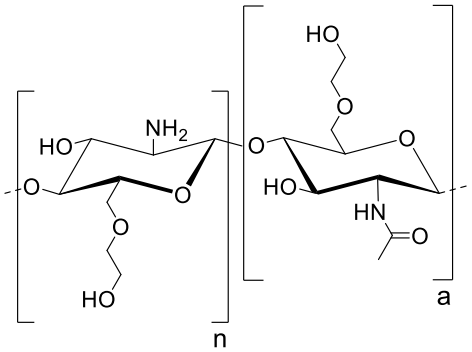

Figure 1.11. Structure of degraded glycol chitosan

As a polysoap, quaternary ammonium palmitoyl glycol chitosan alias GCPQ belongs to amphiphilic polymers, containing hydrophobic side chains (Figure 1.12.) and self assembles into micelles in aqueous solution [81]. GCPQ polymers enable the encapsulation of hydrophilic and lipophilic drugs and can be used as drug delivery system to enter amongst others the brain-blood barrier and epithelium of the gastrointestinal tract.

Based on the nanometre size of GCPQ polymers, the EPR effect can be exploited for passive tumour targeting, enabling an attractive approach for drug delivery of anticancer agents which was already reported in literature [82][83]. The organic anticancer agent selumetinib (AZD6244) was encapsulated in GCPQ micelles and displayed enhanced drug delivery in monolayer experiments and tumouroids compared to the free drug [84]. Moreover, enhanced cellular uptake and tumour targeting potential could be achieved by encapsulation of doxorubicin in GCPQ micelles [83].

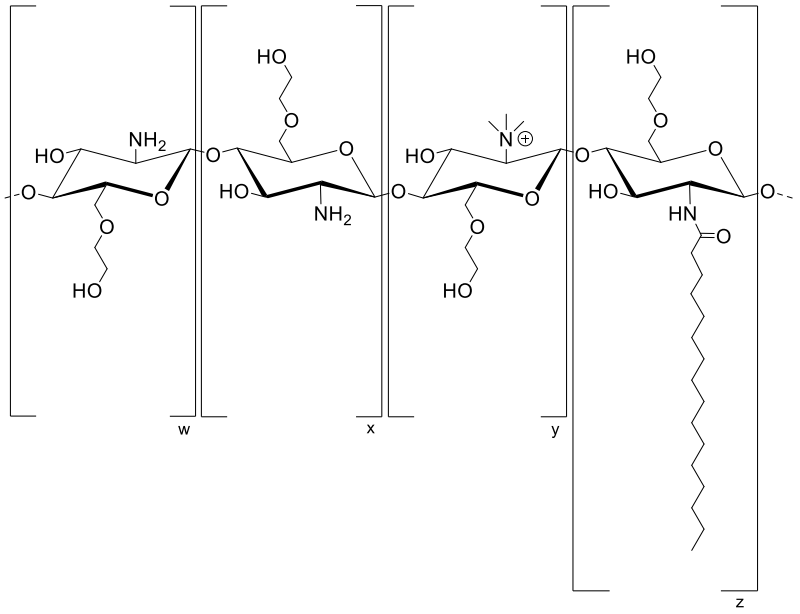

Figure 1.12. Structure of the polysoap GCPQ

2. Research objectives

The general research objective of this thesis was the investigation of the anticancer activity of platinum(IV) complexes conjugated to polymers in the nanometre range in order to exploit the EPR effect and analyse the potential as a more selective anticancer treatment.

2.1 Platinum(IV) complexes conjugated to degraded glycol chitosan (dGC)

Up to now, platinum(II)-based cancer chemotherapy is associated with severe adverse effects, which are responsible for dose limitation and therefore diminish the clinical efficiency of classical platinum(II) drugs [85]. Consequently, the development of anticancer agents with reduced toxicity due to primary tumour targeting is of special interest. The large gaps between endothelial cells of blood vessels of tumour tissue, caused by defective angiogenesis, can be exploited for the penetration of macromolecules in the nanometre range through endocytosis. Additionally, tumour tissue is characterised by defective lymph drainage, leading to accumulation of macromolecules. These two effects are known as EPR effect and enable passive tumour targeting [60]. Therefore, investigations on polymers which can be used as drug delivery systems for anticancer agents, attract more and more attention. Besides non-toxicity and good biocompatibility, chitosan-based polymers display good drug delivery properties, modification possibilities and good solubility (especially glycol chitosan and quaternary ammonium palmitoyl glycol chitosan) [86]. Consequently, the first project aimed to investigate the potential of degraded glycol chitosan (dGC) polymers combined with platinum(IV) complexes as a novel anticancer treatment approach. In total twenty dGC-platinum(IV)-conjugates were synthesised and characterised. Their cytotoxicity was tested in human cancer cell lines and a biodistribution study in non-tumour-bearing mice was performed of one conjugate.

2.2 Platinum(IV) complexes conjugated to quaternary ammonium palmitoyl glycol chitosan (GCPQ)

Similar to degraded glycol chitosan, quaternary ammonium palmitoyl glycol chitosan is able to penetrate into and accumulate in tumour cells due to the EPR effect. Based to the amphiphilic character, GCPQ polymers spontaneously form micelles in aqueous solution and thus show excellent solubilising and drug delivery properties [87][88]. Additionally, the level of palmitoylation and quaternisation can be varied, leading to different toxicological profiles and solubility properties. Therefore, the second project of this thesis focused on the conjugation of platinum(IV) complexes to various GCPQ polymers. Twelve synthesised conjugates were tested in human cancer cell lines and one conjugate was further investigated *in vivo*.

2.3 Platinum(IV) complexes conjugated to PAMAM dendrimers of generation 2 and 4

Dendrimers are synthetically designed polymers in the nanometre range with adjustable functionalities. The most famous representative is the symmetric poly(amidoamine) (PAMAM) dendrimer available in different generations. PAMAM dendrimers are used as drug delivery systems due to the possibility to attach drugs on the surface or encapsulate agents in the interior. Consequently, the third project involved the conjugation of platinum(IV) complexes to PAMAM dendrimers of generation 2 and 4 via amide bond formation in order to investigate their potential as a selective anticancer drug delivery system. Twenty-four conjugates were characterised, and their cytotoxicity was investigated in human cancer cell lines. Finally, one conjugate was further evaluated in biodistribution and activity studies.

3. Publications

3.1 Platinum(IV)-loaded degraded glycol chitosan as efficient platinum(IV) drug delivery platform

Yvonne Lerchbammer-Kreith[1,†], Nadine S. Sommerfeld[1,†], Klaudia Cseh[1], Xian Weng-Jiang[2], Uchechukwu Odunze[2], Andreas G. Schätzlein[2], Ijeoma F. Uchegbu[2], Mathea S. Galanski[1], Michael A. Jakupec[1,3,*] and Bernhard K. Keppler[1,3]

Pharmaceutics, published on March 24th, 2023

[1] Institute of Inorganic Chemistry, Faculty of Chemistry, University of Vienna, Waehringer Strasse 42, 1090 Vienna, Austria

[2] School of Pharmacy, University College London, Brunswick Square 29-39, London WC1N 1AX, UK

[3] Research Cluster "Translational Cancer Therapy Research", University of Vienna, Waehringer Strasse 42, 1090 Vienna, Austria

[*] Correspondence: michael.jakupec@univie.ac.at

[†] These authors contributed equally to this work.

As first author of the publication, I synthesised and characterised all platinum(IV) complexes and the majority of the conjugates (17 out of 20) and I wrote the majority of the manuscript.

pharmaceutics

MDPI

Article

Platinum(IV)-Loaded Degraded Glycol Chitosan as Efficient Platinum(IV) Drug Delivery Platform

Yvonne Lerchbammer-Kreith [1,†], Nadine S. Sommerfeld [1,†], Klaudia Cseh [1], Xian Weng-Jiang [2], Uchechukwu Odunze [2], Andreas G. Schätzlein [2], Ijeoma F. Uchegbu [2], Mathea S. Galanski [1], Michael A. Jakupec [1,3,*] and Bernhard K. Keppler [1,3]

[1] Institute of Inorganic Chemistry, Faculty of Chemistry, University of Vienna, Waehringer Strasse 42, 1090 Vienna, Austria
[2] School of Pharmacy, University College London, Brunswick Square 29-39, London WC1N 1AX, UK
[3] Research Cluster "Translational Cancer Therapy Research", University of Vienna, Waehringer Strasse 42, 1090 Vienna, Austria
* Correspondence: michael.jakupec@univie.ac.at
† These authors contributed equally to this work.

Abstract: A new class of anticancer prodrugs was designed by combining the cytotoxicity of platinum(IV) complexes and the drug carrier properties of glycol chitosan polymers: Unsymmetrically carboxylated platinum(IV) analogues of cisplatin, carboplatin and oxaliplatin, namely (OC-6-44)-acetatodiammine(3-carboxypropanoato)dichloridoplatinum(IV), (OC-6-44)-acetaodiammine(3-carboxypropanoato)(cyclobutane-1,1-dicarboxylato)platinum(IV) and (OC-6-44)-acetato(3-carboxypropanoato)(1R,2R-cyclohexane-1,2-diamine)oxalatoplatinum(IV) were synthesised and conjugated via amide bonding to degraded glycol chitosan (dGC) polymers with different chain lengths (5, 10, 18 kDa). The 15 conjugates were investigated with ^{1}H and ^{195}Pt NMR spectroscopy, and average amounts of platinum(IV) units per dGC polymer molecule with ICP-MS, revealing a range of 1.3–22.8 platinum(IV) units per dGC molecule. Cytotoxicity was tested with MTT assays in the cancer cell lines A549, CH1/PA-1, SW480 (human) and 4T1 (murine). IC_{50} values in the low micromolar to nanomolar range were obtained, and higher antiproliferative activity (up to 72 times) was detected with dGC-platinum(IV) conjugates in comparison to platinum(IV) counterparts. The highest cytotoxicity (IC_{50} of 0.036 ± 0.005 μM) was determined in CH1/PA-1 ovarian teratocarcinoma cells with a cisplatin(IV)–dGC conjugate, which is hence 33 times more potent than the corresponding platinum(IV) complex and twice more potent than cisplatin. Biodistribution studies of an oxaliplatin(IV)–dGC conjugate in non-tumour-bearing Balb/C mice showed an increased accumulation in the lung compared to the unloaded oxaliplatin(IV) analogue, arguing for further activity studies.

Keywords: platinum(IV) complexes; glycol chitosan; anticancer; drug delivery

Citation: Lerchbammer-Kreith, Y.; Sommerfeld, N.S.; Cseh, K.; Weng-Jiang, X.; Odunze, U.; Schätzlein, A.G.; Uchegbu, I.F.; Galanski, M.S.; Jakupec, M.A.; Keppler, B.K. Platinum(IV)-Loaded Degraded Glycol Chitosan as Efficient Platinum(IV) Drug Delivery Platform. *Pharmaceutics* **2023**, *15*, 1050. https://doi.org/10.3390/pharmaceutics15041050

Academic Editor: Kenneth K. W. To

Received: 2 February 2023
Revised: 17 March 2023
Accepted: 20 March 2023
Published: 24 March 2023

1. Introduction

Platinum(II)-based chemotherapy is indispensable in modern clinical oncology, with an expectedly growing global market for the three major drugs, cisplatin, carboplatin and oxaliplatin [1]. Despite the tremendous success of those three platinum(II) complexes, which are in global clinical use and together are integrated in about 50% of all chemotherapies [2], no other platinum complex has reached worldwide marketing approval. The major limitation of platinum(II)-based anticancer treatment is the minor selectivity towards tumour tissue, leading to severe side effects, especially nephrotoxicity and neurotoxicity [3,4]. The clinical efficacy is highly diminished by cancer resurgence and intrinsic as well as acquired therapy resistance [5]. The platinum(IV) prodrug strategy is one attempt to overcome the downsides of platinum(II) drugs. This strategy is driven by the possibility to overcome resistances and to reduce toxicities by introduction of two axial ligands, leading

to higher kinetic inertness and less indiscriminate reactions with biological nucleophiles [6]. Additionally, platinum(IV) complexes follow the "activation by reduction" concept and evolve their cytotoxic properties by releasing their axial ligands [7]. The required reduction is especially facilitated by the characteristic acidic and oxygen-deficient environment in tumour tissue [8]. Initial investigation of mainly axially symmetric platinum(IV) compounds such as tetraplatin, iproplatin, LA-12 and, in particular, satraplatin, in clinical trials has remained unsuccessful [2,9]. Our group made significant progress in the diversification of the platinum(IV) ligand sphere over the last decade(s), with an exceptional focus on mixed axial ligands [10–12] and multifunctionality [13]. The platinum(IV) paradigm shifted towards the integration of moieties with drug-targeting abilities, easily accessible via the additional ligands, for optimising pharmacokinetic and -dynamic properties [14].

The natural chitosan polymers as emerging drug-targeting moieties seem to be promising candidates for improved application and biodistribution of platinum(IV) complexes. They are extensively studied based on their advantageous properties, such as biodegradability, biocompatibility and their polyelectrolyte character [15,16]. The polysaccharide chitosan can be obtained from the natural source chitin, occurring in shells of crustaceans, exoskeletons of insects or cell walls of fungi, via deacetylation. However, harsh conditions from using hydroxides in combination with high temperatures during the deacetylation process can lead to a decrease in molecular weight. According to the desired final properties, chitosan with different degrees of acetylation (DA) can be obtained. Consequently, chitosan consists of two different monosaccharide units: N-acetyl-D-glucosamine and D-glucosamine, which are connected via β (1→4) bonds [17,18]. The DA strongly influences the solubility. Whereas chitin with a very high DA lacks in solubility, chitosan with DA lower than 50 mol% is soluble in water under acidic conditions [19]. The solubility can be further improved by derivatisation, leading to high solubility in water at acidic and neutral pH and organic solvents, for derivatives such as glycol chitosan [17,20]. In addition to glycol chitosan, various derivatives such as different quaternised and alkylated chitosan polymers were synthesised and investigated based on the ease of modification of the chitosan structure via chemical and enzymatic procedures [17,21]. Due to the possibility of crosslinks with various reagents and the polycationic nature, chitosan can be obtained in various forms such as powders, tablets, solutions, gels, membranes or sponges, enabling numerous administration routes such as oral, parenteral and transdermal. Furthermore, chitosan's antioxidant, anti-inflammatory, antibacterial, antimicrobial and antitumour properties in combination with its nontoxicity and biocompatibility are used in different application fields, reaching from food preservation to cosmetics (Scheme 1) [19,21,22]. Especially, medical purposes, such as chitosan being used as artificial skin and as a drug carrier, attract more and more attention [23]. Due to their nontoxicity, adsorption capacities and facile derivatisation [24], chitosan polymers are promising platforms for encapsulation or conjugation with different agents such as anticancer compounds. As a result of their nanometre size, the enhanced permeability and retention effect (EPR effect) can be exploited for passive tumour targeting. Due to defective angiogenesis during tumour growth, large gaps (600–800 nm) between endothelial cells of blood vessels are formed, and small polymers can enter tumour cells by endocytosis. Continuous accumulation of polymers is further supported by malfunctioning lymph drainage. Additionally, drug release is facilitated by the acidic and hypoxic environment in tumour tissue [25–27].

Accordingly, the combination of the drug delivery properties of chitosan polymers and platinum-based anticancer agents opens up a promising strategy for reducing systemic toxicity and overcoming resistance. Recently, platinum(IV) analogues of cisplatin encapsulated in modified chitosan nanoparticles showed higher potency in cisplatin-sensitive as well as resistant lung cancer cells compared to cisplatin alone [28]. Furthermore, hydrophobically modified glycol chitosan nanocarriers loaded with cisplatin were investigated recently in in vivo studies with tumour-bearing mice. The accumulation in cancerous tissue was demonstrated with near-infrared fluorescence imaging technology, and higher tumour-inhibiting activity combined with reduced adverse effects was found in comparison to free cisplatin [29]. Reduced adverse effects compared to cisplatin were also detected in in vivo

studies by using self-assembled chitosan polymers loaded with cisplatin. Renal, hepatic and testicular cells were monitored by physiological and histopathological investigations after the application of cisplatin-loaded chitosan polymers, revealing improved conditions of the respective cells compared to the cisplatin control. Additionally, the treatment with cisplatin increased the serum levels of different liver, kidney and testicular markers, whereas the application of cisplatin–chitosan nanoparticles revealed normal levels [30]. Finally, self-assembled micelles of N-octyl-N,O-succinyl chitosan loaded with cisplatin significantly decreased cisplatin-induced apoptosis in renal cells and maintained cell viability. In addition to the reduced nephrotoxicity compared to cisplatin, the platinum(II)-loaded chitosan derivatives showed moderate anticancer activity [31].

Driven by these promising results in combination with the favourable solubility profile as well as the possibility of surface modifications and variation of molecular weights, we chose glycol chitosan as drug delivery system. We aimed to synthesise, characterise and investigate platinum(IV)-loaded degraded glycol chitosan (dGC) nanoparticles. In contrast to previously published studies using encapsulated cisplatin, platinum(IV) analogues of cisplatin, carboplatin and oxaliplatin were conjugated via amide bonds to the surface of dGC polymers with three different chain lengths. The various conjugates were characterised with NMR spectroscopy and inductively coupled plasma MS (ICP-MS). The conjugates were investigated for their cytotoxicity in different human and murine cancer cell lines, leading to a comparative in vivo study of the most promising oxaliplatin-based conjugate in comparison to its platinum(IV) analogue (Scheme 2).

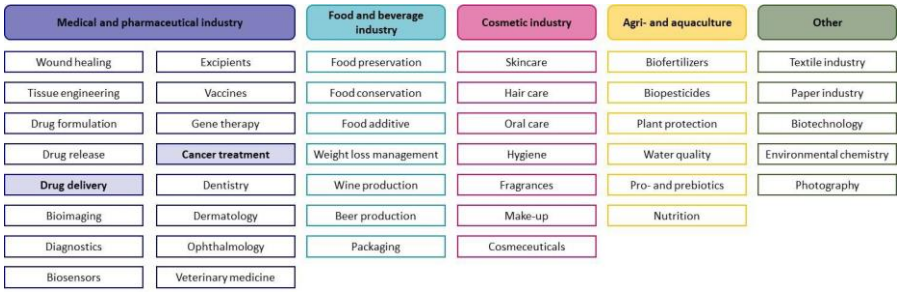

Scheme 1. Overview of different application areas of chitosan and its derivatives (not exhaustive) [22].

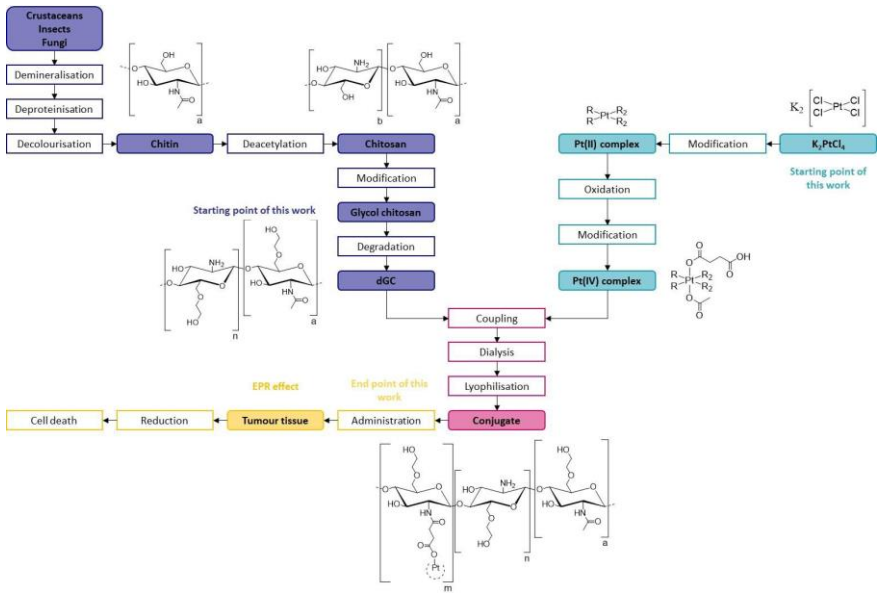

Scheme 2. Overview of process steps and delivery concept of platinum(IV)–dGC conjugates [26,32]. In the presented work, the synthesis of dGC polymers started with degradation of glycol chitosan, whereas platinum(IV) complexes were obtained by modification and oxidation of K_2PtCl_4. Additionally, in vivo studies were performed in non-tumour-bearing mice.

2. Materials and Methods

2.1. Materials

All solvents and chemicals were purchased from commercial suppliers and were used as received. The following chemicals were used without further purification for the synthesis: $K_2[PtCl_4]$ (Assay: 46.69% Pt) (Johnson Matthey, Zurich, Switzerland), glycol chitosan (Assay: 78.2%) (Wako, Osaka, Japan), succinic anhydride (≥99%) (Sigma Aldrich, Steinheim, Germany), acetic anhydride (≥97.0%) (Fisher Scientific, Schwerte, Germany), absolute DMF (99.8%, extra dry, water <50 ppm) (Acros Organics, Geel, Belgium), absolute DMSO (99.7%, extra dry, water <50 ppm) (Acros Organics, Geel, Belgium), triethylamine (99%) (Acros Organics, Geel, Belgium).

Trial Kit Spectra/Por® 3 (molecular weight cut off (MWCO) = 3.5 kDa) and Spectra/Por® 7 (MWCO = 1.0 kDa) dialysis tubing was purchased from Carl Roth (Karlsruhe, Germany). All aqueous solutions were performed with Milli-Q water (18.2 MΩ cm, Milli-Q Advantage). Reactions containing platinum complexes were conducted with glass-coated magnetic stirring bars and protected from light.

2.2. NMR Spectroscopy

NMR spectra were measured with a Bruker Avance NEO 500 MHz NMR spectrometer at 500.32 (^{1}H), 125.81 (^{13}C), 50.70 (^{15}N) and 107.55 MHz (^{195}Pt) in d_6-DMSO, d_7-DMF or D_2O at 298 K. ^{1}H and ^{13}C NMR spectra were measured relative to the solvent resonances (d_6-DMSO: δ = 2.50 ppm (^{1}H), δ = 39.51 ppm (^{13}C); d_7-DMF: δ = 2.75 ppm (high field signal) (^{1}H), δ = 29.76 ppm (high field signal) (^{13}C); D_2O: δ = 4.79 ppm (^{1}H)). $K_2[PtCl_4]$ and NH_4Cl were used as external standards for ^{195}Pt und ^{15}N NMR spectra.

2.3. RP-HPLC

An Agilent 1200 Series system equipped with a XBridge® Prep C18 10 µm OBD™ Column (19 mm × 250 mm) and an Atlantis® T3 Prep 10 µm OBD™ Column (19 mm × 250 mm) from Waters was used for preparative RP-HPLC. All runs were performed with a mixture of Milli-Q water and acetonitrile, or Milli-Q water and methanol with addition of 0.1% formic acid.

2.4. Elemental Analysis

The elemental analysis (C, H, N) of the platinum(IV) complexes was performed by the Microanalytical Laboratory of the Faculty of Chemistry of the University of Vienna with an Eurovector EA3000 elemental analyser. The obtained and calculated values are within a ±0.4% range.

2.5. Synthesis

2.5.1. Platinum(IV) Complexes

The dihydroxidoplatinum(IV) analogues of cisplatin, carboplatin and oxaliplatin were synthesised according to standard procedures [33–35]. The carboxylation of the platinum(IV) compounds was adapted from previously published synthetic pathways [13,36].

General Procedure 1: Carboxylation of Dihydroxidoplatinum(IV) Complexes with Succinic Anhydride

The corresponding dihydroxidoplatinum(IV) complex and succinic anhydride were stirred overnight in absolute DMSO under an argon atmosphere at 50 °C. The solvent was removed under reduced pressure.

1. (OC-6-44)-Diammine(3-carboxypropanoato)dichloridohydroxidoplatinum(IV) (1)

The reaction was performed according to general procedure 1, using diamminedichloridodihydroxidoplatinum(IV) (655 mg, 1.96 mmol, 1 eq), succinic anhydride (196 mg, 1.96 mmol, 1 eq) and absolute DMSO (10 mL). Yield: 845 mg (crude product used for next step).

2. (OC-6-44)-Diammine(3-carboxypropanoato)(cyclobutane-1,1-dicarboxylato) hydroxidoplatinum(IV) (3)

The reaction was performed according to general procedure 1 using diammine (cyclobutane-1,1-dicarboxylato)dihydroxidoplatinum(IV) (1.416 g, 3.49 mmol, 1 eq), succinic anhydride (349.9 mg, 3.49 mmol, 1 eq) and absolute DMSO (80 mL). Yield: 1.564 g (crude product used for next step).

3. (OC-6-44)-(3-carboxypropanoato)(1R,2R-cyclohexane-1,2-diamine) hydroxidooxalatoplatinum(IV) (5)

The reaction was performed according to general procedure 1 using (1R,2R-cyclohexane-1,2-diamine)dihydroxidooxalatoplatinum(IV) (337 mg, 0.78 mmol, 1 eq.), succinic anhydride (79 mg, 0.78 mmol, 1 eq) and absolute DMSO (50 mL). The crude product was purified by using preparative RP-HPLC (column: XBridge®, isocratic, MeOH:Milli-Q water = 5:95 + 0.1% formic acid). Yield: 217 mg (52%). ^{1}H NMR (d_6-DMSO): δ = 12.08 (b, 2H, O*H*), 8.43 (b, 1H, NH_2), 8.10 (b, 1H, NH_2), 7.82 (b, 1H, NH_2), 7.08 (b, 1H, NH_2); overlapping of the C*H* (DACH) signal with the DMSO solvent peak, 2.40–2.44 (m, 2H, CH_2, succinato), 2.34–2.39 (m, 2H, CH_2, succinato), 2.00–2.10 (m, 2H, CH_2, DACH), 1.41–1.53 (m, 3H, CH_2, DACH), 1.25–1.36 (m, 1H, CH_2, DACH), 1.08–1.15 (m, 2H, CH_2, DACH) ppm.

General Procedure 2: Introduction of the Acetato Ligand

The (3-carboxypropanoato)hydroxidoplatinum(IV) complex was suspended in absolute DMF. Acetic anhydride was added, and the reaction mixture was stirred overnight at 45 °C under an argon atmosphere. The solvent was removed, and the crude product was purified via preparative RP-HPLC. The final product was freeze-dried.

1. (OC-6-44)-Acetatodiammine(3-carboxypropanoato)dichloridoplatinum(IV) (2)

The reaction was performed according to general procedure 2 using **1** (845 mg, impure, 1.95 mmol, 1eq), acetic anhydride (1 mL, 10.6 mmol, 5.4 eq) and absolute DMF (15 mL). Preparative RP-HPLC (column: Atlantis®, isocratic, MeOH:Milli-Q water = 1:95 + 0.1% formic acid). Yield: 157 mg. ^{1}H NMR (d_6-DMSO): δ = 6.50 (b, 6H, NH_3); one of the CH_2 signals of the succinato ligand in part overlapped with the DMSO solvent peak, 2.32–2.39 (m, 2H, CH_2, succinato), 1.90 (s, 3H, CH_3) ppm. ^{13}C NMR (d_6-DMSO): δ = 179.6 (*C*=O, succinato), 178.2 (*C*=O, acetato), 173.8 (*C*=O, succinato), 30.5 (CH_2, succinato), 29.8 (CH_2, succinato), 22.8 (CH_3) ppm. ^{15}N NMR (d_6-DMSO): δ = −41.2 (NH_3) ppm. ^{195}Pt NMR (d_6-DMSO): δ = 2857 ppm. Elemental analysis: $C_6H_{14}Cl_2N_2O_6Pt \cdot H_2O$; calcd. C 14.58, H 3.26, N 5.67, found C 14.40, H 3.14, N 5.64.

2. (OC-6-44)-Acetaodiammine(3-carboxypropanoato)(cyclobutane-1,1-dicarboxylato) platinum(IV) (4)

The reaction was performed according to general procedure 2 using **3** (200 mg, 0.40 mmol, 1 eq), acetic anhydride (0.5 mL, 0.53 mmol, 1.3 eq) and absolute DMF (10 mL). Preparative RP-HPLC (column: XBridge®, isocratic, MeOH:Milli-Q water = 17:83 + 0.1% formic acid). Yield: 107 mg. ^{1}H NMR (d_7-DMF): δ = 6.76 (t, ^{1}J (^{14}N, ^{1}H) = 52.8 Hz, 6H, NH_3), 2.62 (m, 4H, CH_2-C, cyclobutyl), 2.51 (m, 2H, CH_2, succinato), 2.45 (m, 2H, CH_2, succinato), 1.89 (p, ^{3}J (^{1}H, ^{1}H = 8.0 Hz), 2H, CH_2, cyclobutyl), 1.86 (s, 3H, CH_3) ppm. ^{13}C NMR (d_7-DMF): δ = 179.8 (*C*=O, succinato), 178.3 (*C*=O, acetato), 177.0 (*C*=O, dicarboxylato), 174.1 (*C*=O, succinato), 56.5 (*C*, cyclobutyl), 32.4 (CH_2-C, cyclobutyl), 31.8 (CH_2-C, cyclobutyl), 30.7 (CH_2, succinato); one of the CH_2 signals of the succinato ligand over- lapped with the DMF solvent peak, 22.0 (CH_3), 16.2 (CH_2, cyclobutyl) ppm. ^{15}N NMR (d_7-DMF): δ = −54.3 (NH_3) ppm. ^{195}Pt NMR (d_7-DMF): δ = 3562 ppm. Elemental analysis: $C_{12}H_{20}N_2O_{10}Pt$; calcd. C 26.33, H 3.68, N 5.12, found C 25.99, H 3.46, N 5.00.

3. (OC-6-44)-Acetato(3-carboxypropanoato)(1R,2R-cyclohexane-1,2-diamine) oxalatoplatinum(IV) (6)

The reaction was performed according to general procedure 2 using **5** (217 mg, 0.41 mmol, 1 eq), acetic anhydride (0.5 mL, 0.53 mmol, 1.3 eq) and absolute DMF (10 mL). Preparative RP-HPLC (column: XBridge®, isocratic, ACN:Milli-Q water = 5:95 + 0.1% formic acid). Yield: 74 mg (32%). ^{1}H NMR (d_6-DMSO): δ = 12.11 (b, 1H, O*H*), 8.29 (m, 4H, NH_2), 2.55–2.63 (m, 2H, C*H*, DACH); one of the CH_2 signals of the succinato ligand overlapped with the DMSO solvent peak, 2.38 (m, 2H, CH_2, succinato), 2.07–2.15 (m, 2H, CH_2, DACH), 1.96 (s, 3H, CH_3), 1.33–1.56 (m, 4H, CH_2, DACH), 1.10–1.22 (m, 2H, CH_2, DACH) ppm. ^{13}C NMR (d_6-DMSO): δ = 179.6 (*C*=O, succinato), 178.6 (*C*=O, acetato), 173.7 (*C*=O, succinato), 163.41 (*C*=O, oxalato), 163.35 (C=O, oxalato), 60.9 (CH, DACH), 60.8 (CH, DACH), 30.9 (CH_2, DACH), 30.8 (CH_2, DACH), 30.5 (CH_2, succinato), 29.6 (CH_2, succinato), 23.5 (CH_2, DACH), 23.4 (CH_2, DACH), 23.0 (CH_3) ppm. ^{15}N NMR (d_6-DMSO): δ = −6.4 (NH_2) ppm. ^{195}Pt NMR (d_6-DMSO): δ = 3242 ppm. Elemental analysis: $C_{14}H_{22}N_2O_{10}Pt \cdot H_2O$; calcd. C 28.43, H 4.09, N 4.74, found C 28.46, H 3.82, N 4.92.

2.5.2. Degradation of Glycol Chitosan (dGC)

The degradation of glycol chitosan (GC) was carried out as previously reported [37]. GC polymer chains (MW~120 kDa, 20 g) were suspended in HCl (4 M, 760 mL) and stirred for 20 min at room temperature. Subsequently, the solution was degraded with continuous stirring by means of a water bath at 50 °C. In order to obtain specific molecular weights, the following three time points were chosen: 2 h (for MW~18 kDa), 8 h (for MW~10 kDa), and 24 h (for MW~5 kDa). The solution was allowed to cool down (30 min) and dialysed exhaustively against water using a dialysis membrane (MWCO = 3.5 kDa). The dialysed solution was then freeze-dried to yield a white fibrous solid. Yield = 45–80%.

2.5.3. Platinum(IV)–dGC Conjugates

General Procedure 3: Conjugation of Platinum(IV) Complex to dGC Polymer

The corresponding platinum(IV) complex was dissolved in DMSO (1 mL). CDI was added, and the mixture was stirred for about 15 min. The dGC polymer was dissolved in DMSO (1 mL) and trimethylamine (TEA). Both solutions were merged together and stirred overnight at room temperature. Two slightly different purification steps were performed:

(a) Dialysis was conducted against distilled water and 0.1 M hydrochloric acid (in each case 6 changes within 24 h). Dialysis tubing with MWCO = 1.0 kDa for **P1** and MWCO = 3.5 kDa for **P2** and **P3** was used. The product was obtained via lyophilisation and stored under an argon atmosphere at −30 °C.

(b) Dialysis was conducted against Milli-Q water (10 changes within 12 h) with dialysis tubing with MWCO = 1.0 kDa for **P1** and MWCO = 3.5 kDa for **P2** and **P3**. Afterwards the solution was adjusted to pH = 3 with hydrochloric acid and freeze-dried. The product was stored under an argon atmosphere at −30 °C.

1. Complex 2 Coupled to dGC P1 (C1)

The reaction was performed according to general procedure 3b using **2** (35 mg, 0.70 mmol, 1 eq), CDI (60 mg, 0.37 mmol, 5 eq), dGC **P1** (60 mg, 0.29 mmol, 4 eq/monomer unit) and trimethylamine (41 µL, 0.29 mmol, 4 eq). Yield: 46 mg. ICP-MS (Pt): 77.7 g/kg. ^{1}H NMR (D_2O): δ = 4.86 (b, O-C*H*-O, backbone of dGC), 3.46–4.28 (m, backbone of dGC), 3.19 (b, C*H*-NH/NH_2, backbone of dGC), 2.56–2.75 (m, CH_2, succinato), 2.12 (s, CH_3), 2.05–2.11 (m, residues of acetylated dGC monomers) ppm. ^{195}Pt NMR (D_2O): δ = 2705 ppm.

2. Complex 2 Coupled to dGC P2 (C2)

The reaction was performed according to general procedure 3a using **2** (73 mg, 0.15 mmol, 1 eq), CDI (125 mg, 0.77 mmol, 5 eq), dGC **P2** (60 mg, 0.29 mmol, 2 eq/monomer unit) and trimethylamine (76 µL, 0.55 mmol, 4 eq). Yield: 75 mg. ICP-MS (Pt): 160.4 g/kg.

^{1}H NMR (D_2O): δ = 4.87 (b, O-C*H*-O, backbone of dGC), 3.56–4.10 (m, backbone of dGC), 3.19 (b, C*H*-NH/NH_2, backbone of dGC), 2.56–2.70 (m, CH_2, succinato), 2.11 (s, CH_3), 2.04–2.10 (m, residues of acetylated dGC monomers) ppm. ^{195}Pt NMR (D_2O): δ = 2705 ppm.

3. Complex 4 Coupled to dGC P1 (C3)

The reaction was performed according to general procedure 3b using **4** (70 mg, 0.13 mmol, 1 eq), CDI (103 mg, 0.64 mmol, 5 eq), dGC **P1** (52 mg, 0.26 mmol, 2 eq/monomer unit) and trimethylamine (71 µL, 0.51 mmol, 4 eq). Yield: 97 mg. ICP-MS (Pt): 42.6 g/kg. ^{1}H NMR (D_2O): δ = 4.87 (b, O-C*H*-O, backbone of dGC), 3.46–4.14 (m, backbone of dGC), 3.19 (b, C*H*-NH/NH_2, backbone of dGC), 2.64–2.71 (m, CH_2, succinato + CH_2-C, cyclobutyl), 2.58–2.62 (m, CH_2, succinato), 2.08 (s, CH_3), 2.05–2.11 (m, residues of acetylated dGC monomers), 2.03 (m, CH_2, cyclobutyl) ppm. ^{195}Pt NMR (D_2O): δ = 3508 ppm.

4. Complex 4 Coupled to dGC P1 (C4)

The reaction was performed according to general procedure 3b using **4** (35 mg, 0.6 mmol, 1 eq), CDI (52 mg, 0.32 mmol, 5 eq), dGC **P1** (52 mg, 0.26 mmol, 4 eq/monomer unit) and trimethylamine (35 µL, 0.26 mmol, 4 eq). Yield: 51 mg. ICP-MS (Pt): 84.5 g/kg. ^{1}H NMR (D_2O): δ = 4.87 (b, O-C*H*-O, backbone of dGC), 3.57–4.11 (m, backbone of dGC), 3.19 (b, C*H*-NH/NH_2, backbone of dGC), 2.64–2.71 (m, CH_2, succinato + CH_2-C, cyclobutyl), 2.57–2.62 (m, CH_2, succinato), 2.08 (s, CH_3), 2.05–2.11 (m, residues of acetylated dGC monomers), 2.03 (m, CH_2, cyclobutyl) ppm. ^{195}Pt NMR (D_2O): δ = 3508 ppm.

5. Complex 4 Coupled to dGC P2 (C5)

The reaction was performed according to general procedure 3b using **4** (70 mg, 0.13 mmol, 1 eq), CDI (104 mg, 0.64 mmol, 5 eq), dGC **P2** (53 mg, 0.26 mmol, 2 eq/monomer unit) and trimethylamine (71 µL, 0.51 mmol, 4 eq). Yield: 88 mg. ICP-MS (Pt): 171.5 g/kg. ^{1}H NMR (D_2O): δ = 4.87 (b, O-C*H*-O, backbone of dGC), 3.47–4.19 (m, backbone of dGC), 3.18 (b, C*H*-NH/NH_2, backbone of dGC), 2.64–2.72 (m, CH_2, succinato + CH_2-C, cyclobutyl), 2.58–2.62 (m, CH_2, succinato), 2.08 (s, CH_3), 2.05–2.11 (m, residues of acetylated dGC monomers), 2.03 (m, CH_2, cyclobutyl) ppm. ^{195}Pt NMR (D_2O): δ = 3509 ppm.

6. Complex 6 Coupled to dGC P1 (C6)

The reaction was performed according to general procedure 3b using **6** (70 mg, 0.12 mmol, 1 eq), CDI (99 mg, 0.61 mmol, 5 eq), dGC **P1** (50 mg, 0.24 mmol, 2 eq/monomer unit) and TEA (68 µL, 0.49 mmol, 4 eq). Yield: 83 mg. ICP-MS (Pt): 100.3 g/kg. ^{1}H NMR (D_2O): δ = 4.87 (b, O-C*H*-O, backbone of dGC), 3.59–4.14 (m, backbone of dGC), 3.18 (b, C*H*-NH/NH_2, backbone of dGC), 2.84–2.95 (m, C*H*, DACH), 2.64–2.69 (m, CH_2, succinato), 2.59–2.64 (m, CH_2, succinato), 2.27–2.34 (m, CH_2, DACH), 2.08 (s, CH_3), 2.06–2.08 (m, residues of acetylated dGC monomers, overlapped with acetato signal), 1.53–1.70 (m, CH_2, DACH), 1.20–1.32 (m, CH_2, DACH) ppm. ^{195}Pt NMR (D_2O): δ = 3213 ppm.

7. Complex 6 Coupled to dGC P1 (C7)

The reaction was performed according to general procedure 3b using **6** (70 mg, 0.12 mmol, 1 eq), CDI (99 mg, 0.61 mmol, 5 eq), dGC **P1** (50 mg, 0.24 mmol, 2 eq/monomer unit) and TEA (68 µL, 0.49 mmol, 4 eq). Yield: 71 mg. ICP-MS (Pt): 148.1 g/kg. ^{1}H NMR (D_2O): δ = 4.87 (b, O-C*H*-O, backbone of dGC), 3.60–4.08 (m, backbone of dGC), 3.18 (b, C*H*-NH/NH_2, backbone of dGC), 2.83–2.96 (m, C*H*, DACH), 2.64–2.70 (m, CH_2, succinato), 2.59–2.63 (m, CH_2, succinato), 2.26–2.34 (m, CH_2, DACH), 2.07 (s, CH_3), 2.05–2.08 (m, residues of acetylated dGC monomers), 1.53–1.71 (m, CH_2, DACH), 1.23–1.32 (m, CH_2, DACH) ppm. ^{195}Pt NMR (D_2O): δ = 3214 ppm.

8. Complex 6 Coupled to dGC P2 (C8)

The reaction was performed according to general procedure 3a using **6** (70 mg, 0.12 mmol, 1 eq), CDI (104 mg, 0.63 mmol, 5 eq), dGC **P2** (50 mg, 0.24 mmol, 2 eq/monomer unit) and TEA (64 µL, 0.46 mmol, 4 eq). Yield: 58 mg. ICP-MS (Pt): 73.4 g/kg. ^{1}H NMR (D_2O): δ = 4.87 (b, O-C*H*-O, backbone of dGC), 3.55–4.30 (m, backbone of dGC), 3.19 (b,

C*H*-NH/NH_2, backbone of dGC), 2.83–2.98 (m, C*H*, DACH), 2.64–2.74 (m, CH_2, succinato), 2.59–2.64 (m, CH_2, succinato), 2.26–2.36 (m, CH_2, DACH), 2.08 (s, CH_3), 2.04–2.11 (m, residues of acetylated dGC monomers), 1.53–1.71 (m, CH_2, DACH), 1.20–1.32 (m, CH_2, DACH) ppm. ^{195}Pt NMR (D_2O): δ = 3213 ppm.

9. Complex 6 Coupled to dGC P2 (C9)

The reaction was performed according to general procedure 3b using **6** (70 mg, 0.12 mmol, 1 eq), CDI (99 mg, 0.61 mmol, 5 eq), **P2** (50 mg, 0.24 mmol, 2 eq/monomer unit) and TEA (68 µL, 0.49 mmol, 4 eq). Yield: 96 mg. ICP-MS (Pt): 116.5 g/kg. ^{1}H NMR (D_2O): δ = 4.87 (b, O-C*H*-O, backbone of dGC), 3.56–4.15 (m, backbone of dGC), 3.19 (b, C*H*-NH/NH_2, backbone of dGC), 2.83–2.95 (m, C*H*, DACH), 2.65–2.70 (m, CH_2, succinato), 2.59–2.64 (m, CH_2, succinato), 2.27–2.34 (m, CH_2, DACH), 2.07 (s, CH_3), 2.05–2.11 (m, residues of acetylated dGC monomers), 1.52–1.71 (m, CH_2, DACH), 1.22–1.32 (m, CH_2, DACH) ppm. ^{195}Pt NMR (D_2O): δ = 3214 ppm.

10. Complex 6 Coupled to dGC P2 (C10)

The reaction was performed according to general procedure 3b using **6** (70 mg, 0.12 mmol, 1 eq), CDI (99 mg, 0.61 mmol, 5 eq), **P2** (50 mg, 0.24 mmol, 2 eq/monomer unit) and TEA (68 µL, 0.49 mmol, 4 eq). Yield: 88 mg. ICP-MS (Pt): 150.6 g/kg. ^{1}H NMR (D_2O): δ = 4.87 (b, O-C*H*-O, backbone of dGC), 3.59–4.11 (m, backbone of dGC), 3.18 (b, C*H*-NH/NH_2, backbone of dGC), 2.84–2.95 (m, C*H*, DACH), 2.64–2.69 (m, CH_2, succinato), 2.58–2.63 (m, CH_2, succinato), 2.26–2.34 (m, CH_2, DACH), 2.08 (s, CH_3), 2.05–2.11 (m, residues of acetylated dGC monomers), 1.52–1.70 (m, CH_2, DACH), 1.23–1.32 (m, CH_2, DACH) ppm. ^{195}Pt NMR (D_2O): δ = 3214 ppm.

11. Complex 6 Coupled to dGC P2 (C11)

The reaction was performed according to general procedure 3a using **6** (70 mg, 0.12 mmol, 1 eq), CDI (103 mg, 0.63 mmol, 5 eq), **P2** (50 mg, 0.24 mmol, 2 eq/monomer unit) and TEA (64 µL, 0.46 mmol, 4 eq). Yield: 43 mg. ICP-MS (Pt): 200.3 g/kg. ^{1}H NMR (D_2O): δ = 4.87 (b, O-C*H*-O, backbone of dGC), 3.55–4.12 (m, backbone of dGC), 3.19 (b, C*H*-NH/NH_2, backbone of dGC), 2.82–2.99 (m, C*H*, DACH), 2.64–2.75 (m, CH_2, succinato), 2.58–2.64 (m, CH_2, succinato), 2.25–2.36 (m, CH_2, DACH), 2.07 (s, CH_3), 2.05–2.11 (m, residues of acetylated dGC monomers), 1.53–1.71 (m, CH_2, DACH), 1.19–1.32 (m, CH_2, DACH) ppm. ^{195}Pt NMR (D_2O): δ = 3214 ppm.

12. Complex 6 Coupled to dGC P3 (C12)

The reaction was performed according to general procedure 3b using **6** (50 mg, 0.09 mmol, 1 eq), CDI (71 mg, 0.44 mmol, 5 eq), **P3** (72 mg, 0.35 mmol, 4 eq/monomer unit) and TEA (48 µL, 0.35 mmol, 4 eq). Yield: 99 mg. ICP-MS (Pt): 102.7 g/kg. ^{1}H NMR (D_2O): δ = 4.87 (b, O-C*H*-O, backbone of dGC), 3.54–4.12 (m, backbone of dGC), 3.18 (b, C*H*-NH/NH_2, backbone of dGC), 2.84–2.95 (m, C*H*, DACH), 2.64–2.69 (m, CH_2, succinato), 2.59–2.64 (m, CH_2, succinato), 2.26–2.35 (m, CH_2, DACH), 2.08 (s, CH_3), 2.05–2.11 (m, residues of acetylated dGC monomers), 1.53–1.71 (m, CH_2, DACH), 1.21–1.33 (m, CH_2, DACH) ppm. ^{195}Pt NMR (D_2O): δ = 3213 ppm.

13. Complex 6 Coupled to dGC P1 (V1)

The reaction was performed according to general procedure 3a using **6** (71 mg, 0.12 mmol, 1 eq), CDI (41 mg, 0.25 mmol, 2 eq), dGC **P1** (50 mg, 0.24 mmol, 2 eq/monomer unit) and TEA (64 µL, 0.46 mmol, 4 eq). Yield: 43 mg. ICP-MS (Pt): 46.5 g/kg. ^{1}H NMR (D_2O): δ = 4.85 (b, O-C*H*-O, backbone of dGC), 3.55–4.12 (m, backbone of dGC), 3.18 (b, C*H*-NH/NH_2, backbone of dGC), 2.85–2.96 (m, C*H*, DACH), 2.37–2.75 (m, CH_2, succinato), 2.27–2.36 (m, CH_2, DACH), 2.08 (b, CH_3), 2.03–2.15 (m, residues of acetylated dGC monomers), 1.55–1.69 (m, CH_2, DACH), 1.12–1.40 (m, CH_2, DACH) ppm.

14. Complex 6 Coupled to dGC P2 (V2)

The reaction was performed according to general procedure 3a using **6** (72 mg, 0.13 mmol, 1 eq), CDI (41 mg, 0.25 mmol, 2 eq), dGC **P2** (50 mg, 0.24 mmol, 2 eq/monomer unit) and TEA (64 µL, 0.46 mmol, 4 eq). Yield: 39 mg. ICP-MS (Pt): 65.1 g/kg. ^{1}H NMR (D_2O): δ = 4.84 (b, O-C*H*-O, backbone of dGC), 3.54–4.13 (m, backbone of dGC), 3.17 (b, C*H*-NH/NH_2, backbone of dGC), 2.86–2.97 (m, C*H*, DACH), 2.44–2.74 (m, CH_2, succinato), 2.26–2.34 (m, CH_2, DACH), 2.08 (b, CH_3), 2.02–2.15 (m, residues of acetylated dGC monomers), 1.53–1.71 (m, CH_2, DACH), 1.13–1.39 (m, CH_2, DACH) ppm.

15. Complex 6 Coupled to dGC P3 (V3)

The reaction was performed according to general procedure 3a using **6** (70 mg, 0.12 mmol, 1 eq), CDI (41 mg, 0.25 mmol, 2 eq), dGC **P3** (50 mg, 0.24 mmol, 2 eq/monomer unit) and TEA (64 µL, 0.46 mmol, 4 eq). Yield: 38 mg. ICP-MS (Pt): 67.4 g/kg. ^{1}H NMR (D_2O): δ = 4.86 (b, O-C*H*-O, backbone of dGC), 3.52–4.12 (m, backbone of dGC), 3.18 (b, C*H*-NH/NH_2, backbone of dGC), 2.86–2.97 (m, C*H*, DACH), 2.50–2.70 (m, CH_2, succinato), 2.22–2.26 (m, CH_2, DACH), 2.09 (b, CH_3), 2.03–2.15 (m, residues of acetylated dGC monomers), 1.57–1.66 (m, CH_2, DACH), 1.13–1.39 (m, CH_2, DACH) ppm.

16. Complex 2 Coupled to dGC P3 (S1)

The reaction was performed according to general procedure 3a using **2** (55 mg, 0.11 mmol, 1 eq), CDI (98 mg, 0.60 mmol, 5 eq), dGC **P3** (47 mg, 0.23 mmol, 2 eq/monomer unit) and trimethylamine (64 µL, 0.46 mmol, 4 eq). Yield: 51 mg. ICP-MS (Pt): 88.7 g/kg. ^{1}H NMR (D_2O): δ = 3.50–4.10 (m, backbone of dGC), 3.14 (b, C*H*-NH/NH_2, backbone of dGC), 2.56–2.75 (m, CH_2, succinato), 2.08 (s, CH_3), 1.99–2.07 (m, residues of acetylated dGC monomers) ppm.

17. Complex 2 Coupled to dGC P3 (S2)

The reaction was performed according to general procedure 3b using **2** (70 mg, 0.15 mmol, 1 eq), CDI (119 mg, 0.74 mmol, 5 eq), dGC **P3** (60 mg, 0.29 mmol, 2 eq/monomer unit) and trimethylamine (82 µL, 0.59 mmol, 4 eq). Yield: 35 mg. ICP-MS (Pt): 117.8 g/kg. ^{1}H NMR (D_2O): δ = 3.53–4.11 (m, backbone of dGC), 3.18 (b, C*H*-NH/NH_2, backbone of dGC), 2.70–2.76 (m, CH_2, succinato), 2.58–2.62 (m, CH_2, succinato), 2.12 (s, CH_3), 2.04–2.11 (m, residues of acetylated dGC monomers) ppm. ^{195}Pt NMR (D_2O): δ = 2705 ppm.

18. Complex 4 Coupled to dGC P3 (S3)

The reaction was performed according to general procedure 3b using **4** (150 mg, 0.30 mmol, 1 eq), CDI (240 mg, 1.48 mmol, 5 eq), dGC **P3** (122 mg, 0.59 mmol, 2 eq/monomer unit) and trimethylamine (165 µL, 1.19 mmol, 4 eq). Yield: 80 mg. ICP-MS (Pt): 91.9 g/kg. ^{1}H NMR (D_2O): δ = 3.54–4.01 (m, backbone of dGC), 3.10 (b, C*H*-NH/NH_2, backbone of dGC), 2.45–2.72 (m, CH_2, succinato + CH_2-C, cyclobutyl), 2.03 (m, CH_2, cyclobutyl) 2.00 (s, CH_3), 1.93–2.09 (m, residues of acetylated dGC monomers) ppm.

19. Complex 4 Coupled to dGC P3 (S4)

The reaction was performed according to general procedure 3b using **4** (50 mg, 0.09 mmol, 1 eq), CDI (74 mg, 0.46 mmol, 5 eq), dGC **P3** (75 mg, 0.037 mmol, 4 eq/monomer unit) and trimethylamine (51 µL, 0.37 mmol, 4 eq). Yield: 92 mg. ICP-MS (Pt): 109.5 g/kg. ^{1}H NMR (D_2O): δ = 3.55–4.10 (m, backbone of dGC), 3.19 (b, C*H*-NH/NH_2, backbone of dGC), 2.63–2.72 (m, CH_2, succinato + CH_2-C, cyclobutyl), 2.57–2.62 (m, CH_2, succinato), 2.07 (s, CH_3), 2.03 (m, CH_2, cyclobutyl), 2.00–2.11 (m, residues of acetylated dGC monomers) ppm. ^{195}Pt NMR (D_2O): δ = 3508 ppm.

20. Complex 6 Coupled to dGC P3 (S5)

The reaction was performed according to general procedure 3b using **6** (71 mg, 0.12 mmol, 1 eq), CDI (99 mg, 0.61 mmol, 5 eq), **P3** (50 mg, 0.24 mmol, 2 eq/monomer unit) and TEA (68 µL, 0.49 mmol, 4 eq). Yield: 71 mg. ICP-MS (Pt): 88.7 g/kg. ^{1}H NMR (D_2O): δ = 4.87 (b, O-C*H*-O, backbone of dGC), 3.52–4.15 (m, backbone of dGC), 3.19 (b,

C*H*-NH/NH_2, backbone of dGC), 2.84–2.96 (m, C*H*, DACH), 2.64–2.69 (m, CH_2, succinato), 2.59–2.64 (m, CH_2, succinato), 2.27–2.34 (m, CH_2, DACH), 2.08 (s, CH_3), 2.04–2.12 (m, residues of acetylated dGC monomers), 1.54–1.70 (m, CH_2, DACH), 1.21–1.33 (m, CH_2, DACH) ppm. ^{195}Pt NMR (D_2O): δ = 3214 ppm.

2.6. ICP-MS

Platinum(IV)–dGC conjugates (0.5–1.5 mg) were digested in 2 mL of HNO_3 (20%) and 0.1 mL of H_2O_2 (30%) with a temperature-controlled heating plate of graphite from Labter. Afterwards the samples were diluted (1:10,000) with HNO_3 (3%), and the total platinum concentration was detected with an Agilent 7800 ICP-MS instrument using rhenium as an internal reference. An Agilent SPS 4 autosampler was used to carry out 10 replicates for each sample, and the data were evaluated with the Agilent MassHunter software.

2.7. Cell Culture

Cell culture of the cell lines CH1/PA-1, SW480 and A549 was performed as described in reference [38]. 4T1 cells were purchased from American Type Culture Collection, stored in a liquid nitrogen dewar and cultured in Roswell Park Memorial Institute (RPMI)-1640 medium supplemented with 10% foetal bovine serum (FBS) (Thermo Fisher, Waltham, MA, USA).

2.8. Cytotoxicity

Cytotoxicity tests (96 h incubation) in the cell lines CH1/PA-1, SW480 and A549 were conducted as described in reference [38]. Compounds were dissolved in supplemented minimum essential medium (MEM), except for compound **C10,** which was dissolved in sterile Milli-Q water.

To seed 4T1 cells at a density of 1×10^4 cells per well, 96-well plates were used. 4T1 cells were incubated at 37 °C in 5% CO_2, 95% in air for 24 h in Roswell Park Memorial Institute (RPMI)-1640 medium supplemented with 10% foetal bovine serum (FBS). Just before treatment, the medium was removed, and the cells were washed twice with phosphate buffered saline (PBS, pH = 7.4). Conjugates **V1**, **V2** and **V3** (1 mg/mL) were suspended in Hank's Balanced Salt Solution (HBSS) and 200 µL volume was dispensed into each well and left for 2 h. HBSS was used as the negative control, while a 1% Triton X-100 solution in PBS was used as the positive control. The treatment was subsequently removed by pipetting and the cells were washed twice with PBS. A stock solution of the MTT reagent (5 mg/mL) was prepared by suspending in PBS, after which a 0.5 mg/mL working solution was prepared from the stock; then, 200 µL of the working solution was transferred into each well, and the plate was incubated until the formed purple formazan crystals could be detected by means of a microscope (typically 2 h). The MTT reagent was subsequently removed from the wells by pipetting, and the crystals were dissolved by adding 200 µL of DMSO to each well and shaking on an orbital shaker for 15 min, protected from light. The plates were subsequently read on an UV spectrophotometer at a wavelength of 570 nm. Cell viability was further determined as a percentage of the negative control (HBSS).

2.9. Biodistribution Study: 1 h and 24 h

The Animal Welfare and Ethical Review Body at University College London (UCL) authorised all animal experiments, which were performed under license from the Home Office, UK. All animals were kept in a pathogen-free environment and treated in accordance with the Institutional Committees on Animal Welfare of the U.K. Home Office (the Home Office Animals Scientific Procedures Act, 1986). Biodistribution studies on a platinum-loaded polymer **V3** compared to the platinum(IV) complex **6** were carried out, using female Balb/C mice (20–22.5 g) (Harlan, UK) divided into 2 time points (t_1 = 1 h, t_2 = 24 h, 4 groups n = 5). The used concentrations of 0.41 mg/100 µL for compound **V3** and 0.15 mg/100 µL for complex **6** are equivalent to 2.75 mg/kg oxaliplatin and 5.5 mg/kg, respectively. All substances were applied intravenously (100 µL stock/20 g body weight) via tail vein

injection. At the chosen time points, animals were culled with CO_2, and the major organs (lung, heart, liver, spleen and kidneys) were collected and frozen in liquid nitrogen. The samples were transferred to the Institute of Inorganic Chemistry, University of Vienna, Austria, where the total platinum content of each sample was determined with an Agilent 7500 ICP-quadrupole MS instrument.

3. Results and Discussion

3.1. Synthesis

Previously published synthetic routes served as a template and were modified for the synthesis of platinum(IV) complexes **1–6** with a mixed axial ligand sphere (Scheme 3) [13,36].

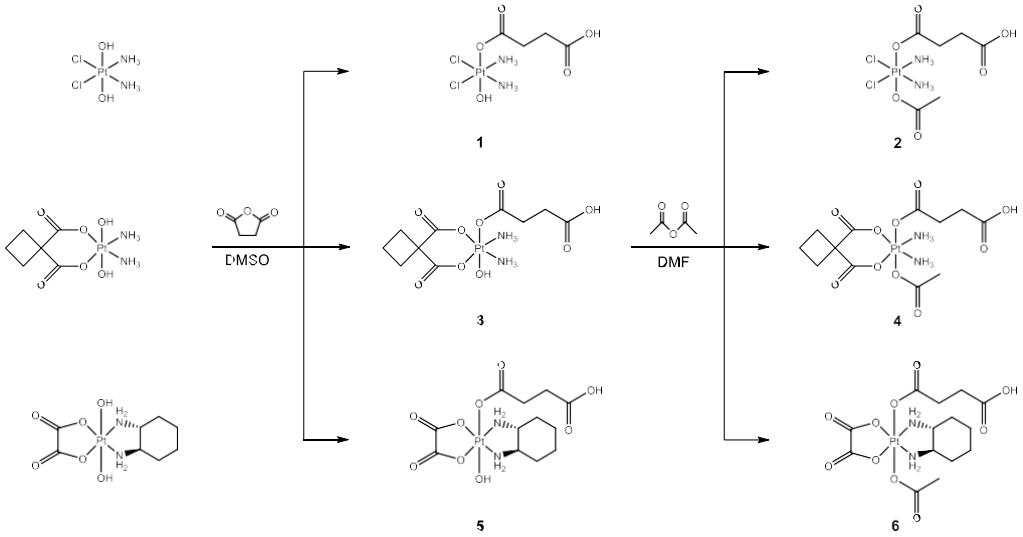

Scheme 3. Synthetic pathway for platinum(IV) complexes **1–6** with mixed axial ligands and a free carboxylic acid group to enable the introduction of drug delivery platforms.

Starting from the corresponding dihydroxidoplatinum(IV) complex, compounds **1**, **3**, and **5** were synthesised via carboxylation with succinic anhydride in absolute DMSO. Afterwards, the addition of acetic anhydride in absolute DMF and purification by preparative RP-HPLC resulted in the final products **2**, **4**, and **6**.

Glycol chitosan polymer chains (MW~120 kDa) were degraded by using hydrochloric acid followed by time-dependent incubation at 50 °C. As longer degradation times lead to shorter chain lengths, the following three time points were chosen: 2, 8, and 24 h to obtain MW~18 kDa (**P3**), MW~10 kDa (**P2**), and MW~5 kDa (**P1**), respectively. Afterwards, the solutions were freeze-dried to yield white fibrous solids (Scheme 4).

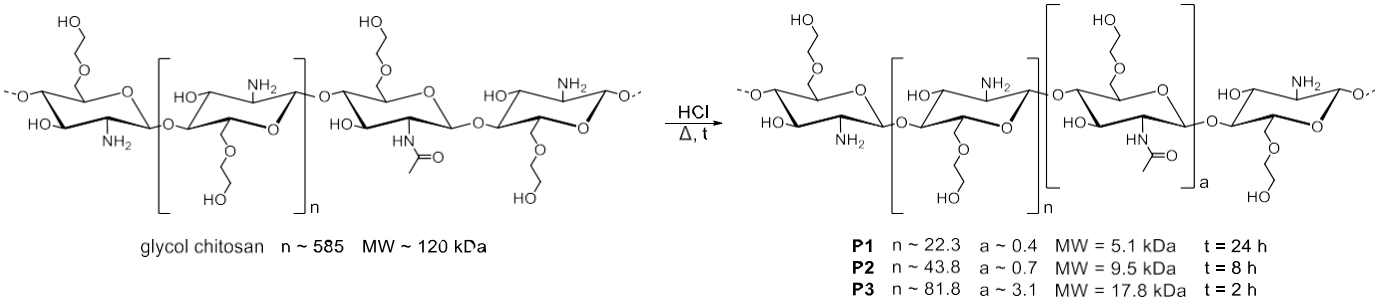

Scheme 4. Time-dependent acidic degradation of glycol chitosan results in dGC polymers with different molecular weights (MW) **P1–P3**. The remaining degree of acetylation was determined with ^{1}H NMR spectroscopy and was detected as about 1% for **P1**, 2% for **P2**, and 4% for **P3**.

In particular, unsymmetrically carboxylated platinum(IV) complexes are in accordance with an optimised reduction potential preventing premature reduction to the corresponding platinum(II) species [39]. The free carboxylic acid group of complexes **2**, **4**, and **6** in axial position enables the attachment to the primary amine of the dGC polymer via amide bond formation. The coupling reaction was thereby performed in the presence of the peptide coupling reagent 1,1′-carbonyldiimidazole (CDI). First, the carboxylic acid moiety of compound **2**, **4**, or **6** was activated with CDI, resulting in the reactive imidazolide. In parallel, CO_2 and imidazole were released. Afterwards, the activated carboxylic acid was brought to reaction with the NH_2 moiety of the dGC polymers, leading to amide bond formation [40,41]. Afterwards, the conjugates (**C1–C12**, **S1–S5**, **V1–V3**) were purified via dialysis against distilled water and 0.1 M hydrochloric acid, in succession, in order to remove unreacted CDI, uncoupled platinum(IV) complexes and imidazole. Finally, the conjugates were freeze-dried and obtained as whitish fibrous solids (Scheme 5).

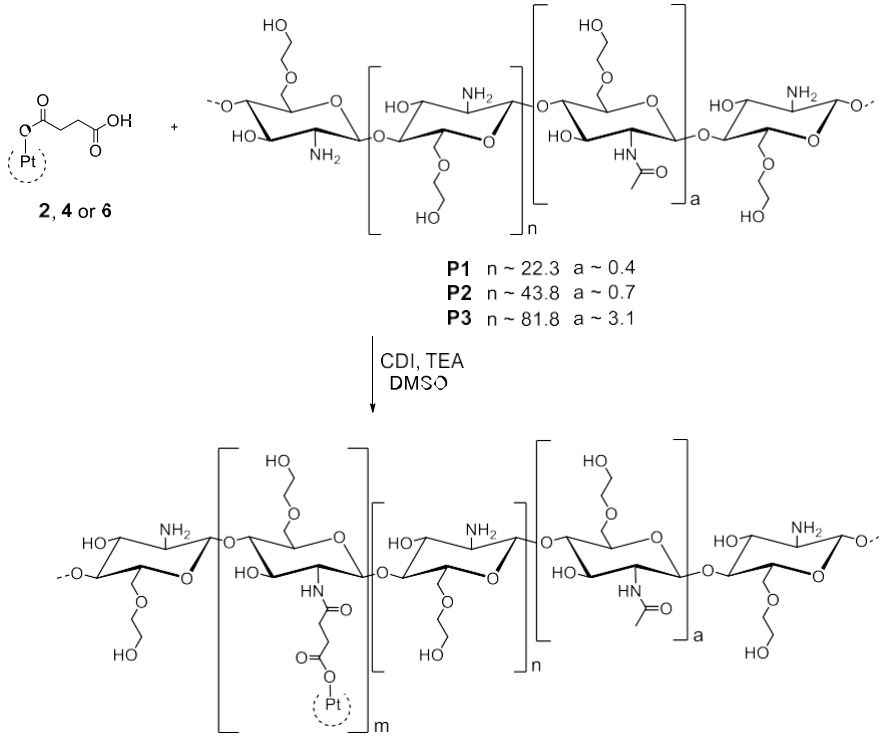

C1	m ~ 2.5	n ~ 19.9	a ~ 0.4	Pt(IV) = **2**	dGC = **P1**
C2	m ~ 12.6	n ~ 31.2	a ~ 0.7	Pt(IV) = **2**	dGC = **P2**
C3	m ~ 1.3	n ~ 21.1	a ~ 0.4	Pt(IV) = **4**	dGC = **P1**
C4	m ~ 2.9	n ~ 19.5	a ~ 0.4	Pt(IV) = **4**	dGC = **P1**
C5	m ~ 15.7	n ~ 28.1	a ~ 0.7	Pt(IV) = **4**	dGC = **P2**
C6	m ~ 3.7	n ~ 18.7	a ~ 0.4	Pt(IV) = **6**	dGC = **P1**
C7	m ~ 6.7	n ~ 15.7	a ~ 0.4	Pt(IV) = **6**	dGC = **P1**
C8	m ~ 4.5	n ~ 39.3	a ~ 0.7	Pt(IV) = **6**	dGC = **P2**
C9	m ~ 8.5	n ~ 35.3	a ~ 0.7	Pt(IV) = **6**	dGC = **P2**
C10	m ~ 12.9	n ~ 30.9	a ~ 0.7	Pt(IV) = **6**	dGC = **P2**
C11	m ~ 22.8	n ~ 21.0	a ~ 0.7	Pt(IV) = **6**	dGC = **P2**
C12	m ~ 13.3	n ~ 68.5	a ~ 3.1	Pt(IV) = **6**	dGC = **P3**
S1	m ~ 10.3	n ~ 71.5	a ~ 3.1	Pt(IV) = **2**	dGC = **P3**
S2	m ~ 14.9	n ~ 66.9	a ~ 3.1	Pt(IV) = **2**	dGC = **P3**
S3	m ~ 11.2	n ~ 70.6	a ~ 3.1	Pt(IV) = **4**	dGC = **P3**
S4	m ~ 14.2	n ~ 67.6	a ~ 3.1	Pt(IV) = **4**	dGC = **P3**
S5	m ~ 10.9	n ~ 70.9	a ~ 3.1	Pt(IV) = **6**	dGC = **P3**
V1	m ~ 1.4	n ~ 20.9	a ~ 0.4	Pt(IV) = **6**	dGC = **P1**
V2	m ~ 3.9	n ~ 39.9	a ~ 0.7	Pt(IV) = **6**	dGC = **P2**
V3	m ~ 7.6	n ~ 74.2	a ~ 3.1	Pt(IV) = **6**	dGC = **P3**

Scheme 5. Scheme of CDI coupling reaction of the unsymmetric platinum(IV) complexes and dGC polymers, yielding 20 conjugates with a platinum(IV) to dGC polymer ratio between 1.3 and 22.8.

In addition to CDI, varying coupling reagents as well as different solvents and complex to polymer ratios were evaluated. Overall, the best results were observed in DMSO with maximum 0.5 equivalents of the corresponding CDI-activated platinum(IV) complex. The complex:polymer ratio of a maximum of 1:2 is crucial for the solubility, especially with the longest dGC polymer **P3**. In addition to conjugate **C12**, another conjugation of complex **6** and dGC polymer **P3** (**S5**) as well as the coupling of complex **2** and **4** to **P3** were successfully performed (**S1–S4**) with complex:polymer ratios of 1:2 and 1:4, respectively. Based on the best solubility, a series of conjugates (**V1–V3**) with oxaliplatin(IV) analogue **6** and all three dGC batches (**P1–P3**) were synthesised de novo for subsequent in vivo experiments. In addition to lower complex to polymer ratios, acidic conditions before freeze-drying affected the solubility. As a result of the change from distilled water to 0.1 M hydrochloric acid at the end of the dialysis process, the adjustment to pH 3 significantly improved the solubility of the product, possibly due to the formation of amine salts. Finally, a continuous decline of solubility was detected by conjugates over time. However, the solubility loss could be substantially decelerated by storage of the conjugates under an argon atmosphere at −30 °C.

3.2. Analysis

The final platinum(IV) complexes **2**, **4**, and **6** were characterised with one- and two-dimensional NMR spectroscopy (^{1}H, ^{13}C, ^{15}N, ^{195}Pt) (Supporting Information, Figures S1–S9), and their purity (>95%) was confirmed by elemental analysis.

The molecular weight of the different dGC batches **P1–P3** was determined by gel permeation chromatography with multi-angle laser light scattering (GPC-MALLS); the results are presented in Table 1. Additionally, one representative NMR spectrum of the dGC polymer can be found in the Supporting Information (Figure S10).

Table 1. Overview of the different molecular weights of the dGC polymers **P1–P3**.

dGC Batch	Degradation Time (h)	MW (kDa)
P1	24	5.074
P2	8	9.539
P3	2	17.830

The characterisation of the conjugates **C1–C12** was performed with ^{1}H and ^{195}Pt NMR spectroscopy, proving the presence of the corresponding platinum(IV) complexes (Supporting Information, Figures S13–S18). The ^{195}Pt NMR spectra showed characteristic signals for platinum(IV) species between 2700 and 3500 ppm. Especially, the superimposition of the ^{1}H NMR spectra of the platinum(IV) analogue of oxaliplatin **6** and the unloaded dGC polymer highlights the additional peaks in the upfield region between 1.0 and 3.0 ppm of the NMR spectra of the corresponding conjugates (Supporting Information, Figure S17).

The average levels of platinum(IV) complexes per dGC polymer for all conjugates were determined by means of inductively coupled plasma MS (ICP-MS) and were in the range of 5.4% to 49.8%, equivalent to 1.3–22.8 platinum(IV) units per polymer molecule. The obtained platinum(IV) units per dGC polymer molecule were used for the calculation of the molecular weight of all conjugates (Table 2), and the amount of platinum(IV) units affected the solubility. In general, lower platinum(IV) loading levels, and the resulting smaller molecular weights resulted in better solubility. This relationship is particularly distinct for conjugates with the same dGC polymer, platinum(IV) complex and molecular weights ~15 kDa. Conjugates with molecular weights ~20 kDa, mainly achieved with **P3**, showed the lowest solubility of all conjugates. Additionally, solubility differences between conjugates containing different dGC polymers and platinum(IV) complexes were identified in the following order, starting with the best solubility: **P1** > **P2** > **P3** and **6** > **4** > **2** (Supporting Information, Table S1).

Table 2. Overview of the platinum(IV) units per dGC polymer molecule and average loading levels of conjugates **C1–C12**, **S1–S5**, **V1–V3**.

Sample	Pt (IV) Precursor	dGC	Monomer Units *	Pt Loading [%] **	MW [kDa] Unloaded	MW [kDa] Loaded
C1	**2**	**P1**	24.3	10.3	5.1	6.6
C2	**2**	**P2**	45.8	27.5	9.5	15.7
C3	**4**	**P1**	24.3	5.4	5.1	6.2
C4	**4**	**P1**	24.3	11.9	5.1	7.0
C5	**4**	**P2**	45.8	34.3	9.5	18.3
C6	**6**	**P1**	24.3	15.2	5.1	7.5
C7	**6**	**P1**	24.3	27.6	5.1	9.2
C8	**6**	**P2**	45.8	9.8	9.5	12.5
C9	**6**	**P2**	45.8	18.6	9.5	14.7
C10	**6**	**P2**	45.8	28.2	9.5	17.1
C11	**6**	**P2**	45.8	49.8	9.5	22.6
C12	**6**	**P3**	83.8	15.9	17.8	25.6
S1	**2**	**P3**	83.8	12.3	17.8	22.9
S2	**2**	**P3**	83.8	17.8	17.8	25.1
S3	**4**	**P3**	83.8	13.4	17.8	24.2
S4	**4**	**P3**	83.8	16.9	17.8	25.8
S5	**6**	**P3**	83.8	13.0	17.8	24.3
V1	**6**	**P1**	24.3	5.8	5.1	6.3
V2	**6**	**P2**	45.8	8.5	9.5	12.1
V3	**6**	**P3**	83.8	9.1	17.8	22.5

* Amount of monomer units without acetylated monomer units. ** Referred to monomer units without acetylation.

3.3. Cytotoxicity

Based on the required solubility, conjugates **C1–C12** were forwarded for cytotoxicity assessments, whereas conjugates **S1–S5** could not be tested due to solubility issues (Supporting Information, Table S1). The twelve substances **C1–C12** were examined in comparison to the free platinum(IV) complexes and the unloaded dGC polymers with three different chain lengths for their cytotoxic activity in vitro. For this purpose, the colorimetric MTT assay was used in three human cancer cell lines (A549 (non-small-cell lung carcinoma), CH1/PA-1 (ovarian teratocarcinoma) and SW480 (colon adenocarcinoma)), yielding IC_{50} values in the low micromolar to nanomolar concentration range for all conjugates (Table 3, Supporting Information, Figures S18–S20). The three tested cell lines differ in their platinum sensitivity. SW480 and A549 cells are intrinsically cisplatin- and carboplatin-resistant due to their low expression of CTR1, whereas CH1/PA-1 cells show high chemosensitivity, particularly to platinum drugs [42,43].

In general, platinum(IV) complexes exert even slower biological effects than their platinum(II) analogues; consequently, complexes **2**, **4**, and **6** exhibited lower cytotoxic potencies than their platinum(II) counterparts. The dGC polymers **P1**, **P2**, and **P3** showed negligible cytotoxicity within 96 h, with IC_{50} values higher than 100 µM, with the exception of **P3,** displaying an IC_{50} value of 77 ± 25 µM in CH1/PA-1 cells.

On the contrary, conjugates (**C1–C12**) revealed different antiproliferative activities in the three tested cell lines, exhibiting the highest activity against the commonly most sensitive cell line CH1/PA-1, moderate activity in the cell line SW480, and the lowest activity in the intrinsically more chemoresistant A549 cell line (Figure 1).

Remarkably, the most potent conjugate **C2**, with IC_{50} values of 0.036 ± 0.005 µM (CH1/PA-1), 1.9 ± 0.5 µM (A549) and 0.65 ± 0.07 µM (SW480), was two times more active in CH1/PA-1 and A549 cells and three-and-a-half times more active in the cell line SW480 than its platinum(II) counterpart cisplatin. Compared with the corresponding platinum(IV) complex **2**, **C2** demonstrated an enormous increase in cytotoxicity by factors of 33 (CH1/PA-1), 52 (A549) and 72 (SW480), based on IC_{50} values. The second most cytotoxic compound was **C11**, containing the highest loading with platinum(IV) units

(22.8 per polymer) of all examined conjugates. In contrast to **C2**, **C11** did not reveal a higher antiproliferative effect than the platinum(II) counterpart (oxaliplatin). However, it displayed significantly enhanced cytotoxicity compared to the corresponding platinum(IV) complex **6** by factors of 22 (CH1/PA-1), 25 (SW480), and 41 (A549). Conjugate **C3** yielded the lowest antiproliferative activity of all conjugates, in line with the overall highest IC_{50} value of carboplatin(IV) analogue **4** and lowest loading with platinum(IV) units (1.3 per polymer molecule).

Within the set of all dGC polymers bearing platinum(IV) complexes, cisplatin(IV)-containing conjugates **C1** and **C2** were more favourable in terms of antiproliferative activity, correlating very well with the high cytotoxicity of cisplatin. **C1** appeared less potent, containing five times less platinum(IV) units than **C2**, which revealed the highest cytotoxic potency of all conjugates. Both, **C1** and **C2** showed higher antiproliferative activity in all tested cell lines than their platinum(IV) analogue **2**.

The conjugate group of carboplatin(IV) derivatives **C3–C5** featured the highest IC_{50} values, consistent with the low cytotoxicity of carboplatin(IV) complex **4**. **C3** and **C4**, both coupled to **P1**, differ in their amount of conjugated platinum(IV) units, demonstrating a clear correlation with cytotoxicity. Expectedly, the higher platinum(IV) loading of **C4** resulted in lower IC_{50} values compared to **C3**. Otherwise, **C5** exhibited the lowest IC_{50} values in CH1/PA-1 and SW480 cells within this group of conjugates, likely correlated with a higher platinum(IV) loading level. Collectively, all three conjugates **C3–C5** revealed enhanced antiproliferative activity compared to the corresponding platinum(IV) complex **4**.

Table 3. IC_{50} values of conjugates **C1–C12** in comparison to platinum(II) and free platinum(IV) complexes (**2**, **4**, **6**) as well as to unloaded dGC polymers (**P1–P3**) in the human cancer cell lines A549, CH1/PA-1 and SW480.

Sample	Pt(IV)	dGC	Pt(IV) Units per Polymer	IC_{50} [µM] A549	IC_{50} [µM] CH1/PA-1	IC_{50} [µM] SW480
Cisplatin [38]	-		-	3.8 ± 1.0	0.073 ± 0.001	2.3 ± 0.2
Carboplatin [38]	-		-	38 ± 3	0.79 ± 0.11	42 ± 10
Oxaliplatin [38]	-		-	0.98 ± 0.21	0.18 ± 0.01	0.29 ± 0.05
2	**2**		-	99 ± 17	1.2 ± 0.5	47 ± 10
4	**4**		-	>200	16 ± 6	>200
6	**6**		-	70 ± 29	4.1 ± 0.6	22 ± 8
P1	-	**P1**	-	>190	>100	>190
P2	-	**P2**	-	>180	>180	>180
P3	-	**P3**	-	>230	77 ± 25	205 ± 16
C1	**2**	**P1**	2.5	9.6 ± 0.7	0.32 ± 0.09	5.5 ± 1.1
C2	**2**	**P2**	12.6	1.9 ± 0.5	0.036 ± 0.005	0.65 ± 0.07
C3	**4**	**P1**	1.3	>90	4.0 ± 1.5	66 ± 21
C4	**4**	**P1**	2.9	35 ± 9	2.9 ± 0.4	35 ± 5
C5	**4**	**P2**	15.7	45 ± 9	1.5 ± 0.4	16 ± 5
C6	**6**	**P1**	3.7	7.1 ± 1.4	0.78 ± 0.11	1.9 ± 0.2
C7	**6**	**P1**	6.7	4.4 ± 0.5	0.54 ± 0.08	1.5 ± 0.1
C8	**6**	**P2**	4.5	4.4 ± 0.4	0.38 ± 0.08	1.7 ± 0.2
C9	**6**	**P2**	8.5	3.2 ± 0.5	0.33 ± 0.08	0.97 ± 0.06
C10	**6**	**P2**	12.9	2.6 ± 0.4	0.27 ± 0.02	0.80 ± 0.08
C11	**6**	**P2**	22.8	1.7 ± 0.4	0.18 ± 0.02	0.86 ± 0.11
C12	**6**	**P3**	13.3	2.1 ± 0.3	0.26 ± 0.02	0.64 ± 0.07

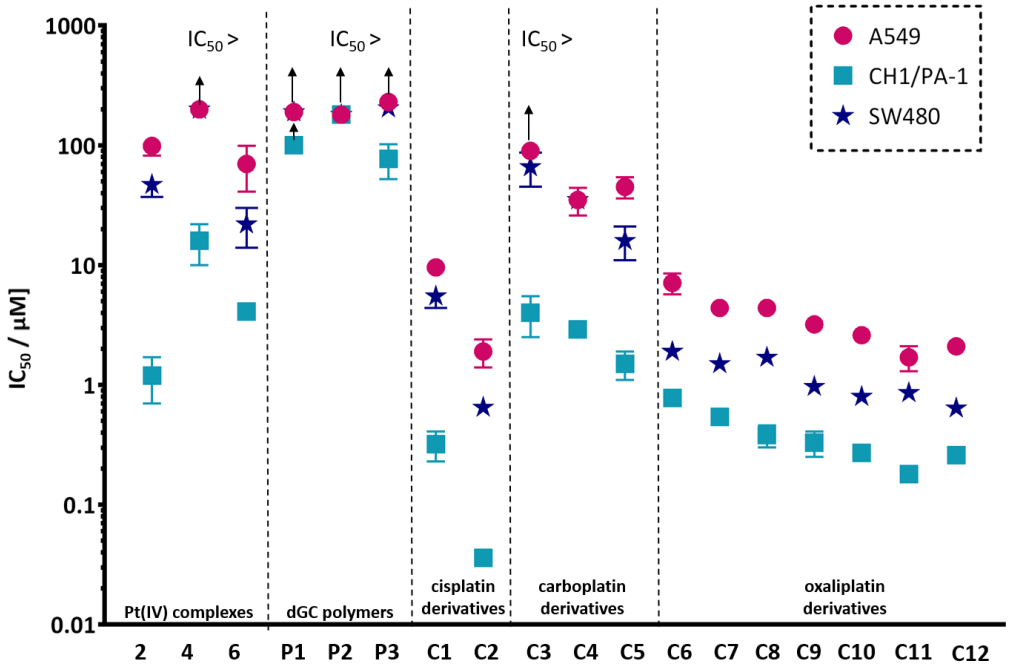

Figure 1. Structure–activity relationship of the studied platinum(IV) complexes, dGC polymers and conjugates. The y-axis represents IC_{50} values (means ± standard deviations) in all three cell lines on a logarithmic scale. The arrows indicate IC_{50} values higher than the indicated value.

Compounds **C6–C12**, featuring oxaliplatin analogues in the oxidation state IV, covered a wide cytotoxic activity span, with IC_{50} values ranging from 0.18 µM to 7.1 µM. The above-mentioned correlation, based on the number of coordinated platinum(IV) units leading to higher cytotoxicity, was further observed within groups of the same chain lengths. Accordingly, **C7** displayed advantageously lower IC_{50} values in all cell lines than **C6**. The dGC polymer **P2,** containing series **C8–C11,** showed different amounts of platinum(IV) units, ranging from 4.5 to 22.8 per polymer molecule, showing again a pronounced dependency of cytotoxicity on the number of platinum(IV) units. Therefore, **C8** exhibited the lowest, whereas **C11** displayed the highest antiproliferative activity in all cell lines. The only exception to this pattern was observed for **C11**, with a higher IC_{50} value in SW480 cells. Due to low solubility of conjugate **S5**, **C12** was the only tested compound based on dGC polymer **P3**, and it revealed one of the highest antiproliferative effects. **C10** and **C12**, with a negligible difference in amount of platinum(IV) units and thus mainly differing in the polymer carrier, revealed comparable IC_{50} values in each and every cell line. On the contrary, the correlation of platinum(IV) loading and higher cytotoxicity was not as pronounced for conjugates with different dGC batches, such as **C7** and **C8**. Consequently, the polymer chain length has a minor effect on the cytotoxic activity.

Additionally, the correlation between IC_{50} values and platinum(IV) load of oxaliplatin derivatives (**C6–C12**) was studied and is shown in Figure 2. In all three cell lines, the same trend could be observed: the higher the platinum(IV) load, the lower the IC_{50} value of the tested conjugates. An unpaired *t*-test with Welch's correction was performed between the most (**C11**) and the least (**C6**) cytotoxic complexes, revealing significant differences, with $p < 0.05$ (A549), $p < 0.01$ (CH1/PA-1) and $p < 0.01$ (SW480).

In order to further investigate the influence of conjugation on the cytotoxicity, the concentration levels of the corresponding platinum(IV) units at the IC_{50} value of conjugates **C1–C12** and **V1–V3** were calculated (Table 4). The comparison of the normalised IC_{50} values with the IC_{50} values of the uncoupled platinum(IV) complexes **2**, **4**, **6** displayed an evident increase in cytotoxicity through conjugation. This connection could be observed for all conjugates except for **C5** in all cell lines. Depending on the coupled platinum(IV)

complex and the cell line, the factors for increased cytotoxicity varied between 1.0 and 5.7, following the trend **4** < **6** < **2** and CH1/PA-1 < A549 ≈ SW480.

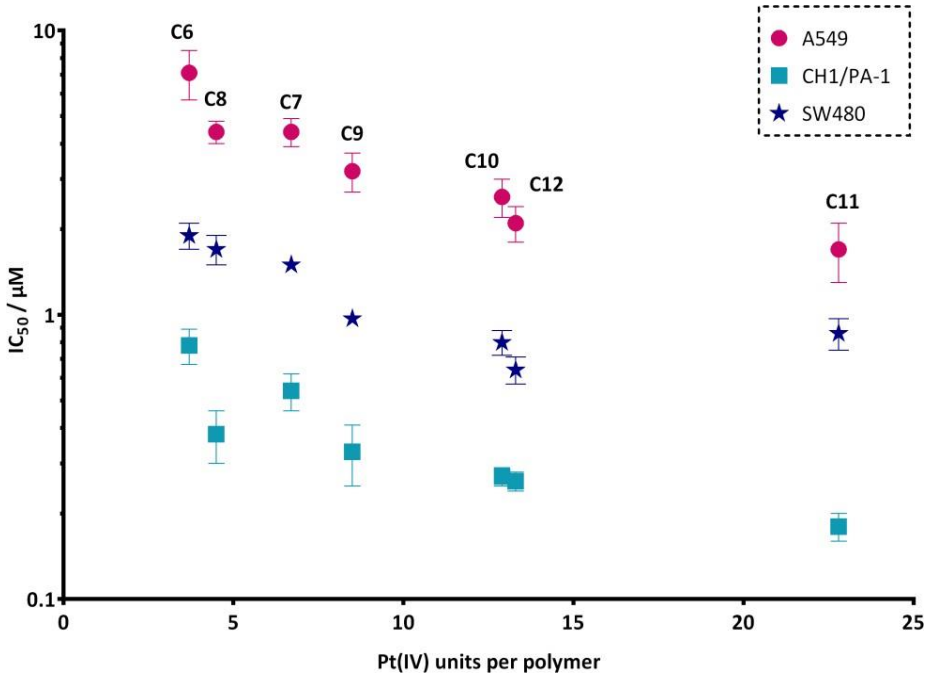

Figure 2. Correlation between IC_{50} values and platinum(IV) loading of oxaliplatin derivatives (**C6–C12**). The y-axis represents IC_{50} values (means ± standard deviations) in all three cell lines on a logarithmic scale; the x-axis is related to the platinum(IV) units per polymer.

Table 4. Overview of the concentration levels of platinum(IV) unit at the IC_{50} value calculated on the basis of the measured IC_{50} values of conjugates **C1–C12** and **V1–V3** in the corresponding cancer cell lines.

		Concentration of Pt(IV) Units at IC_{50} [µM]			
Sample	**Pt(IV)**	**A549**	**CH1/PA-1**	**SW480**	**4T1**
2	**2**	99 ± 17	1.2 ± 0.5	47 ± 10	-
4	**4**	>200	16 ± 6	>200	-
6	**6**	70 ± 29	4.1 ± 0.6	22 ± 8	-
C1	**2**	24	0.80	14	-
C2	**2**	24	0.45	8.2	-
C3	**4**	117	5.2	86	-
C4	**4**	102	8.4	102	-
C5	**4**	707	24	251	-
C6	**6**	26	2.9	7.0	-
C7	**6**	29	3.6	10	-
C8	**6**	20	1.7	7.7	-
C9	**6**	27	2.8	8.2	-
C10	**6**	34	3.5	10	-
C11	**6**	39	4.1	20	-
C12	**6**	28	3.5	8.5	-
V1	**6**	-	-	-	25
V2	**6**	-	-	-	41
V3	**6**	-	-	-	28

Based on these observations, it can be concluded that in general, conjugation of platinum(IV) complexes to dGC polymers led to increased cytotoxicity. Furthermore, higher

loading with platinum(IV) units consistently enhanced the antiproliferative activity within the group of the same dGC polymer. On the other hand, no systematic structure–activity relationship could be observed with regard to conjugates differing in the chain length of dGC. Overall, conjugates with lower chain lengths and high platinum(IV) loading levels are the most promising candidates, based on good solubility combined with high potency. Moreover, all conjugates showed enhanced cytotoxicity compared to the corresponding platinum(IV) complexes.

Based on the highly promising results, we chose to push the most active compounds offering favourable solubility forward, based on dGC polymer chain length and platinum core. Despite accurate controlling of the reaction parameters, it remains a challenge to precisely control the platinum(IV) load. For animal experiments, oxaliplatin(IV)-based conjugates **V1–V3** were resynthesised with 1.4, 3.9, and 7.6 units of platinum(IV) per dGC polymer molecule, respectively. Their cytotoxicity was investigated in murine mammary carcinoma cell line 4T1, used for the in vivo experiments in mice. In general, IC_{50} values in the low micromolar range were revealed, and these results emphasise the previously examined structure–activity relationships of platinum(IV) loading levels and cytotoxic activity, with **V1** exhibiting the lowest antiproliferative effect, whereas **V3** was the most active conjugate (Table 5).

Table 5. IC_{50} values of conjugates **V1–V3** with the platinum(IV) analogue of oxaliplatin in the murine mammary carcinoma cell line 4T1.

Sample	Pt(IV)	dGC	Pt(IV) Units per Polymer	IC_{50} [µM] 4T1
V1	**6**	**P1**	1.4	18.0 ± 6.4
V2	**6**	**P2**	3.9	10.4 ± 3.0
V3	**6**	**P3**	7.6	3.7 ± 1.3

3.4. Biodistribution Studies

Conjugate **V3**, offering both high cytotoxicity and sufficient solubility, was investigated for its biodistribution in vivo in comparison to its respective free platinum(IV) complex **6**. Intravenously, 0.15 mg/100 µL of platinum(IV) complex **6** and 0.41 mg/100 µL of conjugate **V3** were administered to five non-tumour-bearing female Balb/C mice per group. The used concentrations are equivalent to 5.5 mg/kg and 2.75 mg/kg oxaliplatin, respectively, and were well tolerated without signs of toxicity or any other negative impact on mouse health. The major organs of liver, lung, heart, kidney and spleen were collected after two specific time points (1 h and 24 h), and the platinum content of each organ was evaluated with ICP-MS analysis (Figure 3).

The free platinum(IV) complex **6** was similarly distributed in lung, heart, and spleen and displayed the highest concentrations in the excretory organs (kidney and liver) 1 h post administration. After 24 h, the platinum amount was only slightly raised in all systemic organs. The highest increase of 2.1-fold was in the kidneys, as indication of excretion. The high platinum levels in the kidney are in accordance with previously published data of an oxaliplatin(IV) analogue and other platinum(IV) complexes [44,45]. However, complex **6** displayed significantly lower platinum amounts in the liver, possibly caused by the lower lipophilicity of compound **6**.

On the contrary, conjugate **V3** showed the highest accumulation in the kidneys, followed by the lungs and heart, and the lowest amounts in the liver and spleen after 1 h, indicating higher renal excretion of the conjugates compared to complex **6**. Platinum concentrations decreased in all organs for conjugate **V3** 24 h post injection but remained high in the kidney. These results are in accordance with previously published studies of dGC polymers loaded with other chemotherapeutics, such as doxorubicin [46,47]. The renal uptake is characteristic for glycol chitosan polymers based on their ability to bind to the megalin receptor in tubular cells of the kidney [48–50]. Cisplatin-associated nephrotoxicity is not reported for oxaliplatin [51], and together with the nontoxicity of glycol chitosan

polymers [49], a safe pharmacokinetic profile for conjugate **V3** can be expected. Additionally, the biodistribution study of conjugate **V3** revealed an increased accumulation in lung tissue compared to complex **6** and other platinum(IV) complexes [44,45].

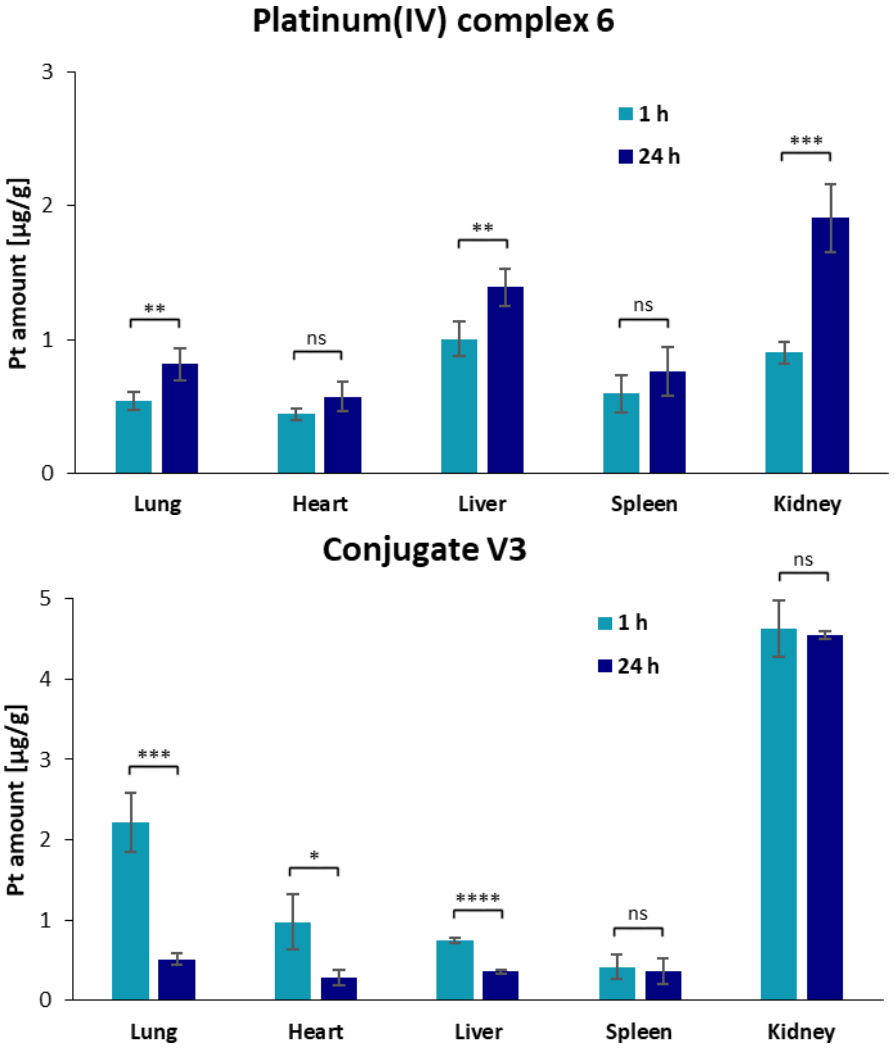

Figure 3. Overview of the accumulation of platinum in different organs, measured with ICP-MS, as result of the biodistribution studies for platinum(IV) complex **6** and conjugate **V3** after 1 h and 24 h after intravenous administration. Additionally, significance of the increase and decrease in the platinum amount between 1 h and 24 h of complex **6** (upper figure) and conjugate **V3** (lower figure) was further examined via unpaired *t*-test with Welch's correction, with the following abbreviations: ns = not significant; * $p < 0.05$; ** $p < 0.01$; *** $p < 0.001$; **** $p < 0.0001$.

Finally, the altered kinetic profile of platinum(IV) complexes through coupling to dGC polymers reveals a promising approach for future cancer research, maybe also with respect to cancer of the lung or lung metastases.

4. Conclusions

The synthesis of a series of platinum(IV) analogues of cisplatin, carboplatin and oxaliplatin coordinated to dGC polymers with different molecular weights resulted in 15 conjugates with various average platinum(IV) loading levels. In vitro cytotoxicity assays displayed promising cytotoxic activity in human cancer cell lines, with IC_{50} values in the low micromolar to nanomolar range. All conjugates revealed lower IC_{50} values than the corresponding unconjugated platinum(IV) complex and were comparable with the platinum(II) counterparts. Generally, it can be concluded that conjugation of platinum(IV)

complexes to dGC polymers led to increased cytotoxicity. Additionally, a tendency with higher amounts of platinum(IV) units per dGC polymer leading to lower IC_{50} values could be observed. One oxaliplatin(IV)–dGC conjugate was further investigated in a biodistribution experiment in non-tumour-bearing Balb/C mice, revealing an enhanced accumulation in the lung compared to the free oxaliplatin(IV) analogue. Consequently, these results imply a great potential for a novel anticancer treatment, especially with regard to lung cancer types and lung metastases. Therefore, activity studies in tumour-bearing mice would be the next step in order to evaluate the promising potential of platinum(IV)–dGC conjugates.

Supplementary Materials: The following supporting information can be downloaded at https://www.mdpi.com/article/10.3390/pharmaceutics15041050/s1, Figures S1–S9: NMR spectra of platinum(IV) complexes; Figure S10: NMR spectra of dGC polymers; Figures S11–S17: NMR spectra of conjugates; Figures S18–S20: Concentration–effect curves; Table S1: solubility data.

Author Contributions: Conceptualization, Y.L.-K., N.S.S., I.F.U. and M.S.G.; Data curation, Y.L.-K., N.S.S., K.C., X.W.-J., U.O. and M.A.J.; Formal analysis, K.C. and U.O.; Funding acquisition, Y.L.- K., N.S.S., A.G.S., I.F.U., M.S.G. and B.K.K.; Investigation, Y.L.-K., N.S.S., K.C., X.W.-J. and U.O.; Methodology, Y.L.-K., N.S.S., I.F.U. and M.S.G.; Project administration, Y.L.-K., N.S.S., I.F.U. and M.S.G.; Resources, A.G.S., I.F.U., M.S.G., M.A.J. and B.K.K.; Supervision, A.G.S., I.F.U., M.S.G., M.A.J. and B.K.K.; Validation, Y.L.-K., N.S.S., I.F.U., M.S.G. and M.A.J.; Visualization, Y.L.-K., N.S.S. and K.C.; Writing—original draft, Y.L.-K., N.S.S., K.C. and U.O.; Writing—review and editing, Y.L.-K., N.S.S., K.C., X.W.-J., U.O., A.G.S., I.F.U., M.S.G., M.A.J. and B.K.K. All authors have read and agreed to the published version of the manuscript.

Funding: The research was funded by the University of Vienna.

Institutional Review Board Statement: The animal study protocol was approved by the Ethics Committee of University College London, and the studies were performed in accordance with the UK Animals (Scientific Procedures) Act 1986.

Informed Consent Statement: Not applicable.

Data Availability Statement: The data presented in this study are available in the supplementary material.

Acknowledgments: The authors gratefully acknowledge the support of Rui Manuel Jesus Lopes, Sophie Neumayer, Asya Petkova, Verena Pichler, Tatjana Schafarik, Martin Schaier, David Workmann and Zilan Zhou. Open access funding by the University of Vienna.

Conflicts of Interest: The authors declare no conflict of interest.

References

1. Polaris Market Research. *Global Platinum Based Cancer Drugs Market Share, Size, Trends, Industry Analysis Report By Drug Type (Cisplatin, Oxaliplatin, Carboplatin, Other), By Application (Colorectal Cancer, Ovarian Cancer, Lung Cancer, Other); By Regions, and Segment Forecast, 2019–2026*; Polaris Market Research & Consulting LLP: Pune, India, 2019.
2. Varbanov, H.P.; Göschl, S.; Heffeter, P.; Theiner, S.; Roller, A.; Jensen, F.; Jakupec, M.A.; Berger, W.; Galanski, M.; Keppler, B.K. A Novel Class of Bis-and Tris-Chelate Diam(m)Inebis(Dicarboxylato) Platinum(IV) Complexes as Potential Anticancer Prodrugs. *J. Med. Chem.* **2014**, *57*, 6751–6764. [CrossRef] [PubMed]
3. Wexselblatt, E.; Gibson, D. What Do We Know about the Reduction of Pt(IV) pro-Drugs? *J. Inorg. Biochem.* **2012**, *117*, 220–229. [CrossRef] [PubMed]
4. Deo, K.M.; Ang, D.L.; McGhie, B.; Rajamanickam, A.; Dhiman, A.; Khoury, A.; Holland, J.; Bjelosevic, A.; Pages, B.; Gordon, C.; et al. Platinum Coordination Compounds with Potent Anticancer Activity. *Coord. Chem. Rev.* **2018**, *375*, 148–163. [CrossRef]
5. Jia, C.; Deacon, G.B.; Zhang, Y.; Gao, C. Platinum(IV) Antitumor Complexes and Their Nano-Drug Delivery. *Coord. Chem. Rev.* **2021**, *429*, 213640. [CrossRef]
6. Gibson, D. Platinum(IV) Anticancer Agents; Are We En Route to the Holy Grail or to a Dead End? *J. Inorg. Biochem.* **2021**, *217*, 111353. [CrossRef] [PubMed]
7. Johnstone, T.C.; Suntharalingam, K.; Lippard, S.J. The Next Generation of Platinum Drugs: Targeted Pt(II) Agents, Nanoparticle Delivery, and Pt(IV) Prodrugs. *Chem. Rev.* **2016**, *116*, 3436–3486. [CrossRef]

8. Liang, S.; Deng, X.; Xu, G.; Xiao, X.; Wang, M.; Guo, X.; Ma, P.; Cheng, Z.; Zhang, D.; Lin, J. A Novel Pt–TiO2 Heterostructure with Oxygen-Deficient Layer as Bilaterally Enhanced Sonosensitizer for Synergistic Chemo-Sonodynamic Cancer Therapy. *Adv. Funct. Mater.* **2020**, *30*, 1908598. [CrossRef]
9. Apps, M.G.; Choi, E.H.Y.; Wheate, N.J. The State-of-Play and Future of Platinum Drugs. *Endocr. Relat. Cancer* **2015**, *22*, R219–R233. [CrossRef]
10. Pichler, V.; Göschl, S.; Meier, S.M.; Roller, A.; Jakupec, M.A.; Galanski, M.; Keppler, B.K. Bulky N (,N)-(Di)Alkylethane-1,2-Diamineplatinum(II) Compounds as Precursors for Generating Unsymmetrically Substituted Platinum(IV) Complexes. *Inorg. Chem.* **2013**, *52*, 8151–8162. [CrossRef]
11. Pichler, V.; Heffeter, P.; Valiahdi, S.M.; Kowol, C.R.; Egger, A.; Berger, W.; Jakupec, M.A.; Galanski, M.; Keppler, B.K. Unsymmetric Mono- and Dinuclear Platinum(IV) Complexes Featuring an Ethylene Glycol Moiety: Synthesis, Characterization, and Biological Activity. *J. Med. Chem.* **2012**, *55*, 11052–11061. [CrossRef]
12. Pichler, V.; Valiahdi, S.M.; Jakupec, M.A.; Arion, V.B.; Galanski, M.; Keppler, B.K. Mono-Carboxylated Diaminedichloridoplatinum(IV) Complexes—Selective Synthesis, Characterization, and Cytotoxicity. *Dalton Trans.* **2011**, *40*, 8187–8192. [CrossRef] [PubMed]
13. Harringer, S.; Hejl, M.; Enyedy, É.A.; Jakupec, M.A.; Galanski, M.S.; Keppler, B.K.; Dyson, P.J.; Varbanov, H.P. Multifunctional Pt(IV) Prodrug Candidates Featuring the Carboplatin Core and Deferoxamine. *Dalton Trans.* **2021**, *50*, 8167–8178. [CrossRef] [PubMed]
14. Kenny, R.G.; Chuah, S.W.; Crawford, A.; Marmion, C.J. Platinum(IV) Prodrugs—A Step Closer to Ehrlich's Vision? *Eur. J. Inorg. Chem.* **2017**, *2017*, 1596–1612. [CrossRef]
15. Shukla, S.K.; Mishra, A.K.; Arotiba, O.A.; Mamba, B.B. Chitosan-Based Nanomaterials: A State-of-the-Art Review. *Int. J. Biol. Macromol.* **2013**, *59*, 46–58. [CrossRef] [PubMed]
16. Martau, G.A.; Mihai, M.; Vodnar, D.C. The Use of Chitosan, Alginate, and Pectin in the Biomedical and Food Sector-Biocompatibility, Bioadhesiveness, and Biodegradability. *Polymers* **2019**, *11*, 1837. [CrossRef]
17. Morin-Crini, N.; Lichtfouse, E.; Torri, G.; Crini, G. Fundamentals and Applications of Chitosan. In *Sustainable Agriculture Reviews 35*; Springer: Cham, Switzerland, 2019; Volume 35, ISBN 9783030165376.
18. Muxika, A.; Etxabide, A.; Uranga, J.; Guerrero, P.; de la Caba, K. Chitosan as a Bioactive Polymer: Processing, Properties and Applications. *Int. J. Biol. Macromol.* **2017**, *105*, 1358–1368. [CrossRef]
19. Younes, I.; Rinaudo, M. Chitin and Chitosan Preparation from Marine Sources. Structure, Properties and Applications. *Mar. Drugs* **2015**, *13*, 1133–1174. [CrossRef]
20. Lin, F.; Jia, H.R.; Wu, F.G. Glycol Chitosan: A Water-Soluble Polymer for Cell Imaging and Drug Delivery. *Molecules* **2019**, *24*, 4371. [CrossRef]
21. Huq, T.; Khan, A.; Brown, D.; Dhayagude, N.; He, Z.; Ni, Y. Sources, Production and Commercial Applications of Fungal Chitosan: A Review. *J. Bioresour. Bioprod.* **2022**, *7*, 85–98. [CrossRef]
22. Morin-Crini, N.; Lichtfouse, E.; Torri, G.; Crini, G. Applications of Chitosan in Food, Pharmaceuticals, Medicine, Cosmetics, Agriculture, Textiles, Pulp and Paper, Biotechnology, and Environmental Chemistry. *Environ. Chem. Lett.* **2019**, *17*, 1667–1692. [CrossRef]
23. Kumar, M.N.V.R. A Review of Chitin and Chitosan Applications. *React. Funct. Polym.* **2000**, *46*, 1–27. [CrossRef]
24. Yan, L.; Crayton, S.H.; Thawani, J.P.; Amirshaghaghi, A.; Tsourkas, A.; Cheng, Z. A PH-Responsive Drug-Delivery Platform Based on Glycol Chitosan-Coated Liposomes. *Small* **2015**, *11*, 4870–4874. [CrossRef]
25. Danhier, F.; Feron, O.; Préat, V. To Exploit the Tumor Microenvironment: Passive and Active Tumor Targeting of Nanocarriers for Anti-Cancer Drug Delivery. *J. Control. Release* **2010**, *148*, 135–146. [CrossRef] [PubMed]
26. Shanmuganathan, R.; Edison, T.N.J.I.; LewisOscar, F.; Kumar, P.; Shanmugam, S.; Pugazhendhi, A. Chitosan Nanopolymers: An Overview of Drug Delivery against Cancer. *Int. J. Biol. Macromol.* **2019**, *130*, 727–736. [CrossRef] [PubMed]
27. Herdiana, Y.; Wathoni, N.; Shamsuddin, S.; Joni, I.M.; Muchtaridi, M. Chitosan-Based Nanoparticles of Targeted Drug Delivery System in Breast Cancer Treatment. *Polymers* **2021**, *13*, 1717. [CrossRef]
28. Nascimento, A.V.; Singh, A.; Bousbaa, H.; Ferreira, D.; Sarmento, B.; Amiji, M.M. Combinatorial-Designed Epidermal Growth Factor Receptor-Targeted Chitosan Nanoparticles for Encapsulation and Delivery of Lipid-Modified Platinum Derivatives in Wild-Type and Resistant Non-Small-Cell Lung Cancer Cells. *Mol. Pharm.* **2015**, *12*, 4466–4477. [CrossRef] [PubMed]
29. Kim, J.H.; Kim, Y.S.; Park, K.; Lee, S.; Nam, H.Y.; Min, K.H.; Jo, H.G.; Park, J.H.; Choi, K.; Jeong, S.Y.; et al. Antitumor Efficacy of Cisplatin-Loaded Glycol Chitosan Nanoparticles in Tumor-Bearing Mice. *J. Control. Release* **2008**, *127*, 41–49. [CrossRef]
30. El-Shafai, N.M.; Farrag, F.; Shukry, M.; Mehany, H.; Aboelmaati, M.; Abu-Ali, O.; Saleh, D.; Ramadan, M.; El-Mehasseb, I. Effect of a Novel Hybrid Nanocomposite of Cisplatin–Chitosan on Induced Tissue Injury as a Suggested Drug by Reducing Cisplatin Side Effects. *Biol. Trace Elem. Res.* **2022**, *200*, 4017–4026. [CrossRef]
31. Soodvilai, S.; Soodvilai, S.; Sajomsang, W.; Rojanarata, T.; Patrojanasophon, P.; Opanasopit, P. Chitosan Polymeric Micelles for Prevention of Cisplatin-Induced Nephrotoxicity and Anticancer Activity of Cisplatin. In Proceedings of the ACM International Conference Proceeding Series, 25–28 October 2010, Beijing, China; Association for Computing Machinery: New York, NY, USA, 2020; pp. 197–201.
32. Madni, A.; Kousar, R.; Naeem, N.; Wahid, F. Recent Advancements in Applications of Chitosan-Based Biomaterials for Skin Tissue Engineering. *J. Bioresour. Bioprod.* **2021**, *6*, 11–25. [CrossRef]

33. Varbanov, H.P.; Valiahdi, S.M.; Kowol, C.R.; Jakupec, M.A.; Galanski, M.; Keppler, B.K. Novel Tetracarboxylatoplatinum(Iv) Complexes as Carboplatin Prodrugs. *Dalton Trans.* **2012**, *41*, 14404–14415. [CrossRef]
34. Ghosh, S. Cisplatin: The First Metal Based Anticancer Drug. *Bioorg. Chem.* **2019**, *88*, 102925. [CrossRef]
35. Kidani, Y.; Inagaki, K.; Iigo, M.; Hoshi, A.; Kuretani, K. Antitumor Activity of 1,2-Diaminocyclohexane-Platinum Complexes against Sarcoma-180 Ascites Form. *J. Med. Chem.* **1978**, *21*, 1315–1318. [CrossRef] [PubMed]
36. Zhang, J.Z.; Bonnitcha, P.; Wexselblatt, E.; Klein, A.V.; Najajreh, Y.; Gibson, D.; Hambley, T.W. Facile Preparation of Mono-, Di- and Mixed-Carboxylato Platinum(IV) Complexes for Versatile Anticancer Prodrug Design. *Chem. – A Eur. J.* **2013**, *19*, 1672–1676. [CrossRef]
37. Wang, W.; McConaghy, A.M.; Tetley, L.; Uchegbu, I.F. Controls on Polymer Molecular Weight May Be Used to Control the Size of Palmitoyl Glycol Chitosan Polymeric Vesicles. *Langmuir* **2001**, *17*, 631–636. [CrossRef]
38. Cseh, K.; Geisler, H.; Stanojkovska, K.; Westermayr, J.; Brunmayr, P.; Wenisch, D.; Gajic, N.; Hejl, M.; Schaier, M.; Koellensperger, G.; et al. Arene Variation of Highly Cytotoxic Tridentate Naphthoquinone-Based Ruthenium(II) Complexes and In-Depth In Vitro Studies. *Pharmaceutics* **2022**, *14*, 2466. [CrossRef] [PubMed]
39. Chen, S.; Yao, H.; Zhou, Q.; Tse, M.K.; Gunawan, Y.F.; Zhu, G. Stability, Reduction, and Cytotoxicity of Platinum(IV) Anticancer Prodrugs Bearing Carbamate Axial Ligands: Comparison with Their Carboxylate Analogues. *Inorg. Chem.* **2020**, *59*, 11676–11687. [CrossRef]
40. Lafrance, D.; Bowles, P.; Leeman, K.; Rafka, R. Mild Decarboxylative Activation of Malonic Acid Derivatives by 1,1^{t}-Carbonyldiimidazole. *Org. Lett.* **2011**, *13*, 2322–2325. [CrossRef]
41. Engstrom, K.M. Practical Considerations for the Formation of Acyl Imidazolides from Carboxylic Acids and N, N^{t}-Carbonyldiimidazole: The Role of Acid Catalysis. *Org. Process Res. Dev.* **2018**, *22*, 1294–1297. [CrossRef]
42. Varbanov, H.P.; Jakupec, M.A.; Roller, A.; Jensen, F.; Galanski, M.; Keppler, B.K. Theoretical Investigations and Density Functional Theory Based Quantitative Structure-Activity Relationships Model for Novel Cytotoxic Platinum(IV) Complexes. *J. Med. Chem.* **2013**, *56*, 330–344. [CrossRef]
43. Varbanov, H.; Valiahdi, S.M.; Legin, A.A.; Jakupec, M.A.; Roller, A.; Galanski, M.; Keppler, B.K. Synthesis and Characterization of Novel Bis(Carboxylato) Dichloridobis(Ethylamine)Platinum(IV) Complexes with Higher Cytotoxicity than Cisplatin. *Eur. J. Med. Chem.* **2011**, *46*, 5456–5464. [CrossRef]
44. Theiner, S.; Varbanov, H.P.; Galanski, M.; Egger, A.E.; Berger, W.; Heffeter, P.; Keppler, B.K. Comparative in Vitro and in Vivo Pharmacological Investigation of Platinum(IV) Complexes as Novel Anticancer Drug Candidates for Oral Application. *J. Biol. Inorg. Chem.* **2015**, *20*, 89–99. [CrossRef] [PubMed]
45. Göschl, S.; Schreiber-Brynzak, E.; Pichler, V.; Cseh, K.; Heffeter, P.; Jungwirth, U.; Jakupec, M.A.; Berger, W.; Keppler, B.K. Comparative Studies of Oxaliplatin-Based Platinum(Iv) Complexes in Different in Vitro and in Vivo Tumor Models. *Metallomics* **2017**, *9*, 309–322. [CrossRef] [PubMed]
46. Park, K.; Kim, J.H.; Nam, Y.S.; Lee, S.; Nam, H.Y.; Kim, K.; Park, J.H.; Kim, I.S.; Choi, K.; Kim, S.Y.; et al. Effect of Polymer Molecular Weight on the Tumor Targeting Characteristics of Self-Assembled Glycol Chitosan Nanoparticles. *J. Control. Release* **2007**, *122*, 305–314. [CrossRef] [PubMed]
47. Son, Y.J.; Jang, J.S.; Cho, Y.W.; Chung, H.; Park, R.W.; Kwon, I.C.; Kim, I.S.; Park, J.Y.; Seo, S.B.; Park, C.R.; et al. Biodistribution and Anti-Tumor Efficacy of Doxorubicin Loaded Glycol-Chitosan Nanoaggregates by EPR Effect. *J. Control. Release* **2003**, *91*, 135–145. [CrossRef]
48. On, K.C.; Rho, J.; Yoon, H.Y.; Chang, H.; Yhee, J.Y.; Yoon, J.S.; Jeong, S.Y.; Kim, H.K.; Kim, K. Tumor-Targeting Glycol Chitosan Nanoparticles for Image-Guided Surgery of Rabbit Orthotopic VX2 Lung Cancer. *Pharmaceutics* **2020**, *12*, 621. [CrossRef]
49. Kim, C.S.; Mathew, A.P.; Uthaman, S.; Moon, M.J.; Bae, E.H.; Kim, S.W.; Park, I.K. Glycol Chitosan-Based Renal Docking Biopolymeric Nanomicelles for Site-Specific Delivery of the Immunosuppressant. *Carbohydr. Polym.* **2020**, *241*, 116255. [CrossRef]
50. Kato, Y.; Onishi, H.; Machida, Y. Contribution of Chitosan and Its Derivatives to Cancer Chemotherapy. *In Vivo* **2005**, *19*, 301–310.
51. Moraleja, I.; Esteban-Fernández, D.; Lázaro, A.; Humanes, B.; Neumann, B.; Tejedor, A.; Mena, M.L.; Jakubowski, N.; Gómez-Gómez, M.M. Printing Metal-Spiked Inks for LA-ICP-MS Bioimaging Internal Standardization: Comparison of the Different Nephrotoxic Behavior of Cisplatin, Carboplatin, and Oxaliplatin. *Anal. Bioanal. Chem.* **2016**, *408*, 2309–2318. [CrossRef]

Supporting Information

Platinum(IV) loaded degraded glycol chitosan as efficient platinum(IV) drug delivery platform

Yvonne Lerchbammer-Kreith [1,†], Nadine S. Sommerfeld [1,†], Klaudia Cseh [1], Xian Weng-Jiang [2], Uchechukwu Odunze [2], Andreas G. Schätzlein [2], Ijeoma F. Uchegbu [2], Mathea S. Galanski [1], Michael A. Jakupec [1,3,*] and Bernhard K. Keppler [1,3]

[1] Institute of Inorganic Chemistry, Faculty of Chemistry, University of Vienna, Waehringer Strasse 42, 1090 Vienna, Austria
[2] School of Pharmacy, University College London, Brunswick Square 29-39, London WC1N 1AX, UK
[3] Research Cluster "Translational Cancer Therapy Research", University of Vienna, Waehringer Strasse 42, 1090 Vienna, Austria
* Correspondence: michael.jakupec@univie.ac.at
† These authors contributed equally to this work.

Table of Contents

1. NMR spectra of platinum(IV) complexes

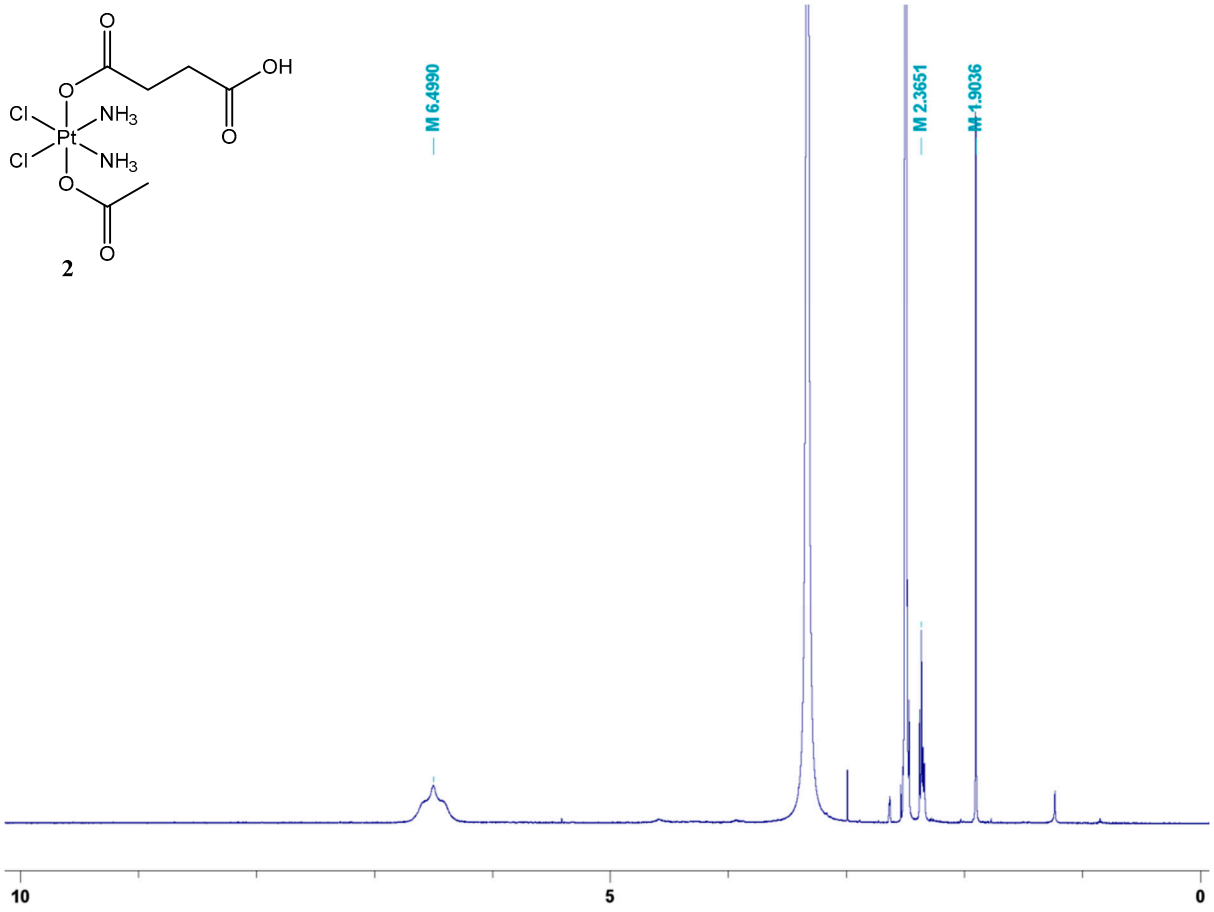

Figure S1. ^{1}H NMR spectrum of complex **2** in d_6-DMSO.

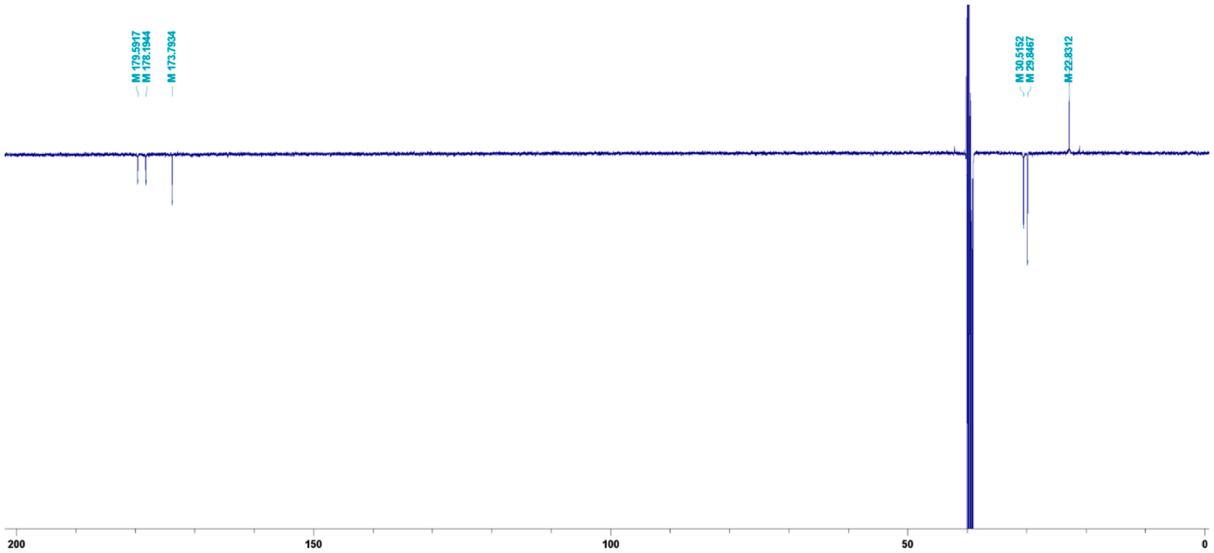

Figure S2. ^{13}C NMR spectrum of complex **2** in d_6-DMSO.

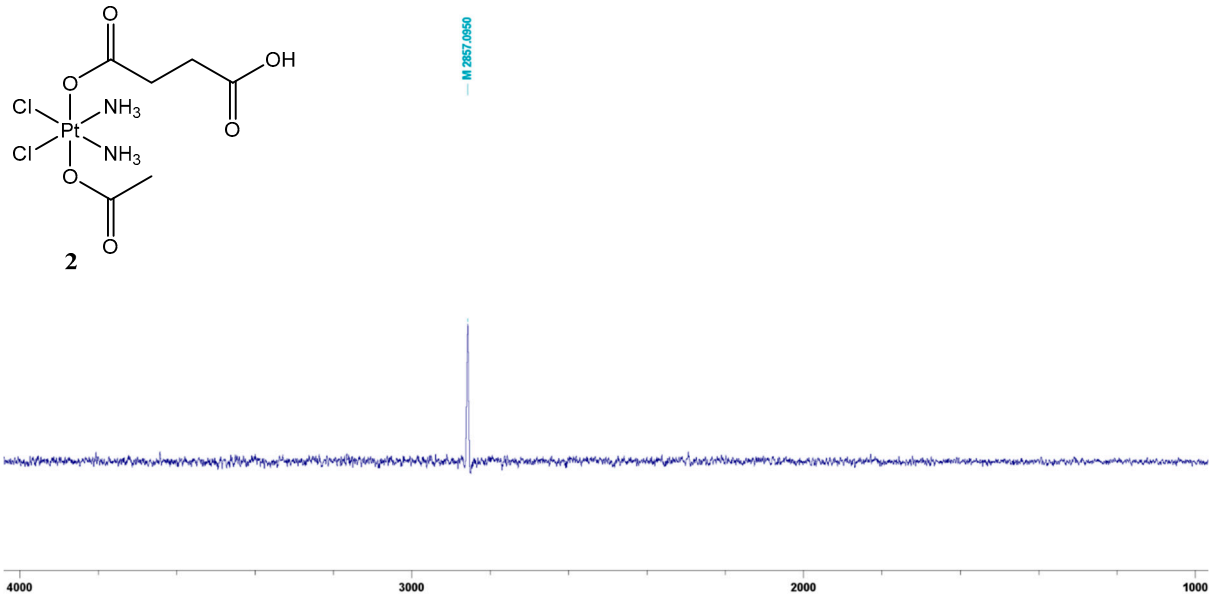

Figure S3. ^{195}Pt NMR spectrum of complex **2** in d_6-DMSO.

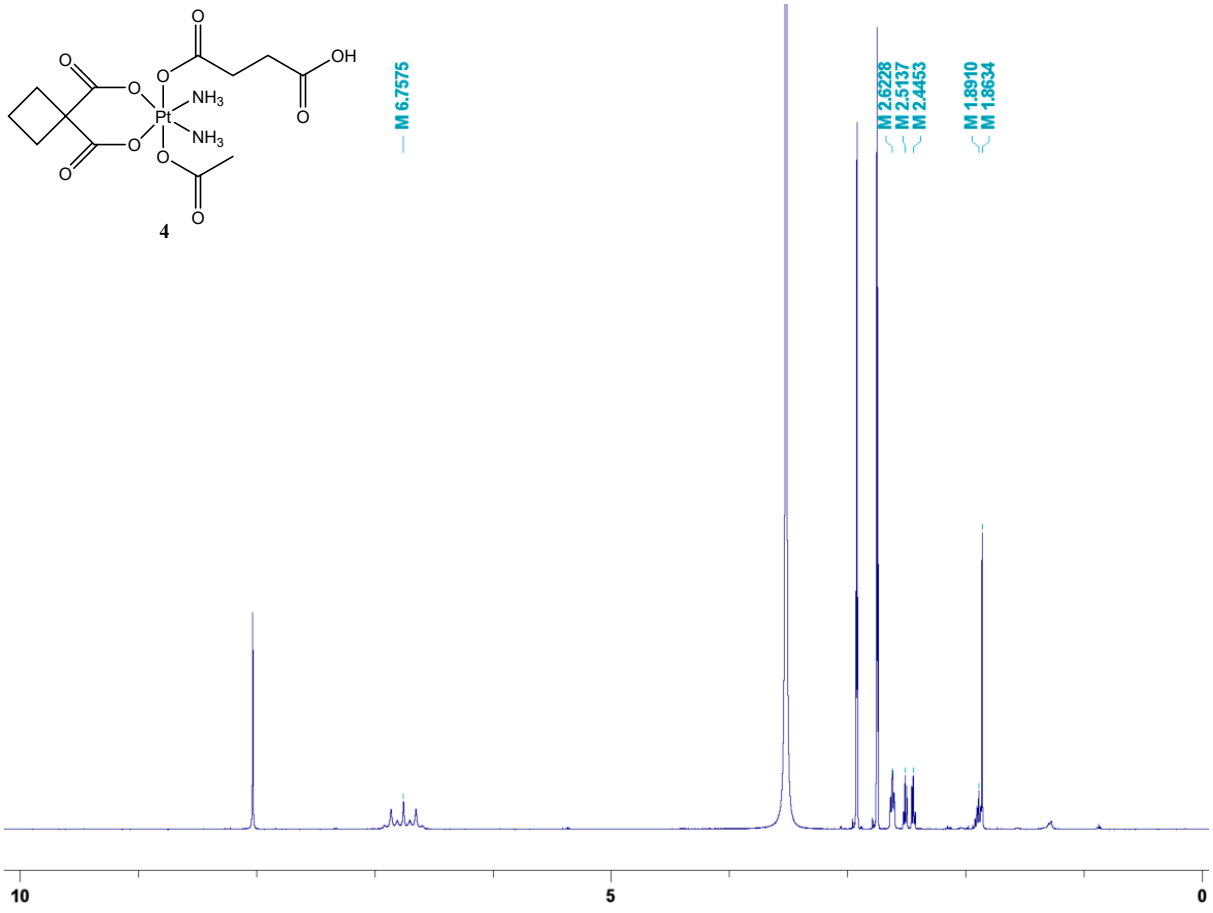

Figure S4. ^{1}H NMR spectrum of complex **4** in d$_7$-DMF.

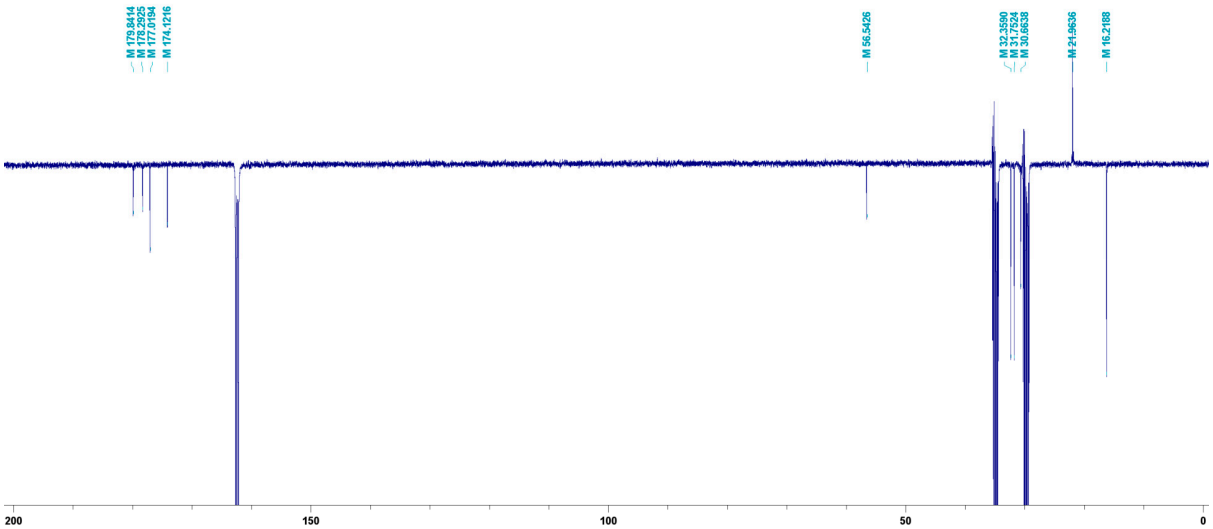

Figure S5. ^{13}C NMR spectrum of complex **4** in d$_7$-DMF.

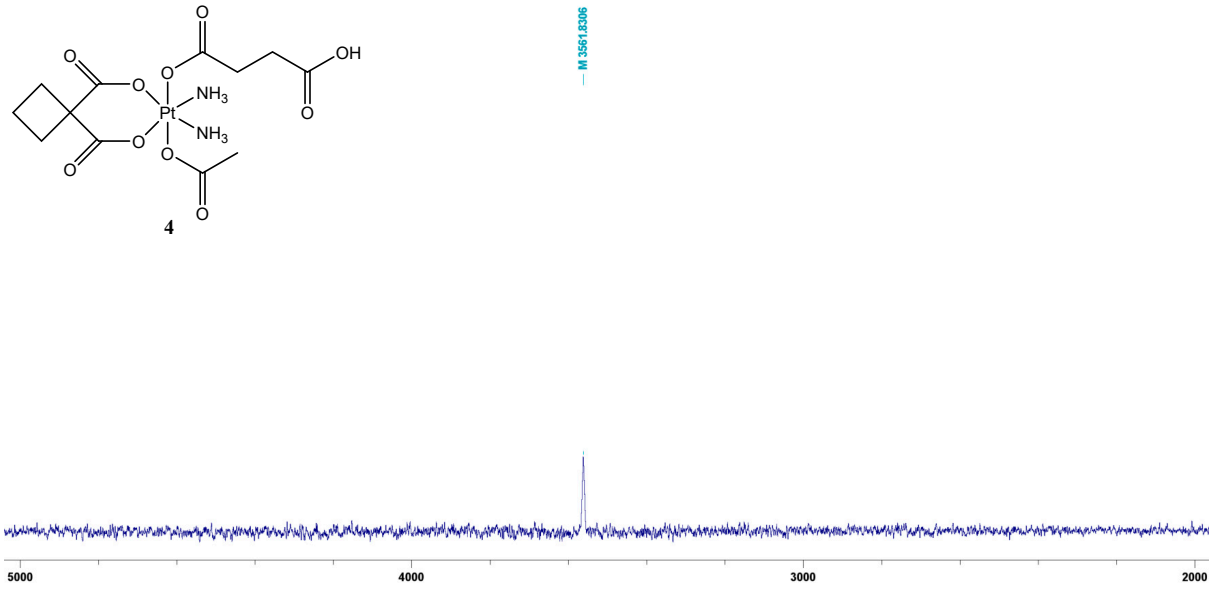

4

Figure S6. ^{195}Pt NMR spectrum of complex **4** in d$_7$-DMF.

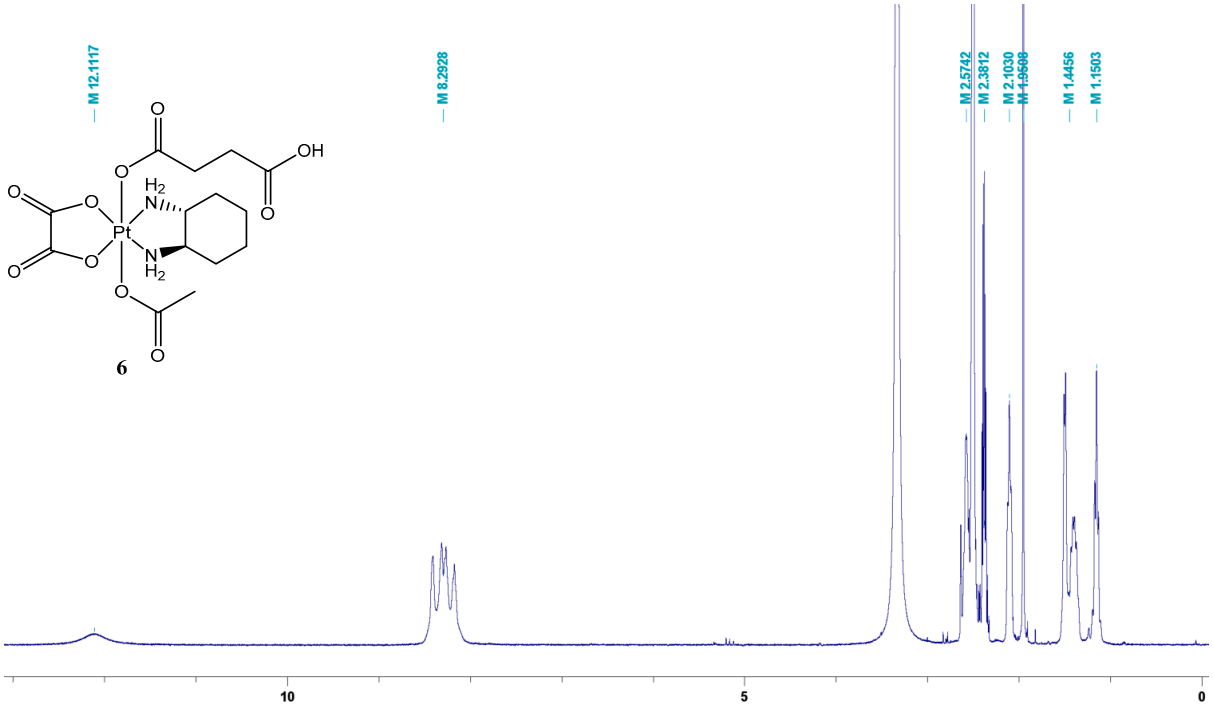

Figure S7. ^{1}H NMR spectrum of complex **6** in d_6-DMSO.

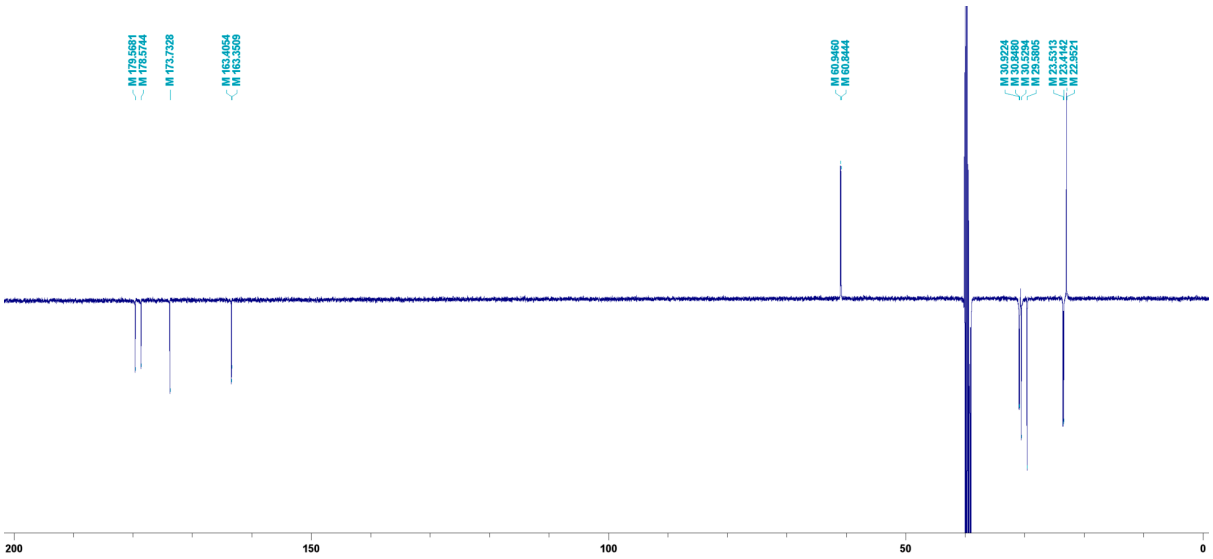

Figure S8. ^{13}C NMR spectrum of complex **6** in d_6-DMSO.

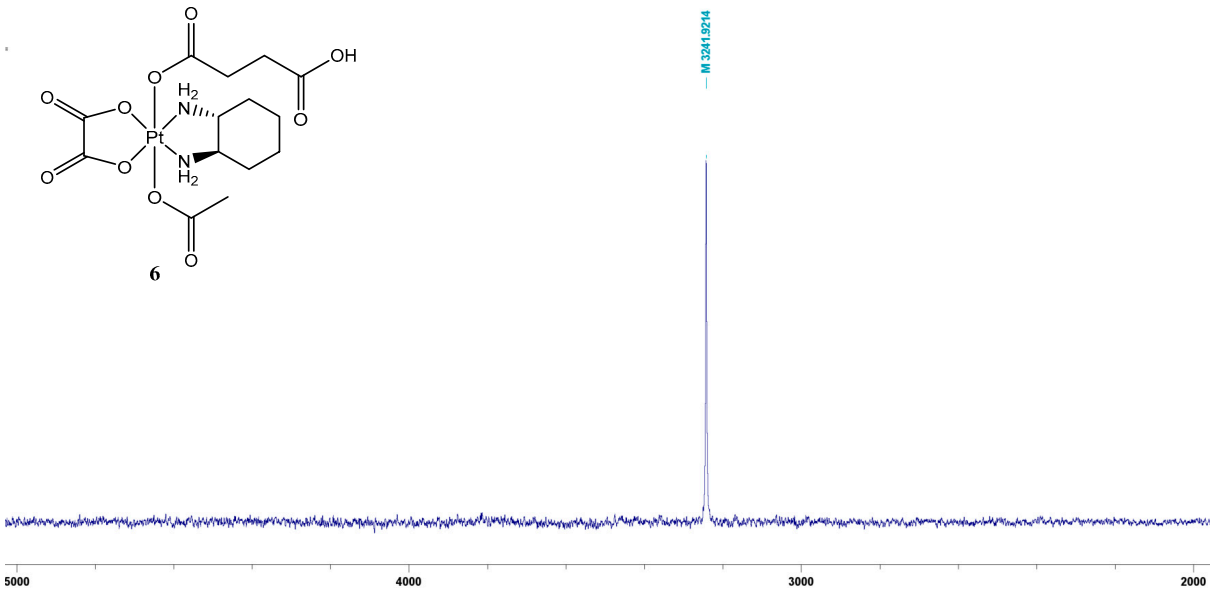

Figure S9. ^{195}Pt NMR spectrum of complex **6** in d_6-DMSO.

2. NMR spectra of dGC polymers

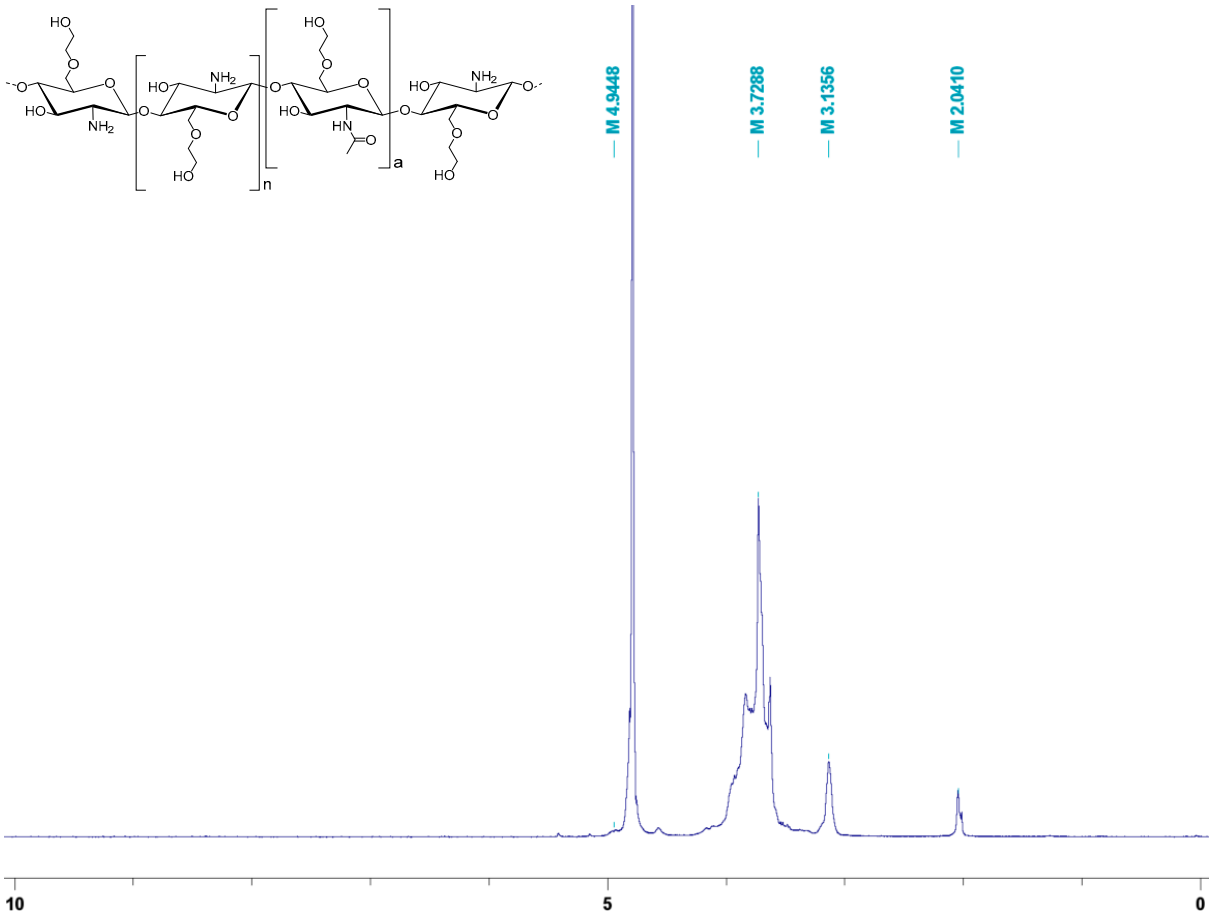

Figure S10. ^{1}H NMR spectrum of dGC polymer **P2** in D_2O.

3. NMR spectra of conjugates

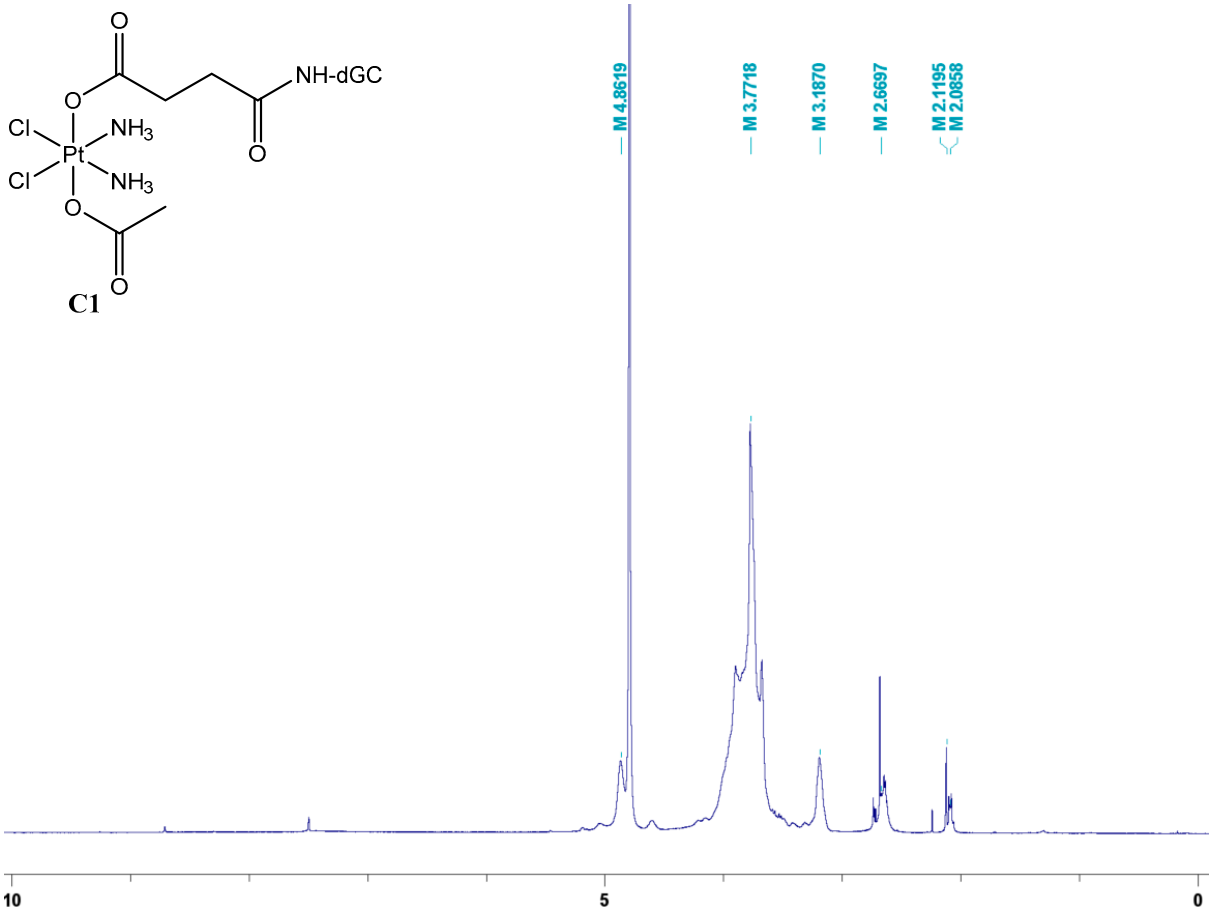

Figure S11. ^{1}H NMR spectrum of conjugate **C1** in D_2O.

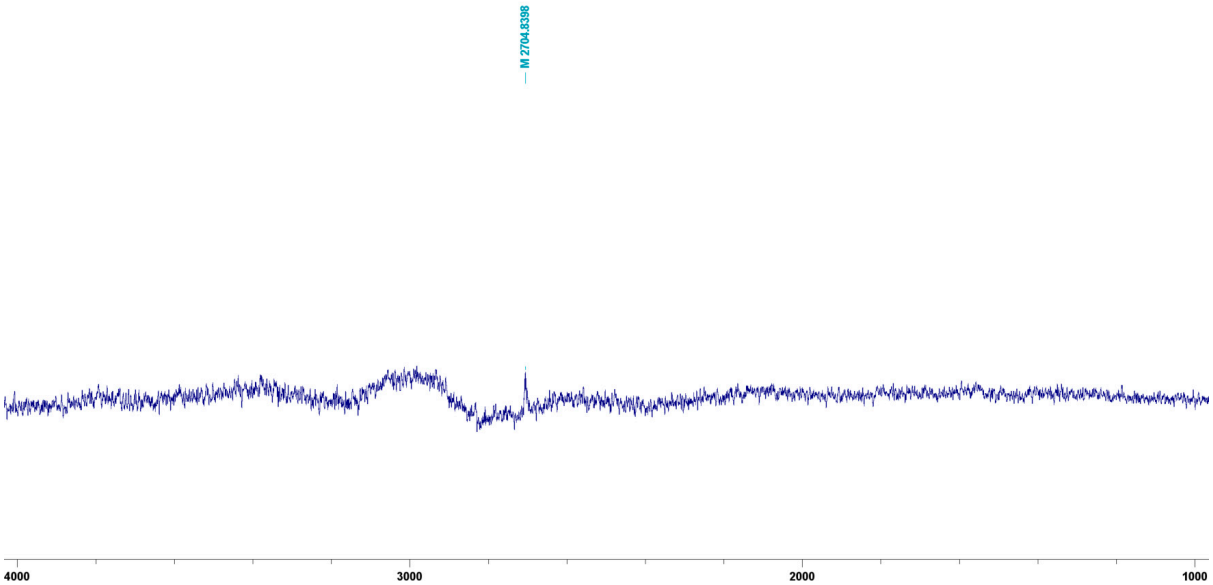

Figure S12. ^{195}Pt NMR spectrum of conjugate **C1** in D_2O.

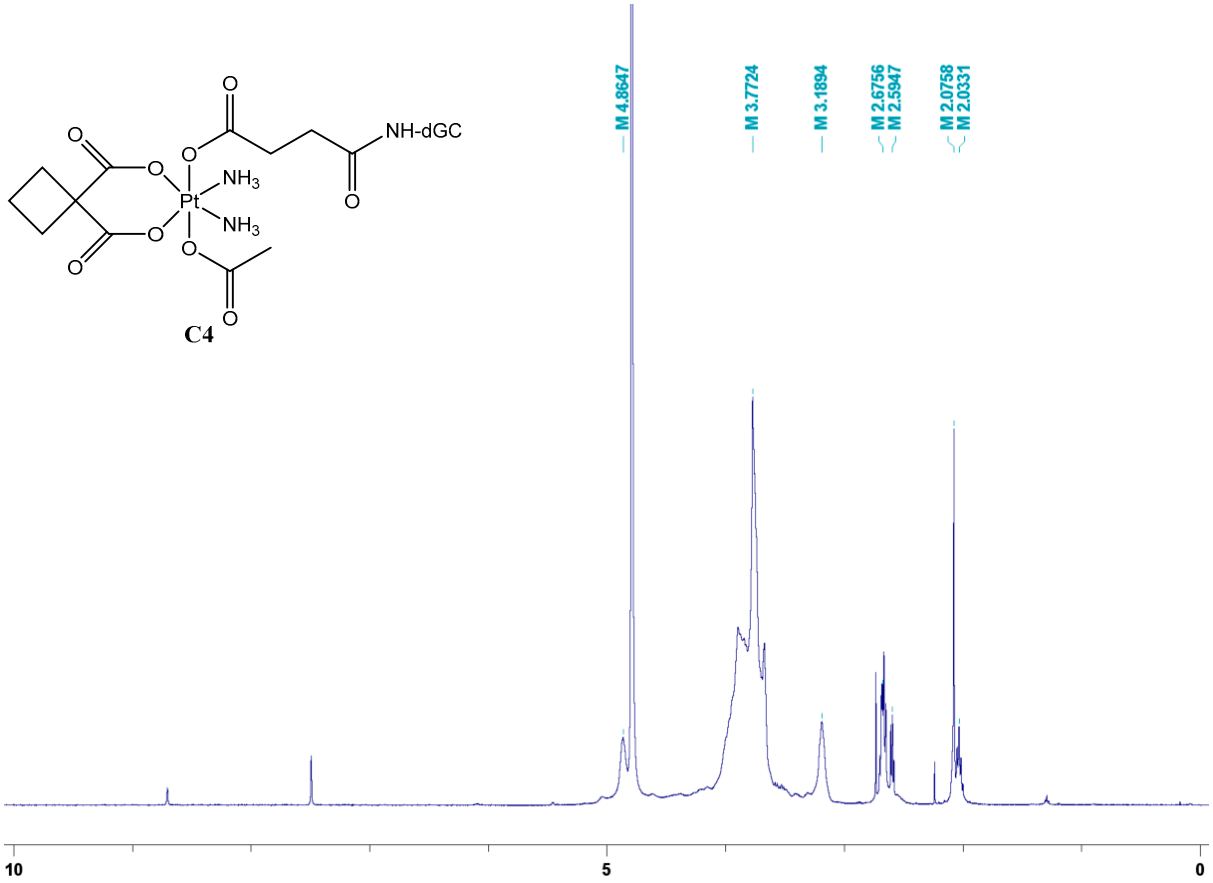

Figure S13. ^{1}H NMR spectrum of conjugate **C4** in D_2O.

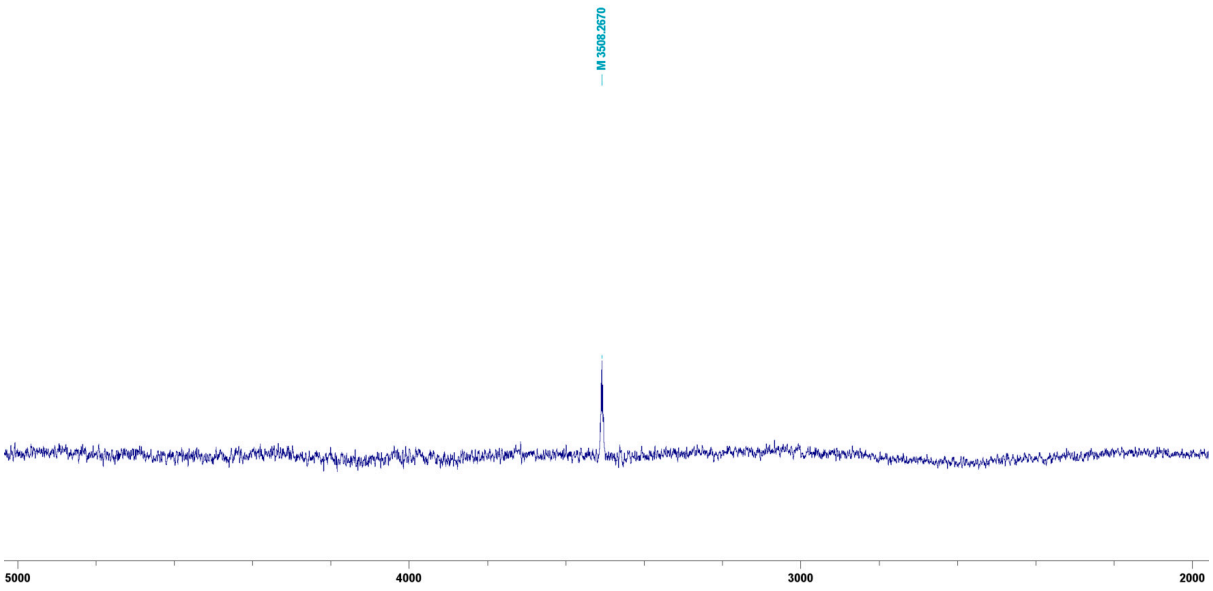

Figure S14. ^{195}Pt NMR spectrum of conjugate **C4** in D_2O.

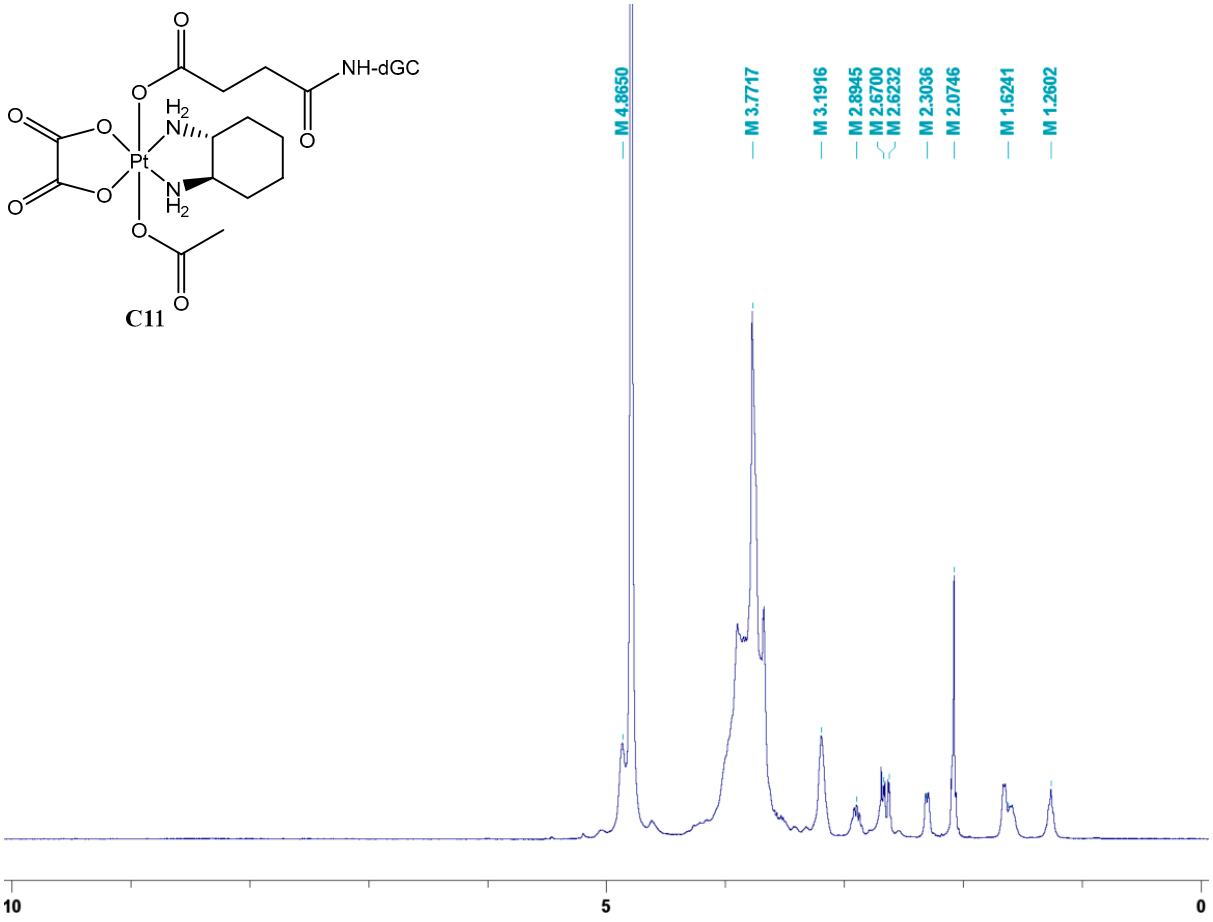

Figure S15. ^{1}H NMR spectrum of conjugate **C11** in D_2O.

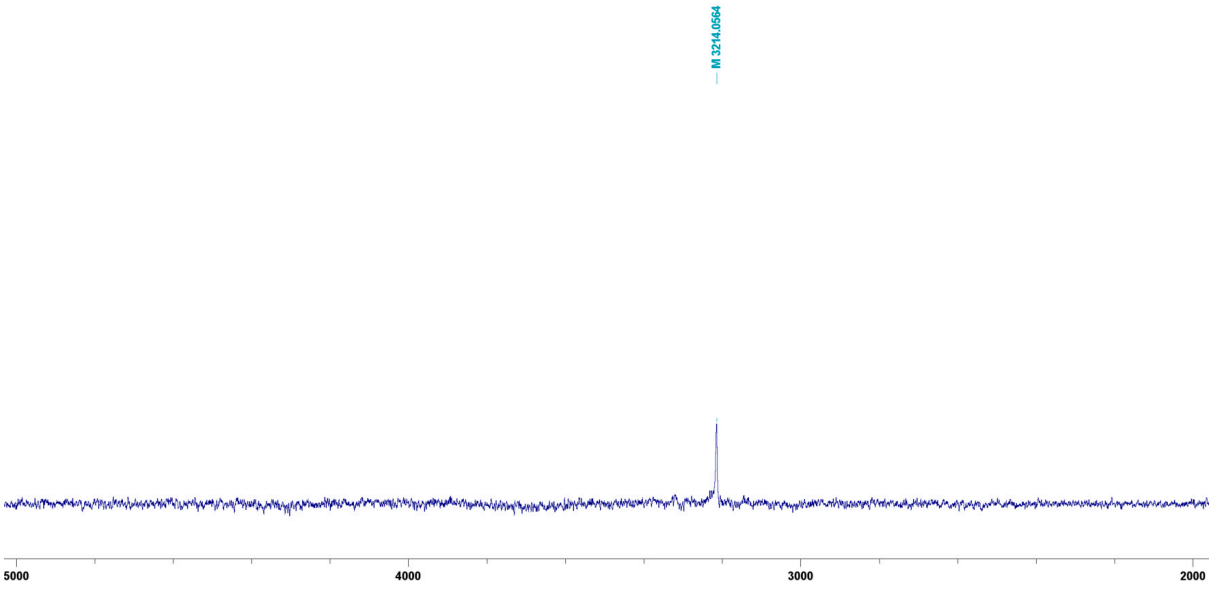

Figure S16. ^{195}Pt NMR spectrum of conjugate **C11** in D_2O.

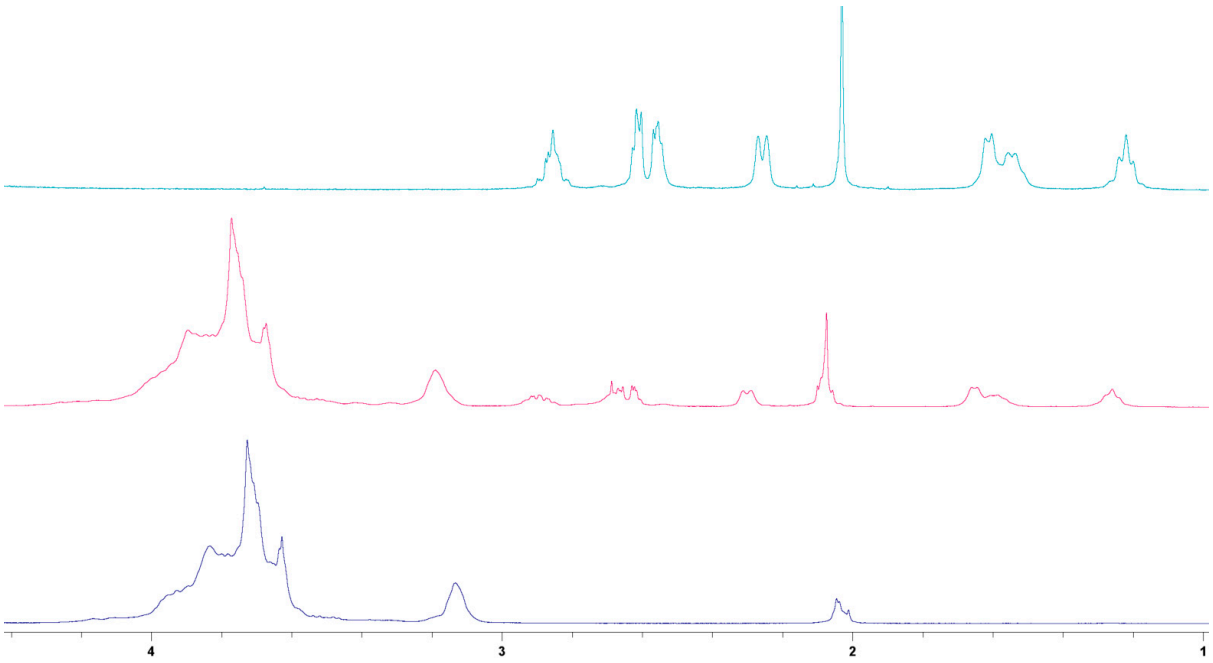

Figure S17. ^{1}H NMR spectra measured in D_2O of platinum(IV) complex **6** (above), conjugate **C11** (middle) and dGC polymer **P2** (below).

4. Concentration-effect curves

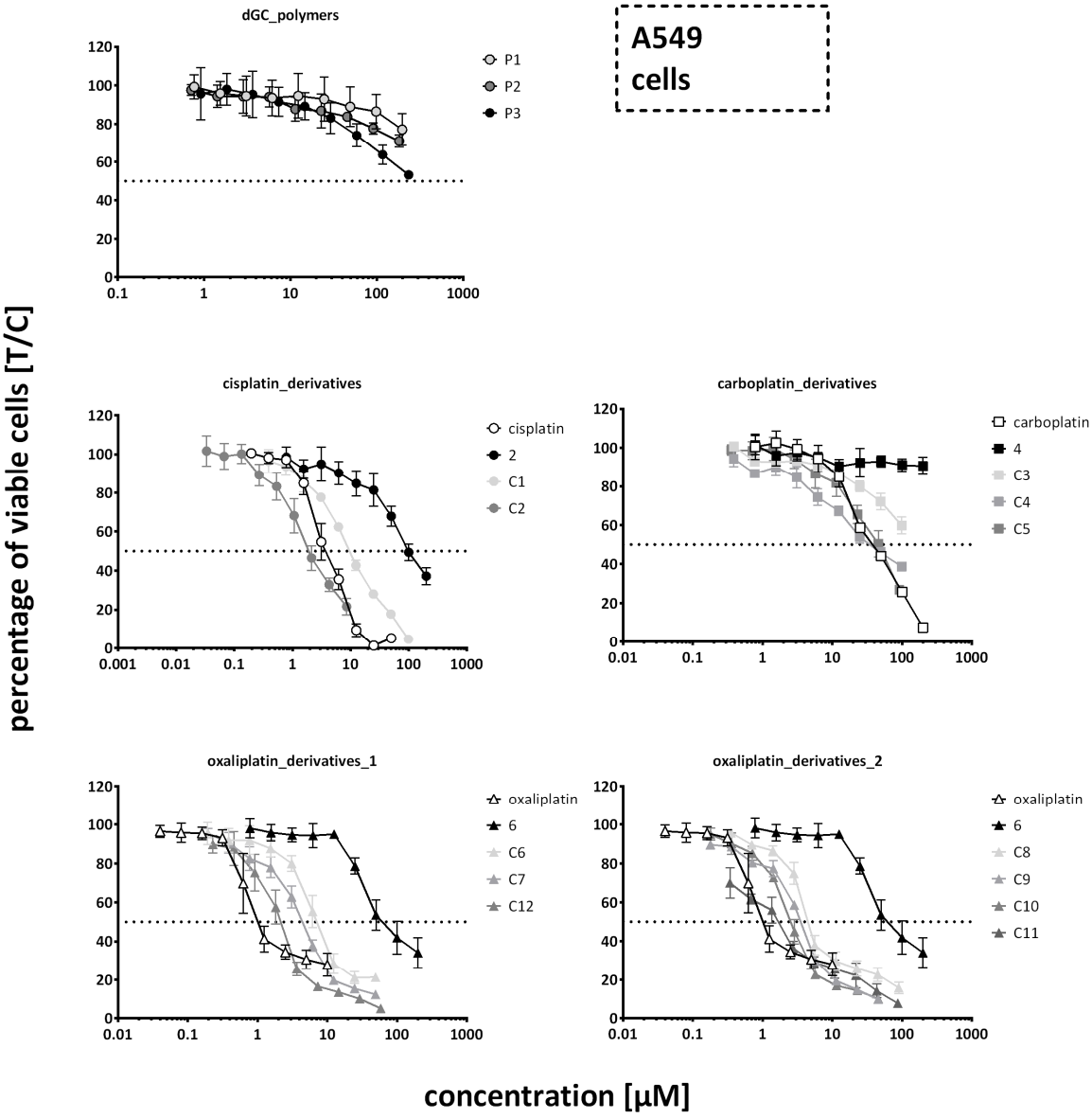

Figure S18. Concentration-effect curves in human cancer cell line A549 in MTT assays.

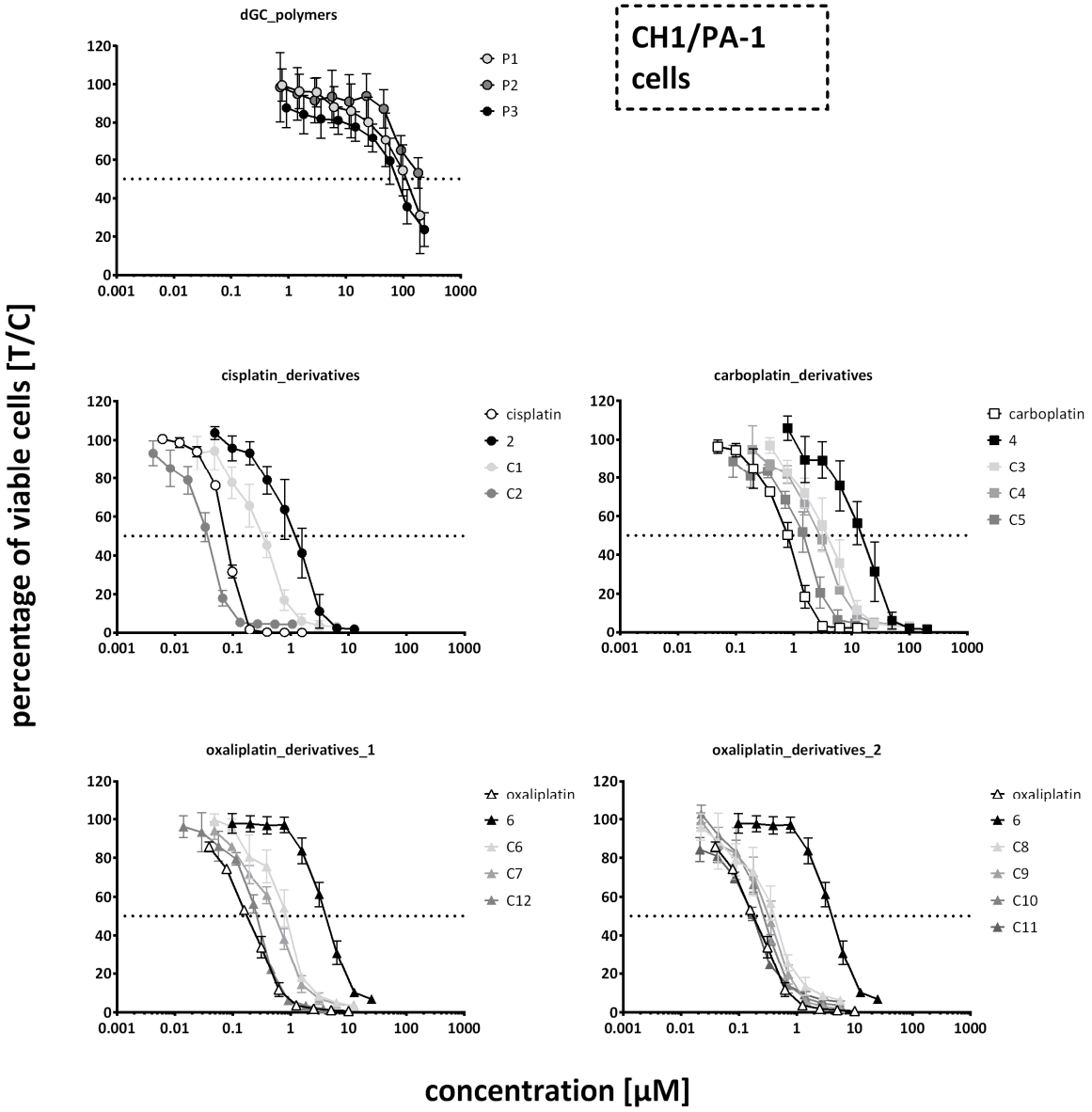

Figure S19. Concentration-effect curves in human cancer cell line CH1/PA-1 in MTT assays.

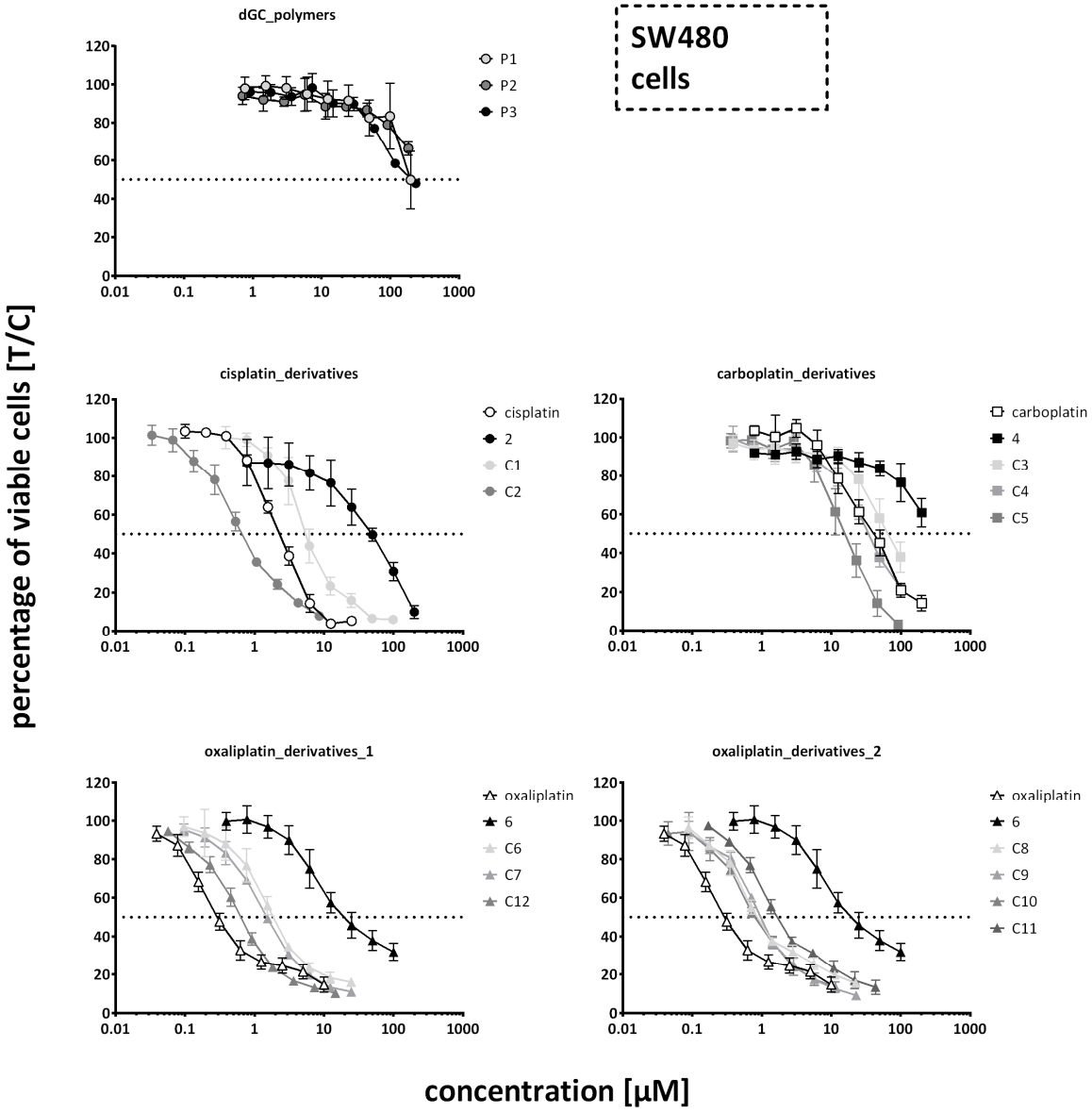

Figure S20. Concentration-effect curves in human cancer cell line SW480 in MTT assays.

5. Solubility data

Table S1. Overview of the water solubility of conjugates **C1**-**C12**, **S1**-**S5**, **V1**-**V3** measured by visual judgement in Milli-Q water at room temperature.

Sample	Pt(IV)	dGC	Water solubility [mg/mL]
C1	**2**	**P1**	>36
C2	**2**	**P2**	~1
C3	**4**	**P1**	>39
C4	**4**	**P1**	~14
C5	**4**	**P2**	~7
C6	**6**	**P1**	>48
C7	**6**	**P1**	>38
C8	**6**	**P2**	>19
C9	**6**	**P2**	>22
C10	**6**	**P2**	>15
C11	**6**	**P2**	~4
C12	**6**	**P3**	~2
S1	**2**	**P3**	<0.5
S2	**2**	**P3**	<0.5
S3	**4**	**P3**	<0.5
S4	**4**	**P3**	<0.5
S5	**6**	**P3**	<0.5
V1	**6**	**P1**	>55
V2	**6**	**P2**	>21
V3	**6**	**P3**	~9

3.2 Quaternary ammonium palmitoyl glycol chitosan (GCPQ) loaded with platinum-based anticancer agents – A novel polymer formulation for anticancer therapy

Yvonne Lerchbammer-Kreith[1], Michaela Hejl[1], Nadine S. Sommerfeld[1], Xian Weng-Jiang[2], Uchechukwu Odunze[2], Ryan D. Mellor[2], David G. Workman[2], Michael A. Jakupec[1,3], Andreas G. Schätzlein[2], Ijeoma F. Uchegbu[2,*], Mathea S. Galanski[1,*] and Bernhard K. Keppler[1,3]

Pharmaceuticals, published on July 19th, 2023

[1] Institute of Inorganic Chemistry, Faculty of Chemistry, University of Vienna, Waehringer Strasse 42, 1090 Vienna, Austria

[2] School of Pharmacy, University College London, Brunswick Square 29-39, London WC1N 1AX, UK

[3] Research Cluster "Translational Cancer Therapy Research", University of Vienna, Waehringer Strasse 42, 1090 Vienna, Austria

[*] Correspondence: ijeoma.uchegbu@ucl.ac.uk (I.F.U.); mathea.galanski@univie.ac.at (M.S.G.)

As first author of the publication, I synthesised and characterised the majority of the polymers (4 out of 5) and conjugates (12 out of 13) and I wrote the majority of the manuscript.

pharmaceuticals

MDPI

Article

Quaternary Ammonium Palmitoyl Glycol Chitosan (GCPQ) Loaded with Platinum-Based Anticancer Agents—A Novel Polymer Formulation for Anticancer Therapy

Yvonne Lerchbammer-Kreith [1], Michaela Hejl [1], Nadine S. Sommerfeld [1], Xian Weng-Jiang [2], Uchechukwu Odunze [2], Ryan D. Mellor [2], David G. Workman [2], Michael A. Jakupec [1,3], Andreas G. Schätzlein [2], Ijeoma F. Uchegbu [2,*], Mathea S. Galanski [1,*] and Bernhard K. Keppler [1,3]

[1] Institute of Inorganic Chemistry, Faculty of Chemistry, University of Vienna, Waehringer Strasse 42, 1090 Vienna, Austria
[2] School of Pharmacy, University College London, Brunswick Square 29-39, London WC1N 1AX, UK
[3] Research Cluster "Translational Cancer Therapy Research", University of Vienna, Waehringer Strasse 42, 1090 Vienna, Austria
* Correspondence: ijeoma.uchegbu@ucl.ac.uk (I.F.U.); mathea.galanski@univie.ac.at (M.S.G.)

Abstract: Quaternary ammonium palmitoyl glycol chitosan (GCPQ) has already shown beneficial drug delivery properties and has been studied as a carrier for anticancer agents. Consequently, we synthesised cytotoxic platinum(IV) conjugates of cisplatin, carboplatin and oxaliplatin by coupling via amide bonds to five GCPQ polymers differing in their degree of palmitoylation and quaternisation. The conjugates were characterised by ^{1}H and ^{195}Pt NMR spectroscopy as well as inductively coupled plasma mass spectrometry (ICP-MS), the latter to determine the amount of platinum(IV) units per GCPQ polymer. Cytotoxicity was evaluated by the MTT assay in three human cancer cell lines (A549, non-small-cell lung carcinoma; CH1/PA-1, ovarian teratocarcinoma; SW480, colon adenocarcinoma). All conjugates displayed a high increase in their cytotoxic activity by factors of up to 286 times compared to their corresponding platinum(IV) complexes and mostly outperformed the respective platinum(II) counterparts by factors of up to 20 times, also taking into account the respective loading of platinum(IV) units per GCPQ polymer. Finally, a biodistribution experiment was performed with an oxaliplatin-based GCPQ conjugate in non-tumour-bearing BALB/c mice revealing an increased accumulation in lung tissue. These findings open promising opportunities for further tumouricidal activity studies especially focusing on lung tissue.

Keywords: platinum(IV) complexes; quaternary ammonium glycol chitosan (GCPQ); anticancer; drug delivery

Citation: Lerchbammer-Kreith, Y.; Hejl, M.; Sommerfeld, N.S.; Weng-Jiang, X.; Odunze, U.; Mellor, R.D.; Workman, D.G.; Jakupec, M.A.; Schätzlein, A.G.; Uchegbu, I.F.; et al. Quaternary Ammonium Palmitoyl Glycol Chitosan (GCPQ) Loaded with Platinum-Based Anticancer Agents—A Novel Polymer Formulation for Anticancer Therapy. *Pharmaceuticals* **2023**, *16*, 1027. https://doi.org/10.3390/ph16071027

Academic Editor: Martina Benešová-Schäfer

Received: 21 June 2023
Revised: 5 July 2023
Accepted: 14 July 2023
Published: 19 July 2023

1. Introduction

Platinum(II) complexes such as the worldwide approved drugs cisplatin, carboplatin and oxaliplatin are first-line anticancer agents against different tumour types and these compounds still play an essential role in modern cancer chemotherapy [1–3]. However, their clinical success is limited due to severe adverse effects such as nephrotoxicity and neurotoxicity as well as intrinsic and acquired therapy resistance [4,5]. The introduction of additional ligands in the axial position leads to platinum(IV) complexes with higher kinetic inertness which enables the promising possibility of overcoming platinum(II)-based drawbacks [6,7]. Platinum(IV) prodrugs demonstrate their cytotoxic activity after the reduction to the corresponding platinum(II) counterparts by releasing their axial ligands [8,9]. Supportive conditions for the required reduction are provided by the acidic and oxygen-deficient milieu of tumour tissue, resulting in a potentially improved selectivity for platinum(IV) complexes towards cancerous tissue [10,11]. Additionally, the octahedral

structure of platinum(IV) agents can be exploited for introducing targeting moieties as well as enabling the fine-tuning of pharmacokinetic properties [12,13].

The attachment of platinum(IV) compounds to different types of nanoparticles via axial ligands is a promising approach for drug delivery purposes [14–16]. In particular, passive tumour targeting by exploiting the enhanced permeability and retention effect (EPR effect) is attracting more and more interest. The EPR effect is a characteristic of tumour tissue based on the existence of large gaps between the endothelial cells in combination with dysfunctional lymphatic drainage. Thereby, the penetration and accumulation in tumour tissue by molecules in the nanometre range is facilitated [17,18].

Promising nanoparticles with excellent drug delivery properties can be found in the class of chitosan, a naturally obtained polysaccharide [19–21]. Chitosan is only soluble at acid pH in aqueous media; however, modifications lead to derivatives such as *N*-palmitoyl-*N*-monomethyl-*N*,*N*-dimethyl-*N*,*N*,*N*-trimethyl-6-*O*-glycolchitosan (GCPQ) which self-assembles in aqueous media into stable colloids [22,23]. As an amphiphile, GCPQ spontaneously forms these micellar nano-sized clusters in aqueous media and is also able to facilitate the aqueous incorporation of lipophilic compounds by effectively solubilising them [24–26]. GCPQ functions as an improved transporter for hydrophobic and amphiphilic agents through the epithelium of the gastrointestinal tract and the cornea as well as to the brain via the nose-to-brain route. Due to the encapsulation inside GCPQ nanoparticles, drug degradation in the gastrointestinal tract can theoretically be prevented [25,27].

GCPQ is a non-toxic carrier that forms particles in the nanometre range; therefore, it is hypothesised that tumour targeting through passive diffusion caused by the EPR effect is possible. Consequently, the use of GCPQ polymers could build the basis for a promising drug delivery strategy for anticancer agents [28]. Recent in vitro experiments with GCPQ micelles serving as nanocarriers for selumetinib (AZD6244), an organic kinase inhibitor and anticancer agent, showed very promising results. In comparison to the free drug, GCPQ-based nanoparticles were superior in monolayer cell culture experiments and tumouroids in spite of their poor diffusion through the tumouroid tissue [29]. Furthermore, the lipophilic anticancer agent etoposide was encapsulated in GCPQ micelles, leading to enhanced cellular uptake in mammary cancer cells. Additionally, biodistribution studies in A431 xenografted mice showed a successful delivery of loaded GCPQ polymers to the solid tumour [30]. Additionally, GCPQ polymers loaded with the anticancer drug doxorubicin showed improved cellular uptake and increased cytotoxic activity compared to free doxorubicin. Furthermore, in vivo studies in a skin tumour model revealed enhanced accumulation in cancerous tissue, detected by fluorescence imaging [31].

Inspired by the promising use of GCPQ micelles as drug delivery systems, we developed and investigated GCPQ polymers loaded with cytotoxic platinum(IV) complexes. In analogy to a previously published study [19], platinum(IV) analogues of cisplatin, carboplatin and oxaliplatin were conjugated via amide bonds to GCPQ nanoparticles, differing in levels of palmitoylation and quaternisation. Characterisation of the conjugates was performed by NMR spectroscopy and inductively coupled plasma mass spectrometry (ICP-MS). IC_{50} values in three different human cancer cell lines were determined via the MTT assay. Finally, the biodistribution of an oxaliplatin-based GCPQ conjugate compared to its carrier-free platinum(IV) counterpart was investigated in non-tumour-bearing mice.

2. Results and Discussion

2.1. Synthesis

The synthesis of GCPQ polymers was conducted according to procedures previously reported (Scheme 1) [24]. Starting from acidic degradation of glycol chitosan (MW ≈ 120 kDa) with hydrochloric acid, the obtained degraded glycol chitosan (dGC) was derivatised by reaction with palmitic acid *N*-hydroxysuccinimide (PNS). The formed palmitoyl glycol chitosan (PGC) was further treated with sodium hydroxide, sodium iodide and methyl iodide under a nitrogen atmosphere in order to produce quaternary ammo-

nium groups. Besides quaternisation, di- and methylamine side chains were additionally formed, whereas some amino groups did not react at all. The corresponding levels of palmitoylation and quaternisation can be controlled by the amount of PNS and methyl iodide as well as reaction time. Consequently, five GCPQ polymers were synthesised, differing by the proportion of palmitoylated and quaternised monomers. These GCPQ polymers were synthesised in order to determine the effects of different palmitoylation and quaternisation levels on cytotoxicity and biodistribution. Polymers with a palmitoylation and quaternisation level of 7% will be described as **GCP7Q7**, whereas in **GCP21Q27**, the level of palmitoylation and quaternisation is 21% and 27%, respectively (Table 1).

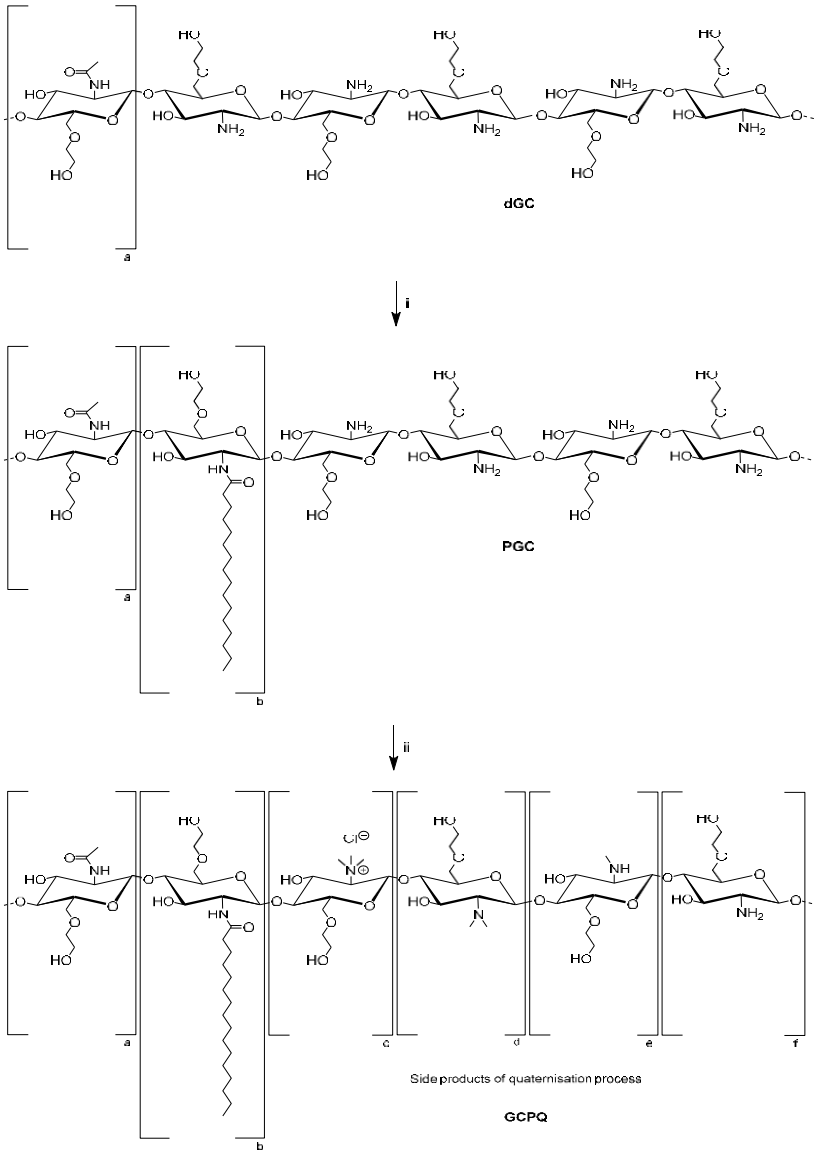

Scheme 1. Synthetic steps for preparation of GCPQ polymers starting from degraded glycol chitosan (dGC), containing approximately 5% of acetylated monomers. (**i**) Palmitic acid *N*-hydroxysuccinimide (PNS), DMSO/triethylamine (TEA), (**ii**) sodium hydroxide, sodium iodide, methyl iodide, *N*-methyl-2-pyrrolidon (NMP), nitrogen atmosphere. Following monomers are shown: (a) acetylated GC, (b) palmitoylated GC, (c) quaternised GC, (d) dimethylamine GC, (e) methylamine GC, (f) GC.

Table 1. Summary of parameters of the five synthesised GCPQ polymers.

Sample	Mol % Palmitoylation	Mol % Quaternisation	QPR *	MW [kDa]
GCP7Q7	7	7	1.0	13.1
GCP8Q10	8	10	1.3	9.6
GCP21Q12	21	12	0.6	12.0
GCP21Q27	21	27	1.3	11.5
GCP22Q33	22	33	1.5	18.0

The following nomenclature is used for the GCPQ polymers: GCPxQy with x = mol % of palmitoylation and y = mol % of quaternisation. * QPR = (mol % quaternisation)/(mol % palmitoylation), parameter for hydrophilicity.

Synthesis of platinum(IV) complexes **1–3** as well as conjugation to GCPQ polymer followed a synthetic pathway published previously [19].

Conjugation of platinum(IV) complexes to GCPQ was performed via amide bond formation between the acid group of platinum(IV) compounds and primary amines of GCPQ polymers, using 1,1^t-carbonyldiimidazole (CDI) as a coupling agent (Scheme 2). The resulting conjugates **C1–C11**, **V1** (Table 2) were dialysed against Milli-Q water, treated with HCl to adjust a pH of approximately 3 and finally obtained by freeze-drying. The complex-to-polymer ratios affected the aqueous solubility of the conjugates; therefore, it was important to avoid an overload of GCPQ polymers with platinum(IV) complexes in order to prevent precipitation of the conjugates.

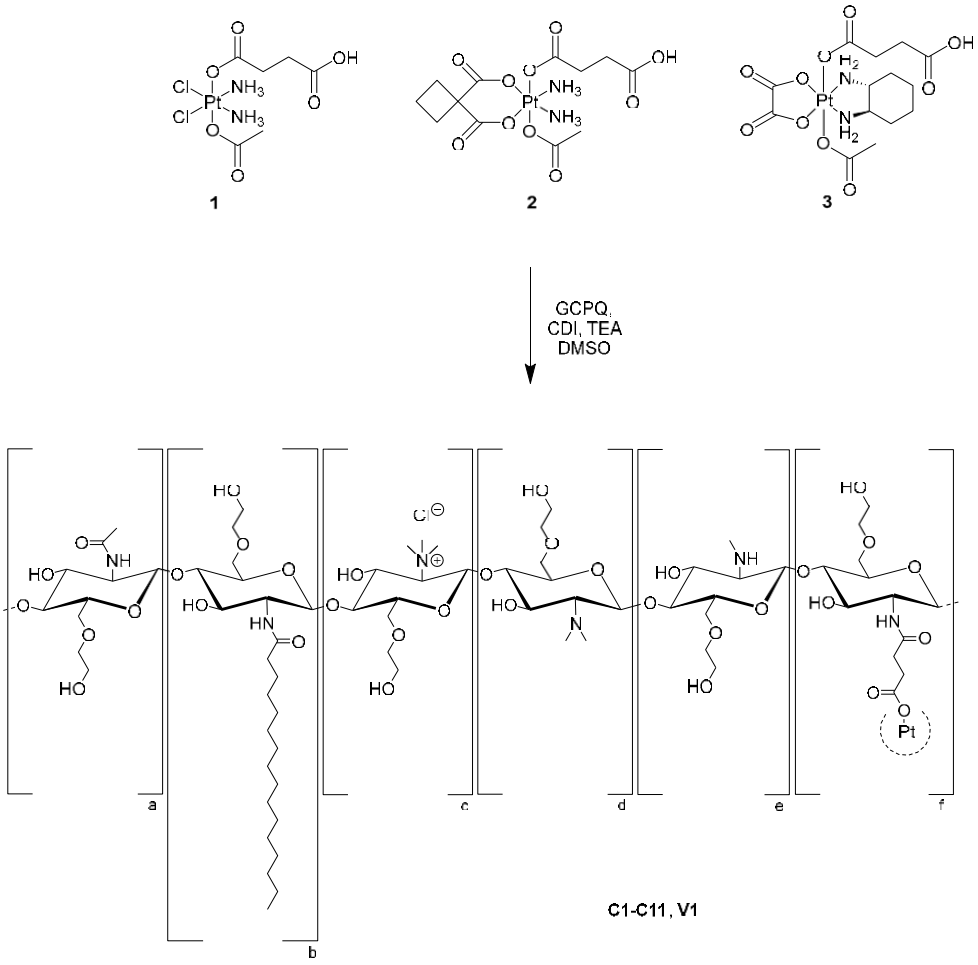

Scheme 2. Illustration of the coupling reaction of platinum(IV) complexes **1–3** to five different GCPQ polymers resulting in conjugates **C1–C11**, **V1**.

Table 2. Overview of the newly developed platinum(IV)-containing conjugates **C1–C11**, **V1**.

Sample	Pt(IV)	GCPQ	Pt(IV) Units Per GCPQ	MW [kDa]
C1	**1**	**GCP7Q7**	3.9	14.9
C2	**1**	**GCP21Q12**	2.5	13.1
C3	**1**	**GCP21Q27**	2.3	12.6
C4	**1**	**GCP22Q33**	5.3	20.5
C5	**2**	**GCP21Q12**	4.6	14.4
C6	**2**	**GCP21Q27**	1.6	12.4
C7	**2**	**GCP22Q33**	7.5	22.0
C8	**3**	**GCP7Q7**	1.7	14.0
C9	**3**	**GCP21Q12**	11.0	18.1
C10	**3**	**GCP21Q27**	7.3	15.6
C11	**3**	**GCP22Q33**	11.0	24.1
V1	**3**	**GCP8Q10**	1.5	10.4

In particular, conjugates containing the cisplatin-based complex **1** as well as the carboplatin-based complex **2** tended to precipitate during the dialysis process. Thus, equivalents of GCPQ polymers were increased to prevent precipitation and significantly improved the solubility of **C1–C6**. Despite increased polymer equivalents, conjugation of complex **2** to **GCP7Q7** could not be successfully performed due to low water solubility and accompanying precipitation during dialysis.

2.2. Analysis

The different levels of palmitoylation and quaternisation of the five synthesised GCPQ polymers were determined via ^{1}H NMR spectroscopy by comparing the ratios of terminal methyl protons of the palmitoyl moiety, the protons of the quaternary ammonium group and protons of the sugar backbone, respectively (Supporting Information, Figure S1) [24]. The synthesised GCPQ polymers featured 7–22 mol % palmitoylation and 7–33 mol % quaternisation, respectively. The molecular weights (MW) of the GCPQ polymers were measured by gel permeation chromatography with multiangle laser light scattering (GPC-MALLS) and they ranged from 9.6 to 18.0 kDa (Table 1).

^{1}H and ^{195}Pt NMR spectra were utilised for characterisation of conjugates **C1–C11**, **V1** confirming the successful attachment of platinum(IV) complexes to the GCPQ polymers. Prominent signals of the acetato ligand of the platinum(IV) complexes were detected in the ^{1}H NMR spectra between 2.03 and 2.12 ppm, as well as multiplets of the succinato ligand between 2.46 and 2.72 ppm. Additionally, peaks, referring to the cyclobutane-1,1-dicarboxylato ligand of carboplatin-based complex **2** as well as the cyclohexane-1,2-diamine ligand of oxaliplatin analogue **3**, were found in the upfield region of the NMR spectra. Characteristic ^{195}Pt signals between 2705 and 3509 ppm further proved the presence of the corresponding platinum(IV) species (Supporting Information, Figures S2–S8). The average platinum(IV) units per GCPQ polymer were calculated based on inductively coupled plasma mass spectrometry (ICP-MS) measurements and were further used for the calculation of molecular weights of the conjugates (Table 2).

Conjugates **C1–C11** displayed a different pattern of solubility, depending on the respective GCPQ polymer and platinum(IV) complex. In general, the following trend in the GCPQ influence could be observed, starting with the highest solubility for conjugates containing: **GCP22Q33** > **GCP21Q27** > **GCP21Q12** > **GCP7Q7**. This observation mostly corresponded to the ratio of the degree of quaternisation to palmitoylation (QPR, Table 1), a parameter for hydrophilicity of GCPQ polymers [25]. Furthermore, conjugates loaded with the oxaliplatin analogue **3** displayed the highest solubility, whereas conjugates featuring cisplatin (**1**) and carboplatin moieties (**2**) were less soluble (Supporting Information, Table S1).

2.3. Cytotoxicity

A comparison of cytotoxic potencies in three human cancer cell lines according to results from the MTT assay after 96 h exposure (Tables 3 and 4, Supporting Information, Figures S9–S12) revealed certain patterns of cytotoxicity: While it has been shown previously that platinum(IV) derivatives of the established platinum(II) drugs show (by 1–2 orders of magnitude) diminished cytotoxicity due to their higher inertness as expected [19], coupling to GCPQ polymers usually compensates for most of this loss, and in the majority of cases even overcompensates it. This effect was most conspicuous for conjugates **C10** and **C11**. Taking into account the loading of approximately 7.3 and 11.0 platinum(IV) units per polymer, respectively, these two products were 96–286 times (Table 4, based on IC_{50} values, depending on the cell line) more potent than platinum(IV) derivative **3**. Additionally, they also outperformed their parent drug oxaliplatin, especially in CH1/PA-1 teratocarcinoma cells (by factors of 6.8 and 9.1) and the colon carcinoma cell line SW480 (by factors of 3.5 and 3.8), the latter representing a malignancy typically treated with this drug.

Table 3. IC_{50} values (means ± standard deviations from at least three independent experiments) of conjugates **C1–C11** as well as their corresponding platinum(II) and platinum(IV) complexes in the three human cancer cell lines according to the MTT assay (96 h exposure).

Sample	Pt(IV)	GCPQ	Pt(IV) Units Per Polymer	IC_{50} [µM] A549	IC_{50} [µM] CH1/PA-1	IC_{50} [µM] SW480
cisplatin [32]	-	-	-	3.8 ± 1.0	0.073 ± 0.001	2.3 ± 0.2
carboplatin [32]	-	-	-	38 ± 3	0.79 ± 0.11	42 ± 10
oxaliplatin [32]	-	-	-	0.98 ± 0.21	0.18 ± 0.01	0.29 ± 0.05
1 [19]	**1**	-	-	99 ± 17	1.2 ± 0.5	47 ± 10
2 [19]	**2**	-	-	>200	16 ± 6	>200
3 [19]	**3**	-	-	70 ± 29	4.1 ± 0.6	22 ± 8
GCP7Q7	-	**GCP7Q7**	-	>12.5	2.4 ± 0.4	5.0 ± 0.6
GCP21Q12 *	-	**GCP21Q12**	-	-	-	-
GCPQ21Q27	-	**GCPQ21Q27**	-	2.2 ± 0.5	1.6 ± 0.1	1.1 ± 0.1
GCP22Q33	-	**GCP22Q33**	-	1.8 ± 0.2	0.95 ± 0.13	0.83 ± 0.08
C1 **	**1**	**GCP7Q7**	3.9	-	-	-
C2	**1**	**GCP21Q12**	2.5	8.7 ± 2.0	0.015 ± 0.005	1.1 ± 0.2
C3	**1**	**GCP21Q27**	2.3	1.3 ± 0.4	0.0046 ± 0.0015	0.12 ± 0.03
C4	**1**	**GCP22Q33**	5.3	1.5 ± 0.4	0.0025 ± 0.0005	0.20 ± 0.04
C5	**2**	**GCP21Q12**	4.6	>12.5	0.25 ± 0.09	1.3 ± 0.1
C6	**2**	**GCP21Q27**	1.6	2.3 ± 0.9	0.028 ± 0.007	1.3 ± 0.2
C7	**2**	**GCP22Q33**	7.5	2.0 ± 0.3	0.018 ± 0.002	0.64 ± 0.13
C8	**3**	**GCP7Q7**	1.7	2.0 ± 0.9	0.040 ± 0.012	0.21 ± 0.03
C9	**3**	**GCP21Q12**	11.0	0.15 ± 0.07	0.0058 ± 0.0016	0.014 ± 0.004
C10	**3**	**GCP21Q27**	7.3	0.10 ± 0.03	0.0036 ± 0.0014	0.011 ± 0.002
C11	**3**	**GCP22Q33**	11.0	0.040 ± 0.011	0.0018 ± 0.0005	0.0070 ± 0.0013

* Could not be determined due to precipitation in the test medium. ** Could not be determined due to insufficient solubility.

Relative to the palpably least potent of the parent drugs, i.e., carboplatin, conjugates **C7** and **C6** performed comparably well (factors of 2.5–8.8, depending on the cell line) or even better (factors of 10.5–20.3), respectively. In two of the three cell lines, however, the performance of these two conjugates may be explained by the cytotoxicity that the unloaded polymers exert by themselves, as reflected in the rather similar IC_{50} values of **C6** and **GCPQ21Q27** as well as **C7** and **GCP22Q33** in A549 and SW480 cells. Generally, substantial but unselective cytotoxic potencies were observed for the three unloaded polymers that were suitable for testing, with IC_{50} values mostly in the low micromolar range and a minor dependency on the cell line (i.e., no hypersensitivity of CH1/PA-1 cells, in contrast to all the platinum-containing substances except for oxaliplatin).

Table 4. Factors of increase (decrease) in cytotoxicity of conjugates **C2–C11** in human cancer cell lines compared to corresponding platinum(II) and (IV) complexes by taking into account the respective number of platinum(IV) units per GCPQ polymer of the conjugates.

	Cytotoxicity Factors Compared to Pt(II)			Cytotoxicity Factors Compared to Pt(IV)		
Sample	**A549**	**CH1/PA-1**	**SW480**	**A549**	**CH1/PA-1**	**SW480**
C2	0.17	1.9	0.81	4.5	32	17
C3	1.3	7.4	8.3	33	121	170
C4	0.48	6.0	2.2	13	98	44
C5	-	0.69	7.1	-	14	34
C6	11	18	20	55	357	97
C7	2.5	5.9	8.8	13	119	42
C8	0.29	2.6	0.81	29	60	62
C9	0.64	2.8	2.0	46	64	150
C10	1.3	6.8	3.5	96	156	265
C11	2.2	9.1	3.8	159	207	286

Nevertheless, most of the other comparisons revealed distinct increases in cytotoxicity as a result of platinum loading. Moreover, the factors by which potencies of conjugates **C8**, **C10** and **C11** exceeded those of the corresponding unloaded polymers (A549: >6.3, 22, 45; CH1/PA-1: 60, 444, 528; SW480: 24, 100, 119 times, respectively) suggest a fairly good correlation with the degree of platinum loading (1.7, 7.3 and 11.0 platinum(IV) units per polymer, respectively). Assessment of correlation remained incomplete, however, because precipitation of **GCP21Q12** in the test medium made a comparison with **C9** impossible.

Based on the promising results, we decided to further investigate an oxaliplatin-based conjugate in vivo due to its favourable combination of solubility and cytotoxicity. Despite accurate controlling of the reaction parameters, the exact resynthesis of GCPQ polymers and the following platinum(IV) loading is challenging. Therefore, conjugate **V1**, a close analogue of **C8**, was synthesised de novo with 1.5 platinum(IV) units per **GCP8Q10** polymer. The cytotoxic activity was tested in the murine mammary carcinoma cell line 4T1, revealing an IC_{50} value in the high nanomolar range (Table 5).

Table 5. IC_{50} value (means ± standard error) of conjugate **V1** in the murine mammary carcinoma cell line 4T1. The IC_{50} value was obtained from 2 independent MTT assays.

Sample	Pt(IV)	GCPQ	Pt(IV) Units Per GCPQ	IC_{50} [µM] 4T1
V1	**3**	**GCP8Q10**	1.51	0.82 ± 0.08

2.4. Biodistribution

In order to obtain a deeper understanding of the target organs for these novel conjugates, biodistribution studies were performed with oxaliplatin analogue **3** in comparison to its conjugate **V1**. Doses of 0.15 mg/100 µL of **3** and 0.95 mg/100 µL of **V1** equivalent to 5.5 mg/kg oxaliplatin were injected intravenously into healthy BALB/c mice. The administered concentration was well tolerated by the mice and did not reveal any signs of gross toxicity. One hour after administration, the major organs were collected and their platinum content was determined via ICP-MS (Figures 1 and 2).

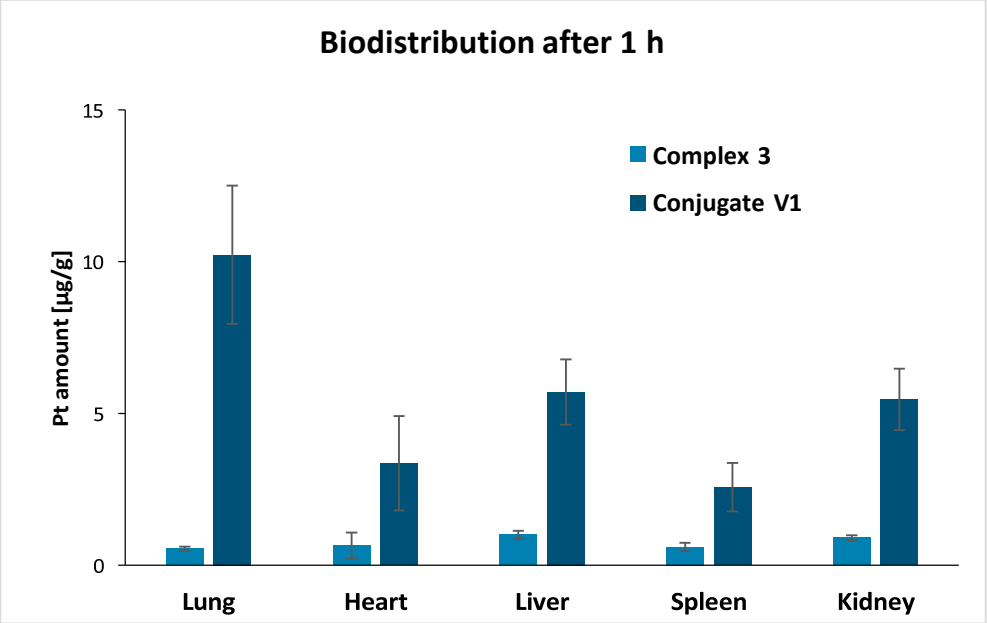

Figure 1. Comparison of the biodistribution investigation of platinum(IV) complex **3** and conjugate **V1** showing the accumulation of platinum in different organs 1 h after administration (complex 3: n = 5, conjugate V1: n = 4). The values are presented as mean ± SD. The data of complex **3** were published previously [19].

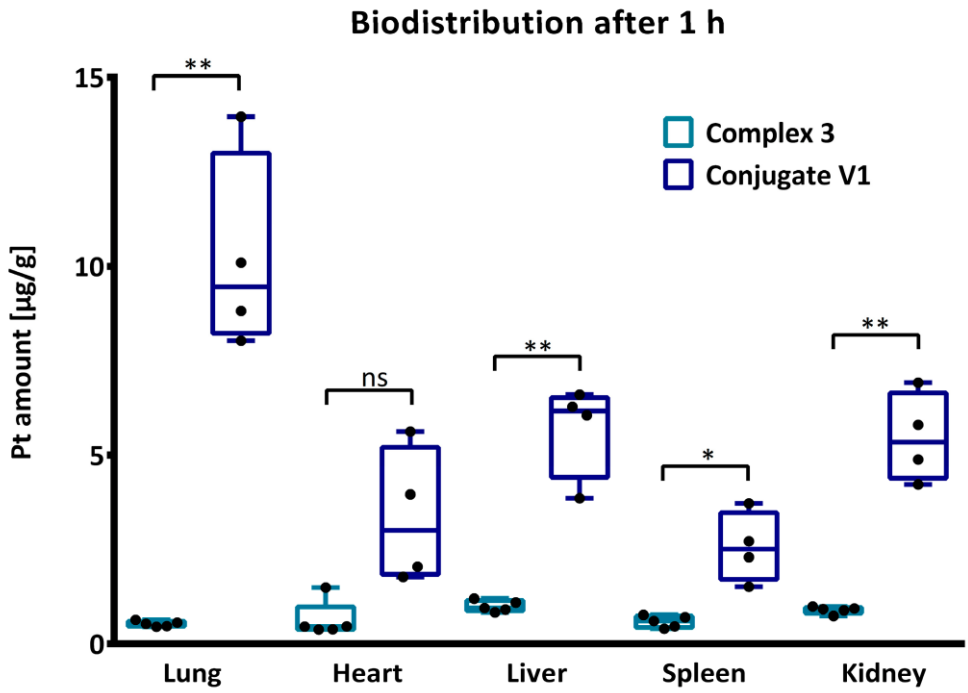

Figure 2. For the biodistribution, unpaired t-test with Welch's correction was conducted for the determination of significances using following abbreviations: ns = not significant, * $p < 0.05$, ** $p < 0.01$. The values are presented as mean ± SEM.

Complex **3** displayed a relatively equal distribution in lung, heart and liver, whereas the highest platinum level was detected in liver followed by kidneys similar to previously reported findings [33]. Contrary, the lung was the significantly preferred organ of conjugate **V1** followed by liver and kidney. Interestingly, the high accumulation in the lung was

not observed in previous biodistribution studies of GCPQ polymers [34,35], enabling interesting opportunities for further investigations.

3. Materials and Methods

3.1. Materials

All solvents and chemicals were acquired from commercial suppliers and were used as received. The following chemicals were used for the synthesis: K_2PtCl_4 (Assay: 46.69% Pt) (Johnson Matthey, Zurich, Switzerland), glycol chitosan (Assay: 78.2%) (Wako, Osaka, Japan), palmitic acid *N*-hydroxysuccinimide (PNS) (99%) (Biosynth Carbosynth, Billingham, UK), *N*-methyl-2-pyrrolidon (NMP) (99%) (Fischer Scientific, Schwerte, Germany), sodium hydroxide (97%) (Sigma-Aldrich, St. Louis, MO, USA), sodium iodide (≥99%) (Acros Organics, Geel, Belgium), methyl iodide (99%) (Thermo Scientific, Budapest, Hungary), carbonyldiimidazole (CDI) (≥97%) (Sigma Aldrich, Steinheim, Germany), Amberlite® IRA-410 chloride form (Sigma Aldrich, Saint-Quentin-Fallavier, France), *tert*-butyl methyl ether (>99.5%) (Fisher Scientific, Svhwerte, Germany), acetone (>99.5%) (Sigma-Aldrich, Saint-Quentin-Fallavier, France), DMSO (>99.8%) (Acros Organics, Geel, Belgium), triethylamine (99%) (Acros Organics, Geel, Belgium). Dialysis tubing (molecular weight cut off (MWCO) = 3.5 kDa) from Medicell Membranes (London, UK) was used for the dialysis of GCPQ polymers, whereas Trial Kit Spectra/Por® 3 (MWCO = 3.5 kDa) dialysis tubing was used for all conjugates and was obtained from Carl Roth (Karlsruhe, Germany). Milli-Q water (18.2 MΩ cm, Milli-Q Advantage) was used for dialysis. Conjugation reactions containing platinum(IV) complexes were performed in darkness with glass coated magnetic stirring bars.

3.2. NMR Spectroscopy

NMR spectroscopy measurements were performed with a Bruker Avance NEO 500 MHz NMR spectrometer at 500.32 (^{1}H) and 107.55 MHz (^{195}Pt) in D_2O at 298 K. ^{1}H NMR spectra were measured relative to the solvent resonance of δ = 4.79 ppm, whereas $K_2[PtCl_4]$ was used as external reference for ^{195}Pt NMR spectra.

3.3. Inductively Coupled Plasma Mass Spectrometry (ICP-MS)

For digestion, the conjugates (0.5–1.5 mg) were dissolved in 2 mL of HNO_3 (20%) and 0.1 mL of H_2O_2 (30%) and heated over a period of 6 h with a temperature-controlled heating plate of graphite from Labter. Dilutions of 1:10,000 were prepared with HNO_3 (3%) for all samples, and afterwards, the total platinum amount was determined with an Agilent 7800 ICP-MS instrument using rhenium as internal reference. Ten replicates for each sample were measured and analysed with the Agilent MassHunter software package (Workstation Software, Version C.01.04, 2018, Agilent, Santa Clara, CA, USA).

3.4. Gel permeation Chromatography Coupled to Multiangle Laser Light Scattering Detector (GPC-MALLS)

The used mobile phase consisted of acetate buffer and methanol (65:35). The acetate buffer (pH = 4) was prepared by dissolving sodium acetate (3.05 g) in 800 mL of H_2O, adjusting the pH with acetic acid (11 mL), and, finally, the volume was made up to 1 L with H_2O. A primary sample was prepared by dissolving the GCPQ samples (25 mg) in mobile phase (2.5 mL) and filtering through a 0.2 µm PTFE syringe filter. For dn/dc determination, primary samples were diluted in mobile phase to concentrations of 0.1, 0.2, 0.3, 0.4, 0.5 and 0.6 mg/mL. Each dilution was then injected directly into the Optilab TrEX, allowing the change in refractive index (dRI) to settle between injections (≈30 s). The experiment was started and ended with an injection of mobile phase to be used as a baseline. For molecular weight determination, the primary sample without dilution (100 µL, 100 µg) was analysed using the mobile phase described above, at a flow rate of 0.7 mL/min, and separated using a PolySep-GFC-P 4000 column fitted with a PolySep-GFC-P guard column. The signal was

detected using DAWN HELEOS II and Optilab TrEX detectors from Wyatt Technology (Cambridge, UK) and analysed using ASTRA software version 5.3.4.14.

3.5. Synthesis

3.5.1. GCPQ Polymers

The degradation of glycol chitosan, as well as the palmitoylation and quaternisation, was adapted according to standard procedures [24]. The levels of palmitoylation and quaternisation were calculated by the comparison of the ratios of palmitoyl methyl protons, quaternary ammonium protons and sugar backbone protons, respectively, by means of ^{1}H NMR spectroscopy.

General Procedure 1: Degradation and Palmitoylation of Glycol Chitosan

Glycol chitosan (MW ≈ 120 kDa) was heated with hydrochloric acid between 14 and 21 h resulting in degraded glycol chitosan (dGC). Afterwards, dGC and palmitic acid *N*-hydroxysuccinimide (PNS) were dissolved in a DMSO/trimethylamine (TEA) mixture and stirred overnight under the absence of light. The formed palmitoyl glycol chitosan (PGC) was precipitated by a mixture of acetone/*tert*-butyl methyl ether (1:2), filtered off and dried under reduced pressure.

1. Palmitoyl glycol chitosan (**P7GC**)

General procedure 1. dGC (15 h) (5.031 g), PNS (591 mg), DMSO + 3.7% TEA (155 mL). Yield: 1.664 g.

2. Palmitoyl glycol chitosan (**P8GC**)

General procedure 1. dGC (21 h) (2.500 g), PNS (328 mg), DMSO + 3.7% TEA (75 mL). Yield: 1.310 g.

3. Palmitoyl glycol chitosan (**P21aGC**)

General procedure 1. dGC (16 h) (5.001 g), PNS (1.760 g), DMSO + 3.7% TEA (155 mL). Yield: 3.084 g.

4. Palmitoyl glycol chitosan (**P21bGC**)

General procedure 1. dGC (15 h) (4.533 g), PNS (1.607 g), DMSO + 3.7% TEA (140 mL). Yield: 5.551 g.

5. Palmitoyl glycol chitosan (**P22GC**)

General procedure 1. dGC (14 h) (5.045 g), PNS (1.695 g), DMSO + 3.7% TEA (156 mL). Yield: 4.529 g.

General Procedure 2: Quaternisation of Palmitoyl Glycol Chitosan

PGC was dissolved in *N*-methyl-2-pyrrolidon (NMP) and sodium hydroxide, sodium iodide and methyl iodide were added under a nitrogen atmosphere. The reaction solution was stirred at 36 °C between 1 and 25 h. The crude GCPQ was precipitated by 0.1 M NaOH and collected via filtration. GCPQ was resuspended in methanol and dialysed (MWCO = 3.5 kDa) against distilled water over 48 h. Afterwards, the product solution was stirred with Amberlite IRA 410 ion exchange resin for approximately 20 min to remove iodide. Amberlite was filtered off and the product containing filtrate was adjusted to pH between 3 and 4 by adding concentrated HCl. Finally, GCPQ was obtained via freeze-drying.

1. Quaternary ammonium palmitoyl glycol chitosan **GCP7Q7**

General procedure 2. **P7GC** (1.664 g), NMP (97 mL), NaOH (225 mg), NaI (259 mg), ICH_3 (2.5 mL), reaction time: 1 h. Yield: 1.434 g. ^{1}H NMR (D_2O): δ = 5.37 + 4.89–5.19 (m, O-C*H*-O, GCPQ backbone), 3.45–4.58 (m, GCPQ backbone), 3.21–3.37 (m, N(CH_3)$_3$, GCPQ), 3.01 + 2.81 (b, N(CH_3)$_2$ and NCH_3, GCPQ), 2.24 (b, (C=O)CH_2, palmitoyl), 1.94–2.07 (m,

acetyl-CH_3, GCPQ), 1.53 (b, (C=O)CH$_2$CH_2, palmitoyl), 1.20 (b, CH_2, palmitoyl), 0.76–0.86 (m, CH_3, palmitoyl) ppm.

2. Quaternary ammonium palmitoyl glycol chitosan **GCP8Q10**

General procedure 2. **P8GC** (1.310 g), NMP (104 mL), NaOH (169 mg), ICH$_3$ (5.0 mL), reaction time: 1 h, precipitated with diethyl ether. Yield: 808 g. ^{1}H NMR (MeOD + 5 µL DCl): δ = 5.40 + 4.70–5.15 (m, O-C*H*-O, GCPQ backbone), 3.50–4.68 (m, GCPQ backbone), 3.31–3.43 (m, N(CH_3)$_3$, GCPQ), 3.00–3.20 (m, N(CH_3)$_2$ and NCH_3, GCPQ), 2.30 (b, (C=O)CH_2, palmitoyl), 2.00–2.12 (m, acetyl-CH_3, GCPQ), 1.63 (b, (C=O)CH$_2$CH_2, palmitoyl), 1.25 (b, CH_2, palmitoyl), 0.85–0.91 (m, CH_3, palmitoyl) ppm.

3. Quaternary ammonium palmitoyl glycol chitosan **GCP21Q12**

General procedure 2. **P21aGC** (3.084 g), NMP (179 mL), NaOH (417 mg), NaI (476 mg), ICH$_3$ (4.6 mL), reaction time: 3 h. Yield: 1.062 g. ^{1}H NMR (MeOD + 5µL DCl): δ = 5.13–5.45 (m, O-C*H*-O, GCPQ backbone), 3.54–4.75 (m, GCPQ backbone), 3.40 (b, N(CH_3)$_3$, GCPQ), 3.14 (b, N(CH_3)$_2$ and NCH_3, GCPQ), 2.30 (b, (C=O)CH_2, palmitoyl), 2.04–2.14 (m, acetyl-CH_3, GCPQ), 1.66 (b, (C=O)CH$_2$CH_2, palmitoyl), 1.33 (b, CH_2, palmitoyl), 0.92 (t, ^{3}J (^{1}H, ^{1}H) = 7.1 Hz, CH_3, palmitoyl) ppm.

4. Quaternary ammonium palmitoyl glycol chitosan **GCP21Q27**

General procedure 2. **P21bGC** (5.551 g), NMP (320 mL), NaOH (750 mg), NaI (855 mg), ICH$_3$ (8.3 mL), reaction time: 4 h. Yield: 3.333 g. ^{1}H NMR (D$_2$O): δ = 5.39 + 5.13 (b, O-C*H*-O, GCPQ backbone), 3.46- 4.42 (m, GCPQ backbone), 3.30 (b, N(CH_3)$_3$, GCPQ), 3.03 (b, N(CH_3)$_2$ and NCH_3, GCPQ), 2.26 (b, (C=O)CH_2, palmitoyl), 1.98–2.07 (m, acetyl-CH_3, GCPQ), 1.56 (b, (C=O)CH$_2$CH_2, palmitoyl), 1.25 (b, CH_2, palmitoyl), 0.86 (b, CH_3, palmitoyl) ppm.

5. Quaternary ammonium palmitoyl glycol chitosan **GCP22Q33**

General procedure 2. **P22GC** (4.529 g), NMP (263 mL), NaOH (611 mg), NaI (701 mg), ICH$_3$ (18.0 mL), reaction time: 25 h. Yield: 2.600 g. ^{1}H NMR (D$_2$O): δ = 5.37 + 5.08 (b, O-C*H*-O, GCPQ backbone), 3.44–4.46 (m, GCPQ backbone), 3.28 (b, N(CH_3)$_3$, GCPQ), 3.01 (b, N(CH_3)$_2$ and NCH_3, GCPQ), 2.25 (b, (C=O)CH_2, palmitoyl), 1.94–2.06 (m, acetyl-CH_3, GCPQ), 1.53 (b, (C=O)CH$_2$CH_2, palmitoyl), 1.22 (b, CH_2, palmitoyl), 0.82 (b, CH_3, palmitoyl) ppm.

3.5.2. Platinum(IV)–GCPQ Conjugates

General Procedure 3: Conjugation of Platinum(IV) Complexes to GCPQ

Synthesis of platinum(IV) complexes **1**–**3** as well as conjugation to the GCPQ polymer was performed according to a procedure published previously [19]. Platinum(IV) complex **1**, **2** or **3** dissolved in DMSO was treated with CDI and stirred for half an hour. In the meantime, a solution of GCPQ dissolved in DMSO and trimethylamine (TEA) was prepared and added to the solution containing the platinum(IV) complex. The mixture was stirred overnight at room temperature. Purification was performed via dialysis against Milli-Q water using dialysis tubing with a MWCO = 3.5 kDa. After the adjustment of a pH of 3 with HCl, the final conjugates were obtained by lyophilisation.

1. Complex **1** coupled to **GCP7Q7** (**C1**)

General procedure 3. **1** (25 mg, 0.05 mmol), CDI (21 mg, 0.13 mmol), **GCP7Q7** (72 mg, 0.0055 mmol), TEA (29 µL, 0.21 mmol). Yield: 65 mg. ICP-MS (Pt): 50.7 g/kg. ^{1}H NMR (D$_2$O): δ = 5.10 (b, O-C*H*-O, GCPQ backbone), 3.60–4.43 (m, GCPQ backbone), 3.30–3.44 (m, N(CH_3)$_3$, GCPQ), 3.09 + 2.89 (b, N(CH_3)$_2$ and NCH_3, GCPQ), 2.68–2.72 (m, CH_2, succinato), 2.62- 2.66 (m, CH_2, succinato), 2.32 (b, (C=O)CH_2, palmitoyl), 2.05–2.16 (m, amide-CH_3, GCPQ), 2.12 (b, CH_3, acetato), 1.62 (b, (C=O)CH$_2$CH_2, palmitoyl), 1.29 (b, CH_2, palmitoyl), 0.85–0.97 (m, CH_3, palmitoyl) ppm. ^{195}Pt NMR (D$_2$O): δ = 2705 ppm.

2. Complex **1** coupled to **GCP21Q12** (**C2**)

General procedure 3. **1** (20 mg, 0.04 mmol), CDI (17 mg, 0.11 mmol), **GCP21Q12** (73 mg, 0.0061 mmol), TEA (23 µL, 0.17 mmol). Yield: 65 mg. ICP-MS (Pt): 37.1 g/kg. ^{1}H NMR (D_2O): δ = 5.14 (b, O-C*H*-O, GCPQ backbone), 3.52–4.53 (m, GCPQ backbone), 3.36 (b, N(CH_3)$_3$, GCPQ), 3.09 (b, N(CH_3)$_2$ and NCH_3, GCPQ), 2.67–2.72 (m, CH_2, succinato)(in part overlapping with DMSO signal), 2.61–2.66 (m, CH_2, succinato), 2.32 (b, (C=O)CH_2, palmitoyl), 2.09–2.15 (m, amide-CH_3, GCPQ), 2.12 (b, CH_3, acetato), 1.62 (b, (C=O)CH$_2$CH_2, palmitoyl), 1.32 (b, CH_2, palmitoyl), 0.92 (b, CH_3, palmitoyl) ppm. ^{195}Pt NMR (D_2O): δ = 2705 ppm.

3. Complex **1** coupled to **GCP21Q27** (**C3**)

General procedure 3. **1** (15 mg, 0.03 mmol), CDI (13 mg, 0.08 mmol), **GCP21Q27** (79 mg, 0.0068 mmol), TEA (17 µL, 0.13 mmol). Yield: 72 mg. ICP-MS (Pt): 34.9 g/kg. ^{1}H NMR (D_2O): δ = 5.43 + 5.15 (b, O-C*H*-O, GCPQ backbone), 3.51–4.56 (m, GCPQ backbone), 3.36 (b, N(CH_3)$_3$, GCPQ), 3.08 (b, N(CH_3)$_2$ and NCH_3, GCPQ), 2.67–2.72 (m, CH_2, succinato), 2.61–2.65 (m, CH_2, succinato), 2.32 (b, (C=O)CH_2, palmitoyl), 2.05–2.16 (m, amide-CH_3, GCPQ), 2.12 (b, CH_3, acetato), 1.63 (b, (C=O)CH$_2$CH_2, palmitoyl), 1.33 (b, CH_2, palmitoyl), 0.93 (b, CH_3, palmitoyl) ppm. ^{195}Pt NMR (D_2O): δ = 2705 ppm.

4. Complex **1** coupled to **GCP22Q33** (**C4**)

General procedure 3. **1** (15 mg, 0.03 mmol), CDI (13 mg, 0.08 mmol), **GCP22Q33** (61 mg, 0.0034 mmol), TEA (17 µL, 0.13 mmol). Yield: 52 mg. ICP-MS (Pt): 50.9 g/kg. ^{1}H NMR (D_2O): δ = 5.45 + 5.13 (b, O-C*H*-O, GCPQ backbone), 3.51–4.54 (m, GCPQ backbone), 3.37 (b, N(CH_3)$_3$, GCPQ), 3.09 (b, N(CH_3)$_2$ and NCH_3, GCPQ), 2.68–2.72 (m, CH_2, succinato), 2.62–2.66 (m, CH_2, succinato), 2.33 (b, (C=O)CH_2, palmitoyl), 2.07–2.15 (m, amide-CH_3, GCPQ), 2.12 (b, CH_3, acetato), 1.63 (b, (C=O)CH$_2$CH_2, palmitoyl), 1.32 (b, CH_2, palmitoyl), 0.93 (b, CH_3, palmitoyl) ppm. ^{195}Pt NMR (D_2O): δ = 2705 ppm.

5. Complex **2** coupled to **GCP21Q12** (**C5**)

General procedure 3. **2** (20 mg, 0.04 mmol), CDI (15 mg, 0.09 mmol), **GCP21Q12** (64 mg, 0.0054 mmol), TEA (21 µL, 0.15 mmol). Yield: 58 mg. ICP-MS (Pt): 62.3 g/kg. ^{1}H NMR (D_2O): δ = 5.45 + 5.18 (b, O-C*H*-O, GCPQ backbone), 3.61–4.42 (m, GCPQ backbone), 3.36 (b, N(CH_3)$_3$, GCPQ), 3.09 (b, N(CH_3)$_2$ and NCH_3, GCPQ), 2.63–2.71 (m, CH_2, succinato; C-CH_2, cyclobutyl), 2.57–2.62 (m, CH_2, succinato), 2.32 (b, (C=O)CH_2, palmitoyl), 2.06–2.10 (m, amide-CH_3, GCPQ), 2.07 (b, CH_3, acetato), 2.03 (p, ^{3}J (^{1}H, ^{1}H = 8.2 Hz), CH_2, cyclobutyl), 1.62 (b, (C=O)CH$_2$CH_2, palmitoyl), 1.30 (b, CH_2, palmitoyl), 0.90 (b, CH_3, palmitoyl) ppm. ^{195}Pt NMR (D_2O): δ = 3509 ppm.

6. Complex **2** coupled to **GCP21Q27** (**C6**)

General procedure 3. **2** (50 mg, 0.09 mmol), CDI (37 mg, 0.23 mmol), **GCP21Q27** (114 mg, 0.0099 mmol), TEA (51 µL, 0.37 mmol). Yield: 106 mg. ICP-MS (Pt): 25.4 g/kg. ^{1}H NMR (D_2O): δ = 5.43 + 5.16 (b, O-C*H*-O, GCPQ backbone), 3.50–4.51 (m, GCPQ backbone), 3.36 (b, N(CH_3)$_3$, GCPQ), 3.09 (b, N(CH_3)$_2$ and NCH_3, GCPQ), 2.63–2.71 (m, CH_2, succinato; C-CH_2, cyclobutyl), 2.57–2.62 (m, CH_2, succinato), 2.32 (b, (C=O)CH_2, palmitoyl), 2.05–2.13 (m, amide-CH_3, GCPQ), 2.07 (b, CH_3, acetato), 2.03 (p, ^{3}J (^{1}H, ^{1}H = 8.2 Hz), CH_2, cyclobutyl), 1.62 (b, (C=O)CH$_2$CH_2, palmitoyl), 1.30 (b, CH_2, palmitoyl), 0.90 (b, CH_3, palmitoyl) ppm. ^{195}Pt NMR (D_2O): δ = 3509 ppm.

7. Complex **2** coupled to **GCP22Q33** (**C7**)

General procedure 3. **2** (35 mg, 0.06 mmol), CDI (26 mg, 0.16 mmol), **GCP22Q33** (62 mg, 0.0034 mmol), TEA (35 µL, 0.26 mmol). Yield: 50 mg. ICP-MS (Pt): 66.1 g/kg. ^{1}H NMR (D_2O): δ = 5.42 + 5.15 (b, O-C*H*-O, GCPQ backbone), 3.49–4.43 (m, GCPQ backbone), 3.34 (b, N(CH_3)$_3$, GCPQ), 3.08 (b, N(CH_3)$_2$ and NCH_3, GCPQ), 2.61–2.69 (m, CH_2, succinato; C-CH_2, cyclobutyl), 2.55–2.60 (m, CH_2, succinato), 2.30 (b, (C=O)CH_2, palmitoyl), 2.03–2.11 (m, amide-CH_3, GCPQ), 2.05 (b, CH_3, acetato), 2.00 (p, ^{3}J (^{1}H, ^{1}H = 8.0 Hz), CH_2, cyclobutyl), 1.60 (b, (C=O)CH$_2$CH_2, palmitoyl), 1.28 (b, CH_2, palmitoyl), 0.89 (b, CH_3, palmitoyl) ppm. ^{195}Pt NMR (D_2O): δ = 3509 ppm.

8. Complex **3** coupled to **GCP7Q7** (**C8**)

General procedure 3. **3** (202 mg, 0.35 mmol), CDI (141 mg, 0.87 mmol), **GCP7Q7** (158 mg, 0.0121 mmol), TEA (193 µL, 1.40 mmol). Yield: 129 mg. ICP-MS (Pt): 23.6 g/kg. ^{1}H NMR (D_2O): δ = 4.91–5.22 (m, O-C*H*-O, GCPQ backbone), 3.44–4.44 (m, GCPQ backbone), 3.24–3.40 (m, N(CH_3)$_3$, GCPQ), 2.92–3.20 (m, C*H*, DACH), 2.82 (m, N(CH_3)$_2$ and NCH_3, GCPQ), 2.52–2.68 (m, CH_2, succinato), 1.98–2.06 (m, CH_2, DACH; (C=O)CH_2, palmitoyl), 2.03 (b, CH_3, acetato; amide-CH_3, GCPQ), 1.47–1.63 (m, CH_2, DACH; (C=O)CH$_2$CH_2, palmitoyl), 1.23 (b, CH_2, palmitoyl; CH_2, DACH), 0.78–0.89 (m, CH_3, palmitoyl) ppm. ^{195}Pt NMR (D_2O): δ = 3213 ppm.

9. Complex **3** coupled to **GCP21Q12** (**C9**)

General procedure 3. **3** (35 mg, 0.06 mmol), CDI (25 mg, 0.15 mmol), **GCP21Q12** (53 mg, 0.0044 mmol), TEA (34 µL, 0.24 mmol). Yield: 42 mg. ICP-MS (Pt): 118.5 g/kg. ^{1}H NMR (D_2O): δ = 3.53–4.36 (m, GCPQ backbone), 3.34 (b, N(CH_3)$_3$, GCPQ), 2.84–3.03 (m, C*H*, DACH), 2.49–2.72 (m, CH_2, succinato; N(CH_3)$_2$ and NCH_3, GCPQ), 2.35–2.45 (m, CH_2, succinato), 2.24–2.35 (m, CH_2, DACH; (C=O)CH_2, palmitoyl), 2.07 (b, CH_3, acetato; amide-CH_3, GCPQ), 1.51–1.74 (m, CH_2, DACH; (C=O)CH$_2$CH_2, palmitoyl), 1.31 (b, CH_2, palmitoyl; CH_2, DACH), 0.83–1.00 (m, CH_3, palmitoyl) ppm. ^{195}Pt NMR (D_2O): δ = 3223 ppm.

10. Complex **3** coupled to **GCP21Q27** (**C10**)

General procedure 3. **3** (30 mg, 0.05 mmol), CDI (21 mg, 0.13 mmol), **GCP21Q27** (65 mg, 0.0056 mmol), TEA (29 µL, 0.21 mmol). Yield: 57 mg. ICP-MS (Pt): 91.6 g/kg. ^{1}H NMR (D_2O): δ = 5.46 (b, O-C*H*-O, GCPQ backbone), 3.54–4.42 (m, GCPQ backbone), 3.35 (b, N(CH_3)$_3$, GCPQ), 2.84–3.01 (m, C*H*, DACH), 2.55–2.66 (m, CH_2, succinato), 2.51 (b, N(CH_3)$_2$ and NCH_3, GCPQ), 2.36–2.45 (m, CH_2, succinato), 2.24–2.35 (m, CH_2, DACH; (C=O)CH_2, palmitoyl), 2.04–2.14 (m, amide-CH_3, GCPQ), 2.07 (b, CH_3, acetato), 1.52–1.73 (m, CH_2, DACH; (C=O)CH$_2$CH_2, palmitoyl), 1.33 (b, CH_2, palmitoyl; CH_2, DACH), 0.93 (b, CH_3, palmitoyl) ppm. ^{195}Pt NMR (D_2O): δ = 3223 ppm.

11. Complex **3** coupled to **GCP22Q33** (**C11**)

General procedure 3. **3** (29 mg, 0.05 mmol), CDI (18 mg, 0.11 mmol), **GCP22Q33** (51 mg, 0.0028 mmol), TEA (24 µL, 0.17 mmol). Yield: 41 mg. ICP-MS (Pt): 88.7 g/kg. ^{1}H NMR (D_2O): δ = 5.44 (b, O-C*H*-O, GCPQ backbone), 3.49–4.43 (m, GCPQ backbone), 3.34 (b, N(CH_3)$_3$, GCPQ), 2.84–3.01 (m, C*H*, DACH), 2.55–2.65 (m, CH_2, succinato), 2.51 (b, N(CH_3)$_2$ and NCH_3, GCPQ), 2.36–2.43 (m, CH_2, succinato), 2.25–2.34 (m, CH_2, DACH; (C=O)CH_2, palmitoyl), 2.04–2.13 (m, amide-CH_3, GCPQ), 2.07 (b, CH_3, acetato), 1.53–1.73 (m, CH_2, DACH; (C=O)CH$_2$CH_2, palmitoyl), 1.32 (b, CH_2, palmitoyl; CH_2, DACH), 0.92 (b, CH_3, palmitoyl) ppm. ^{195}Pt NMR (D_2O): δ = 3223 ppm.

12. Complex **3** coupled to **GC8P10** (**V1**)

General procedure 3. **3** (78 mg, 0.14 mmol), CDI (46 mg, 0.29 mmol), **GCP8Q10** (74 mg, 0.0077 mmol), TEA (38 µL, 0.27 mmol). Yield: 25 mg. ICP-MS (Pt): 28.5 g/kg. ^{1}H NMR (MeOD): δ = 5.21 (b, O-C*H*-O, GCPQ backbone), 3.54–4.32 (m, GCPQ backbone), 3.37 (b, N(CH_3)$_3$, GCPQ), 2.86–3.14 (m, N(CH_3)$_2$ and NCH_3, GCPQ; C*H*, DACH), 2.52–2.74 (m, CH_2, succinato), 2.19–2.37 (m, CH_2, DACH; (C=O)CH_2, palmitoyl), 1.98–2.08 (m, amide-CH_3, GCPQ), 1.99 (b, CH_3, acetato), 1.56–1.74 (m, CH_2, DACH; (C=O)CH$_2$CH_2, palmitoyl), 1.32 (b, CH_2, palmitoyl; CH_2, DACH), 0.90 (t, ^{3}J (^{1}H, ^{1}H) = 7.2 Hz, CH_3, palmitoyl) ppm.

3.6. Cytotoxicity Tests

The MTT assay (96 h exposure time) in the human cancer cell lines SW480 (colon carcinoma), CH1/PA-1 (ovarian teratocarcinoma) and A549 (non-small-cell lung cancer) was performed as described in [32], with the exception that conjugates were dissolved either in supplemented MEM or sterile water and then serially diluted in the former medium. These cell lines were chosen to represent three malignancies that are clinical indications for platinum drugs on the one hand but possess different chemosensitivity profiles on the

other, with CH1/PA-1 cells being broadly sensitive, SW480 (expressing P-glycoprotein) intermediately sensitive and A549 (expressing ABC transporters other than P-glycoprotein) multidrug-resistant, reflecting a different demand for improved platinum-based therapies in these malignancies. A description of the conducted MTT assay in the cancer cell line 4T1 (mammary carcinoma, 24 h exposure time) can be found in [19].

3.7. Biodistribution Studies

The Animal Welfare and Ethical Review Body at University College London (UCL) approved all animal experiments performed according to the Home Office Animals Scientific Procedures Act, 1986, United Kingdom. Non-tumour-bearing female BALB/c mice (20–22.5 g) (Harlan, UK) were used for the biodistribution of the oxaliplatin-based GCPQ conjugate and the free platinum(IV) complex **3**. Four to five mice per group were treated with doses of 0.15 mg/100 µL of complex **3** and 0.95 mg/100 µL of conjugate **V1** equivalent to 5.5 mg/kg oxaliplatin. The compounds were injected intravenously into the tail vein (100 µL/20 g body weight). After 1 h, heart, spleen, lung, liver and kidneys were removed, stored under liquid nitrogen and their platinum amount was detected via ICP-MS at the Institute of Inorganic Chemistry of the University of Vienna. For statistical analysis the *t*-test with Welsh's correction was implemented in GraphPad Prism software (Version 6.01). Testing for normal distribution was not possible due to the small sample number (n = 4–5). The values are presented as mean ± SEM.

4. Conclusions

The conjugation of platinum(IV) analogues of cisplatin, carboplatin and oxaliplatin to GCPQ polymers differing in levels of palmitoylation and quaternisation led to a series of twelve novel conjugates with IC_{50} values in the low micromolar to nanomolar range. Remarkably, the conjugates featured higher antiproliferative activity compared to the respective platinum(IV) complex and most of the conjugates even outperformed the cytotoxicity of their corresponding platinum(II) precursors. Notably, increased cytotoxicity of factors up to 11 and 159 compared to platinum(II) and (IV) complexes, respectively, could additionally be observed in the multidrug-resistant non-small-cell lung cancer cell line A549. As a next step, investigations in other cancer cell lines, especially platinum(II)-resistant ones, could further disclose the full potential of platinum(IV)-based GCPQ-conjugates. Furthermore, a biodistribution study in non-tumour-bearing BALB/c mice was conducted with an oxaliplatin-based GCP8Q10 conjugate. The increased accumulation of the conjugate in the lung in comparison to the unloaded platinum(IV) complex combined with increased cytotoxicity in non-small-cell lung cancer cell line A549 revealed promising results for further activity experiments, especially with respect to different lung cancer types and lung metastases. In order to determine the potential of platinum(IV)-based GCPQ conjugates as a favourable new cancer treatment approach, additional investigations of their stability as well as pharmacokinetics and pharmacodynamics could provide clarification of therapeutic benefits and potential side effects. Finally, studies of GCPQ as a drug delivery system for platinum(IV) complexes or combined with other anticancer agents (e.g., doxorubicin) could further result in promising approaches for future cancer treatments.

Supplementary Materials: The following supporting information can be downloaded at: https://www.mdpi.com/article/10.3390/ph16071027/s1, Figure S1: ^{1}H NMR spectrum of polymer **GCP21Q12**; Figure S2: ^{1}H NMR spectrum of conjugate **C2**; Figure S3: ^{195}Pt NMR spectrum of conjugate **C2**; Figure S4: ^{1}H NMR spectrum of conjugate **C6**; Figure S5: ^{195}Pt NMR spectrum of conjugate **C6**; Figure S6: ^{1}H NMR spectrum of conjugate **C11**; Figure S7: ^{195}Pt NMR spectrum of conjugate **C11**; Figure S8: ^{1}H NMR spectra of **3**, **C11** and **GCP22Q33**; Figure S9: Concentration–effect curves of **GCP7Q7** and **C8** in A549, CH1/PA-1 and SW480 cells; Figure S10: Concentration–effect curves of **GCPQ21Q27**, **C3**, **C6** and **C10** in A549, CH1/PA-1 and SW480 cells; Figure S11: Concentration–effect curves of **GCP22Q33**, **C4**, **C7** and **C11** in A549, CH1/PA-1 and SW480 cells; Figure S12: Concentration–effect curves of **C2**, **C5** and **C9** in A549, CH1/PA-1 and SW480 cells; Table S1: Overview of the water solubility of conjugates **C1–C11**.

Author Contributions: Conceptualization, Y.L.-K., N.S.S., I.F.U. and M.S.G.; Methodology, Y.L.-K., N.S.S., I.F.U. and M.S.G.; Validation, Y.L.-K., M.H., U.O., M.A.J., I.F.U. and M.S.G.; Formal analysis, Y.L.-K., M.H., N.S.S. and U.O.; Investigation, Y.L.-K., M.H., N.S.S., X.W.-J., U.O., R.D.M. and D.G.W.; Resources, M.A.J., A.G.S., I.F.U., M.S.G. and B.K.K.; Data curation, Y.L.-K., M.H., N.S.S., X.W.-J., U.O., R.D.M., D.G.W. and M.A.J.; Writing—original draft preparation, Y.L.-K. and M.A.J.; Writing—review and editing, Y.L.-K., M.H., N.S.S., X.W.-J., U.O., R.D.M., D.G.W., M.A.J., A.G.S., I.F.U., M.S.G. and B.K.K.; Visualization, Y.L.-K., N.S.S. and M.A.J.; Supervision, M.A.J., A.G.S., I.F.U., M.S.G. and B.K.K.; Project administration, Y.L.-K., I.F.U. and M.S.G.; Funding acquisition, Y.L.-K., A.G.S., I.F.U., M.S.G. and B.K.K. All authors have read and agreed to the published version of the manuscript.

Funding: The presented work was supported by the Hochschuljubiläumsfonds of the City of Vienna, Austria, under the project number H-320163/2018, which is gratefully acknowledged.

Institutional Review Board Statement: The animal study protocol was approved by the Ethics Committee of University College London (project license PPL 70/8224 approved in October 2014), and the studies were performed in accordance with the UK Animals (Scientific Procedures) Act 1986.

Informed Consent Statement: Not applicable.

Data Availability Statement: The data presented in this study are available in the article and in the Supplementary Materials.

Acknowledgments: The authors gratefully acknowledge the support of Klaudia Cseh, Sophie Neumayer, Tatjana Schafarik and Martin Schaier. Open Access Funding by the University of Vienna.

Conflicts of Interest: The authors declare no conflict of interest.

References

1. Živkovic´, M.D.; Kljun, J.; Ilic-Tomic, T.; Pavic, A.; Veselinovic´, A.; Manojlovic´, D.D.; Nikodinovic-Runic, J.; Turel, I. A New Class of Platinum(II) Complexes with the Phosphine Ligand Pta Which Show Potent Anticancer Activity. *Inorg. Chem. Front.* **2018**, *5*, 39–53. [CrossRef]
2. Ramu, V.; Gill, M.R.; Jarman, P.J.; Turton, D.; Thomas, J.A.; Das, A.; Smythe, C. A Cytostatic Ruthenium(II)-Platinum(II) Bis(Terpyridyl) Anticancer Complex That Blocks Entry into S Phase by up-Regulating P27KIP1. *Chem. A Eur. J.* **2015**, *21*, 9185–9197. [CrossRef]
3. Ghosh, S. Cisplatin: The First Metal Based Anticancer Drug. *Bioorg. Chem.* **2019**, *88*, 102925. [CrossRef]
4. Oun, R.; Moussa, Y.E.; Wheate, N.J. The Side Effects of Platinum-Based Chemotherapy Drugs: A Review for Chemists. *Dalton Trans.* **2018**, *47*, 6645. [CrossRef]
5. Deo, K.M.; Ang, D.L.; McGhie, B.; Rajamanickam, A.; Dhiman, A.; Khoury, A.; Holland, J.; Bjelosevic, A.; Pages, B.; Gordon, C.; et al. Platinum Coordination Compounds with Potent Anticancer Activity. *Coord. Chem. Rev.* **2018**, *375*, 148–163. [CrossRef]
6. Gibson, D. Platinum(IV) Anticancer Agents; Are We En Route to the Holy Grail or to a Dead End? *J. Inorg. Biochem.* **2021**, *217*, 111353. [CrossRef]
7. Marotta, C.; Giorgi, E.; Binacchi, F.; Cirri, D.; Gabbiani, C.; Pratesi, A. An Overview of Recent Advancements in Anticancer Pt(IV) Prodrugs: New Smart Drug Combinations, Activation and Delivery Strategies. *Inorg. Chim. Acta* **2023**, *548*, 121388. [CrossRef]
8. Wexselblatt, E.; Gibson, D. What Do We Know about the Reduction of Pt(IV) pro-Drugs? *J. Inorg. Biochem.* **2012**, *117*, 220–229. [CrossRef]
9. Xu, Z.; Wang, Z.; Deng, Z.; Zhu, G. Recent Advances in the Synthesis, Stability, and Activation of Platinum(IV) Anticancer Prodrugs. *Coord. Chem. Rev.* **2021**, *442*, 213991. [CrossRef]
10. Gibson, D. Platinum(IV) Anticancer Prodrugs-Hypotheses and Facts. *Dalton Trans.* **2016**, *45*, 12983–12991. [CrossRef]
11. Ritacco, I.; Mazzone, G.; Russo, N.; Sicilia, E. Investigation of the Inertness to Hydrolysis of Platinum(IV) Prodrugs. *Inorg. Chem.* **2016**, *55*, 1580–1586. [CrossRef] [PubMed]
12. Kenny, R.G.; Chuah, S.W.; Crawford, A.; Marmion, C.J. Platinum(IV) Prodrugs—A Step Closer to Ehrlich's Vision? *Eur. J. Inorg. Chem.* **2017**, *2017*, 1596–1612. [CrossRef]
13. Hall, M.D.; Mellor, H.R.; Callaghan, R.; Hambley, T.W. Basis for Design and Development of Platinum(IV) Anticancer Complexes. *J. Med. Chem.* **2007**, *50*, 3403–3411. [CrossRef]
14. Han, X.; Sun, J.; Wang, Y.; He, Z. Recent Advances in Platinum (IV) Complex-Based Delivery Systems to Improve Platinum (II) Anticancer Therapy. *Med. Res. Rev.* **2015**, *35*, 1268–1299. [CrossRef] [PubMed]
15. Zhong, Y.; Jia, C.; Zhang, X.; Liao, X.; Yang, B.; Cong, Y.; Pu, S.; Gao, C. Targeting Drug Delivery System for Platinum(IV)-Based Antitumor Complexes. *Eur. J. Med. Chem.* **2020**, *194*, 112229. [CrossRef]
16. Jia, C.; Deacon, G.B.; Zhang, Y.; Gao, C. Platinum(IV) Antitumor Complexes and Their Nano-Drug Delivery. *Coord. Chem. Rev.* **2021**, *429*, 213640. [CrossRef]
17. Subhan, M.A.; Yalamarty, S.S.K.; Filipczak, N.; Parveen, F.; Torchilin, V.P. Recent Advances in Tumor Targeting via Epr Effect for Cancer Treatment. *J. Pers. Med.* **2021**, *11*, 571. [CrossRef]

18. Shi, Y.; van der Meel, R.; Chen, X.; Lammers, T. The EPR Effect and beyond: Strategies to Improve Tumor Targeting and Cancer Nanomedicine Treatment Efficacy. *Theranostics* **2020**, *10*, 7921–7924. [CrossRef] [PubMed]
19. Lerchbammer-Kreith, Y.; Sommerfeld, N.S.; Cseh, K.; Weng-Jiang, X.; Odunze, U.; Schätzlein, A.G.; Uchegbu, I.F.; Galanski, M.S.; Jakupec, M.A.; Keppler, B.K. Platinum(IV)-Loaded Degraded Glycol Chitosan as Efficient Platinum(IV) Drug Delivery Platform. *Pharmaceutics* **2023**, *15*, 1050. [CrossRef]
20. Shukla, S.K.; Mishra, A.K.; Arotiba, O.A.; Mamba, B.B. Chitosan-Based Nanomaterials: A State-of-the-Art Review. *Int. J. Biol. Macromol.* **2013**, *59*, 46–58. [CrossRef]
21. Martau, G.A.; Mihai, M.; Vodnar, D.C. The Use of Chitosan, Alginate, and Pectin in the Biomedical and Food Sector-Biocompatibility, Bioadhesiveness, and Biodegradability. *Polymers* **2019**, *11*, 1837. [CrossRef] [PubMed]
22. Trapani, A.; Sitterberg, J.; Bakowsky, U.; Kissel, T. The Potential of Glycol Chitosan Nanoparticles as Carrier for Low Water Soluble Drugs. *Int. J. Pharm.* **2009**, *375*, 97–106. [CrossRef] [PubMed]
23. Ryu, J.H.; Yoon, H.Y.; Sun, I.C.; Kwon, I.C.; Kim, K. Tumor-Targeting Glycol Chitosan Nanoparticles for Cancer Heterogeneity. *Adv. Mater.* **2020**, *32*, 2002197. [CrossRef] [PubMed]
24. Uchegbu, I.F.; Sadiq, L.; Arastoo, M.; Gray, A.I.; Wang, W.; Waigh, R.D.; Schätzlein, A.G. Quaternary Ammonium Palmitoyl Glycol Chitosan-a New Polysoap for Drug Delivery. *Int. J. Pharm.* **2001**, *224*, 185–199. [CrossRef] [PubMed]
25. Odunze, U.; O'Brien, F.; Godfrey, L.; Schätzlein, A.; Uchegbu, I. Unusual Enthalpy Driven Self Assembly at Room Temperature with Chitosan Amphiphiles. *Pharm. Nanotechnol.* **2019**, *7*, 57–71. [CrossRef]
26. Qu, X.; Khutoryanskiy, V.V.; Stewart, A.; Rahman, S.; Papahadjopoulos-Sternberg, B.; Dufes, C.; McCarthy, D.; Wilson, C.G.; Lyons, R.; Carter, K.C.; et al. Carbohydrate-Based Micelle Clusters Which Enhance Hydrophobic Drug Bioavailability by up to 1 Order of Magnitute. *Biomacromolecules* **2006**, *7*, 3452–3459. [CrossRef]
27. Chong, W.M.; Kadir, E.A. A Brief Review on Hydrophobic Modifications of Glycol Chitosan into Amphiphilic Nanoparticles for Enhanced Drug Delivery. *Sains Malays.* **2021**, *50*, 3693–3703. [CrossRef]
28. Kanwal, U.; Bukhari, N.I.; Raza, A.; Hussain, K.; Abbas, N. *Quaternary Ammonium Palmitoyl Glycol Chitosan-Based Nano-Doxorubicin Delivery System: Potential Applications for Cancer Treatment and Theranostic*; MedDocs Publishers LLC.: Reno, NV, USA, 2019.
29. López-Dávila, V.; Magdeldin, T.; Welch, H.; Dwek, M.V.; Uchegbu, I.; Loizidou, M. Efficacy of DOPE/DC-Cholesterol Liposomes and GCPQ Micelles as AZD6244 Nanocarriers in a 3D Colorectal Cancer in Vitro Model. *Nanomedicine* **2016**, *11*, 331–344. [CrossRef]
30. Raza, A.; de la Fuente, M.; Uchegbu, I.F.; Schätzlein, A. Modified Glycol Chitosan Nanocarriers Carry Hydrophobic Materials into Tumours. *Nanotechnology* **2010**, *3*, 350–353.
31. Kanwal, U.; Bukhari, N.I.; Rana, N.F.; Rehman, M.; Hussain, K.; Abbas, N.; Mehmood, A.; Raza, A. Doxorubicin-Loaded Quaternary Ammonium Palmitoyl Glycol Chitosan Polymeric Nanoformulation: Uptake by Cells and Organs. *Int. J. Nanomed.* **2019**, *14*, 1–15. [CrossRef]
32. Cseh, K.; Geisler, H.; Stanojkovska, K.; Westermayr, J.; Brunmayr, P.; Wenisch, D.; Gajic, N.; Hejl, M.; Schaier, M.; Koellensperger, G.; et al. Arene Variation of Highly Cytotoxic Tridentate Naphthoquinone-Based Ruthenium(II) Complexes and In-Depth In Vitro Studies. *Pharmaceutics* **2022**, *14*, 2466. [CrossRef] [PubMed]
33. Göschl, S.; Schreiber-Brynzak, E.; Pichler, V.; Cseh, K.; Heffeter, P.; Jungwirth, U.; Jakupec, M.A.; Berger, W.; Keppler, B.K. Comparative Studies of Oxaliplatin-Based Platinum(IV) Complexes in Different in Vitro and in Vivo Tumor Models. *Metallomics* **2017**, *9*, 309–322. [CrossRef] [PubMed]
34. Lalatsa, A.; Lee, V.; Malkinson, J.P.; Zloh, M.; Schätzlein, A.G.; Uchegbu, I.F. A Prodrug Nanoparticle Approach for the Oral Delivery of a Hydrophilic Peptide, Leucine5-Enkephalin, to the Brain. *Mol. Pharm.* **2012**, *9*, 1665–1680. [CrossRef] [PubMed]
35. Zia, N.; Iqbal, Z.; Raza, A.; Zia, A.; Shafique, R.; Andleeb, S.; Walker, G.C. Glycol-Chitosan-Based Technetium-99m-Loaded Multifunctional Nanomicelles: Synthesis, Evaluation, and In Vivo Biodistribution. *Nanomaterials* **2022**, *12*, 2198. [CrossRef]

Supporting Information

Quaternary ammonium palmitoyl glycol chitosan (GCPQ) loaded with platinum-based anticancer agents – a novel polymer formulation for anticancer therapy

Yvonne Lerchbammer-Kreith [1], Michaela Hejl [1], Nadine S. Sommerfeld [1], Xian Weng-Jiang [2], Uchechukwu Odunze [2], Ryan D. Mellor [2], David G. Workman [2],Michael A. Jakupec[1,3], Andreas G. Schätzlein [2], Ijeoma F. Uchegbu [2,*], Mathea S. Galanski [1,*], Bernhard K. Keppler [1,3]

[1]University of Vienna, Faculty of Chemistry, Institute of Inorganic Chemistry, Waehringer Strasse 42, 1090 Vienna, Austria

[2]University College London, School of Pharmacy, Brunswick Square 29-39, WC1N 1AX London, United Kingdom

[3]Research Cluster "Translational Cancer Therapy Research", University of Vienna, Waehringer Strasse 42, 1090 Vienna, Austria

*Corresponding authors: E-mail addresses: ijeoma.uchegbu@ucl.ac.uk (I.F.U.); mathea.galanski@univie.ac.at (M.S.G.)

Table of Contents

1. ^{1}H NMR spectrum of GCPQ polymer

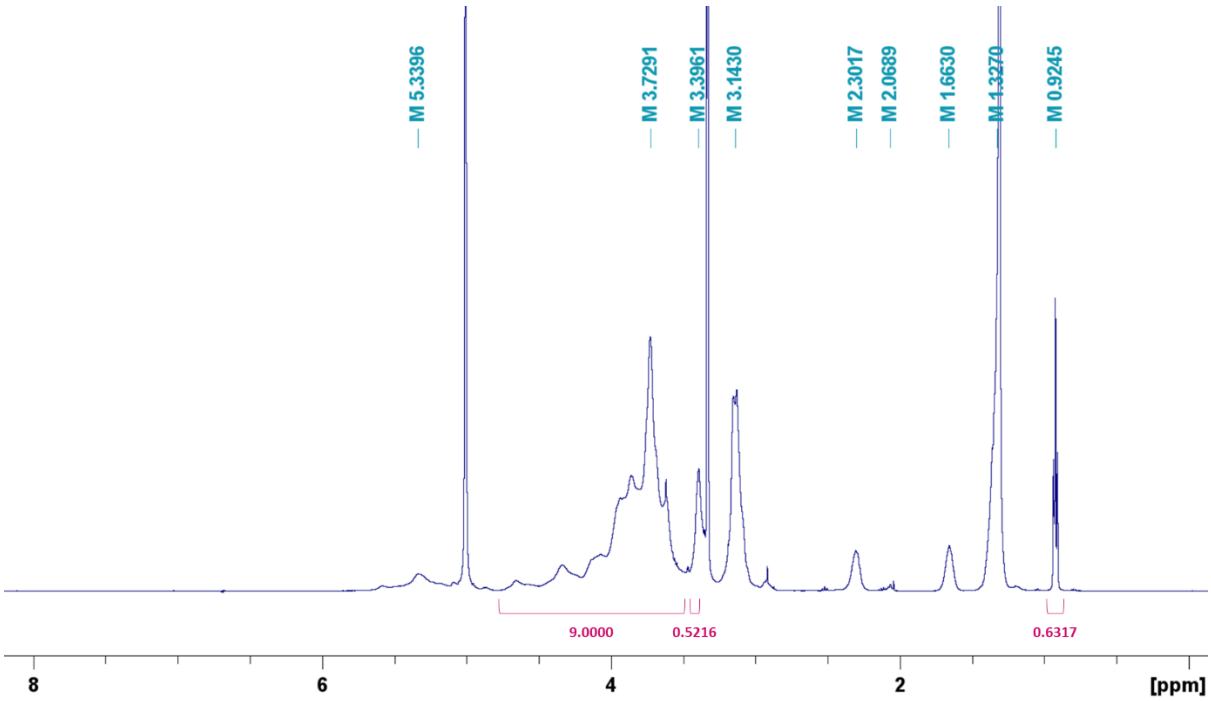

Figure S1. ^{1}H NMR spectrum of polymer **GCP21Q12** in MeOD + 5µL DCl. The levels of palmitoylation and quaternisation were estimated by comparison of the integrals of palmitoyl methyl protons (0.92 ppm, 3H), quaternary ammonium protons (3.40 ppm, 9H, due to the partly overlapping MeOD signal, only half of the quaternary ammonium signal was integrated and accounted as 4.5 protons, provided a symmetrical resonance) and sugar backbone protons (3.54–4.75 ppm, 9H), respectively [1] .

2. Selected NMR spectra of conjugates

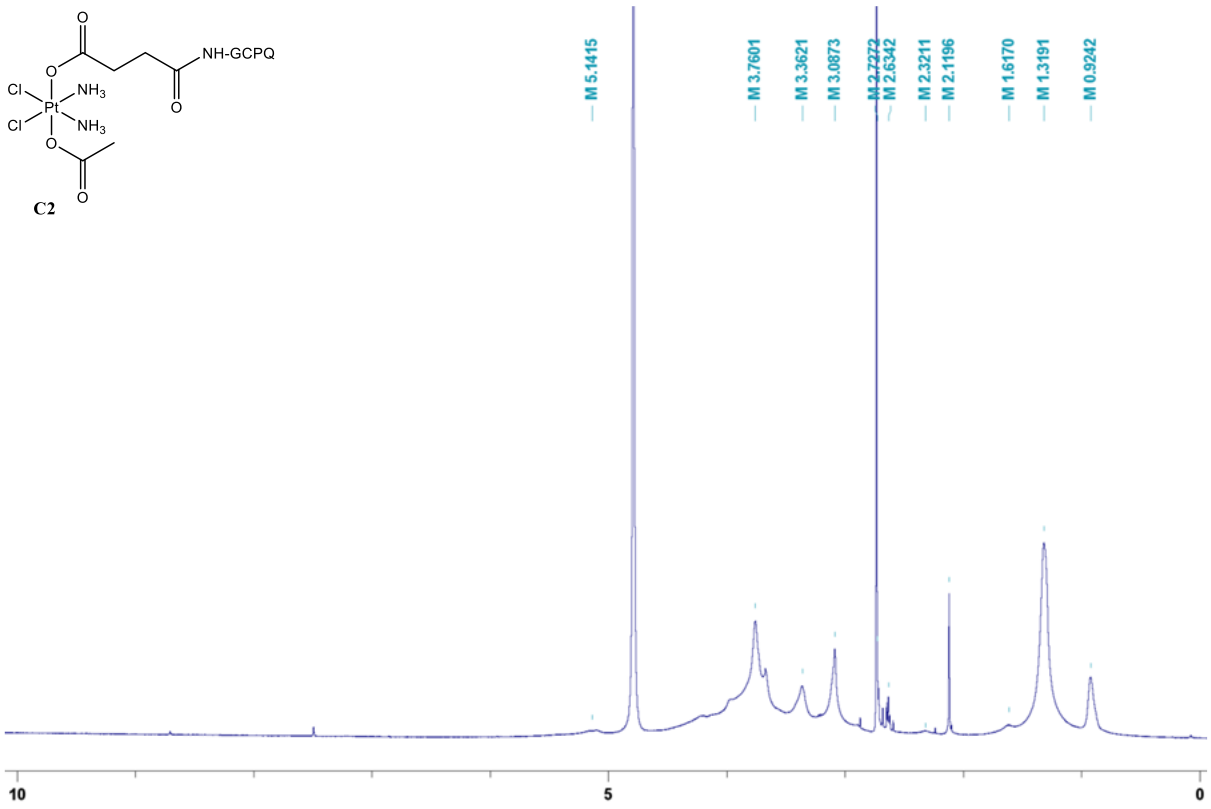

Figure S2. ^{1}H NMR spectrum of conjugate **C2** in D_2O

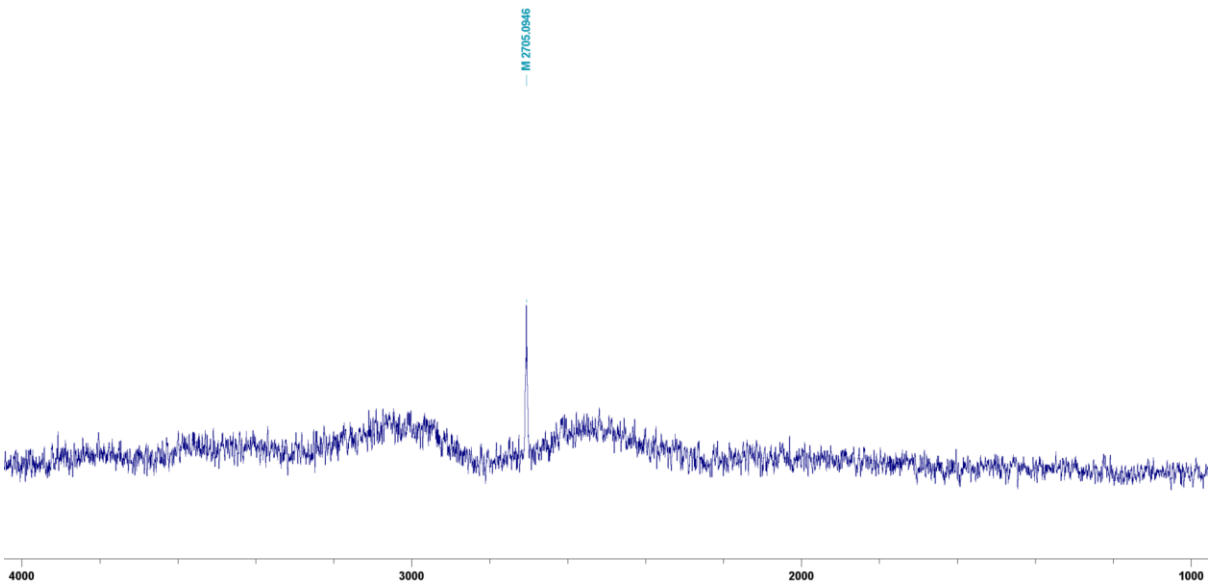

Figure S3. ^{195}Pt NMR spectrum of conjugate **C2** in D_2O.

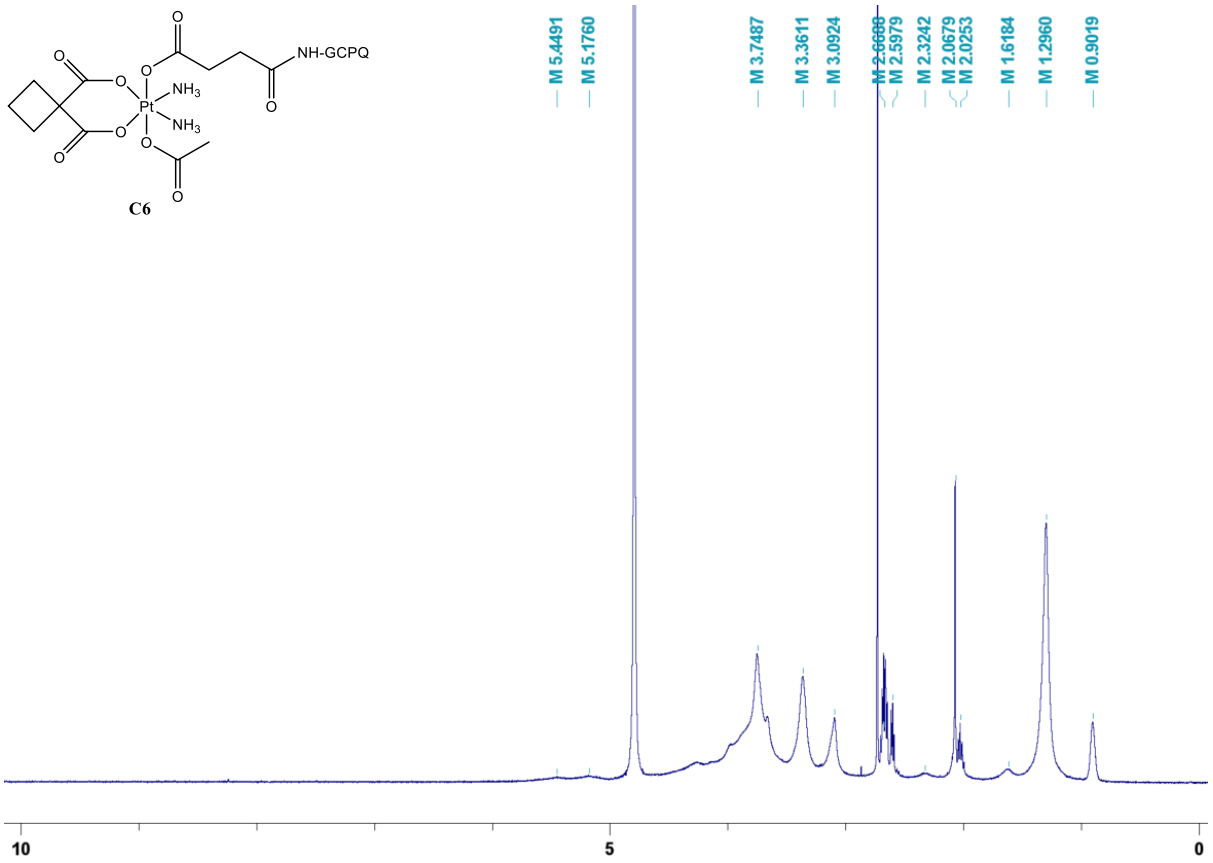

Figure S4. ^{1}H NMR spectrum of conjugate **C6** in D_2O.

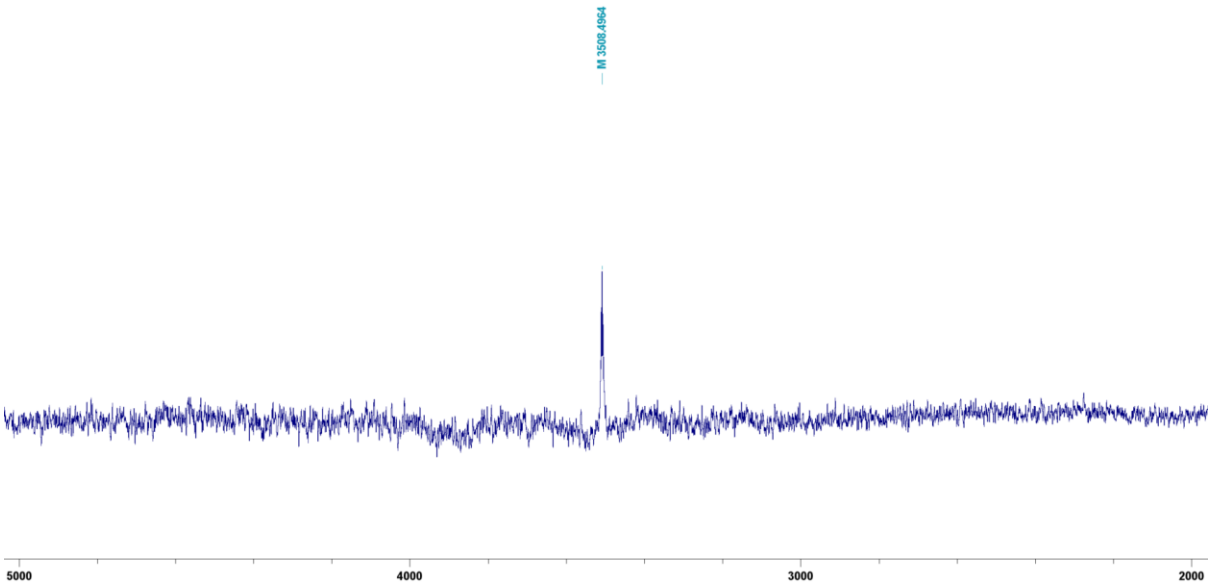

Figure S5. ^{195}Pt NMR spectrum of conjugate **C6** in D_2O.

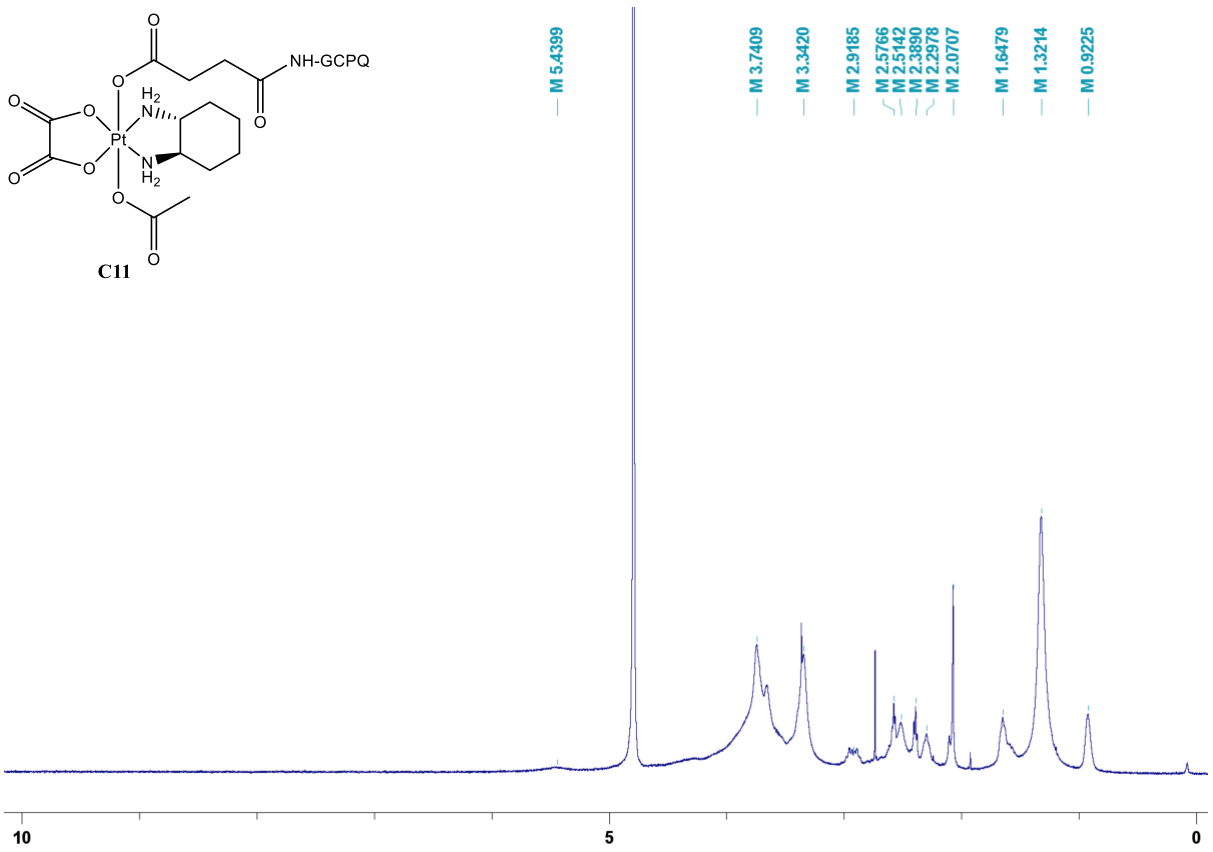

Figure S6. ^{1}H NMR spectrum of conjugate **C11** in D_2O.

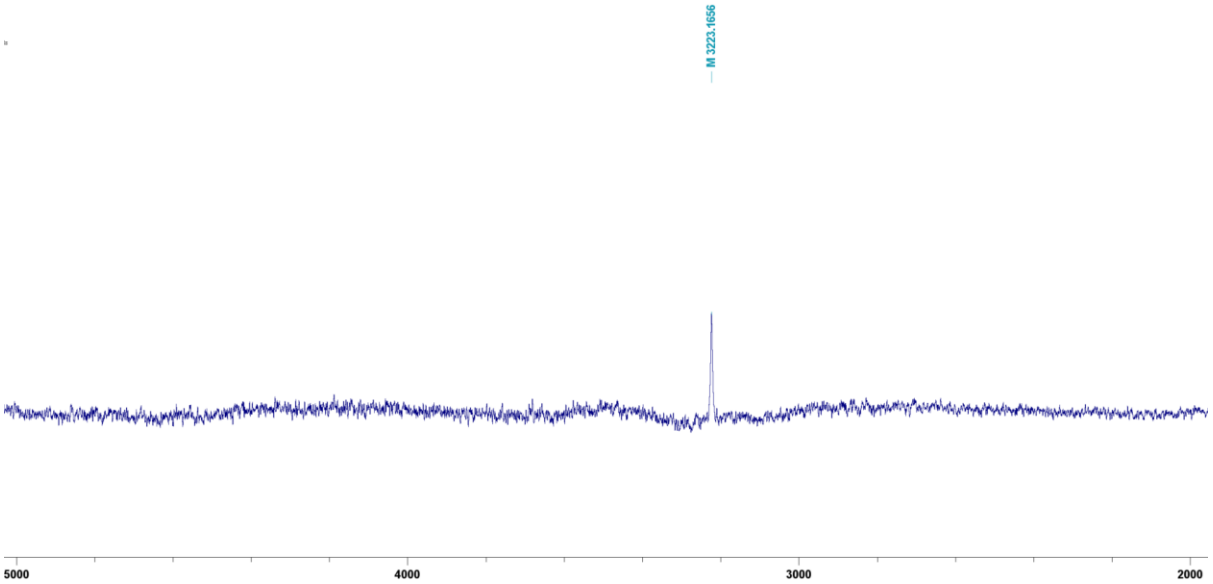

Figure S7. ^{195}Pt NMR spectrum of conjugate **C11** in D_2O.

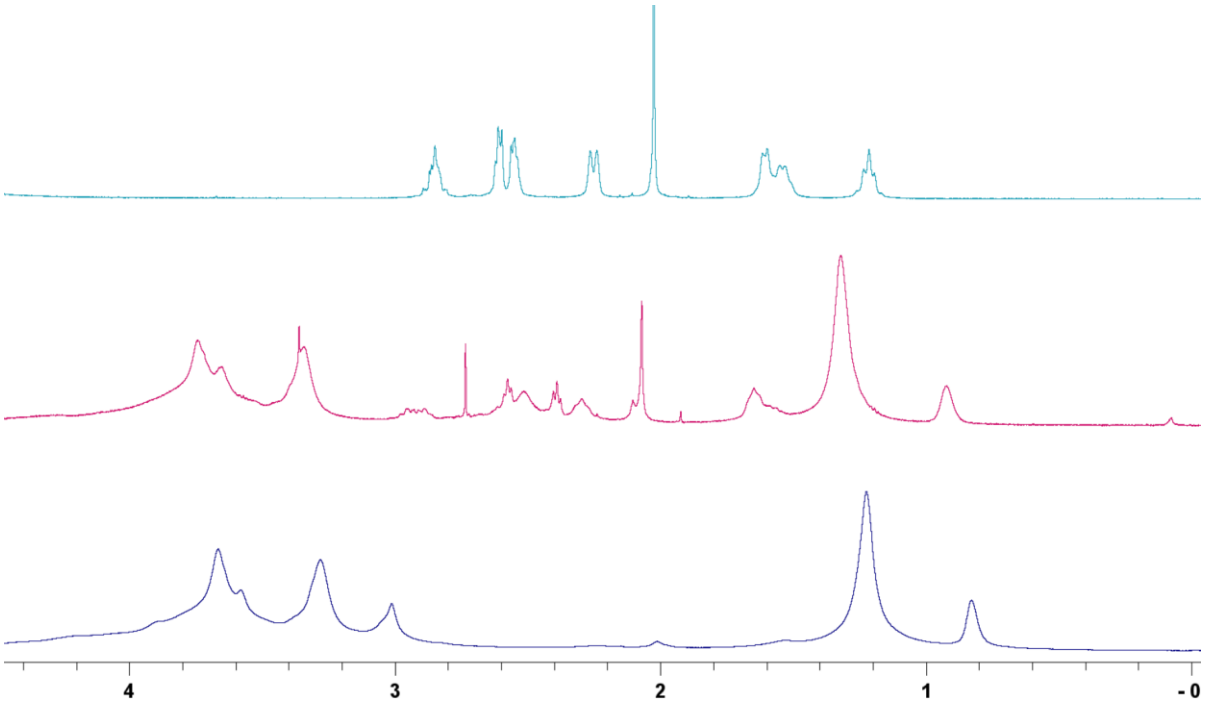

Figure S8. ^{1}H NMR spectra measured in D_2O of platinum(IV) complex **3** (above), conjugate **C11** (middle) and **GCP22Q33** polymer (below).

3. Concentration-effect curves

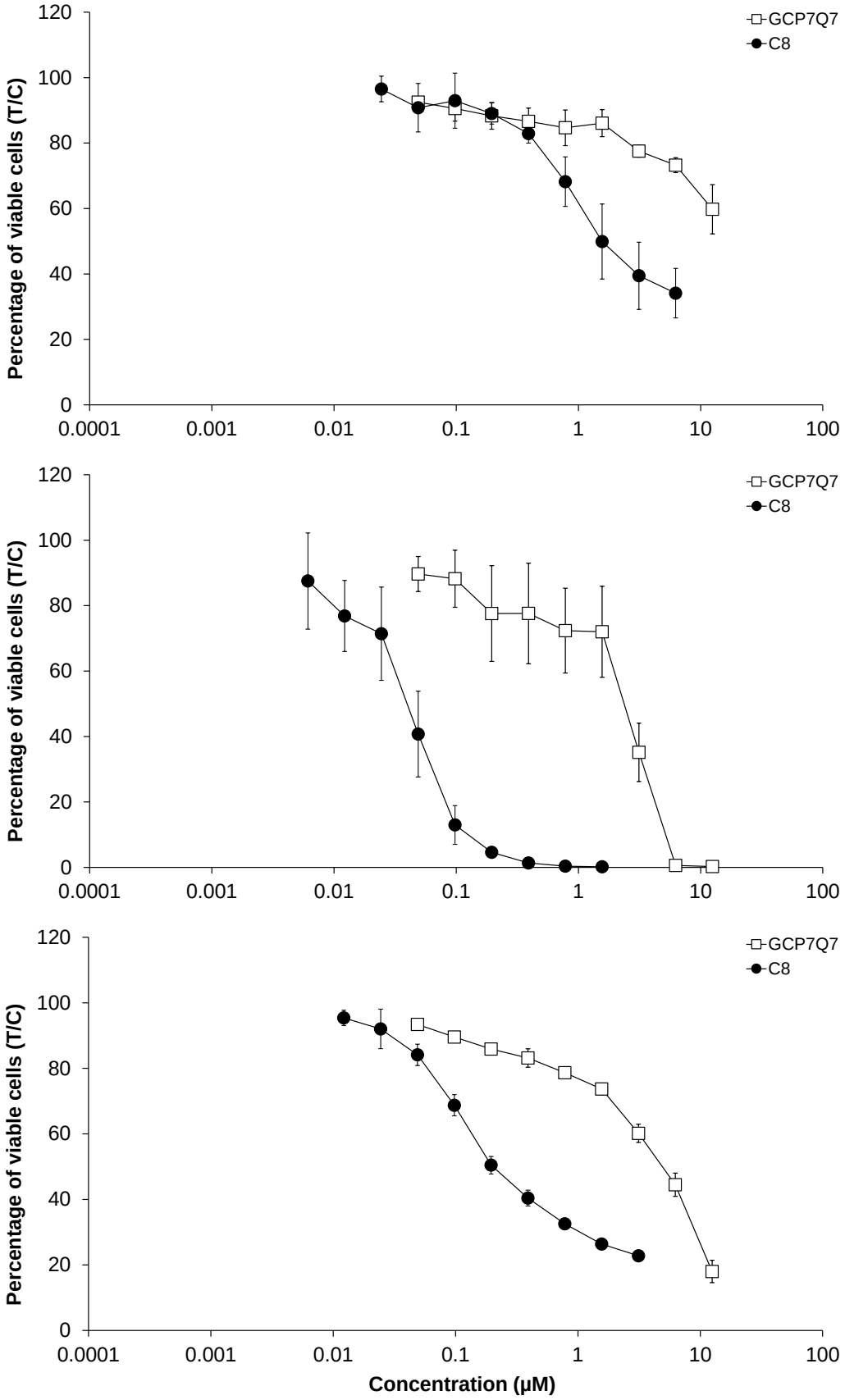

Figure S9. Concentration-effect curves of **GCP7Q7** and **C8** in A549 (top), CH1/PA-1 (middle) and SW480 (bottom) cells, obtained by MTT assays with 96 h exposure time. Values are means ± standard deviations from at least three independent experiments.

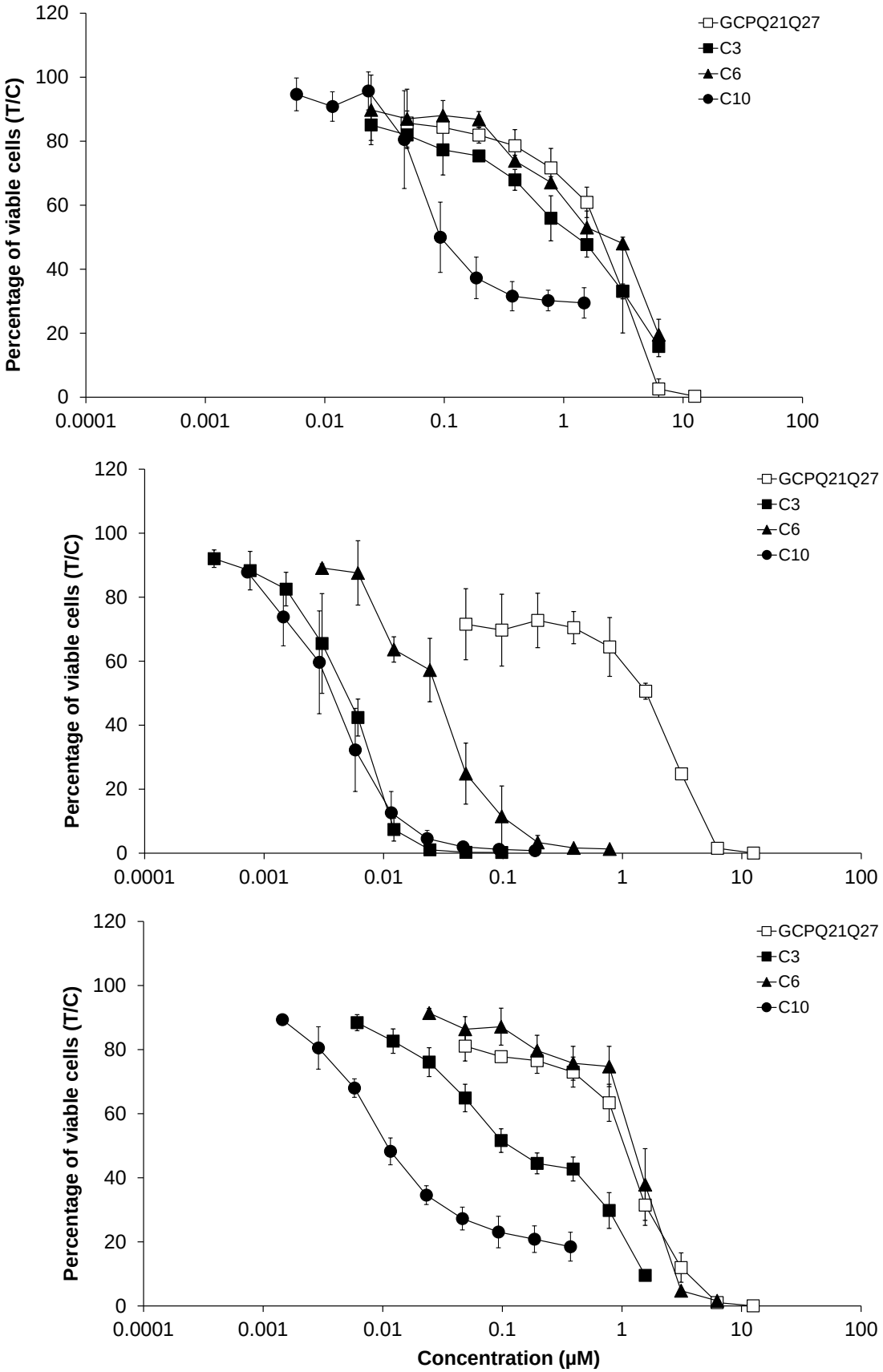

Figure S10. Concentration-effect curves of **GCPQ21Q27**, **C3**, **C6** and **C10** in A549 (top), CH1/PA-1 (middle) and SW480 (bottom) cells, obtained by MTT assays with 96 h exposure time. Values are means ± standard deviations from at least three independent experiments.

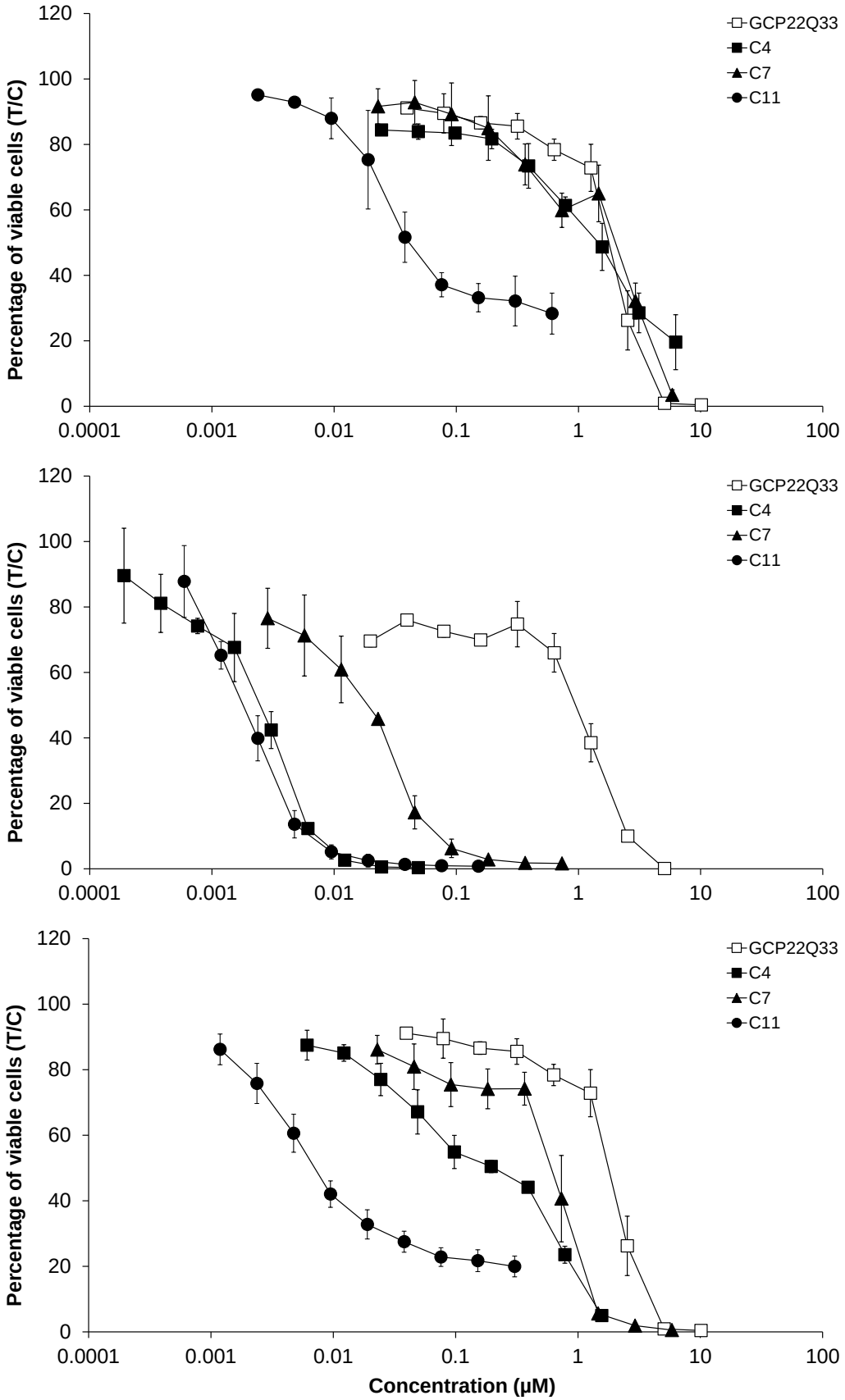

Figure S11. Concentration-effect curves of **GCP22Q33**, **C4**, **C7** and **C11** in A549 (top), CH1/PA-1 (middle) and SW480 (bottom) cells, obtained by MTT assays with 96 h exposure time. Values are means ± standard deviations from at least three independent experiments.

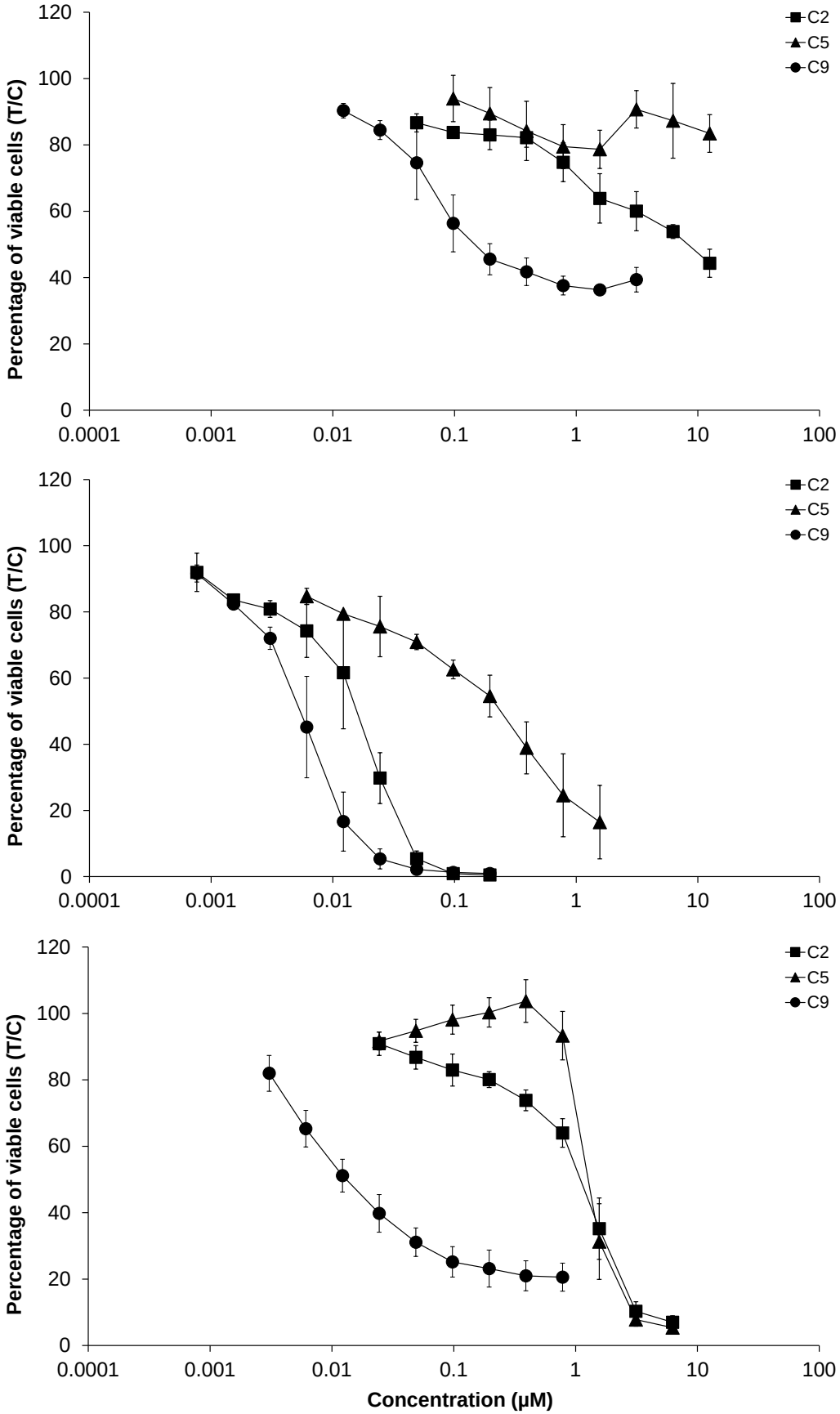

Figure S12. Concentration-effect curves of **C2**, **C5** and **C9** in A549 (top), CH1/PA-1 (middle) and SW480 (bottom) cells, obtained by MTT assays with 96 h exposure time. Values are means ± standard deviations from at least three independent experiments.

4. Solubility data

Table S1. Overview of the water solubility of conjugates **C1**-**C11** measured by visual judgement in Milli-Q water at room temperature.

Sample	Pt(IV)	GCPQ	Water solubility [mg/mL]
C1	**1**	**GCP7Q7**	~1
C2	**1**	**GCP21Q12**	~3
C3	**1**	**GCP21Q27**	~4
C4	**1**	**GCP22Q33**	~5.5
C5	**2**	**GCP21Q12**	~3
C6	**2**	**GCP21Q27**	~5
C7	**2**	**GCP22Q33**	~6
C8	**3**	**GCP7Q7**	~2
C9	**3**	**GCP21Q12**	~4
C10	**3**	**GCP21Q27**	~5
C11	**3**	**GCP22Q33**	~6.5

5. References

1. Uchegbu, I.F.; Sadiq, L.; Arastoo, M.; Gray, A.I.; Wang, W.; Waigh, R.D.; Schätzlein, A.G. Quaternary Ammonium Palmitoyl Glycol Chitosan-a New Polysoap for Drug Delivery. *Int J Pharm* **2001**, *224*, 185–199, doi:10.1016/s0378-5173(01)00763-3.

3.3 Combination of drug delivery properties of PAMAM dendrimers and cytotoxicity of platinum(IV) complexes – A more selective anticancer treatment?

Yvonne Lerchbammer-Kreith[1], Michaela Hejl[1], Petra Vician[2], Michael A. Jakupec[1,3], Walter Berger[2,3], Mathea S. Galanski[1,*] and Bernhard K. Keppler[1,3,*]

Pharmaceutics, published on May 17th, 2023

[1] Institute of Inorganic Chemistry, Faculty of Chemistry, University of Vienna, Waehringer Strasse 42, 1090 Vienna, Austria

[2] Center for Cancer Research and Comprehensive Cancer Center, Medical University of Vienna, Borschkegasse 8a, 1090 Vienna, Austria

[3] Research Cluster "Translational Cancer Therapy Research", University of Vienna, Waehringer Strasse 42, 1090 Vienna, Austria

[*] Correspondence: mathea.galanski@univie.ac.at (M.S.G.); bernhard.keppler@univie.ac.at (B.K.K.)

As first author of the publication, I synthesised and characterised all platinum(IV) complexes and conjugates, determined the reduction behaviour and I wrote the majority of the manuscript.

pharmaceutics

MDPI

Article

Combination of Drug Delivery Properties of PAMAM Dendrimers and Cytotoxicity of Platinum(IV) Complexes—A More Selective Anticancer Treatment?

Yvonne Lerchbammer-Kreith [1], Michaela Hejl [1], Petra Vician [2], Michael A. Jakupec [1,3], Walter Berger [2,3], Mathea S. Galanski [1,*] and Bernhard K. Keppler [1,3,*]

[1] Institute of Inorganic Chemistry, Faculty of Chemistry, University of Vienna, Waehringer Strasse 42, 1090 Vienna, Austria
[2] Center for Cancer Research and Comprehensive Cancer Center, Medical University of Vienna, Borschkegasse 8a, 1090 Vienna, Austria
[3] Research Cluster "Translational Cancer Therapy Research", University of Vienna, Waehringer Strasse 42, 1090 Vienna, Austria
* Correspondence: mathea.galanski@univie.ac.at (M.S.G.); bernhard.keppler@univie.ac.at (B.K.K.)

Abstract: Based on their drug delivery properties and activity against tumors, we combined PAMAM dendrimers with various platinum(IV) complexes in order to provide an improved approach of anticancer treatment. Platinum(IV) complexes were linked to terminal NH_2 moieties of PAMAM dendrimers of generation 2 (G2) and 4 (G4) via amide bonds. Conjugates were characterized by ^{1}H and ^{195}Pt NMR spectroscopy, ICP-MS and in representative cases by pseudo-2D diffusion-ordered NMR spectroscopy. Additionally, the reduction behavior of conjugates in comparison to corresponding platinum(IV) complexes was investigated, showing a faster reduction of conjugates. Cytotoxicity was evaluated via the MTT assay in human cell lines (A549, CH1/PA-1, SW480), revealing IC_{50} values in the low micromolar to high picomolar range. The synergistic combination of PAMAM dendrimers and platinum(IV) complexes resulted in up to 200 times increased cytotoxic activity of conjugates in consideration of the loaded platinum(IV) units compared to their platinum(IV) counterparts. The lowest IC_{50} value of 780 ± 260 pM in the CH1/PA-1 cancer cell line was detected for an oxaliplatin-based G4 PAMAM dendrimer conjugate. Finally, in vivo experiments of a cisplatin-based G4 PAMAM dendrimer conjugate were performed based on the best toxicological profile. A maximum tumor growth inhibition effect of 65.6% compared to 47.6% for cisplatin was observed as well as a trend of prolonged animal survival.

Keywords: platinum(IV) complexes; PAMAM dendrimers; anticancer; drug delivery

Citation: Lerchbammer-Kreith, Y.; Hejl, M.; Vician, P.; Jakupec, M.A.; Berger, W.; Galanski, M.S.; Keppler, B.K. Combination of Drug Delivery Properties of PAMAM Dendrimers and Cytotoxicity of Platinum(IV) Complexes—A More Selective Anticancer Treatment? *Pharmaceutics* **2023**, *15*, 1515. https://doi.org/10.3390/pharmaceutics15051515

Academic Editor: Barbara R. Conway

Received: 25 April 2023
Revised: 11 May 2023
Accepted: 12 May 2023
Published: 17 May 2023

1. Introduction

Five decades after the discovery of the anticancer activity of cisplatin, platinum(II)-based anticancer agents still play an essential role in modern cancer treatment. The breakthrough of platinum(II) complexes was further consolidated by the introduction of carboplatin and oxaliplatin in clinical practice [1–3]. Together, these three platinum(II) drugs are integrated into about 50% of all cancer chemotherapies worldwide and cisplatin belongs to the most lucrative anticancer agents [4,5]. Despite the enormous success, platinum(II)-based cancer treatment lacks selectivity against tumor cells, leading to severe side effects, and is further affected by intrinsic and/or acquired resistance, diminishing its clinical efficacy [6].

The prodrug strategy, employing kinetically more inert platinum(IV) complexes, enabled a new approach to improve selectivity and reduce systemic toxicity. The reduction of the corresponding platinum(II) complexes, required to unleash their cytotoxic capacities, is facilitated by the characteristic oxygen-deficient milieu of tumor tissue [7,8]. Despite

intensive research and promising (pre)clinical studies, platinum(IV) complexes such as tetraplatin, iproplatin, satraplatin and LA-12 could not show an overall improvement so far compared to platinum(II)-based anticancer agents [9–11].

Consequently, in order to improve selectivity, tumor-targeting strategies have attracted more and more attention. Passive tumor targeting exploits the enhanced permeability and retention (EPR) effect, a characteristic of cancerous tissue. The gaps formed between endothelial cells during tumor angiogenesis enable the infiltration of nanoparticles. Additionally, insufficient lymph drainage leads to an enhanced accumulation of macromolecules. Therefore, the development of drug delivery molecules in the nanometer range is of special interest [12,13].

Promising candidates can be found within the class of dendrimers, symmetrically designed polymeric nanostructures with adjustable functionalities such as size, shape and surface groups. The most intensively investigated representative is the poly(amidoamine) (PAMAM) dendrimer, developed by Donald Tomalia in 1985 [14,15]. Sequences of amidoamine units are constituted radially around an ethylenediamine core and the dendritic structure grows symmetrically controlled, using a two-step mechanism. Each full layer thereby represents a full generation, with primary amines serving as terminal groups. The surface functionalities enable covalent bonding or coordination of drugs, whereas small bioactive molecules can be encapsulated in the interior [16–18].

The beneficial combination of platinum complexes and PAMAM dendrimers was already shown in previous studies. Encapsulation of cisplatin led to higher anticancer potency and improved cellular accumulation even in cisplatin-resistant cell lines [19,20]. Additionally, efficacy and biodistribution studies in mice xenografts with ovarian cancer showed an increase in lifespan by up to 40%. Furthermore, the enhanced plasma concentration and tissue accumulation could allow a lower dosage, resulting in decreased side effects [21].

Besides encapsulation, attachment of cisplatin and doxorubicin to the surface of PAMAM dendrimers enabled a more efficacious treatment of breast cancer in animal experiments. Due to the improved accumulation of the conjugate in cancerous tissue, further tumor growth was prevented without noticeable adverse effects [22].

Previously, our group reported on significantly increased cytotoxicity achieved by the formation of amide bonds between oxaliplatin-based platinum(IV) complexes and full-generation PAMAM dendrimers [23].

Hence, we continue investigations into the potential of platinum(IV) compounds in combination with PAMAM dendrimers as anticancer agents in the present work. In total, 24 conjugates with various platinum(IV) complexes and PAMAM dendrimers of generation 2 (G2) and 4 (G4) were synthesized and characterized by multinuclear NMR spectroscopy and inductively coupled plasma mass spectrometry (ICP-MS). Cytotoxicity of the conjugates was compared to that of the corresponding platinum(IV) complexes and unloaded PAMAM dendrimers via the MTT assay in three human cancer cell lines. Finally, biodistribution and anticancer activity were investigated in a murine CT26 solid tumor model.

2. Materials and Methods

2.1. Materials

All chemicals and solvents were purchased from commercial suppliers and were used without further purification. $K_2[PtCl_4]$ was acquired from Johnson Matthey (assay: 46.69% Pt) (Zurich, Switzerland), whereas G2 (20 wt.% in methanol) and G4 PAMAM dendrimers (10 wt.% in methanol) were purchased from Sigma-Aldrich (St. Louis, MO, USA). Additionally, the following chemicals were used as received: succinic anhydride (≥99%) (Sigma-Aldrich, Steinheim, Germany), absolute DMF (99.8%, extra dry, water <50 ppm) (Acros Organics, Geel, Belgium), N-(3-dimethylaminopropyl)-N^t-ethylcarbodiimide hydrochloride (EDC·HCl) (>98%) (TCI Europe, Zwijndrecht, Belgium), N-hydroxysuccinimide (NHS) (98%) (Sigma-Aldrich, Steinheim, Germany).

Trial Kit Spectra/Por® 7 (MWCO 1.0 kDa) and Spectra/Por® 3 (MWCO 3.5 kDa) dialysis tubings were supplied by Carl Roth (Karlsruhe, Germany). Milli-Q water (18.2 MΩ cm, Milli-Q Advantage) was used for aqueous solutions as well as for preparative RP-HPLC purifications. All reactions involving platinum complexes were performed under light protection and with glass-coated magnetic stirring bars.

2.2. Preparative RP-HPLC

An Agilent 1200 Series system controlled by ChemStation® software was used for purifications by preparative RP-HPLC. A XBridge® Prep C18 10 µm OBD™ Column (19 mm × 250 mm) from Waters served as the stationary phase, whereas different ratios of Milli-Q water, acetonitrile and methanol with the addition of 0.1% formic acid were used as eluents.

2.3. Elemental Analysis

The Microanalytical Laboratory of the Faculty of Chemistry at the University of Vienna performed the elemental analyses of the platinum(IV) compounds, using an Eurovector EA3000 elemental analyzer. All obtained values are in the range of ±0.4% of the calculated values, therefore confirming purity of at least 96%.

2.4. NMR Spectroscopy

NMR spectra were recorded on a Bruker AVANCE NEO 500 MHz spectrometer at 500.32 (^{1}H), 125.81 (^{13}C), 50.70 (^{15}N), 470.56 (^{19}F), and 107.38 MHz (^{195}Pt) or an AVANCE III HD 700 MHz spectrometer at 659.03 MHz (^{19}F) at 25 °C. The solvent resonances were used as internal references for ^{1}H (d_6-DMSO, δ = 2.50 ppm; d_7-DMF, δ = 2.75 ppm (high field signal); D_2O, δ = 4.79 ppm) and ^{13}C (d_6-DMSO, δ = 39.51 ppm; d_7-DMF, δ = 29.76 ppm (high field signal)), ^{19}F chemical shifts are given relative to CCl_3F, whereas NH_4Cl and $K_2[PtCl_4]$ served as external reference for ^{15}N and ^{195}Pt NMR spectroscopy.

DOSY experiments were measured with a standard Bruker DOSY pulse sequence without sample spinning in D_2O at 298 K. The diffusion coefficient D, obtained from the spectra, was used for the estimation of the diameter of PAMAM dendrimers and conjugates by assuming a spherical size and using the Stokes–Einstein equation:

$$R_0 = \frac{k_B T}{6\pi\eta D}$$

R_0 is the (hydrodynamic) radius, k_B the Boltzmann constant (JK^{-1}), T the temperature [K], η the viscosity of the liquid (1.095×10^{-3} Pa·s) and D the diffusion coefficient [m^2s^{-1}] [23].

2.5. Reduction Behavior

The reduction of platinum(IV) complexes and representatives of each series of conjugates by ascorbic acid was observed by ^{1}H NMR spectroscopic measurements at ambient temperature. An amount of 1 mM solutions of platinum(IV) complexes **1–3**, **5–7** as well as of the conjugates **C2**, **C11**, **C13**, **C22–C24** referred to their corresponding platinum units were prepared in a D_2O phosphate-buffered solution (50 mM) at physiological pD = 7.4. Afterwards, ascorbic acid was added as a reducing agent (25 mM, 25 eq.) and ^{1}H NMR measurements were performed for several days. The reduction behavior for substances **1–3**, **5**, **6**, **C2**, **C11**, **C13**, **C22**, **C23** was monitored by the resulting decrease in intensity of the acetato signal (release of acetic acid). The percentage of reduced species was determined by using the integration ratios of these two signals. Contrarily, ratios of signals of the succinato ligands and free succinic acid were consulted for the reduction determination of substances **7** and **C24**. However, the reduction half-time of **C24** could not be obtained due to the superimposition of the succinato peaks with other signals.

2.6. ICP-MS

Digestion of all conjugates (0.5–1.5 mg) was performed in 2 mL of HNO_3 (20%) and 0.1 mL of H_2O_2 (30%) with a temperature-controlled heating plate of graphite from Labter. After dilution (1:10,000) of digested samples with HNO_3 (3%), the total platinum amount was determined with an Agilent 7800 ICP-MS instrument. For each sample, 10 measurements were performed and the obtained data were analyzed with the Agilent MassHunter software package (Workstation Software, Version C.01.04, 2018, Agilent, Santa Clara, CA, USA).

2.7. Cytotoxicity Tests

Culture of and 96 h cytotoxicity tests in the human cell lines CH1/PA-1 (ovarian teratocarcinoma), SW480 (colon carcinoma) and A549 (non-small cell lung cancer) were performed as described previously [24], with the exception that test compounds were dissolved either in sterile water or supplemented MEM and then serially diluted in the latter medium.

The MTT assay in the murine cell line CT26 was performed as described in [25].

2.8. In Vivo Experiments and Organ Distribution

Female and male BALB/c mice, bread in-house (originally Janvier), were kept in a controlled environment under pathogen-free conditions. By the toxicity tests, non-tumor-bearing female BALB/c mice were treated intravenously at a dose: G4 PAMAM dendrimer at 0.058 mg/20 g, **C11** at 0.17 mg/20 g, **C12** at 0.075 mg/20 g and 0.15 mg/20 g, **C13** at 0.91 mg/20 g and **C22** at 0.52 mg/20 g three times in the first week. All drugs were dissolved in 0.9% NaCl. For the efficacy study, CT26 (5×10^5 in 50 µL serum-free RMPI medium) murine colon cells were injected into the right flank (subcutaneously) of female BALB/c mice. When all tumors were measurable (at day 5), animals were treated intravenously with solvent (0.9% NaCl, 100 µL/20 g), **C12** (7.5 mg/kg in 0.9% NaCl, 100 µL/20 g) and cisplatin (3 mg/kg in 0.9% NaCl, 100 µL/20 g) twice a week for two weeks. Tumor volume and size (measured by caliper) and body weight were evaluated every working day; the animals were sacrificed by cervical dislocation upon a loss in body weight, tumor size or other indications of deteriorated health. In vivo experiments were done according to the regulations of the Ethics Committee for the Care and Use of Laboratory Animals at the Medical University Vienna (proposal number BMBWF-V/3b 2020-0.380.502).

Organs and tumors for platinum content/distribution were harvested 24 h after the second application of **C12** (7.5 mg/kg in 0.9% NaCl, 100 µL/20 g) and cisplatin (3 mg/kg in 0.9% NaCl, 100 µL/20 g) in male CT26-allograft-bearing BALB/c mice. Blood was taken after 30 min and 24 h after the first application from the facial vein and terminally by cardiac puncture 24 h after the second application. To separate serum from blood pellet, blood was twice spun down at 900 g for 10 min at 4 °C. The platinum amount of all samples was measured by ICP-MS.

2.9. Synthesis

2.9.1. Platinum(IV) Complexes

Acetatohydroxidoplatinum(IV) complexes serving as precursors for substances **1–6** as well as substance **7** were synthesized according to previously published procedures [23,26–28].

General procedure 1: carboxylation of unsymmetrically oxidized platinum(IV) complexes (**1–6**):

The corresponding precursor platinum(IV) complex and succinic anhydride were stirred overnight in absolute DMF under argon atmosphere at 50 °C. The solvent was removed under reduced pressure. Purification was performed by using preparative RP-HPLC. Finally, the product was freeze-dried.

1. (OC-6-44)-Acetatodiammine(3-carboxypropanoato)dichloridoplatinum(IV) (**1**)

The reaction was performed according to general procedure 1. Acetatodiamminedichloridohydroxidoplatinum(IV) (5.171 g, impure, 13.75 mmol, 1 eq.), succinic anhydride (5.502 g, 55.00 mmol, 4 eq.), absolute DMF (100 mL). Preparative RP-HPLC (isocratic, MeOH: Milli-Q water = 5:95 + 0.1% formic acid). Yield: 1.555 g. ^{1}H NMR (d_6-DMSO): δ = 6.51 (b, 6H, NH_3), one of the CH_2 signals of the succinato ligand is in part overlapping with the DMSO solvent peak, 2.34–2.38 (m, 2H, CH_2, succinato), 1.90 (s, 3H, CH_3) ppm. Elemental analysis: $C_6H_{14}Cl_2N_2O_6Pt \cdot H_2O$; calcd. C 14.58, H 3.26, N 5.67, found C 14.40, H 3.14, N 5.64.

2. (OC-6-44)-Acetaodiammine(3-carboxypropanoato)(cyclobutane-1,1-dicarboxylato) platinum(IV) (**2**)

The reaction was performed according to general procedure 1. Acetaodiammine (cyclobutane-1,1-dicarboxylato)hydroxidoplatinum(IV) (2.260 g, impure, 5.05 mmol, 1 eq.), succinic anhydride (2.021 g, 20.21 mmol, 4 eq.), absolute DMF (40 mL). Preparative RP-HPLC (isocratic, MeOH: Milli-Q water = 17:83 + 0.1% formic acid). Yield: 524 mg. ^{1}H NMR (d_6-DMSO): δ = 6.34 (t, $^{1}J(^{14}N, ^{1}H)$ = 50.5 Hz, 6H, NH_3), CH_2-C signal of the cyclobutyl moiety and one of the CH_2 signals of the succinato ligand are in part overlapping with the DMSO solvent peak, 2.35 (m, 2H, CH_2, succinato), 1.89 (s, 3H, CH_3), 1.80 (p, $^{3}J(^{1}H, ^{1}H$ = 8.2 Hz), 2H, CH_2, cyclobutyl) ppm. Elemental analysis: $C_{12}H_{20}N_2O_{10}Pt \cdot H_2O$; calcd. C 25.49, H 3.92, N 4.95, found C 25.80, H 3.66, N 5.12.

3. (OC-6-44)-Acetato(3-carboxypropanoato)(1R,2R-cyclohexane-1,2-diamine) oxalatoplatinum(IV) (**3**)

The reaction was performed according to general procedure 1. Acetato(1R,2R-cyclohexane-1,2-diamine)hydroxidooxalatoplatinum(IV) (7.845 g, impure, 16.64 mmol, 1 eq.), succinic anhydride (6.666 g, 66.71 mmol, 4 eq.), absolute DMF (130 mL). Preparative RP-HPLC (isocratic, ACN: Milli-Q water = 5:95 + 0.1% formic acid). Yield: 2.988 g. Crystals suitable for X-ray diffraction were obtained from a methanol solution by slow evaporation at room temperature. ^{1}H NMR (d_6-DMSO): δ = 12.13 (b, 1H, OH), 8.29 (m, 4H, NH_2), 2.53–2.62 (m, 2H, CH, DACH), one of the CH_2 signals of the succinato ligand is overlapping with the DMSO solvent peak, 2.35–2.41 (m, 2H, CH_2, succinato), 2.06–2.14 (m, 2H, CH_2, DACH), 1.95 (s, 3H, CH_3), 1.47–1.54 (m, 2H, CH_2, DACH), 1.33–1.47 (m, 2H, CH_2, DACH) 1.08–1.21 (m, 2H, CH_2, DACH) ppm. Elemental analysis: $C_{14}H_{22}N_2O_{10}Pt \cdot H_2O$; calcd. C 28.43, H 4.09, N 4.74, found C 28.08, H 4.00, N 4.91.

4. (OC-6-44)-Acetato(3-carboxypropanoato)(1R,2R-cyclohexane-1,2-diamine)($^{13}C_2$) oxalatoplatinum(IV) (**4**)

The reaction was performed according to general procedure 1. Acetato(1R,2R-cyclohexane-1,2-diamine)($^{13}C_2$)hydroxidooxalatoplatinum(IV) (677 mg, impure, 1.42 mmol, 1eq.), succinic anhydride (570 mg, 5.70 mmol, 4 eq.), absolute DMF (30 mL). Preparative RP-HPLC (isocratic, ACN: Milli-Q water = 5:95 + 0.1% formic acid). Yield: 188 mg. ^{1}H NMR (D_2O): δ = 2.83–2.95 (m, 2H, DACH), 2.64–2.69 (m, 2H, succinato), 2.59–2.63 (m, 2H, succinato), 2.27–2.34 (m, 2H, DACH), 2.07 (s, 3H, CH_3), 1.53–1.70 (m, 4H, DACH), 1.20–1.32 (m, 2H, DACH) ppm. ^{13}C NMR (D_2O): δ = 181.9 (C=O, succinato), 181.4 (C=O, acetato), 177.2 (C=O, succinato), 166.4 (^{13}C=O, oxalato), 164.5–165.5 (smaller ^{13}C=O signals, impurities), 61.8 (CH, DACH), 61.3 (CH, DACH), 30.8 (CH_2, DACH), 30.7 (CH_2, succinato), 29.7 (CH_2, succinato), 23.42 (CH_2, DACH), 23.38 (CH_2, DACH), 22.1 (CH_3) ppm. ^{195}Pt NMR (D_2O): δ = 3214 ppm. Elemental analysis: $C_{12}{}^{13}C_2H_{22}N_2O_{10}Pt \cdot 1.5H_2O$; calcd. C 28.00, H 4.20, N 4.67, found C 27.91, H 3.82, N 4.89.

5. (OC-6-54)-Acetato(3-carboxypropanoato)($^{13}C_2$)oxalato(1R,2R,4R/1S,2S,4S)-(4-trifluoromethyl-cyclohexane-1,2-diamine)platinum(IV) (**5**)

The reaction was performed according to general procedure 1. Acetatohydroxido($^{13}C_2$) oxalato(1R,2R,4R/1S,2S,4S)-(4-trifluoromethyl-cyclohexane-1,2-diamine)platinum(IV) (2.588 g, impure, 4.76 mmol, 1 eq.), succinic anhydride (1.192 g, 11.91 mmol, 2.5 eq.), absolute DMF (40 mL). Preparative RP-HPLC (isocratic, MeOH: Milli-Q water = 15:85 + 0.1% formic acid). Yield: 113 mg. ^{1}H NMR (d_6-DMSO): δ = 12.11 (b, 1H, OH), 8.27–8.57 (m, 2H, NH_2),

7.96–8.27 (m, 2H, NH_2), 2.81 (m, 1H, CH, DACH), 2.73 (m, 1H, CH, DACH), one CH_2 signal of the succinato ligand and one CH signal of the DACH ligand is overlapping with the DMSO solvent peak, 2.34–2.43 (m, 2H, CH_2, succinato), 2.20–2.28 (m, 1H, CH_2, DACH), 2.13–2.20 (m, 1H, CH_2, DACH), 1.96+1.95 (b, 3H, CH_3), 1.71–1.78 (m, 1H, CH_2, DACH), 1.48–1.63 (m, 2H, CH_2, DACH), 1.28–1.40 (m, 1H, CH_2, DACH) ppm. ^{13}C NMR (d_6-DMSO): δ = 179.5 + 179.2 (C=O, succinato), 178.4 + 178.2 (C=O, acetato), 173.85 + 173.75 (C=O, succinato), 163.34 + 163.32 (^{13}C=O, oxalato), 162.7–165.8 (smaller ^{13}C=O (coupling) signals based on the asymmetry of labeled oxalate), 126.9 (q, ^{1}J (^{19}F, ^{13}C) = 278.6 Hz, CF_3), 59.9 (CH, DACH), 59.3 (CH, DACH), 59.2 (CH, DACH), 30.64 + 30.58 (CH_2, succinato), 29.8 + 29.7 (CH_2, succinato), 29.1 + 29.0 (CH_2, DACH), 28.1 + 28.0 (CH_2, DACH), 23.0 + 22.9 (CH_3), 22.48 + 22.45 (CH_2, DACH) ppm. ^{15}N NMR (d_6-DMSO): δ = −8.4 (NH_2) ppm. ^{19}F NMR (d_6-DMSO): δ = −71.37/−71.39 (2d, ^{3}J(^{1}H, ^{19}F) = 8.6 Hz, 3F, CF_3) ppm. ^{195}Pt NMR (d_6-DMSO): δ = 3260 (major), 3234 (minor) ppm. Elemental analysis: $C_{13}{}^{13}C_2H_{21}F_3N_2O_{10}Pt \cdot 2H_2O$; calcd. C 26.59, H 3.73, N 4.14, found C 26.58, H 3.42, N 4.31.

6. (OC-6-44)-Acetato(3-carboxypropanoato)dichlorido(1R,2R-cyclohexane-1,2-diamine) platinum(IV) (**6**)

The reaction was performed according to general procedure 1. Acetatodichlorido(1R, 2R-cyclohexane-1,2-diamine)hydroxidoplatinum(IV) (147 mg, 0.32 mmol, 1 eq.), succinic anhydride (82 mg, 0.81 mmol, 2.5 eq.), absolute DMF (15 mL). Preparative RP-HPLC (isocratic, ACN: Milli-Q water = 10:90 + 0.1% formic acid). Yield: 40 mg (22%). ^{1}H NMR (d_6-DMSO): δ = 12.10 (s, 1H, OH), 9.33 (m, 2H, NH_2), 8.30 (b, 1H, NH_2), 8.12 (b, 1H, NH_2), 2.52–2.68 (m, 2H, CH, DACH), 2.33–2.49 (m, 4H, CH_2, succinato signal is in part overlapping with the DMSO solvent peak), 2.14–2.23 (m, 2H, CH_2, DACH), 1.95 (s, 3H, CH_3), 1.46–1.56 (m, 2H, CH_2, DACH), 1.21–1.39 (m, 2H, CH_2, DACH), 1.08–1.20 (m, 2H, CH_2, DACH) ppm. ^{13}C NMR (d_6-DMSO): δ = 181.9 (C=O, succinato), 180.7 (C=O, acetato), 173.7 (C=O, succinato), 62.45 + 62.43 (CH, DACH), 31.2 (CH_2, succinato), 31.0 (CH_2, DACH), 29.6 (CH_2, succinato), 23.53 (CH_3), 23.48 (CH_2, DACH), 23.3 (CH_2, DACH) ppm. ^{15}N NMR (d_6-DMSO): δ = 5.3 (NH_2), 3.7 (NH_2) ppm. ^{195}Pt NMR (d_6-DMSO): δ = 2729 ppm. Elemental analysis: $C_{12}H_{22}Cl_2N_2O_6Pt$; calcd. C 25.91, H 3.99, N 5.04, found C 25.53, H 3.92, N 5.01.

7. (OC-6-44)-(3-carboxypropanoato)(1R,2R-cyclohexanem-1,2-diamine) hydroxidooxalatoplatinum(IV) (**7**)

(1R,2R-cyclohexanediamine)dihydroxidooxalatoplatinum(IV) (57 mg, 0.13 mmol, 1 eq.) and succinic anhydride (13 mg, 0.13 mmol, 1 eq.) were stirred in absolute DMSO (10 mL) for 16 h under argon atmosphere at 50 °C. Afterward, the solvent was removed under reduced pressure. Purification was performed via preparative RP-HPLC (isocratic, MeOH: Milli-Q water = 5:95 + 0.1% formic acid) and the final product was obtained after lyophilization. Yield: 25 mg (36%). ^{1}H NMR (d_6-DMSO): δ = 12.04 (b, 2H, OH), 8.42 (b, 1H, NH_2), 8.09 (b, 1H, NH_2), 7.80 (b, 1H, NH_2), 7.06 (b, 1H, NH_2), the CH signals of the DACH ligand are overlapping with the DMSO solvent peak, 2.40–2.45 (m, 2H, CH_2, succinato), 2.34–2.39 (m, 2H, CH_2, succinato), 2.00–2.11 (m, 2H, CH_2, DACH), 1.39–1.55 (m, 3H, CH_2, DACH), 1.26–1.36 (m, 1H, CH_2, DACH), 1.05–1.18 (m, 2H, CH_2, DACH) ppm. ^{13}C NMR (d_6-DMSO): δ = 180.8 (C=O, succinato), 173.9 (C=O, succinato), 163.9 (C=O, oxalato), 163.8 (C=O, oxalato), 61.2 (CH, DACH), 60.0 (CH, DACH), 31.4 (CH_2, succinato), 30.9 (CH_2, DACH), 30.7 (CH_2, DACH), 29.8 (CH_2, succinato), 23.7 (CH_2, DACH), 23.5 (CH_2, DACH) ppm. ^{15}N NMR (d_6-DMSO): δ = −5.9 (NH_2) and −9.6 (NH_2) ppm. ^{195}Pt NMR (d_6-DMSO): δ = 3039 ppm. Elemental analysis: $C_{12}H_{20}N_2O_9Pt \cdot 2H_2O$; calcd. C 25.40, H 4.25, N 4.94, found C 25.74, H 3.85, N 5.02.

2.9.2. Platinum(IV)-PAMAM Dendrimer Conjugates

General Procedure 2: Coupling of Platinum(IV) Complexes to G2 or G4 PAMAM Dendrimers (**C1**–**C27**)

The corresponding platinum(IV) complex **1**–**7** (1 eq.), N-(3-dimethylaminopropyl)-N′-ethylcarbodiimide hydrochloride (EDC·HCl) (3.5 eq.) and N-hydroxysuccinimide (NHS)

(3.5 eq.) were dissolved in Milli-Q water (5 mL) and the mixture was stirred for about 40 min at room temperature. Afterward, an aqueous solution (15 mL) of PAMAM dendrimer (0.06 eq. for G2 and 0.02 eq. for G4) was added. The reaction time ranged from 6 to 24 h. Purification was performed by dialysis against distilled water (MWCO = 1.0 kDa for G2 and 3.5 kDa for G4, 12 changes within 14 h). Finally, the product was obtained via lyophilization.

1. Complex **1** coupled to G2 PAMAM dendrimer (**C1**)

The reaction was performed according to general procedure 2. **1** (60 mg, 0.13 mmol, 1 eq.), G2 PAMAM (25 mg, 0.0076 mmol, 0.06 eq.), EDC·HCl (85 mg, 0.44 mmol, 3.5 eq.), NHS (51 mg, 0.44 mmol, 3.5 eq.), reaction time of 12 h. Yield: 29 mg. ICP-MS (Pt): 194.1 g/kg, average Pt loading of 37.31%, 5.97 Pt units. ^{195}Pt NMR (D_2O): δ = 2712 ppm.

2. Complex **2** coupled to G2 PAMAM dendrimer (**C2**)

The reaction was performed according to general procedure 2. **2** (60 mg, 0.11 mmol, 1 eq.), G2 PAMAM (21 mg, 0.0066 mmol, 0.06 eq.), EDC·HCl (74 mg, 0.38 mmol, 3.5 eq.), NHS (44 mg, 0.38 mmol, 3.5 eq.), reaction time of 12 h. Yield: 44 mg. ICP-MS (Pt): 161.7 g/kg, average Pt loading of 30.13%, 4.82 Pt units. ^{195}Pt NMR (D_2O): δ = 3507 ppm.

3. Complex **4** coupled to G2 PAMAM dendrimer (**C3**)

The reaction was performed according to general procedure 2. **4** (60 mg, 0.10 mmol, 1 eq.), G2 PAMAM (20 mg, 0.0063 mmol, 0.06 eq.), EDC·HCl (70 mg, 0.37 mmol, 3.5 eq.), NHS (42 mg, 0.37 mmol, 3.5 eq.), reaction time of 12 h. Yield: 23 mg. ICP-MS (Pt): 176.2 g/kg, average Pt loading of 37.06%, 5.93 Pt units. ^{195}Pt NMR (D_2O): δ = 3218 ppm.

4. Complex **5** coupled to G2 PAMAM dendrimer (**C4**)

The reaction was performed according to general procedure 2. **5** (151 mg, 0.23 mmol, 1 eq.), G2 PAMAM (46 mg, 0.014 mmol, 0.06 eq.), EDC·HCl (157 mg, 0.82 mmol, 3.5 eq.), NHS (94 mg, 0.82 mmol, 3.5 eq.), reaction time of 12h. Yield: 148 mg. ICP-MS (Pt): 140.7 g/kg, average Pt loading of 27.38%, 4.38 Pt units. ^{19}F NMR (D_2O): δ = −72.8–(−72.5) (d, $^{3}J(^{1}H, ^{19}F)$ = 8.6 Hz, 3F, CF_3) (several overlapping duplets) ppm. ^{195}Pt NMR (D_2O): δ = 3246 (minor), 3239 (major) ppm.

5. Complex **7** coupled to G2 PAMAM dendrimer (**C5**)

The reaction was performed according to general procedure 2. **7** (80 mg, 0.15 mmol, 1 eq.), G2 PAMAM (29 mg, 0.009 mmol, 0.06 eq.), EDC·HCl (101 mg, 0.53 mmol, 3.5 eq.), NHS (61 mg, 0.53 mmol, 3.5 eq.), reaction time of 12 h. Yield: 45 mg. ICP-MS (Pt): 207.7 g/kg, average Pt loading of 47.88%, 7.66 Pt units. ^{195}Pt NMR (D_2O): δ = 3038 ppm.

6. Complex **1** coupled to G4 PAMAM dendrimer (**C6**)

The reaction was performed according to general procedure 2. **1** (60 mg, 0.13 mmol, 1 eq.), G4 PAMAM (36 mg, 0.0025 mmol, 0.02 eq.), EDC·HCl (85 mg, 0.44 mmol, 3.5 eq.), NHS (51 mg, 0.44 mmol, 3.5 eq.), reaction time of 12 h. Yield: 41 mg. ICP-MS (Pt): 93.2 g/kg, average Pt loading of 13.59%, 8.70 Pt units. ^{195}Pt NMR (D_2O): δ = 2711 ppm.

7. Complex **1** coupled to G4 PAMAM dendrimer (**C7**)

The reaction was performed according to general procedure 2. **1** (60 mg, 0.13 mmol, 1 eq.), G4 PAMAM (36 mg, 0.0025 mmol, 0.02 eq.), EDC·HCl (85 mg, 0.44 mmol, 3.5 eq.), NHS (51 mg, 0.44 mmol, 3.5 eq.), reaction time of 24 h. Yield: 26 mg. ICP-MS (Pt): 102.7 g/kg, average Pt loading of 15.42%, 9.87 Pt units. ^{195}Pt NMR (D_2O): δ = 2712 ppm.

8. Complex **1** coupled to G4 PAMAM dendrimer (**C8**)

The reaction was performed according to general procedure 2. **1** (60 mg, 0.13 mmol, 1 eq.), G4 PAMAM (36 mg, 0.0025 mmol, 0.02 eq.), EDC·HCl (85 mg, 0.44 mmol, 3.5 eq.), NHS (51 mg, 0.44 mmol, 3.5 eq.), reaction time of 12 h. Yield: 34.8 mg. ICP-MS (Pt): 105.3 g/kg, average Pt loading of 15.94%, 10.20 Pt units. ^{195}Pt NMR (D_2O): δ = 2712 ppm.

9. Complex **1** coupled to G4 PAMAM dendrimer (**C9**)

The reaction was performed according to general procedure 2. **1** (60 mg, 0.13 mmol, 1 eq.), G4 PAMAM (36 mg, 0.0025 mmol, 0.02 eq.), EDC·HCl (85 mg, 0.44 mmol, 3.5 eq.), NHS (51 mg, 0.44 mmol, 3.5 eq.), reaction time of 18 h. Yield: 33 mg. ICP-MS (Pt): 111.6 g/kg, average Pt loading of 17.23%, 11.03 Pt units. ^{195}Pt NMR (D_2O): δ = 2712 ppm.

10. Complex **1** coupled to G4 PAMAM dendrimer (**C10**)

The reaction was performed according to general procedure 2. **1** (60 mg, 0.13 mmol, 1 eq.), G4 PAMAM (36 mg, 0.0025 mmol, 0.02 eq.), EDC·HCl (85 mg, 0.44 mmol, 3.5 eq.), NHS (51 mg, 0.44 mmol, 3.5 eq.), reaction time of 21 h. Yield: 28 mg. ICP-MS (Pt): 129.5 g/kg, average Pt loading of 21.20%, 13.57 Pt units. ^{195}Pt NMR (D_2O): δ = 2711 ppm.

11. Complex **1** coupled to G4 PAMAM dendrimer (**C11**)

The reaction was performed according to general procedure 2. **1** (60 mg, 0.13 mmol, 1 eq.), G4 PAMAM (36 mg, 0.0025 mmol, 0.02 eq.), EDC·HCl (85 mg, 0.44 mmol, 3.5 eq.), NHS (51 mg, 0.44 mmol, 3.5 eq.), reaction time of 12 h. Yield: 54 mg. ICP-MS (Pt): 235.8 g/kg, average Pt loading of 60.33%, 38.61 Pt units. ^{195}Pt NMR (D_2O): δ = 2712 ppm.

12. Complex **1** coupled to G4 PAMAM dendrimer (**C12**)

The reaction was performed according to general procedure 2. **1** (300 mg, 0.63 mmol, 1 eq.), G4 PAMAM (179 mg, 0.013 mmol, 0.02 eq.), EDC·HCl (423 mg, 2.21 mmol, 3.5 eq.), NHS (254 mg, 2.21 mmol, 3.5 eq.), reaction time of 12 h. Yield: 325 mg. ICP-MS (Pt): 259.6 g/kg, average Pt loading of 75.98%, 48.63 Pt units. ^{195}Pt NMR (D_2O): δ = 2710 ppm.

13. Complex **2** coupled to G4 PAMAM dendrimer (**C13**)

The reaction was performed according to general procedure 2. **2** (60 mg, 0.131 mmol, 1 eq.), G4 PAMAM (31 mg, 0.0022 mmol, 0.02 eq.), EDC·HCl (73 mg, 0.38 mmol, 3.5 eq.), NHS (44 mg, 0.38 mmol, 3.5 eq.), reaction time of 12 h. Yield: 67 mg. ICP-MS (Pt): 195.1 g/kg, average Pt loading of 47.30%, 30.27 Pt units. ^{195}Pt NMR (D_2O): δ = 3507 ppm.

14. Complex **3** coupled to G4 PAMAM dendrimer (**C14**)

The reaction was performed according to general procedure 2. **3** (60 mg, 0.10 mmol, 1 eq.), G4 PAMAM (33 mg, 0.0021 mmol, 0.02 eq.), EDC·HCl (70 mg, 0.37 mmol, 3.5 eq.), NHS (42 mg, 0.37 mmol, 3.5 eq.), reaction time of 18 h. Yield: 80 mg. ICP-MS (Pt): 86.8 g/kg, average Pt loading of 13.14%, 8.41 Pt units. ^{195}Pt NMR (D_2O): δ = 3217 ppm.

15. Complex **3** coupled to G4 PAMAM dendrimer (**C15**)

The reaction was performed according to general procedure 2. **3** (60 mg, 0.10 mmol, 1 eq.), G4 PAMAM (33 mg, 0.0021 mmol, 0.02 eq.), EDC·HCl (70 mg, 0.37 mmol, 3.5 eq.), NHS (42 mg, 0.37 mmol, 3.5 eq.), reaction time of 15 h. Yield: 56 mg. ICP-MS (Pt): 103.9 g/kg, average Pt loading of 16.81%, 10.76 Pt units. ^{195}Pt NMR (D_2O): δ = 3217 ppm.

16. Complex **3** coupled to G4 PAMAM dendrimer (**C16**)

The reaction was performed according to general procedure 2. **3** (60 mg, 0.10 mmol, 1 eq.), G4 PAMAM (33 mg, 0.0021 mmol, 0.02 eq.), EDC·HCl (70 mg, 0.37 mmol, 3.5 eq.), NHS (42 mg, 0.37 mmol, 3.5 eq.), reaction time of 12 h. Yield: 90 mg. ICP-MS (Pt): 113.2 g/kg, average Pt loading of 19.03%, 12.18 Pt units. ^{195}Pt NMR (D_2O): δ = 3218 ppm.

17. Complex **3** coupled to G4 PAMAM dendrimer (**C17**)

The reaction was performed according to general procedure 2. **3** (60 mg, 0.10 mmol, 1 eq.), G4 PAMAM (33 mg, 0.0021 mmol, 0.02 eq.), EDC·HCl (71 mg, 0.37 mmol, 3.5 eq.), NHS (42 mg, 0.37 mmol, 3.5 eq.), reaction time of 24 h. Yield: 80 mg. ICP-MS (Pt): 119.1 g/kg, average Pt loading of 20.53%, 13.14 Pt units. ^{195}Pt NMR (D_2O): δ = 3218 ppm.

18. Complex **3** coupled to G4 PAMAM dendrimer (**C18**)

The reaction was performed according to general procedure 2. **3** (60 mg, 0.10 mmol, 1 eq.), G4 PAMAM (33 mg, 0.0021 mmol, 0.02 eq.), EDC·HCl (71 mg, 0.37 mmol, 3.5 eq.), NHS (42 mg, 0.37 mmol, 3.5 eq.), reaction time of 6 h. Yield: 81 mg. ICP-MS (Pt): 141.4 g/kg, average Pt loading of 26.98%, 17.27 Pt units. ^{195}Pt NMR (D_2O): δ = 3217 ppm.

19. Complex **3** coupled to G4 PAMAM dendrimer (**C19**)

The reaction was performed according to general procedure 2. **3** (60 mg, 0.10 mmol, 1 eq.), G4 PAMAM (33 mg, 0.0021 mmol, 0.02 eq.), EDC·HCl (70 mg, 0.37 mmol, 3.5 eq.), NHS (42 mg, 0.37 mmol, 3.5 eq.), reaction time of 21 h. Yield: 81 mg. ICP-MS (Pt): 160.7 g/kg, average Pt loading of 33.78%, 21.62 Pt units. ^{195}Pt NMR (D_2O): δ = 3218 ppm.

20. Complex **3** coupled to G4 PAMAM dendrimer (**C20**)

The reaction was performed according to general procedure 2. **3** (60 mg, 0.10 mmol, 1 eq.), G4 PAMAM (33 mg, 0.0021 mmol, 0.02 eq.), EDC·HCl (71 mg, 0.37 mmol, 3.5 eq.), NHS (43 mg, 0.37 mmol, 3.5 eq.), reaction time of 9 h. Yield: 95 mg. ICP-MS (Pt): 181.4 g/kg, average Pt loading of 42.80%, 27.39 Pt units. ^{195}Pt NMR (D_2O): δ = 3218 ppm.

21. Complex **3** coupled to G4 PAMAM dendrimer (**C21**)

The reaction was performed according to general procedure 2. **3** (60 mg, 0.10 mmol, 1 eq.), G4 PAMAM (33 mg, 0.0021 mmol, 0.02 eq.), EDC·HCl (70 mg, 0.37 mmol, 3.5 eq.), NHS (42 mg, 0.37 mmol, 3.5 eq.), reaction time of 24 h. Yield: 76 mg. ICP-MS (Pt): 240.1 g/kg, average Pt loading of 86.73%, 55.51 Pt units. ^{195}Pt NMR (D_2O): δ = 3217 ppm.

22. Complex **4** coupled to G4 PAMAM dendrimer (**C22**)

The reaction was performed according to general procedure 2. **4** (60 mg, 0.10 mmol, 1 eq.), G4 PAMAM (30 mg, 0.0021 mmol, 0.02 eq.), EDC·HCl (70 mg, 0.37 mmol, 3.5 eq.), NHS (43 mg, 0.37 mmol, 3.5 eq.), reaction time of 12 h. Yield: 65 mg. ICP-MS (Pt): 168.1 g/kg, average Pt loading of 37.95%, 24.29 Pt units. ^{195}Pt NMR (D_2O): δ = 3218 ppm.

23. Complex **5** coupled to G4 PAMAM dendrimer (**C23**)

The reaction was performed according to general procedure 2. **5** (60 mg, 0.09 mmol, 1 eq.), G4 PAMAM (27 mg, 0.0019 mmol, 0.02 eq.), EDC·HCl (63 mg, 0.33 mmol, 3.5 eq.), NHS (38 mg, 0.33 mmol, 3.5 eq.), reaction time of 12 h. Yield: 57 mg. ICP-MS (Pt): 125.1 g/kg, average Pt loading of 23.80%, 15.23 Pt units. ^{19}F NMR (D_2O): δ = -72.9-(-72.4) (d, ^{3}J (^{1}H, ^{19}F) = 8.5 Hz, 3F, C*F*$_3$) (several overlapping duplets) ppm. ^{195}Pt NMR (D_2O): δ = 3246 (minor), 3239 (major) ppm.

24. Complex **7** coupled to G4 PAMAM dendrimer (**C24**)

The reaction was performed according to general procedure 2. **7** (80 mg, 0.15 mmol, 1 eq.), G4 PAMAM (43 mg, 0.0030 mmol, 0.02 eq.), EDC·HCl (101 mg, 0.53 mmol, 3.5 eq.), NHS (61 mg, 0.53 mmol, 3.5 eq.), reaction time of 12 h. Yield: 106 mg. ICP-MS (Pt): 152.6 g/kg, average Pt loading of 29.06%, 18.60 Pt units. ^{195}Pt NMR (D_2O): δ = 3038 ppm.

3. Results and Discussion

3.1. Synthesis

Acetatohydroxidoplatinum(IV) precursor complexes were synthesized according to standard procedures via unsymmetric oxidation with hydrogen peroxide in acetic acid [27]. The trifluoromethyl oxaliplatin analog was synthesized as reported recently [26]. Further reaction with succinic anhydride in absolute DMF resulted in complexes **1**–**6** after purification via RP-HPLC [23]. The synthesis of compound **7** followed a method previously published (Scheme 1) [28].

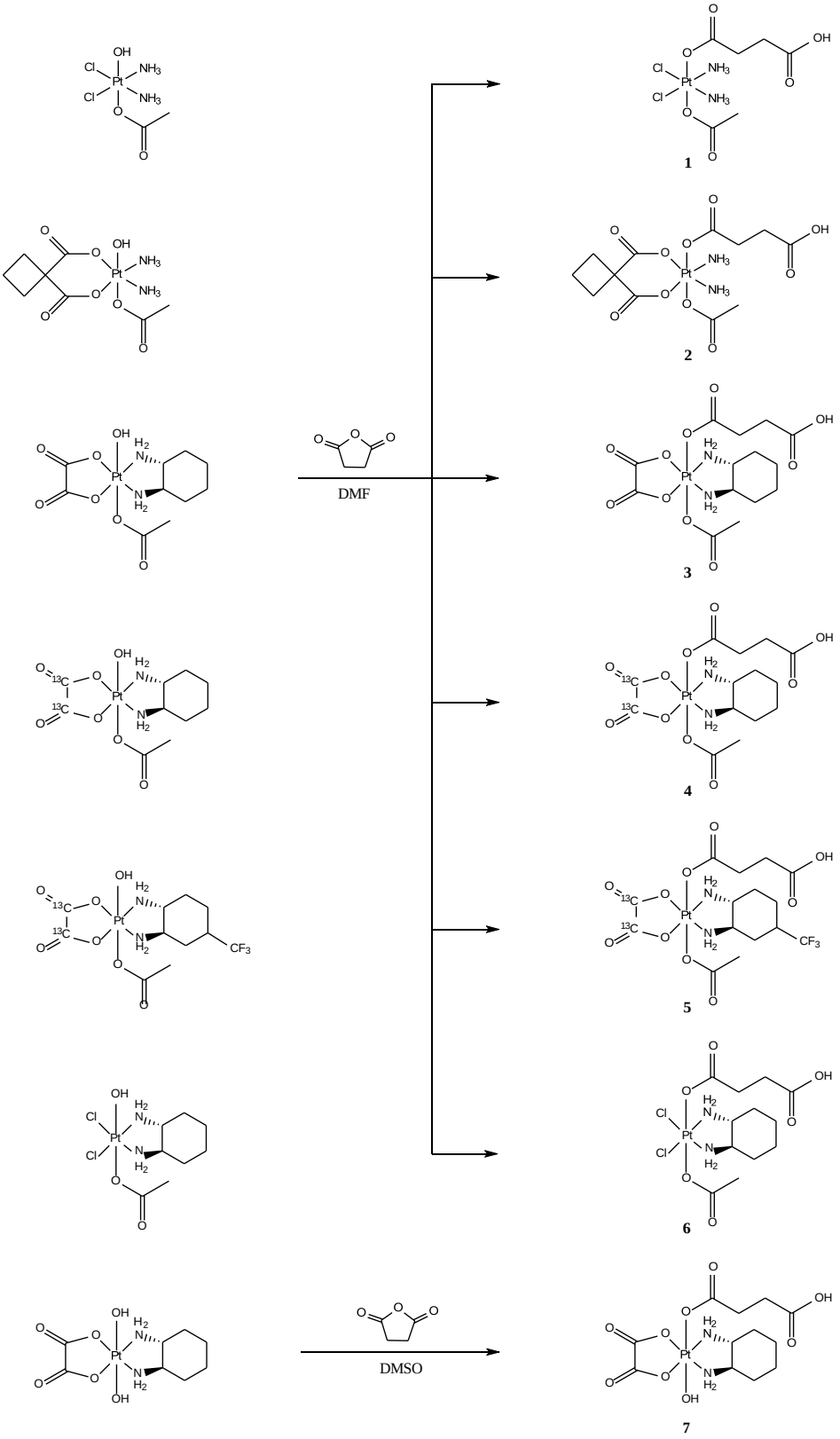

Scheme 1. Synthetic pathway leading to platinum(IV) complexes **1–7**.

The conjugation of platinum(IV) complexes to G2 and G4 PAMAM dendrimers was performed in two steps adapted from a previously published procedure [23]. At first, COOH groups of compounds **1–7** were activated with the coupling reagents N-(3-

dimethylaminopropyl)-N^t-ethylcarbodiimide hydrochloride (EDC·HCl) and N-hydroxysuccinimide (NHS) forming an NHS-ester [29]. The addition of G2 and G4 PAMAM dendrimers containing primary amines as terminal groups resulted in amide bond formations leading to conjugates **C1–C24** (Scheme 2). Purification was performed via dialysis against distilled water using dialysis tubings with a molecular weight cut-off (MWCO) of 1 kDa for conjugates of G2 and MWCO of 3.5 kDa for G4, respectively. The final conjugates, **C1–C24**, were obtained via lyophilization. Additionally, conjugates with platinum(IV) complex **6** were synthesized. However, analysis by NMR spectroscopy revealed an additional signal in ^{195}Pt NMR spectra, probably caused by hydrolysis during the dialysis process. Consequently, these conjugates could not be included in this study. Furthermore, numerous couplings of the G4 PAMAM dendrimer with platinum(IV) complexes **1** and **3** were conducted with different reaction times in order to vary the loading with platinum(IV) complexes (Table 1).

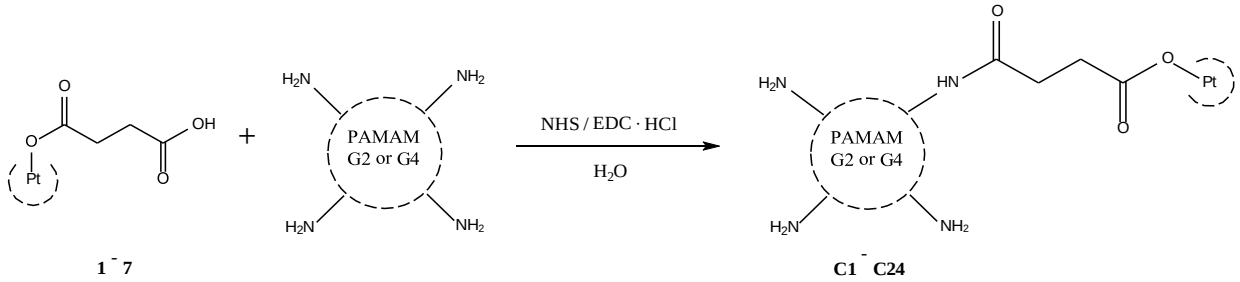

Scheme 2. Schematic illustration of the conjugation reaction of platinum(IV) complexes and PAMAM dendrimers via amide bond formation.

Table 1. Overview of the composition of conjugates **C1–C24** including platinum(IV) units per PAMAM dendrimer, average loading rates and molecular weights (MW).

Sample	Pt(IV)	PAMAM	Number of Terminal NH_2 Moieties	Pt(IV) Units per PAMAM	Average Pt(IV) Loading [%]	MW [kDa]
C1	**1**	G2	16	5.97	37.31	6.0
C2	**2**	G2	16	4.82	30.13	5.8
C3	**4**	G2	16	5.93	37.06	6.6
C4	**5**	G2	16	4.38	27.38	6.0
C5	**7**	G2	16	7.66	47.88	7.2
C6	**1**	G4	64	8.70	13.59	18.2
C7	**1**	G4	64	9.87	15.42	18.7
C8	**1**	G4	64	10.20	15.94	18.9
C9	**1**	G4	64	11.03	17.23	19.3
C10	**1**	G4	64	13.57	21.20	20.4
C11	**1**	G4	64	38.61	60.33	31.9
C12	**1**	G4	64	48.63	75.98	36.5
C13	**2**	G4	64	30.27	47.30	30.2
C14	**3**	G4	64	8.41	13.14	18.9
C15	**3**	G4	64	10.76	16.81	20.2
C16	**3**	G4	64	12.18	19.03	21.0
C17	**3**	G4	64	13.14	20.53	21.5
C18	**3**	G4	64	17.27	26.98	23.8
C19	**3**	G4	64	21.62	33.78	26.2
C20	**3**	G4	64	27.39	42.80	29.4
C21	**3**	G4	64	55.51	86.73	45.0
C22	**4**	G4	64	24.29	37.95	27.8
C23	**5**	G4	64	15.23	23.80	23.7
C24	**7**	G4	64	18.60	29.06	23.8

3.2. Analysis

Characterization of platinum(IV) complexes **1–7** was performed by using multinuclear one- and two-dimensional NMR spectroscopy (^{1}H, ^{13}C, ^{15}N, ^{19}F, ^{195}Pt) (Supporting Information, Figures S1–S10) and their purity was validated by elemental analysis (>95%). The platinum(IV)-PAMAM conjugates **C1–C24** were analyzed by ^{1}H and ^{195}Pt NMR spectroscopy (Supporting Information, Figures S11–S20). ^{195}Pt resonances between 2611 and 3507 ppm are indicative of the presence of platinum(IV) units. As an example, the ^{1}H NMR spectra of G4 PAMAM conjugate **C14** and platinum(IV) complex **3** are shown for comparison (Figure S21). ^{1}H signals of conjugates in the region above 2.2 ppm result in part from signals of the bound platinum(IV) moiety as well as from signals of the inner and outer part of the dendrimer with peripheral amine groups which are free or bound to the platinum complex. Therefore, complete signal assignment in proton NMR spectra was unfortunately not possible.

Furthermore, ICP-MS was used for the determination of the platinum amount of conjugates **C1–C24**. The different platinum(IV) units per dendrimer and the corresponding loading rates are shown in Table 1. The molecular weight of conjugates **C1–C24** was calculated based on the molecular weight of the PAMAM dendrimer (according to Sigma-Aldrich: PAMAM G2 = 3256 g/mol, PAMAM G4 = 14214 g/mol) and the addition of the molecular weight of attached platinum(IV) units, while also considering the release of water molecules during the conjugation process (Table 1).

Additionally, pseudo-2D diffusion-ordered spectroscopy (DOSY) spectra were measured for selected compounds, confirming the conjugation of platinum(IV) complexes to PAMAM dendrimers. As an example, an overlay of DOSY spectra of the conjugate **C14**, the unloaded G4 PAMAM dendrimer and platinum(IV) complex **3** is shown in Figure S22 (Supporting Information). The derived diffusion coefficient was used to estimate the average diameter of unloaded G2 and G4 PAMAM dendrimers as well as of conjugates **C1–C3** and **C12–C14** using the Stokes–Einstein equation and the assumption that the molecules are spherical (Table 2). As expected, the conjugation of platinum(IV) complexes to dendrimers significantly increased the diameter compared to unloaded PAMAM dendrimers. The calculated diameters are consistent with previously published data [23].

Table 2. Estimated diameters using DOSY spectra and Stokes–Einstein equation of G2 and G4 PAMAM dendrimers as well as of conjugates **C1–C3** and **C12–C14**.

Sample	Pt(IV)	PAMAM	Diameter [Å]	Diameter Increase [%]
G2 PAMAM	-	G2	~27.9	-
G4 PAMAM	-	G4	~44.4	-
C1	**1**	G2	~30.4	~9
C2	**2**	G2	~36.9	~32
C3	**3**	G2	~36.5	~31
C12	**1**	G4	~54.4	~23
C13	**2**	G4	~63.6	~43
C14	**3**	G4	~60.0	~35

Moreover, the reduction behavior of conjugates in comparison to unattached platinum(IV) complexes was investigated by time-dependent ^{1}H NMR spectroscopy (Table 3). In general, the reduction behavior is influenced by the nature of the ligands coordinated to the platinum(IV) core. In addition to the axial ligands, the equatorial coordination sphere plays a crucial part as shown by the significantly different rates of reduction of platinum(IV) complexes **1–3**, **5**, **6** featuring the same carboxylato ligands in axial position. In accordance with previous studies [30,31], the cisplatin core of substance **1** led to a faster reduction with a reduction half-time of 6 h, whereas only 6% of the carboplatin(IV) analog **2** was reduced after 95 h. Similar to complex **1**, the two chlorido ligands of compound **6** allow fast electron transfer, thereby supporting rapid reduction [32]. The additional trifluoromethyl group in

position 4 of the DACH ligand of complex **5** seems to cause a faster reduction in comparison to substance **3**, comparable with the discovered relationship of electron-withdrawing power and rate of reduction for axial ligands [33,34]. Furthermore, the strong effect of axial ligands on the reduction behavior is displayed by the comparison of the two oxaliplatin(IV) analogs **3** and **7**. The amine and carboxylato ligands of complex **3** cannot form bridges with the reducing agent and thus do not support the electron transfer from ascorbate to the platinum(IV) atom in the center. Consequently, only 14% of compound **3** was reduced after 165 h. In contrast, the hydroxido ligand of complex **7** facilitates electron transfer and results in a significantly lower reduction half-time of 29 h, consistent with previously published results [35,36]. The same order of rates of reduction was observed for the conjugates of the respective platinum(IV) complexes, except for **C23**. Generally, all conjugates underwent faster reduction compared to their corresponding platinum(IV) complexes, possibly caused by the increased bulkiness of the axial ligand. A potential connection between bulkiness and facilitated reduction has been reported in the literature [37]. As further expected, the influence between G2 and G4 dendrimers on the reduction behavior is marginal due to the huge distance to the platinum(IV) core. Therefore, no significant difference in the rate of reduction between conjugates of G2 and G4 dendrimers was observed based on the measurements of **C2** and **C13**, respectively.

Table 3. Overview of the reduction half-times of platinum(IV) complexes and representative conjugates at ambient temperature (ratio complex: ascorbic acid = 1:25). Due to long reduction half-times, some measurements were stopped before reaching the reduction half-time, and the percentage of the reduced species at this point is mentioned in brackets.

Sample	Pt(IV)	PAMAM	Reduction Half-Time [h]
1	**1**	-	~6
2	**2**	-	>95 (~6%)
3	**3**	-	>165 (~14%)
5	**5**	-	>93 (~23%)
6	**6**	-	~27
7	**7**	-	~29
C2	**2**	G2	>92 (~37%)
C11	**1**	G4	~3
C13	**2**	G4	>95 (~42%)
C22	**4**	G4	~45
C23	**5**	G4	~65
C24	**7**	G4	n/a

Finally, a single crystal of oxaliplatin analog **3** was obtained from a methanol solution by slow evaporation at room temperature and was analyzed by X-ray diffraction. Complex **3** crystallized in the orthorhombic space group $P2_12_12_1$ and confirmed the octahedral coordination sphere with the platinum(IV) atom in the center (Figure 1). The bidentate oxalato and DACH ligand are in equatorial position with bite angles of 84.74(16)° (O5–Pt1–O6) and 83.59(19)° (N1–Pt1–N2), respectively. The structure is completed by two axially coordinated carboxylato ligands featuring an O1–Pt1–O9 angle of 177.1(2)°. The equatorial Pt–N (Pt1–N1, 2.031(5); Pt1–N2, 2.034(5) Å) and Pt–O (Pt1–O5, 2.010(4); Pt1–O6, 2.009(4) Å) distances are comparable to other oxaliplatin analogs reported in the literature [38], whereas Pt–O bond lengths of carboxylato ligands in axial position were found at 2.004(4) (Pt1–O1) and 2.002(4) Å (Pt1–O9), and are comparable with those of previously published platinum(IV) complexes [39]. Additionally, one intra-molecular hydrogen bond N1–H O10 of moderate character with a donor–acceptor contact of 2.715 Å (N1⋯⋯O10) and an angle of 130.1° (N1–H O10) was found in the solid state. Further details about the crystal structure can be found in the Supporting Information (Tables S1–S3).

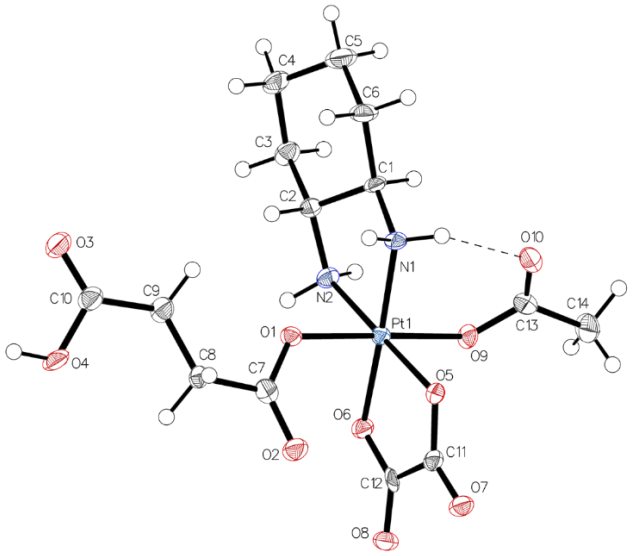

Figure 1. ORTEP view of complex **3**. Asymmetric unit of platinum(IV) complex **3** drawn with 50% displacement ellipsoid with a bond precision for C-C single bonds of 0.0099 Å. The chiral interpretation is done with the help of Flack and Hooft parameters (−0.023, −0.019), and can be determined for C1 (R) and C2 (R). Solvent and disorder (main residue disorder = 4%) were omitted for clarity.

3.3. Cytotoxicity

Three human cancer cell lines differing in their chemosensitivity were employed for testing the cytotoxic potencies of all compounds: the broadly sensitive ovarian teratocarcinoma cell line CH1/PA-1, the multidrug-resistant non-small cell lung cancer cell line A549 and the colon cancer cell line SW480 with mostly intermediate sensitivity. IC_{50} values interpolated from concentration–effect curves (Supporting Information, Figures S23–S29) are listed in Table 4. This pattern of sensitivity also reflects throughout the data compiled here.

As expected due to their higher inertness, platinum(IV) complexes **1**–**3** are by one to two orders of magnitude less potent than the corresponding platinum(II) drugs cisplatin, carboplatin and oxaliplatin. Of the structural modifications imposed on **3**, only the exchange of oxalate for two chlorido ligands had conspicuous consequences for biological activity: IC_{50} values of the dichlorido analog **6** are 9–26 times lower than those of **3**, depending on the cell line, whereas addition of a CF_3 substituent to the DACH ligand (in **5**) or replacement of the axial acetato ligand with a hydroxido group (in **7**) yielded minor, if any, changes in cytotoxic potency.

Except for the rather inefficient conjugate **C2** (where, moreover, a comparison with the unconjugated complex **2** is only partially possible, as some IC_{50} values were not even reached), loading of the platinum(IV) complexes onto G2 PAMAM dendrimers (**C1**, **C3**–**C5**) resulted in products with 4–30 times increased cytotoxic potency in absolute numbers. This implies that the products mostly exert at least the effect that could roughly be expected from their degree of platinum(IV) loading (4–9 platinum(IV) units per dendrimer), but even higher effects were observed in some cases (e.g., compare **C4** with **5** in CH1/PA-1 cells).

Table 4. Cytotoxicity of platinum(IV) complexes **1–3** and **5–7** as well as their dendrimer conjugates **C1–C24** in comparison with parental platinum(II) drugs in three human cancer cell lines. Mean IC_{50} values are indicated ± standard deviations and are obtained from at least three independent MTT assays (96 h exposure) and pertain to dendrimer concentration for **C1–C24**.

Sample	Pt(IV)	PAMAM	Pt(IV) Units per PAMAM	IC_{50} [μM] A549	IC_{50} [μM] CH1/PA-1	IC_{50} [μM] SW480
G2 PAMAM [23]	-	G2	-	>50	67 ± 19	>50
G4 PAMAM [23]	-	G4	-	8.2 ± 2.4	1.5 ± 0.4	6.2 ± 1.1
Cisplatin [24]	-	-	-	3.8 ± 1.0	0.073 ± 0.001	2.3 ± 0.2
Carboplatin [24]	-	-	-	38 ± 3	0.79 ± 0.11	42 ± 10
Oxaliplatin [24]	-	-	-	0.98 ± 0.21	0.18 ± 0.01	0.29 ± 0.05
1 [28]	**1**	-	-	99 ± 17	1.2 ± 0.5	47 ± 11
2 [28]	**2**	-	-	>200	16 ± 6	>200
3 [28]	**3**	-	-	70 ± 29	4.1 ± 0.6	22 ± 8
5	**5**	-	-	54 ± 6	6.0 ± 0.9	33 ± 5
6	**6**	-	-	2.8 ± 0.1	0.44 ± 0.10	0.85 ± 0.14
7	**7**	-	-	66 ± 2	5.2 ± 0.8	20 ± 3
C1	**1**	G2	5.97	10.7 ± 0.3	0.31 ± 0.10	6.4 ± 1.3
C2	**2**	G2	4.82	>200	11 ± 2	122 ± 8
C3	**4**	G2	5.93	6.3 ± 1.3	0.47 ± 0.09	1.7 ± 0.7
C4	**5**	G2	4.38	9.9 ± 0.8	0.20 ± 0.06	2.3 ± 0.4
C5	**7**	G2	7.66	4.0 ± 0.2	0.22 ± 0.02	0.98 ± 0.18
C6	**1**	G4	8.70	1.2 ± 0.3	0.015 ± 0.004	0.42 ± 0.03
C7	**1**	G4	9.87	2.5 ± 0.5	0.029 ± 0.004	1.3 ± 0.2
C8	**1**	G4	10.20	1.1 ± 0.2	0.0084 ± 0.0036	0.31 ± 0.12
C9	**1**	G4	11.03	1.3 ± 0.2	0.011 ± 0.003	0.51 ± 0.05
C10	**1**	G4	13.57	1.2 ± 0.2	0.012 ± 0.003	0.41 ± 0.09
C11	**1**	G4	38.61	1.4 ± 0.1	0.013 ± 0.001	0.71 ± 0.06
C12	**1**	G4	48.63	0.69 ± 0.08	0.0034 ± 0.0016	0.25 ± 0.18
C13	**2**	G4	30.27	9.0 ± 1.8	0.025 ± 0.010	2.5 ± 1.8
C14	**3**	G4	8.41	0.30 ± 0.05	0.017 ± 0.003	0.072 ± 0.007
C15	**3**	G4	10.76	0.092 ± 0.004	0.0078 ± 0.0010	0.038 ± 0.006
C16	**3**	G4	12.18	0.20 ± 0.02	0.013 ± 0.001	0.065 ± 0.017
C17	**3**	G4	13.14	0.85 ± 0.28	0.039 ± 0.013	0.27 ± 0.08
C18	**3**	G4	17.27	1.8 ± 0.3	0.086 ± 0.019	0.50 ± 0.18
C19	**3**	G4	21.62	0.24 ± 0.06	0.011 ± 0.003	0.077 ± 0.021
C20	**3**	G4	27.39	0.052 ± 0.016	0.0024 ± 0.0006	0.022 ± 0.006
C21	**3**	G4	55.51	0.14 ± 0.02	0.0067 ± 0.0005	0.036 ± 0.002
C22	**4**	G4	24.29	0.031 ± 0.006	0.00078 ± 0.00026	0.0062 ± 0.0012
C23	**5**	G4	15.23	27 ± 1	0.37 ± 0.09	6.7 ± 0.7
C24	**7**	G4	18.60	0.191 ± 0.004	0.0069 ± 0.0007	0.056 ± 0.003

Apart from a singular exception (conjugate **C23** containing complex **5**), the effects of loaded G4 PAMAM dendrimers are not less remarkable: the majority of **C6–C12** (loaded with cisplatin analog **1**) and, even more so, **C14–C22** (loaded with oxaliplatin analogs **3** or **4**) is much more to tremendously more potent than could be explained by the mere ratios of platinum(IV) loading (especially compare **C15**, **C20**, **C21** or also **C22** with **3**). Reasons are likely to be multifactorial. It has been reported that dendrimers can enhance membrane permeability and therefore increase the cellular uptake of drugs. The conjugation of anticancer agent paclitaxel to lauryl-modified G3 PAMAM dendrimers led to up to 12-times higher permeability than free paclitaxel in monolayers of the human colon adenocarcinoma cell line Caco-2, as well as in porcine brain endothelial cells [40]. Furthermore, enhanced cellular uptake by a factor of up to 11 was detected with G4 PAMAM dendrimers combined with cisplatin in A2780 ovarian cancer cells compared to free cisplatin [19]. Additionally,

a relationship of fast reduction leading to increased cytotoxicity is widely accepted [41]. According to Ref. [19], the accelerated activation of conjugates by reduction based on faster reduction half-times (Table 2) as compared to their corresponding platinum(IV) complexes may play a significant part in increased cytotoxicity. In addition to enhanced permeability, cellular uptake and faster reduction half-times, it is conceivable that synergies between the individual effects of platinum(IV) complex and G4 PAMAM dendrimer additionally contribute to the extraordinary enhancement of cytotoxicity, since even the unloaded G4 PAMAM dendrimer (in contrast to G2) exerts antiproliferative activity in the low micromolar concentration range in all three cell lines. However, detailed investigations are needed to fully understand the mechanism of significantly increased cytotoxicity of platinum(IV)-based PAMAM dendrimer conjugates. Furthermore, it is intriguing that higher loading than the applied minimum of about 10 platinum(IV) units per dendrimer did not necessarily (or, in fact, rather occasionally and under proportionally) lead to further increase in potency, neither in series **C6–C12** nor **C14–C21**. It is conceivable that reasons are similar to a previously conducted study of half-generation PAMAM dendrimers loaded with cisplatin, in which an incomplete drug release was detected probably caused by intramolecular interactions of platinum complex and dendrimer branches [42].

3.4. In Vivo Studies

In order to validate the in vivo efficacy of the platinum(IV)-loaded dendrimer strategy, one representative conjugate of the platinum(IV) series of cisplatin (**C11**), carboplatin (**C13**), and oxaliplatin (**C22**) was tested in the G4 PAMAM dendrimer background. The toxicity tests were performed by tail vein injection (every second day for 3 injections in total) into non-tumor-bearing mice at a dose equimolar to the released platinum(II) species: **C11**, 0.17 mg/20 g, equimolar to 3 mg/kg cisplatin; **C13**, 0.91 mg/20 g, equimolar to 17 mg/kg carboplatin; **C22**, 0.52 mg/20 g; equimolar to 9 mg/kg oxaliplatin. Out of the three tested substances, the cisplatin-based conjugate **C11** showed by far the best tolerability without significant weight loss or profound changes in behavior and showed only temporal mild hair loss. In contrast, oxaliplatin-based conjugate **C22** led in both treated mice to tail necrosis, forcing the termination of this experimental group based on ethical guidelines. The carboplatin-based conjugate **C13** induced moderate weight and strong hair loss. Thus, the cisplatin-based conjugate was further analyzed in more depth. An additional toxicity assay with **C12**, a higher platinum(IV)-loaded conjugate compared to **C11**, was performed at concentrations equimolar to 1.5 and 3 mg/kg cisplatin and the same application scheme as before. Again, no signs of toxicity were observed.

Consequently, **C12** was chosen for the therapy experiment. As the anticancer activity of platinum drugs includes also immunological mechanisms [43], the colon cancer allograft model was used. As a first step, the impact of cisplatin was tested compared to **C12** in CT26 murine colon cancer cells in vitro. Compound **C12** exerted a more than four-fold lower IC_{50} value as compared to cisplatin (**C12**: 0.43 µM; cisplatin: 1.85 µM, Supporting Information, Figure S30), thus resembling data in the human cancer cell models (compare Table 4).

Based on this higher cytotoxic activity and clearly better tolerability in non-tumor-bearing animals, the efficacy of **C12** (7.5 mg/kg: equimolar to 3 mg/kg cisplatin) was compared with the respective dose of free cisplatin (3 mg/kg) and unloaded G4 PAMAM dendrimer in CT26-allograft-bearing mice. Drugs were given intravenously for two weeks twice a week. The impact of the different treatment groups as compared to solvent control on tumor volume and body weight until day 14 (loss of the first mouse in the solvent group due to big tumor size) are given in Figures 2 and 3, respectively. All treatments significantly reduced tumor volume as compared to the solvent control with a maximum tumor growth inhibition effect of 37% for unloaded G4 PAMAM dendrimer, 47.6% for cisplatin, as well as 65.6% for **C12**. In addition, concerning the tumor growth curves, the strongest activity was exerted by **C12**, although the difference between free cisplatin and **C12** did not reach statistical significance in the multiple comparison tests (p = 0.075). Concerning toxicity,

neither free G4 PAMAM dendrimer nor **C12** led to any loss of body weight. In contrast, free cisplatin at the maximal tolerated dose of 3 mg/kg significantly reduced body weight as compared to all other experimental groups with a maximal loss of body weight of around 20% at day 14 of treatment. This data strongly suggests an improved therapeutic window for cisplatin when given as a PAMAM-dendrimer-based nano-formulation.

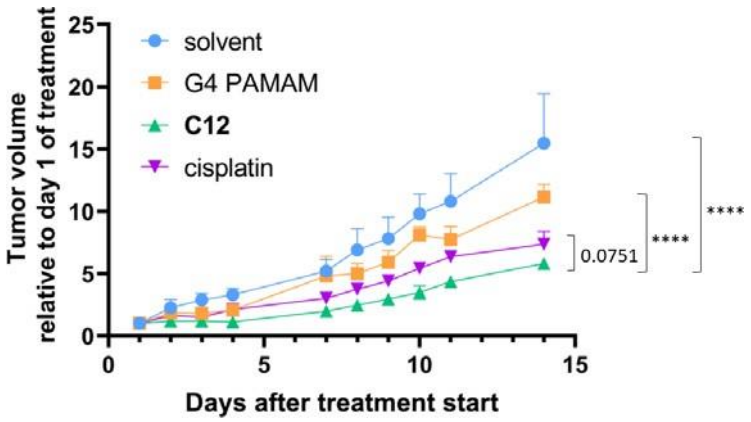

Figure 2. Comparison of the tumor volume development with treatment of solvent, G4 PAMAM, conjugate **C12** and cisplatin in BALB/c mice over 14 days. Significances were determined via Turkey's multiple comparisons test with the following abbreviations: **** $p < 0.0001$.

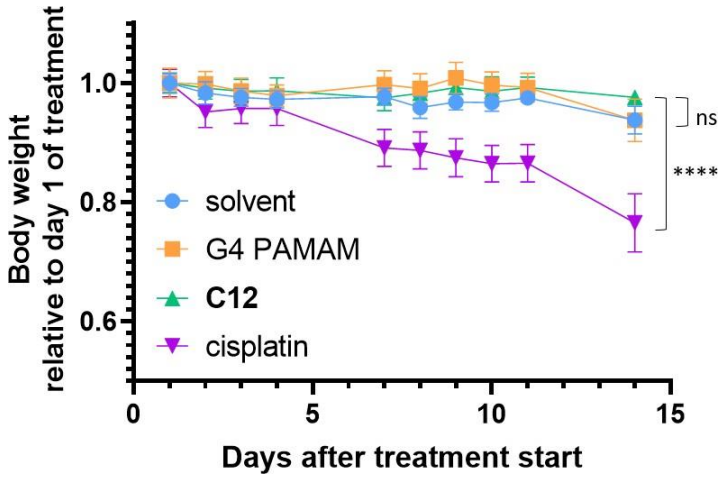

Figure 3. Comparison of the body weight development with treatment of solvent, G4 PAMAM, conjugate **C12** and cisplatin in BALB/c mice over 14 days. Significances were determined via Turkey's multiple comparisons test with the following abbreviations: ns = not significant, **** $p < 0.0001$.

The promising effects further translate into a prolongation trend of animal survival (Figure 4). While in the cisplatin group, weight loss was critical in addition to tumor necrosis, even smaller tumors tended to get necrotic and broke up in **C12**-treated animals, making the sacrifice of the animals necessary due to ethical guidelines. In contrast to the cisplatin and G4 PAMAM dendrimer treatment arms, only the anticancer activity of **C12** showed a trend towards longer survival (p-value of 0.0549 in log-rank and 0.05 in Gehan–Breslow–Wilcoxon test) in the direct comparison with the solvent control arm. A more extended analysis of different doses and schedules is needed to optimize the therapeutic effects of **C12,** but limit the massive necrotizing effects leading to the termination of the experiment due to tumor ulceration.

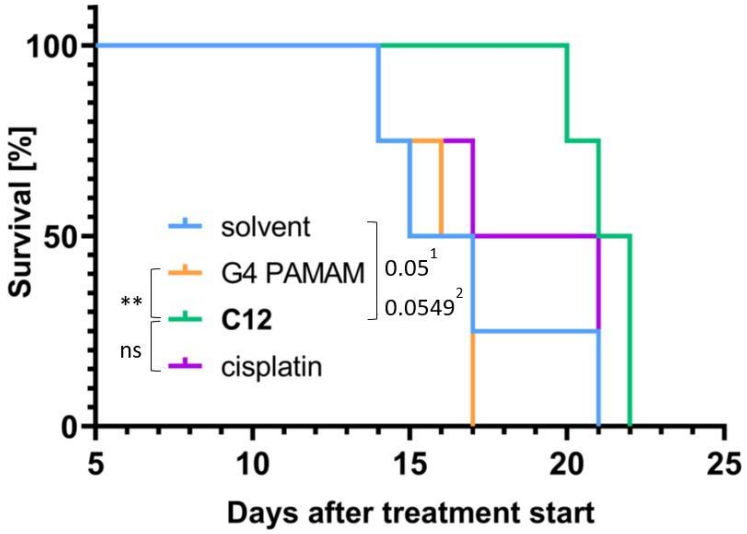

Figure 4. Comparison of the survival time with treatment of solvent, G4 PAMAM, conjugate **C12** and cisplatin in BALB/c mice over 14 days. Significances were determined via log-rank test (LRT) and Gehan–Breslow-Wilcoxon test (GBWT) with the following abbreviations: ns = not significant, ** $p < 0.01$. [1] with GBWT. [2] with LRT.

In addition to tumor growth experiments, the tumor and organ distribution of platinum in mice treated with cisplatin or **C12** were determined by ICP-MS (Figure 5). Unexpectedly, the platinum levels in the tumor did not differ significantly 24 h after the second dosing. In contrast, **C12** led to high platinum levels in the serum at all three time points, while blood cells contained enhanced platinum contents in the case of cisplatin treatment (Supporting Information, Figure S31). This suggests a lower clearance and reduced local interaction with blood cells of **C12**, as compared to cisplatin. In organ distribution (Figure 5), **C12** treatment led to a massive platinum accumulation in the kidney as compared to all other organs, while in the case of cisplatin, higher levels were detected in lung tissue, however, with great inter-individual differences. These data strongly suggest that the PAMAM dendrimer formulation leads to trapping of the nano-formation probably based on filtration in the glomerulus and reabsorbed in the lumen of the proximal tubule. Renal excretion and glomerular filtration are typical for ≤G4 PAMAM dendrimers and in general for nanoparticles smaller than 5 nm [44,45]. The conjugation of complex **1** to G4 PAMAM dendrimers considerably increased the polymer diameter of **C14** from about 4.5 to 5.4 nm. Additionally, the influence of the molecular weight of nanoparticles on the biodistribution behavior was reported previously. Nanoparticles <20 kDa primarily undergo renal clearance, whereas bigger molecules show longer blood circulation times and a shift towards clearance by the reticuloendothelial system [46]. Based on a particle size of over 5 nm and a molecular weight of 36.5 kDa of conjugate **C12**, the renal accumulation is rather unexpected and needs to be investigated in more detail. However, it is obvious that, despite these unwanted conditions, **C12** exerted a comparable tumor accumulation to cisplatin, a tendency to enhance anticancer activity, and an improved therapeutic window. This strongly suggests further modifications of the novel cisplatin dendrimeric remedy to ameliorate kidney accumulation and, in parallel, enhance tumor response. On the contrary, the efficient kidney accumulation of this dendrimer preparation might also be considered in kidney-specific drug delivery approaches [47–49].

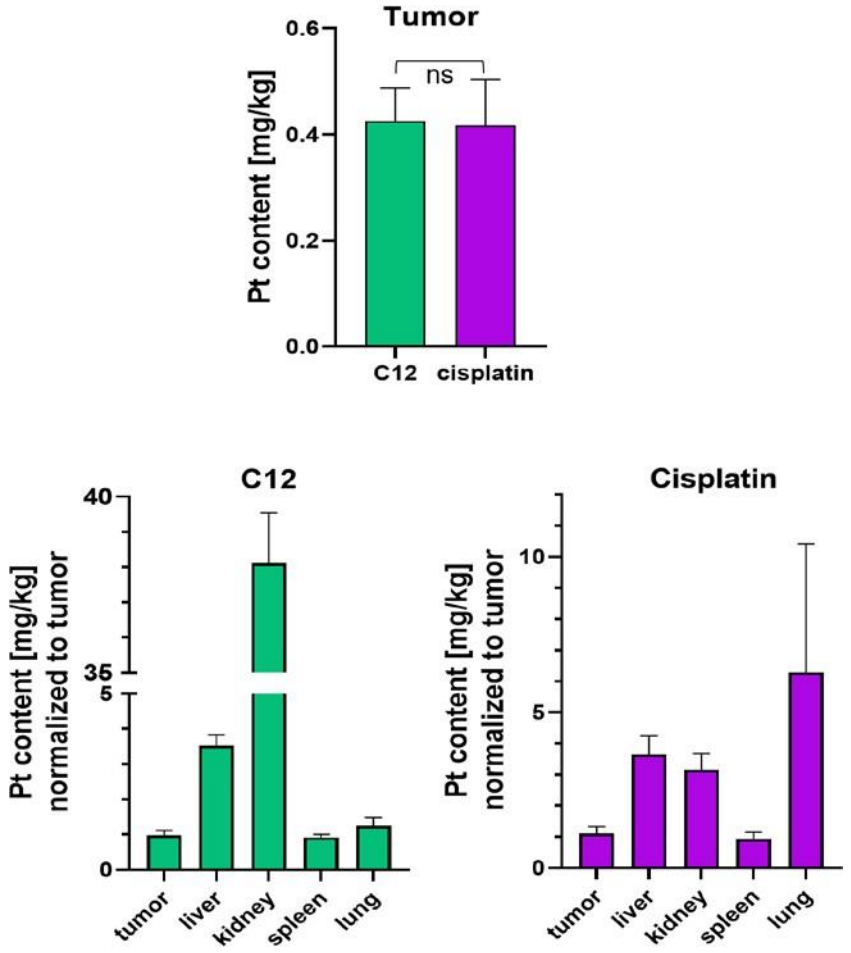

Figure 5. Comparison of the platinum accumulation in tumors and different organs of mice treated with conjugate **C12** (green) and cisplatin (violet) 24 h after second application measured by ICP-MS. Significances were determined via Turkey's multiple comparisons test with the following abbreviation: ns = not significant.

4. Conclusions

In the present study, an alternative antitumor strategy was presented by conjugating various platinum(IV)-analogs of cisplatin, carboplatin and oxaliplatin to the surface of G2 and G4 PAMAM dendrimers. Twenty-four novel conjugates were synthesized and characterized by ^{1}H and ^{195}Pt NMR spectroscopy, as well as DOSY measurements substantiating the successful conjugation. Reduction behavior analysis revealed a significantly faster reduction of all conjugates in comparison to their corresponding platinum(IV) complexes, probably caused by the increased bulkiness of the axial ligands of the conjugates. The accelerated reduction of the conjugates may also, amongst others, be responsible for improved cytotoxicity of the conjugates. Specifically, the conjugation of platinum(IV) complexes to G4 PAMAM dendrimers resulted in IC_{50} values in the low micro- to the nanomolar range, tremendously lower compared to the corresponding platinum(IV) or even platinum(II) complexes. Remarkably, an oxaliplatin(IV)-based conjugate even reached an IC_{50} value of 780 ± 260 pM in the CH1/PA-1 cancer cell line.

Furthermore, the cisplatin(IV)-based conjugate **C12** was investigated in vivo in CT26-allograft-bearing mice due to its best toxicological profile. Concentrations of the conjugate equimolar to 3 mg/kg cisplatin (maximum tolerated dosage [50]) were very well tolerated and even higher doses could be considered in further investigations. Additionally, biodistribution was analyzed in tumor-bearing mice 24 h after the second application. Unexpectedly, increased accumulation in the kidney was detected despite a higher cut-

off molecular weight and particle size of **C12.** It needs to be investigated in more detail, whether **C12** behaves like nanoparticles with a hydrodynamic diameter between 5 nm and 100 nm efficiently crossing the endothelial layer, but blocked by the glomerular basement membrane [51]. Due to the connection of preferred renal excretion with small molecular weights and particle sizes as well as cationic surface charges, supporting attraction to the negatively charged endothelial and podocyte glycocalyx, the use of amine-terminated PAMAM dendrimers >G4 could be considered to reduce renal accumulation. Nevertheless, besides increased molecular weight and size, higher generations of cationic PAMAM dendrimers (>G4) are accompanied by a sharp increase in cytotoxicity based on their increased positive charge density [52,53]. However, additional surface modifications (e.g., PEGylation) of the terminal positively charged amines under physiological conditions could reduce undesired toxicities and further decrease the preference for renal excretion [54,55].

The following anticancer activity experiments revealed a maximum tumor growth inhibition effect of 65.6% for **C12** compared to 47.6% for cisplatin. Additionally, the treatment with **C12** had no negative influence on body weight, whereas cisplatin application led to a maximal loss of body weight of around 20%, enabling an improved therapeutic window for **C12** compared to cisplatin. Furthermore, a trend of extended animal survival with the treatment of **C12** could be observed compared to the solvent control and cisplatin group.

Finally, it can be concluded that the combination of platinum(IV) complexes coupled with PAMAM dendrimers enables a promising approach to further improve existing anticancer therapy. The full potential could be exploited by further investigations of the therapeutic window as well as adjustments on the surface of PAMAM dendrimers to further optimize pharmacological properties.

Supplementary Materials: The following supporting information can be downloaded at https://www.mdpi.com/article/10.3390/pharmaceutics15051515/s1, Figures S1–S10: NMR Spectra of Platinum(IV) Complexes **5**–**7**; Figures S11–S22: NMR Spectra of selected conjugates; Tables S1–S3: X-Ray diffraction analysis; Figures S23–S30: concentration–effect curves; Figure S31: in vivo data. References [56–62] are cited in the supplementary materials.

Author Contributions: Conceptualization, Y.L.-K. and M.S.G.; data curation, Y.L.-K., M.H., P.V., M.A.J., W.B. and M.S.G.; formal analysis, P.V. and W.B.; funding acquisition, Y.L.-K., W.B., M.S.G. and B.K.K.; investigation, Y.L.-K., M.H. and P.V.; methodology, Y.L.-K., W.B. and M.S.G.; project administration, Y.L.-K. and M.S.G.; resources, M.A.J., W.B., M.S.G. and B.K.K.; supervision, M.A.J., W.B., M.S.G. and B.K.K.; validation, Y.L.-K., M.H., P.V., M.A.J., W.B. and M.S.G.; visualization, Y.L.-K., P.V. and M.A.J.; writing—original draft, Y.L.-K., P.V., M.A.J. and W.B.; writing—review and editing, Y.L.-K., P.V., M.A.J., W.B., M.S.G. and B.K.K. All authors have read and agreed to the published version of the manuscript.

Funding: The authors gratefully acknowledge the Uni:docs Fellowship Programme at the University of Vienna for funding this research and the FWF (L568) for their support.

Institutional Review Board Statement: The animal study was performed in accordance with the Ethics Committee for the Care and Use of Laboratory Animals at the Medical University Vienna (proposal number BMBWF-V/3b 2020-0.380.502).

Informed Consent Statement: Not applicable.

Data Availability Statement: The data presented in this study are available in the supplementary material.

Acknowledgments: The authors gratefully acknowledge the support of Sophie Neumayer, Alexander Prado-Roller, Tatjana Schafarik and Martin Schaier. Open Access Funding by the University of Vienna.

Conflicts of Interest: The authors declare no conflict of interest.

References

1. Ghosh, S. Cisplatin: The First Metal Based Anticancer Drug. *Bioorg. Chem.* **2019**, *88*, 102925. [CrossRef] [PubMed]
2. Brown, A.; Kumar, S.; Tchounwou, P.B. Cisplatin-Based Chemotherapy of Human Cancers. *J. Cancer Sci. Ther.* **2019**, *11*, 97–103.

3. Fennell, D.A.; Summers, Y.; Cadranel, J.; Benepal, T.; Christoph, D.C.; Lal, R.; Das, M.; Maxwell, F.; Visseren-Grul, C.; Ferry, D. Cisplatin in the Modern Era: The Backbone of First-Line Chemotherapy for Non-Small Cell Lung Cancer. *Cancer Treat. Rev.* **2016**, *44*, 42–50. [CrossRef] [PubMed]
4. Varbanov, H.P.; Göschl, S.; Heffeter, P.; Theiner, S.; Roller, A.; Jensen, F.; Jakupec, M.A.; Berger, W.; Galanski, M.; Keppler, B.K. A Novel Class of Bis-and Tris-Chelate Diam(m)Inebis(Dicarboxylato) Platinum(IV) Complexes as Potential Anticancer Prodrugs. *J. Med. Chem.* **2014**, *57*, 6751–6764. [CrossRef] [PubMed]
5. Boulikas, T. Molecular Mechanisms of Cisplatin and Its Liposomally Encapsulated Form, Lipoplatin. Lipoplatin as a Chemotherapy and Antiangiogenesis Drug. *Cancer Ther.* **2007**, *5*, 351–376.
6. Oun, R.; Moussa, Y.E.; Wheate, N.J. The Side Effects of Platinum-Based Chemotherapy Drugs: A Review for Chemists. *Dalton Trans.* **2018**, *47*, 6645–6653. [CrossRef]
7. Gibson, D. Platinum(IV) Anticancer Prodrugs-Hypotheses and Facts. *Dalton Trans.* **2016**, *45*, 12983–12991. [CrossRef]
8. Ritacco, I.; Mazzone, G.; Russo, N.; Sicilia, E. Investigation of the Inertness to Hydrolysis of Platinum(IV) Prodrugs. *Inorg. Chem.* **2016**, *55*, 1580–1586. [CrossRef]
9. Mi, Q.; Shu, S.; Yang, C.; Gao, C.; Zhang, X.; Luo, X.; Bao, C.; Zhang, X.; Niu, J. Current Status for Oral Platinum (IV) Anticancer Drug Development. *Int. J. Med. Phys. Clin. Eng. Radiat. Oncol.* **2018**, *7*, 231–247. [CrossRef]
10. Alassadi, S.; Pisani, M.J.; Wheate, N.J. A Chemical Perspective on the Clinical Use of Platinum-Based Anticancer Drugs. *Dalton Trans.* **2022**, *51*, 10835–10846. [CrossRef]
11. Apps, M.G.; Choi, E.H.Y.; Wheate, N.J. The State-of-Play and Future of Platinum Drugs. *Endocr. Relat. Cancer* **2015**, *22*, R219–R233. [CrossRef] [PubMed]
12. Subhan, M.A.; Yalamarty, S.S.K.; Filipczak, N.; Parveen, F.; Torchilin, V.P. Recent Advances in Tumor Targeting via Epr Effect for Cancer Treatment. *J. Pers. Med.* **2021**, *11*, 571. [CrossRef]
13. Shi, Y.; van der Meel, R.; Chen, X.; Lammers, T. The EPR Effect and beyond: Strategies to Improve Tumor Targeting and Cancer Nanomedicine Treatment Efficacy. *Theranostics* **2020**, *10*, 7921–7924. [CrossRef] [PubMed]
14. Tomalia, D.A.; Baker, H.; Dewald, J.; Hall, M.; Kallos, G.; Martin, S.; Roeck, J.; Ryder, J.; Smith, P. A New Class of Polymers: Starburst-Dendritic Macromolecules. *Polym. J.* **1985**, *17*, 117–132. [CrossRef]
15. Tomalia, D.A.; Fréchet, J.M.J. Discovery of Dendrimers and Dendritic Polymers: A Brief Historical Perspective. *J. Polym. Sci. A Polym. Chem.* **2002**, *40*, 2719–2728. [CrossRef]
16. Rolland, O.; Turrin, C.O.; Caminade, A.M.; Majoral, J.P. Dendrimers and Nanomedicine: Multivalency in Action. *New J. Chem.* **2009**, *33*, 1809–1824. [CrossRef]
17. Abbasi, E.; Aval, S.F.; Akbarzadeh, A.; Milani, M.; Nasrabadi, H.T.; Joo, S.W.; Hanifehpour, Y.; Nejati-Koshki, K.; Pashaei-Asl, R. Dendrimers: Synthesis, Applications, and Properties. *Nanoscale Res. Lett.* **2014**, *9*, 247. [CrossRef]
18. Harper, B.W.; Krause-Heuer, A.M.; Grant, M.P.; Manohar, M.; Garbutcheon-Singh, K.B.; Aldrich-Wright, J.R. Advances in Platinum Chemotherapeutics. *Chem. Eur. J.* **2010**, *16*, 7064–7077. [CrossRef]
19. Yellepeddi, V.K.; Kumar, A.; Maher, D.M.; Chauhan, S.C.; Vangara, K.K.; Palakurthi, S. Biotinylated PAMAM Dendrimers for Intracellular Delivery of Cisplatin to Ovarian Cancer: Role of SMVT. *Anticancer Res.* **2011**, *31*, 897–906.
20. Yellepeddi, V.K.; Vangara, K.K.; Palakurthi, S. Poly(Amido)Amine (PAMAM) Dendrimer-Cisplatin Complexes for Chemotherapy of Cisplatin-Resistant Ovarian Cancer Cells. *J. Nanopart. Res.* **2013**, *15*, 1897. [CrossRef]
21. Yellepeddi, V.K.; Vangara, K.K. In Vivo Efficacy of PAMAM-Dendrimer-Cisplatin Complexes in SKOV-3 Xenografted Balb/C Nude Mice. *J Biotechnol. Biomater.* **2013**, *S13*, 003. [CrossRef]
22. Guo, X.L.; Kang, X.X.; Wang, Y.Q.; Zhang, X.J.; Li, C.J.; Liu, Y.; Du, L.B. Co-Delivery of Cisplatin and Doxorubicin by Covalently Conjugating with Polyamidoamine Dendrimer for Enhanced Synergistic Cancer Therapy. *Acta Biomater.* **2019**, *84*, 367–377. [CrossRef]
23. Sommerfeld, N.S.; Hejl, M.; Klose, M.H.M.; Schreiber-Brynzak, E.; Bileck, A.; Meier, S.M.; Gerner, C.; Jakupec, M.A.; Galanski, M.; Keppler, B.K. Low-Generation Polyamidoamine Dendrimers as Drug Carriers for Platinum(IV) Complexes. *Eur. J. Inorg. Chem.* **2017**, *2017*, 1713–1720. [CrossRef]
24. Cseh, K.; Geisler, H.; Stanojkovska, K.; Westermayr, J.; Brunmayr, P.; Wenisch, D.; Gajic, N.; Hejl, M.; Schaier, M.; Koellensperger, G.; et al. Arene Variation of Highly Cytotoxic Tridentate Naphthoquinone-Based Ruthenium(II) Complexes and In-Depth In Vitro Studies. *Pharmaceutics* **2022**, *14*, 2466. [CrossRef]
25. Fronik, P.; Gutmann, M.; Vician, P.; Stojanovic, M.; Kastner, A.; Heffeter, P.; Pirker, C.; Keppler, B.K.; Berger, W.; Kowol, C.R. A Platinum(IV) Prodrug Strategy to Overcome Glutathione-Based Oxaliplatin Resistance. *Commun. Chem.* **2022**, *5*, 46. [CrossRef] [PubMed]
26. Hizal, S.; Hejl, M.; Jungmann, C.; Jakupec, M.A.; Galanski, M.; Keppler, B.K. Synthesis, Characterization, Cytotoxicity, and Time-Dependent NMR Spectroscopic Studies of (*SP*-4-3)-Oxalato[(1*R*,2*R*,4*R*/1*S*,2*S*,4*S*)-(4-Trifluoromethyl-Cyclohexane-1,2-Diamine)]Platinum(II). *Eur. J. Inorg. Chem.* **2019**, *2019*, 856–864. [CrossRef]
27. Zhang, J.Z.; Bonnitcha, P.; Wexselblatt, E.; Klein, A.V.; Najajreh, Y.; Gibson, D.; Hambley, T.W. Facile Preparation of Mono-, Di- and Mixed-Carboxylato Platinum(IV) Complexes for Versatile Anticancer Prodrug Design. *Chem. Eur. J.* **2013**, *19*, 1672–1676. [CrossRef]

28. Lerchbammer-Kreith, Y.; Sommerfeld, N.S.; Cseh, K.; Xian, W.-J.; Odunze, U.; Schätzlein, A.G.; Uchegbu, I.F.; Galanski, M.S.; Jakupec, M.A.; Keppler, B.K. Platinum(IV)-Loaded Degraded Glycol Chitosan as Efficient Platinum(IV) Drug Delivery Platform. *Pharmaceutics* **2023**, *15*, 1050. [CrossRef]
29. Yan, Q.; Zheng, H.N.; Jiang, C.; Li, K.; Xiao, S.J. EDC/NHS Activation Mechanism of Polymethacrylic Acid: Anhydride versus NHS-Ester. *RSC Adv.* **2015**, *5*, 69939–69947. [CrossRef]
30. Banfic, J.; Adib-Razavi, M.S.; Galanski, M.; Keppler, B.K. Platinum(IV) Complexes Featuring Axial (1,4-$^{13}C_2$)Succinato Ligands—Synthesis, Characterization, and Preliminary Investigations in Cancer Cell Lysates. *Z. Anorg. Allg. Chem.* **2013**, *639*, 1613–1620. [CrossRef]
31. Kastner, A.; Poetsch, I.; Mayr, J.; Burda, J.V.; Roller, A.; Heffeter, P.; Keppler, B.K.; Kowol, C.R. A Dogma in Doubt: Hydrolysis of Equatorial Ligands of PtIV Complexes under Physiological Conditions. *Angew. Chem.* **2019**, *131*, 7542–7547. [CrossRef]
32. Wexselblatt, E.; Gibson, D. What Do We Know about the Reduction of Pt(IV) pro-Drugs? *J. Inorg. Biochem.* **2012**, *117*, 220–229. [CrossRef] [PubMed]
33. Choi, S.; Filotto, C.; Bisanzo, M.; Delaney, S.; Lagasee, D.; Whitworth, J.L.; Jusko, A.; Li, C.; Wood, N.A.; Willingham, J.; et al. Reduction and Anticancer Activity of Platinum(IV) Complexes. *Inorg. Chem.* **1998**, *37*, 2500–2504. [CrossRef]
34. Wexselblatt, E.; Yavin, E.; Gibson, D. Platinum(IV) Prodrugs with Haloacetato Ligands in the Axial Positions Can Undergo Hydrolysis under Biologically Relevant Conditions. *Angew. Chem. Int. Ed.* **2013**, *52*, 6059–6062. [CrossRef]
35. Zhang, J.Z.; Wexselblatt, E.; Hambley, T.W.; Gibson, D. Pt(Iv) Analogs of Oxaliplatin That Do Not Follow the Expected Correlation between Electrochemical Reduction Potential and Rate of Reduction by Ascorbate. *Chem. Commun.* **2012**, *48*, 847–849. [CrossRef] [PubMed]
36. Lemma, K.; Sargeson, A.M.; Elding, L.I. Kinetics and Mechanism for Reduction of Oral Anticancer Platinum(IV) Dicarboxylate Compounds by L-Ascorbate Ions. *J. Chem. Soc. Dalton Trans.* **2000**, 1167–1172. [CrossRef]
37. Ellis, L.T.; Er, H.M.; Hambley, T.W. The Influence of the Axial Ligands of a Series of Platinum(IV) Anti-Cancer Complexes on Their Reduction to Platinum(II) and Reaction with DNA. *Aust. J. Chem.* **1995**, *48*, 793–806. [CrossRef]
38. Galanski, M.S.; Yasemi, A.; Slaby, S.; Jakupec, M.A.; Arion, V.B.; Rausch, M.; Nazarov, A.A.; Keppler, B.K. Synthesis, Crystal Structure and Cytotoxicity of New Oxaliplatin Analogues Indicating That Improvement of Anticancer Activity Is Still Possible. *Eur. J. Med. Chem.* **2004**, *39*, 707–714. [CrossRef]
39. Song, R.; Kim, K.M.; Lee, S.S.; Sohn, Y.S. Electrophilic Substitution of (Diamine)Tetrahydroxoplatinum(IV) with Carboxylic Anhydrides. Synthesis and Characterization of (Diamine)Platinum(IV) Complexes of Mixed Carboxylates. *Inorg. Chem.* **2000**, *39*, 3567–3571. [CrossRef] [PubMed]
40. Teow, H.M.; Zhou, Z.; Najlah, M.; Yusof, S.R.; Abbott, N.J.; D'Emanuele, A. Delivery of Paclitaxel across Cellular Barriers Using a Dendrimer-Based Nanocarrier. *Int. J. Pharm.* **2013**, *441*, 701–711. [CrossRef]
41. Leal, J.; Santos, L.; Fernández-Aroca, D.M.; Cuevas, J.V.; Martínez, M.A.; Massaguer, A.; Jalón, F.A.; Ruiz-Hidalgo, M.J.; Sánchez-Prieto, R.; Rodríguez, A.M.; et al. Effect of the Aniline Fragment in Pt(II) and Pt(IV) Complexes as Anti-Proliferative Agents. Standard Reduction Potential as a More Reliable Parameter for Pt(IV) Compounds than Peak Reduction Potential. *J. Inorg. Biochem.* **2021**, *218*, 111403. [CrossRef] [PubMed]
42. Kirkpatrick, G.J.; Plumb, J.A.; Sutcliffe, O.B.; Flint, D.J.; Wheate, N.J. Evaluation of Anionic Half Generation 3.5–6.5 Poly(Amidoamine) Dendrimers as Delivery Vehicles for the Active Component of the Anticancer Drug Cisplatin. *J. Inorg. Biochem.* **2011**, *105*, 1115–1122. [CrossRef] [PubMed]
43. Hato, S.V.; Khong, A.; De Vries, I.J.M.; Lesterhuis, W.J. Molecular Pathways: The Immunogenic Effects of Platinum-Based Chemotherapeutics. *Clin. Cancer Res.* **2014**, *20*, 2831–2837. [CrossRef] [PubMed]
44. Du, B.; Jiang, X.; Das, A.; Zhou, Q.; Yu, M.; Jin, R.; Zheng, J. Glomerular Barrier Behaves as an Atomically Precise Bandpass Filter in a Sub-Nanometre Regime. *Nat. Nanotechnol.* **2017**, *12*, 1096–1102. [CrossRef] [PubMed]
45. Hauser, P.V.; Chang, H.M.; Yanagawa, N.; Hamon, M. Nanotechnology, Nanomedicine, and the Kidney. *Appl. Sci.* **2021**, *11*, 7187. [CrossRef]
46. Kaminskas, L.M.; Boyd, B.J.; Porter, C.J.H. Dendrimer Pharmacokinetics: The Effect of Size, Structure and Surface Characteristics on ADME Properties. *Nanomedicine* **2011**, *6*, 1063–1084. [CrossRef]
47. Li, J.; Duan, Q.; Wei, X.; Wu, J.; Yang, Q. Kidney-Targeted Nanoparticles Loaded with the Natural Antioxidant Rosmarinic Acid for Acute Kidney Injury Treatment. *Small* **2022**, *18*, e2204388. [CrossRef]
48. Matsuura, S.; Katsumi, H.; Suzuki, H.; Hirai, N.; Takashima, R.; Morishita, M.; Sakane, T.; Yamamoto, A. L-Cysteine and l-Serine Modified Dendrimer with Multiple Reduced Thiols as a Kidney-Targeting Reactive Oxygen Species Scavenger to Prevent Renal Ischemia/Reperfusion Injury. *Pharmaceutics* **2018**, *10*, 251. [CrossRef]
49. Matsuura, S.; Katsumi, H.; Suzuki, H.; Hirai, N.; Hayashi, H.; Koshino, K.; Higuchi, T.; Yagi, Y.; Kimura, H.; Sakane, T.; et al. L-Serine-Modified Polyamidoamine Dendrimer as a Highly Potent Renal Targeting Drug Carrier. *Proc. Natl. Acad. Sci. USA* **2018**, *115*, 10511–10516. [CrossRef]
50. Boyle, F.M.; Wheeler, H.R.; Shenfield, G.M. Amelioration of Experimental Cisplatin and Paclitaxel Neuropathy with Glutamate. *J. Neuro-Oncol.* **1999**, *41*, 107–116. [CrossRef]
51. Du, B.; Yu, M.; Zheng, J. Transport and Interactions of Nanoparticles in the Kidneys. *Nat. Rev. Mater.* **2018**, *3*, 358–374. [CrossRef]
52. Haensler, J.; Szoka, F.C. Polyamidoamine Cascade Polymers Mediate Efficient Transfection of Cells in Culture. *Bioconj. Chem.* **1993**, *4*, 372–379. [CrossRef] [PubMed]

53. Shah, N.; Steptoe, R.J.; Parekh, H.S. Low-Generation Asymmetric Dendrimers Exhibit Minimal Toxicity and Effectively Complex DNA. *J. Pept. Sci.* **2011**, *17*, 470–478. [CrossRef] [PubMed]
54. McNerny, D.Q.; Leroueil, P.R.; Baker, J.R. Understanding Specific and Nonspecific Toxicities: A Requirement for the Development of Dendrimer-Based Pharmaceuticals. *Wiley Interdiscip. Rev. Nanomed. Nanobiotechnol.* **2010**, *2*, 249–259. [CrossRef]
55. Shcharbin, D.; Janaszewska, A.; Klajnert-Maculewicz, B.; Ziemba, B.; Dzmitruk, V.; Halets, I.; Loznikova, S.; Shcharbina, N.; Milowska, K.; Ionov, M.; et al. How to Study Dendrimers and Dendriplexes III. Biodistribution, Pharmacokinetics and Toxicity In Vivo. *J. Control. Release* **2014**, *181*, 40–52. [CrossRef]
56. Bruker AXS. *Bruker SAINT v.838B Copyright(C)*; Bruker AXS: Billerica, MA, USA, 2005–2019.
57. Sheldrick, G.M. *Sadabs*; University of Göttingen: Göttingen, Germany, 1996.
58. Dolomanov, O.V.; Bourhis, L.J.; Gildea, R.J.; Howard, J.A.K.; Puschmann, H. OLEX2: A Complete Structure Solution, Refinement and Analysis Program. *J. Appl. Crystallogr.* **2009**, *42*, 339–341. [CrossRef]
59. Hübschle, C.B.; Sheldrick, G.M.; Dittrich, B. ShelXle: A Qt Graphical User Interface for SHELXL. *J. Appl. Crystallogr.* **2011**, *44*, 1281–1284. [CrossRef]
60. Sheldrick, G.M. *SHELXS v 2016/4*; University of Göttingen: Göttingen, Germany, 2015.
61. Sheldrick, G.M. *SHELXL v 2016/4*; University of Göttingen: Göttingen, Germany, 2015.
62. Spek, A.L. Structure Validation in Chemical Crystallography. *Acta Crystallogr. D Biol. Crystallogr.* **2009**, *65*, 148–155. [CrossRef]

Supporting Information

Combination of Drug Delivery Properties of PAMAM Dendrimers and Cytotoxicity of Platinum(IV) Complexes—A More Selective Anticancer Treatment?

Yvonne Lerchbammer-Kreith [1], Michaela Hejl [1], Petra Vician [2], Michael A. Jakupec [1,3], Walter Berger [2,3], Mathea S. Galanski [1,*] and Bernhard K. Keppler [1,3,*]

[1] Institute of Inorganic Chemistry, Faculty of Chemistry, University of Vienna, Waehringer Strasse 42, 1090 Vienna, Austria
[2] Center for Cancer Research and Comprehensive Cancer Center, Medical University of Vienna, Borschkegasse 8a, 1090 Vienna, Austria
[3] Research Cluster "Translational Cancer Therapy Research", University of Vienna, Waehringer Strasse 42, 1090 Vienna, Austria
* Correspondence: mathea.galanski@univie.ac.at (M.S.G.); bernhard.keppler@univie.ac.at (B.K.K.)

Table of Contents

1. NMR Spectra of Platinum(IV) Complexes 5-7

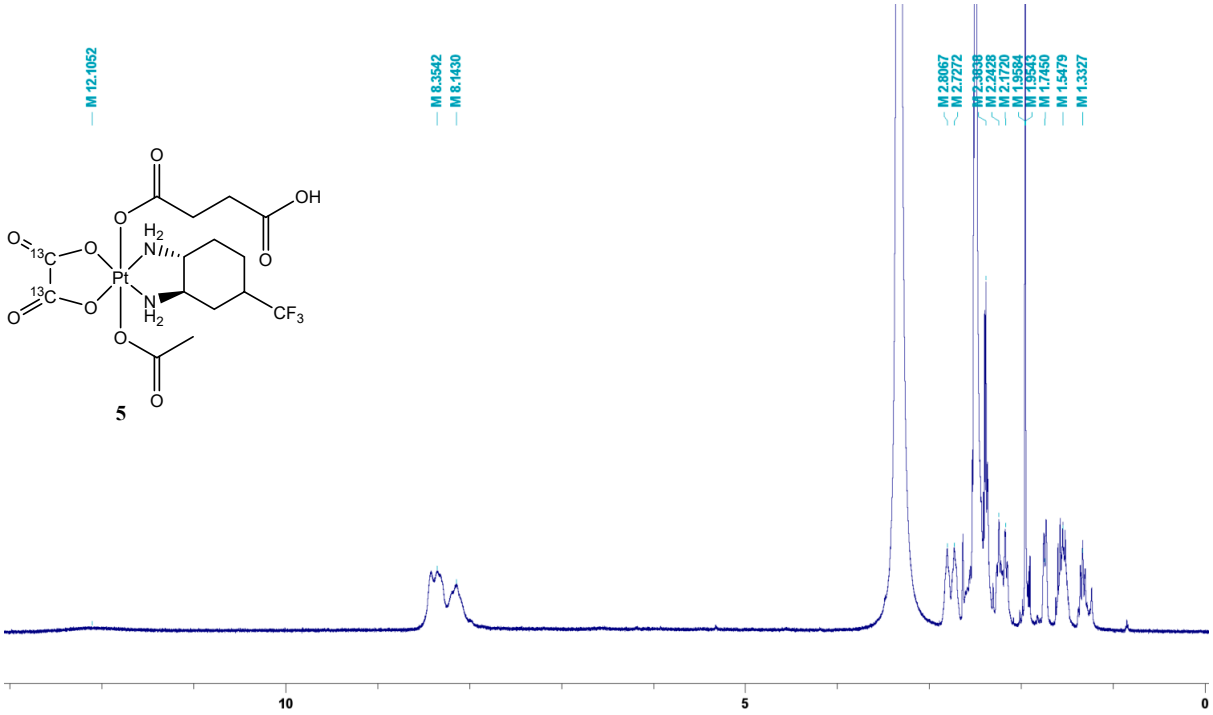

Figure S1. ^{1}H NMR spectrum of complex **5** in d_6-DMSO.

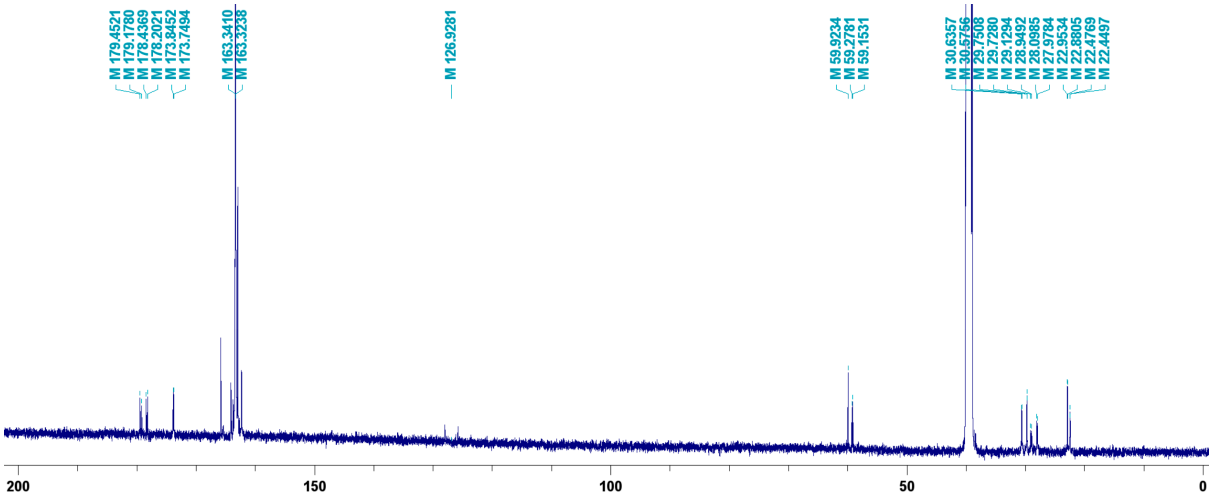

Figure S2. ^{13}C NMR spectrum of complex **5** in d_6-DMSO.

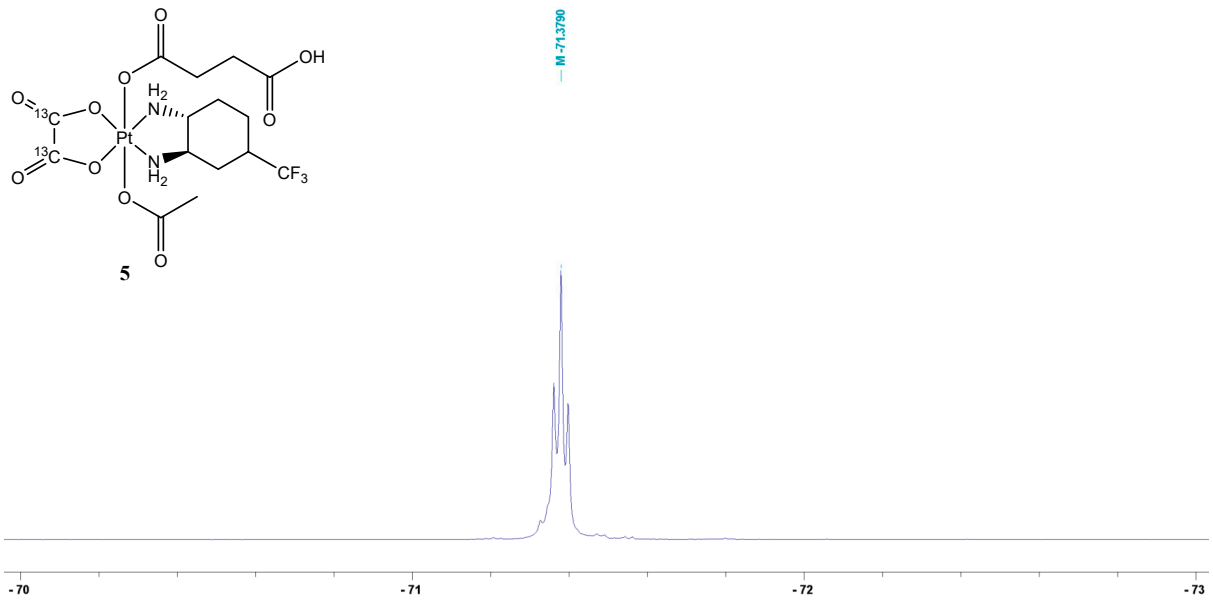

5

Figure S3. ^{19}F NMR spectrum of complex **5** in d_6-DMSO.

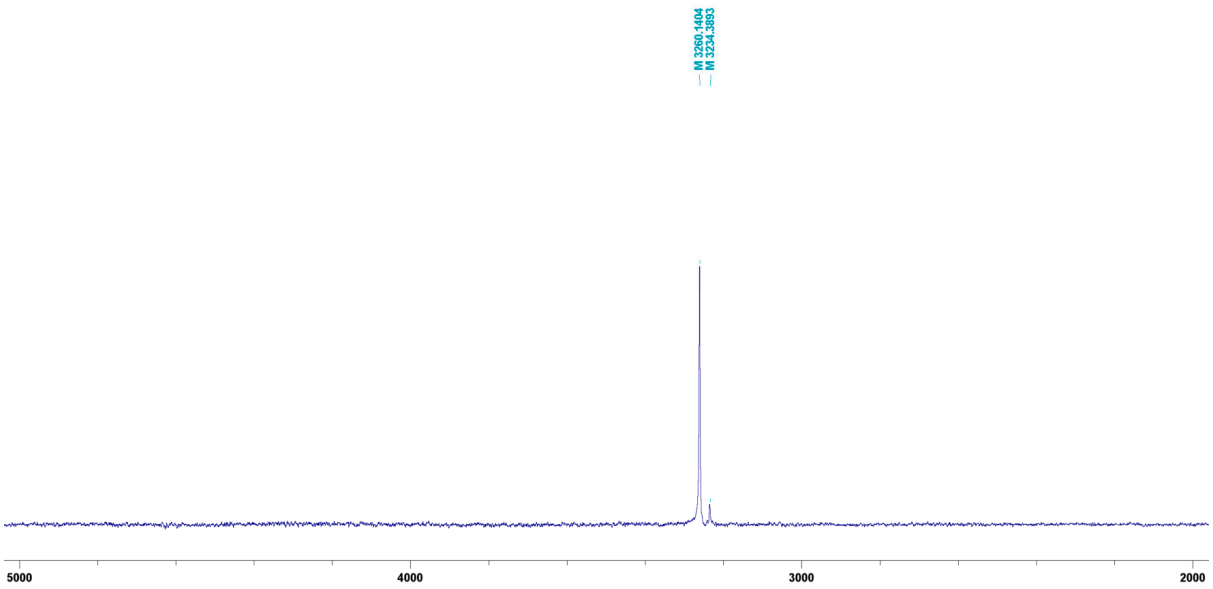

Figure S4. ^{195}Pt NMR spectrum of complex **5** in d_6-DMSO.

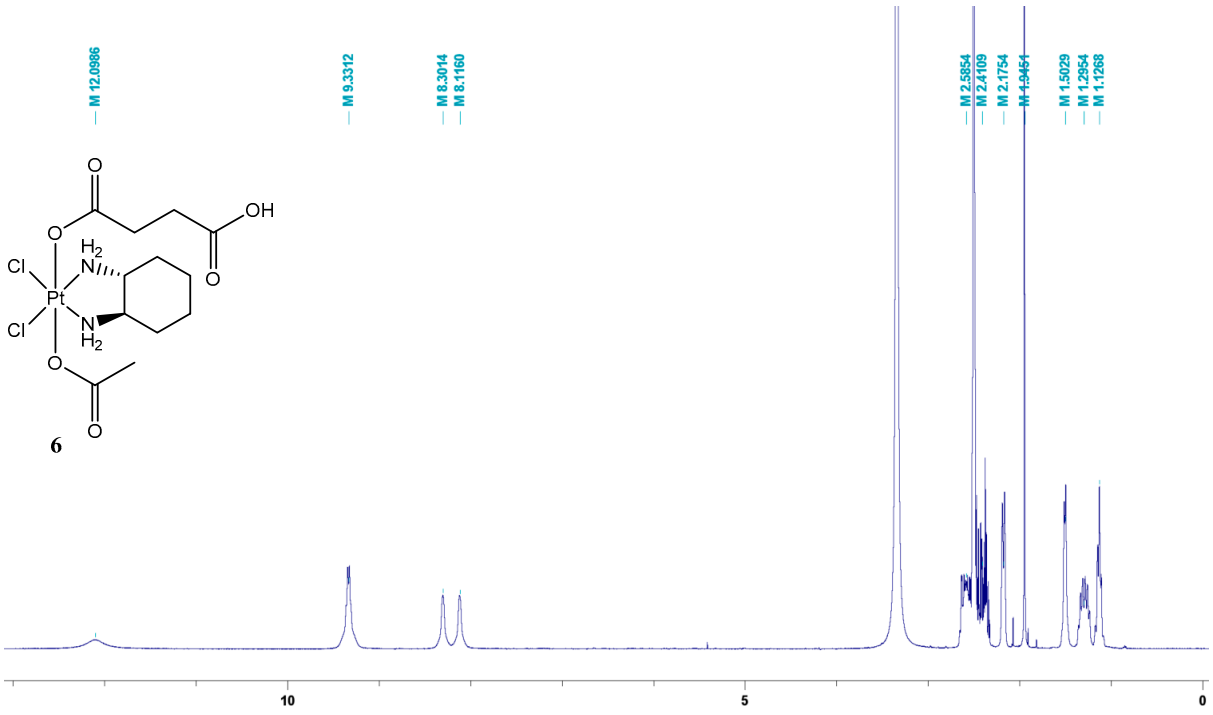

Figure S5. ^{1}H NMR spectrum of complex **6** in d_6-DMSO.

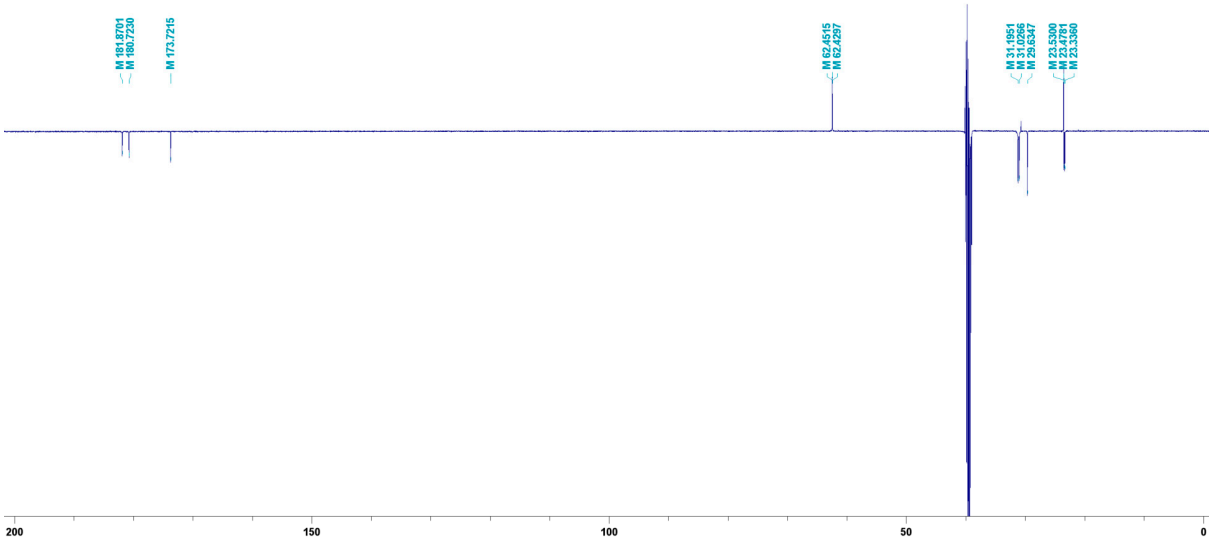

Figure S6. ^{13}C NMR spectrum of complex **6** in d_6-DMSO.

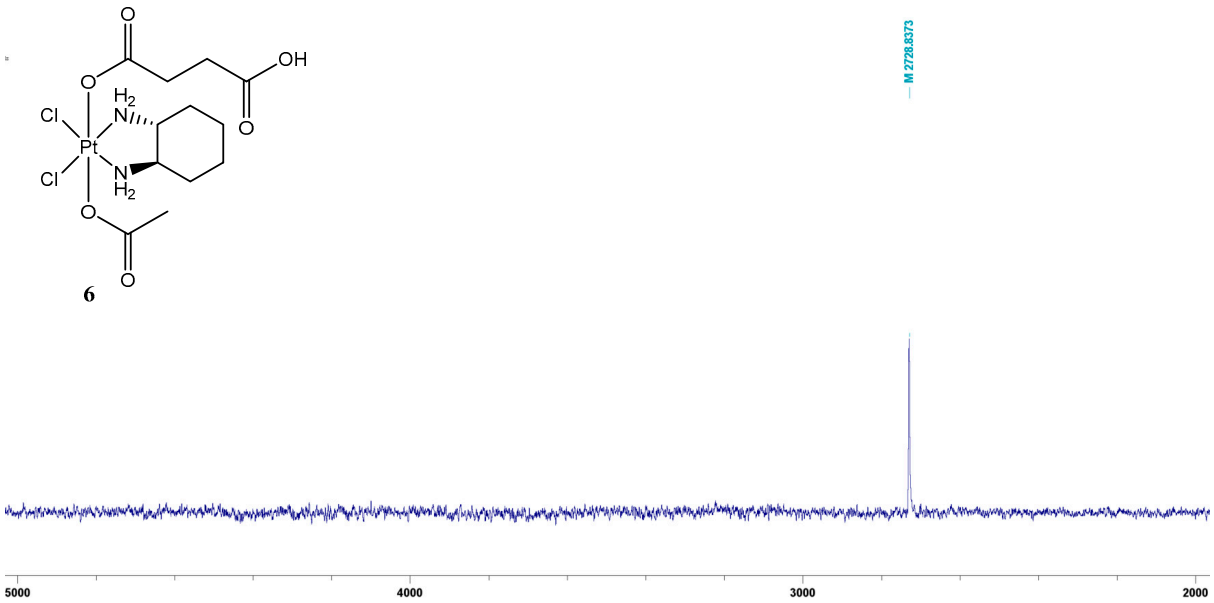

Figure S7. ^{195}Pt NMR spectrum of complex **6** in d_6-DMSO.

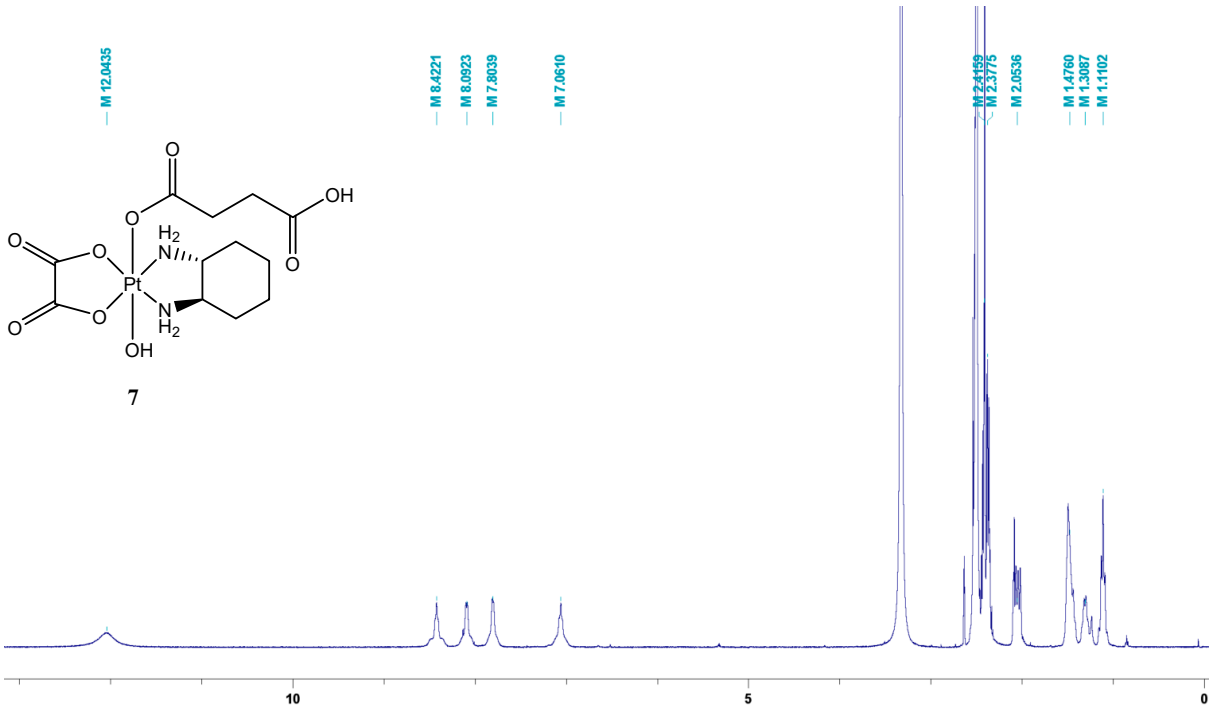

Figure S8. ^{1}H NMR spectrum of complex **7** in d_6-DMSO.

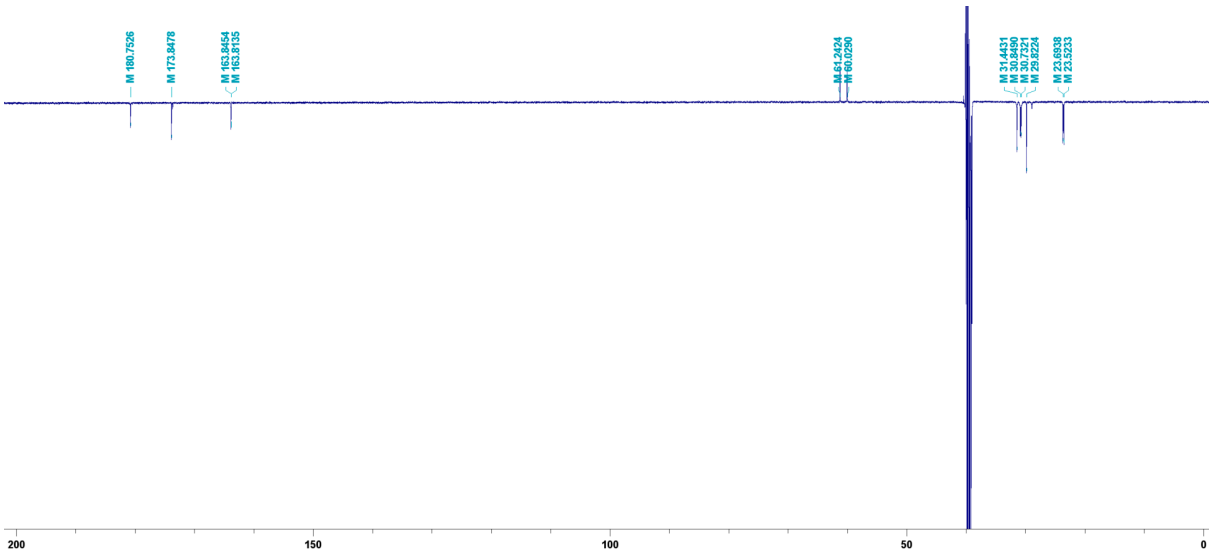

Figure S9. ^{13}C NMR spectrum of complex **7** in d_6-DMSO.

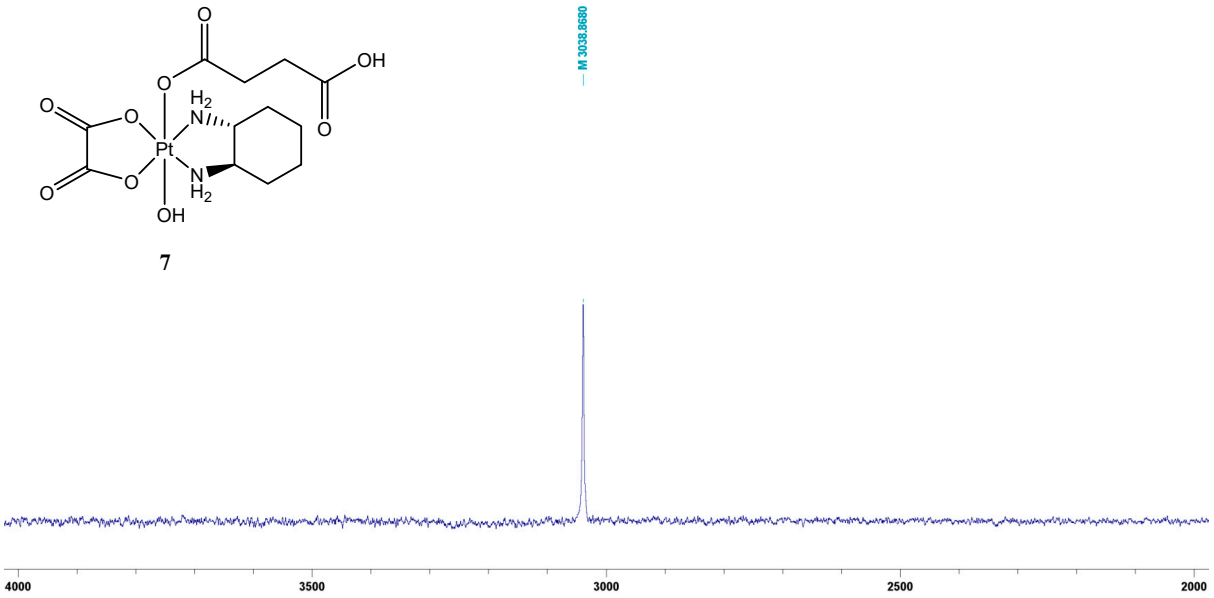

7

Figure S10. ^{195}Pt NMR spectrum of complex **7** in d_6-DMSO.

2. NMR Spectra of Selected Conjugates

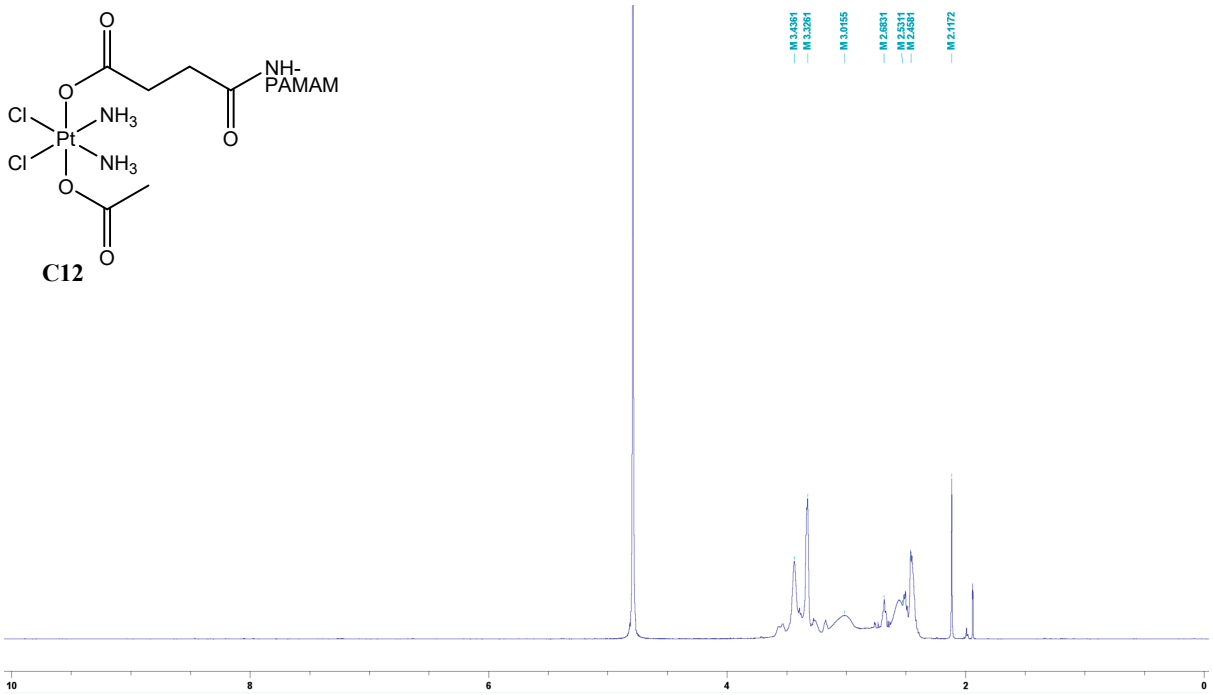

Figure S11. ^{1}H NMR spectrum of conjugate **C12** in D_2O.

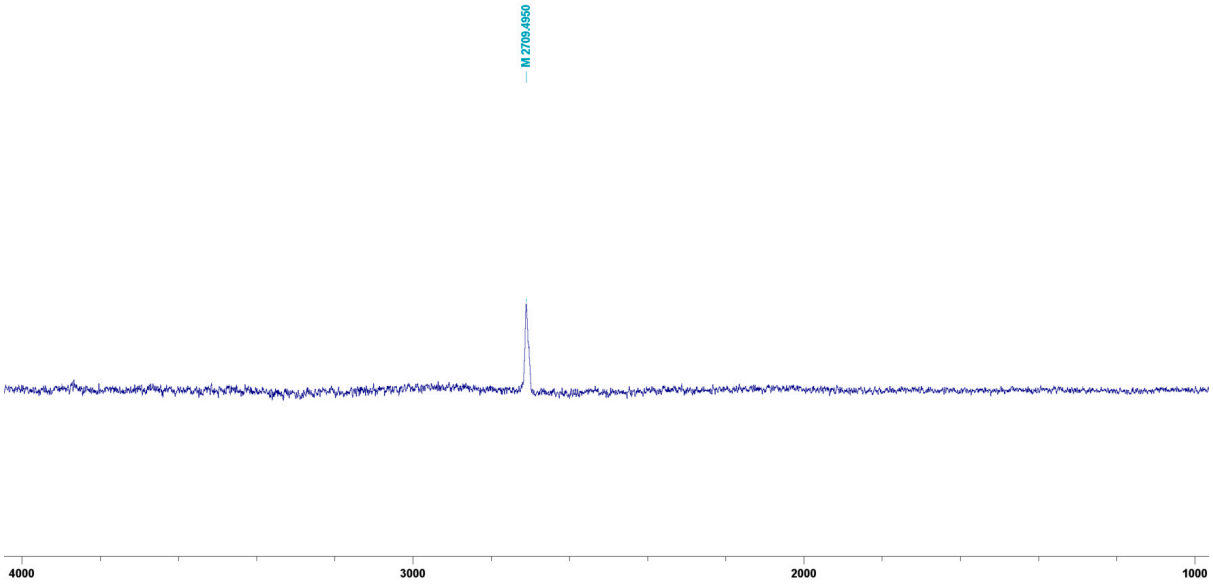

Figure S12. ^{195}Pt NMR spectrum of conjugate **C12** in D_2O.

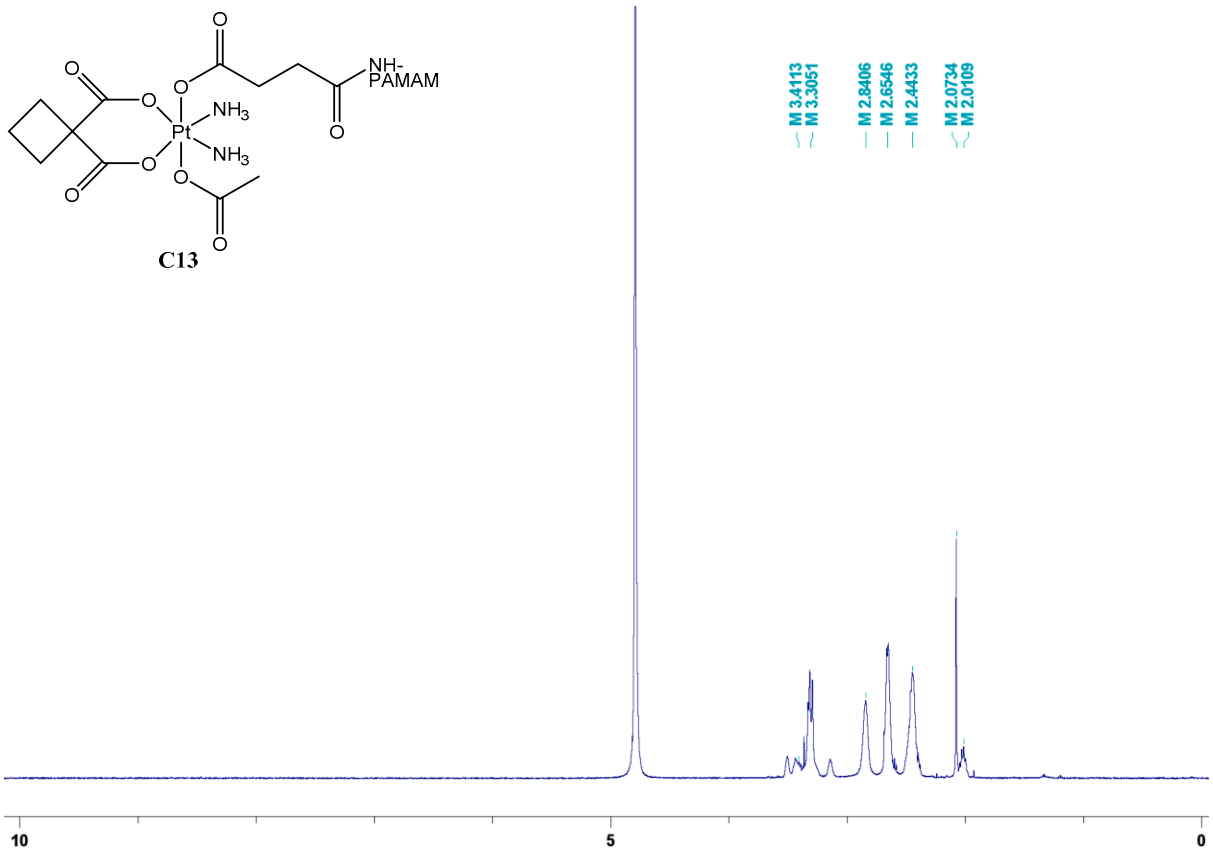

Figure S13. ^{1}H NMR spectrum of conjugate **C13** in D_2O.

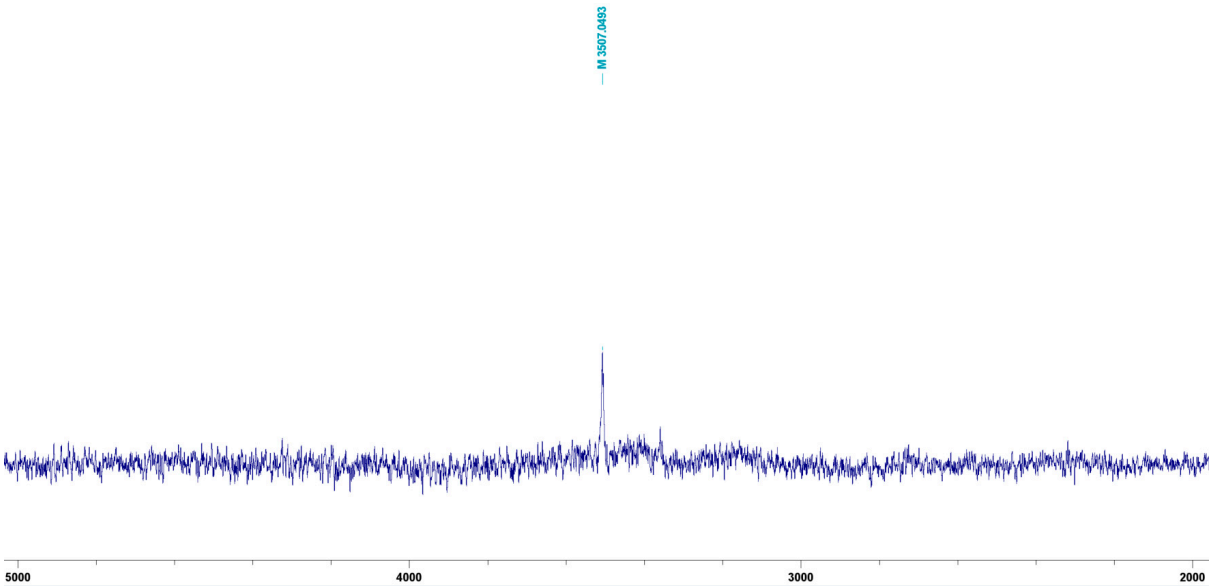

Figure S14. ^{195}Pt NMR spectrum of conjugate **C13** in D_2O.

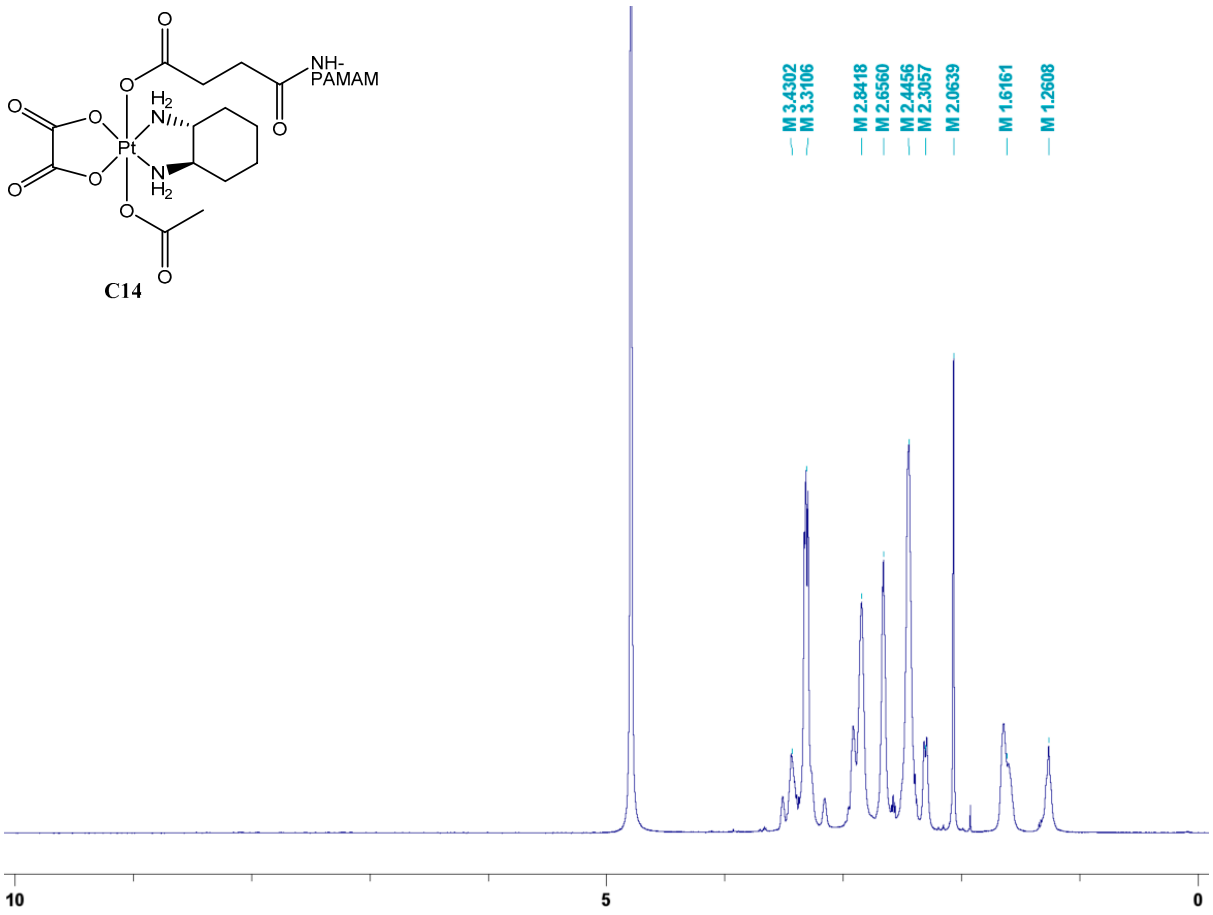

Figure S15. ^{1}H NMR spectrum of conjugate **C14** in D_2O.

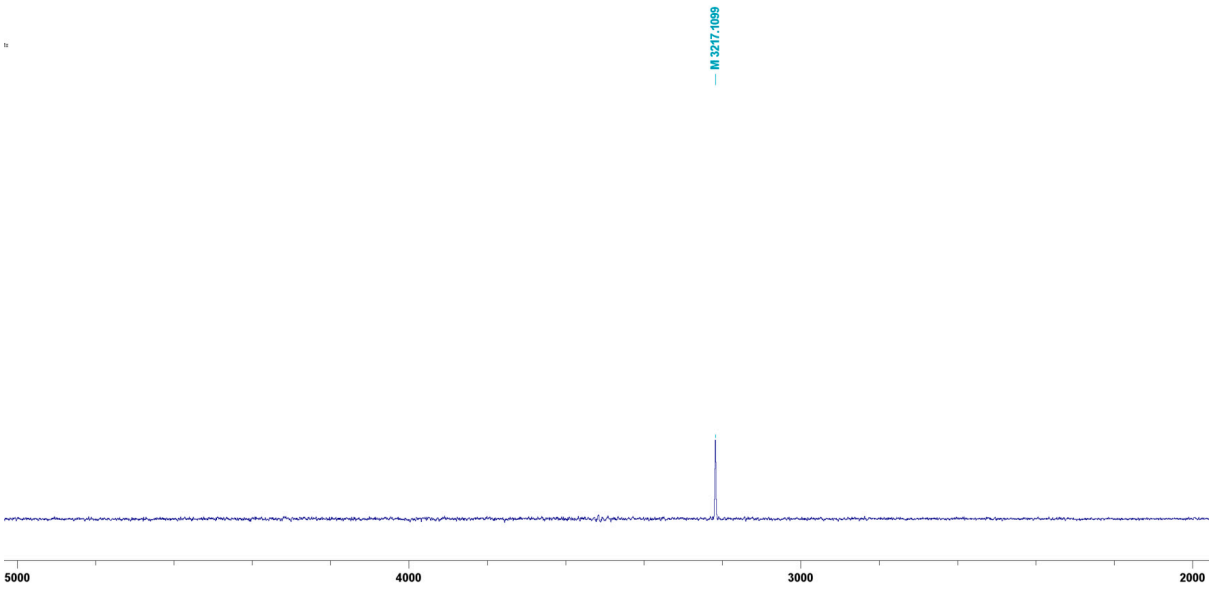

Figure S16. ^{195}Pt NMR spectrum of conjugate **C14** in D_2O.

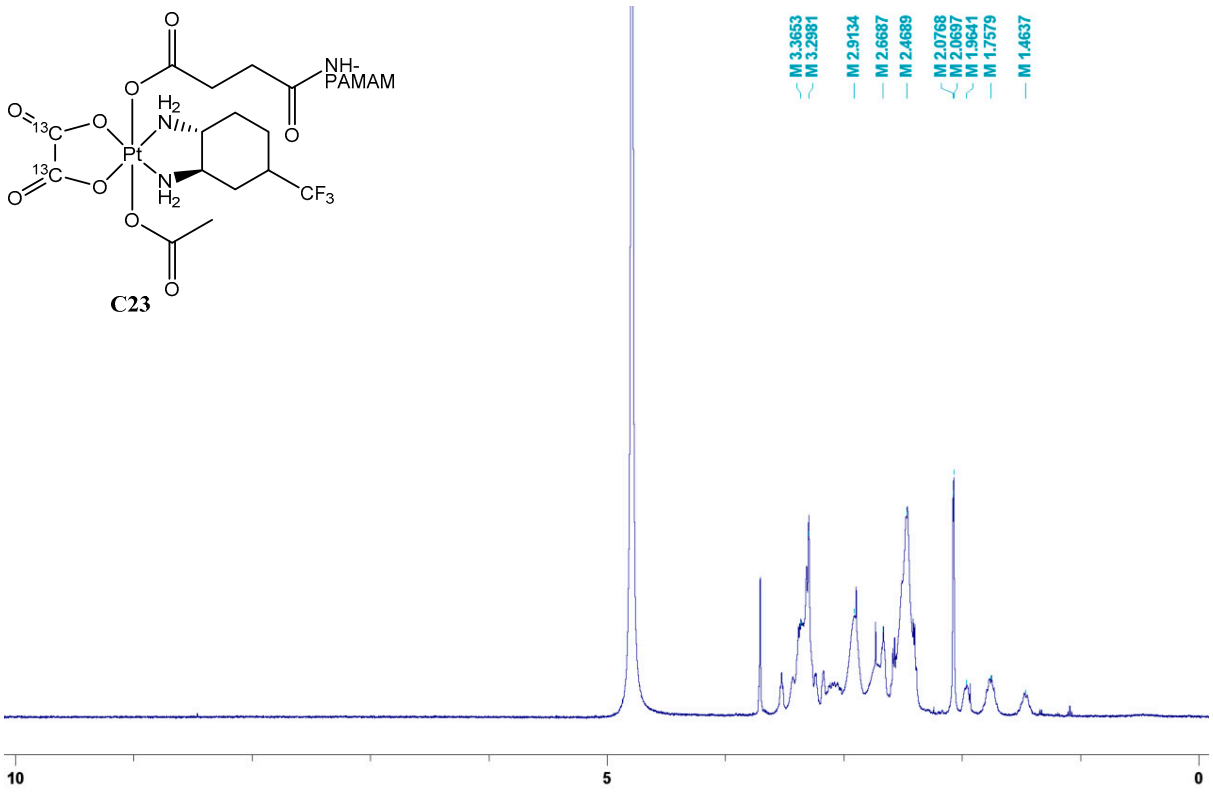

Figure S17. ^{1}H NMR spectrum of conjugate **C23** in D_2O.

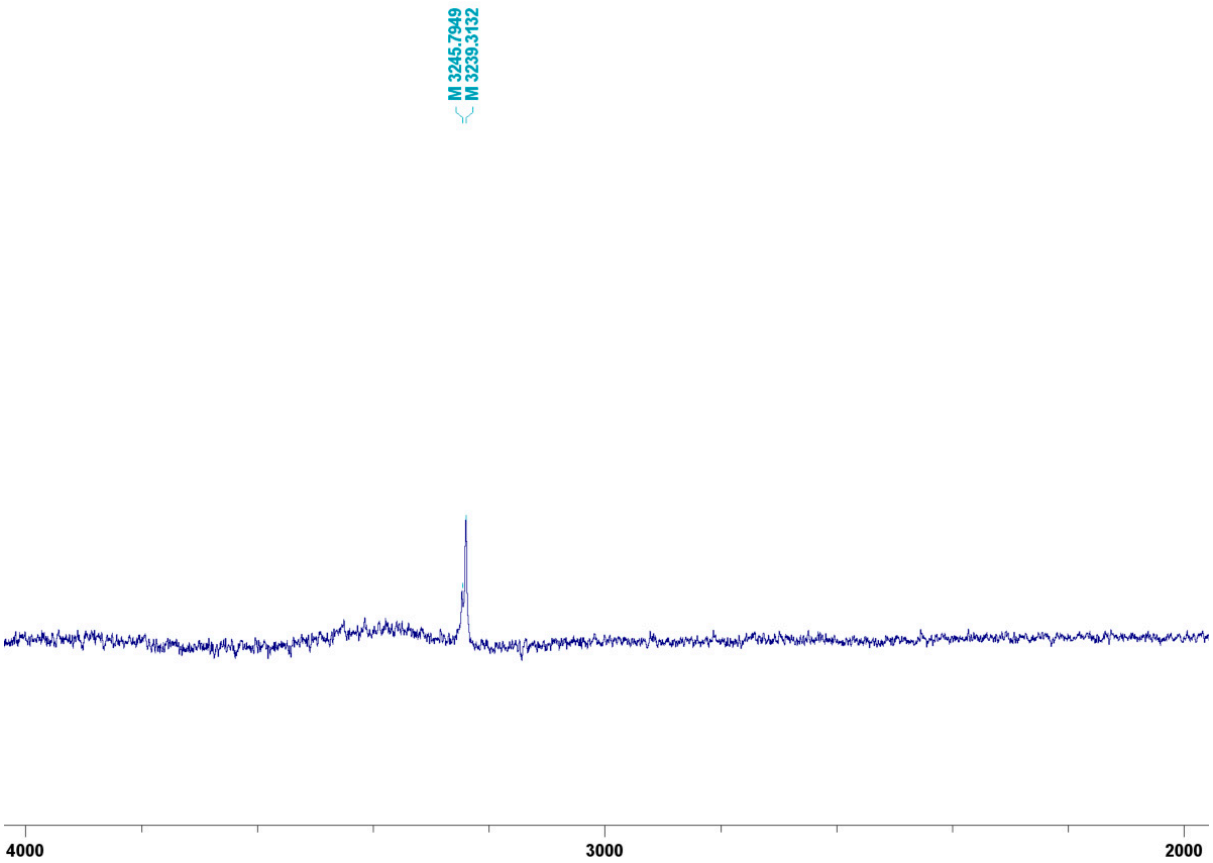

Figure S18. ^{195}Pt NMR spectrum of conjugate **C23** in D_2O.

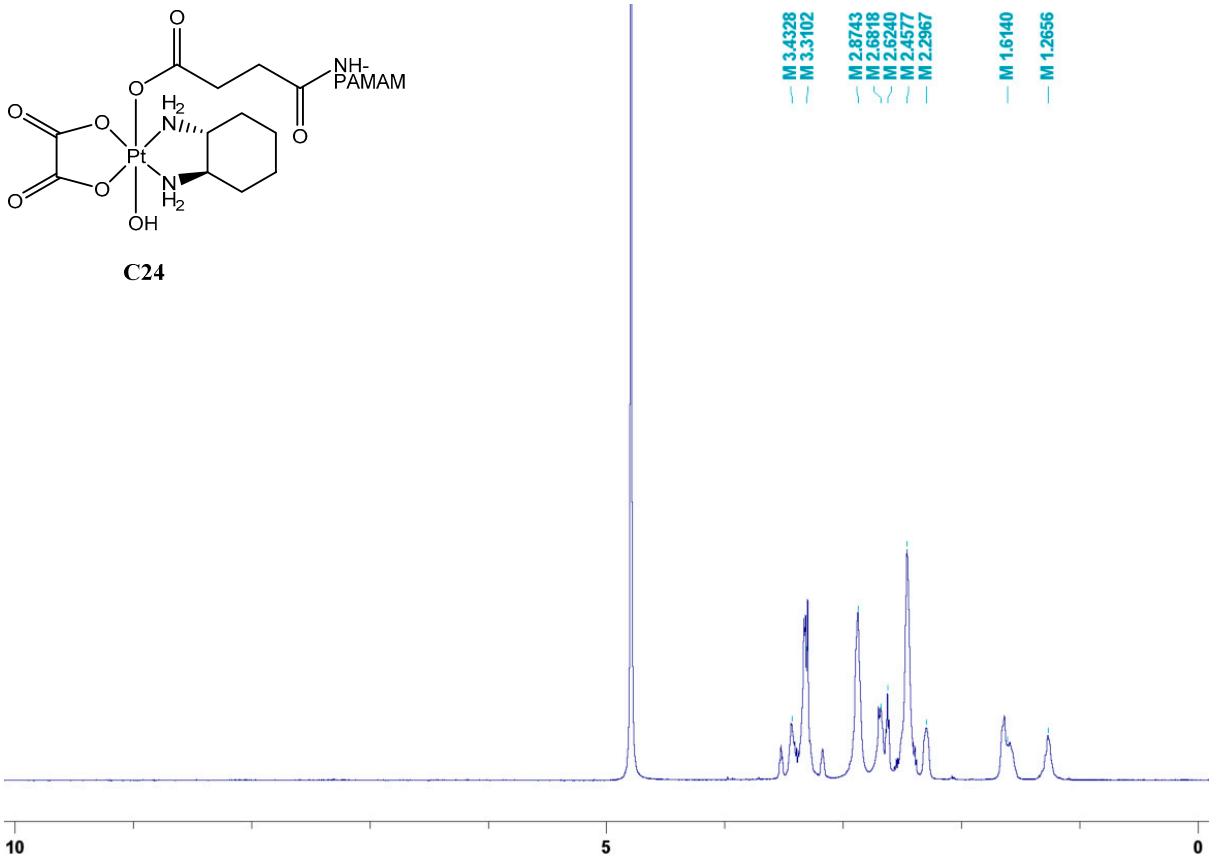

C24

Figure S19. ^{1}H NMR spectrum of conjugate **C24** in D_2O.

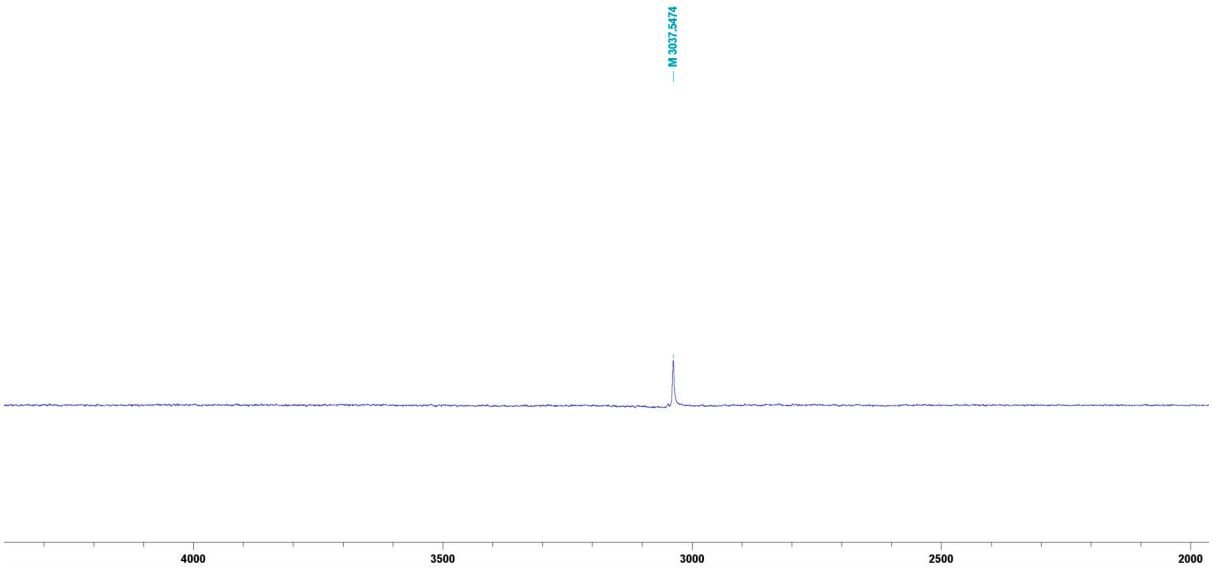

Figure S20. ^{195}Pt NMR spectrum of conjugate **C24** in D_2O.

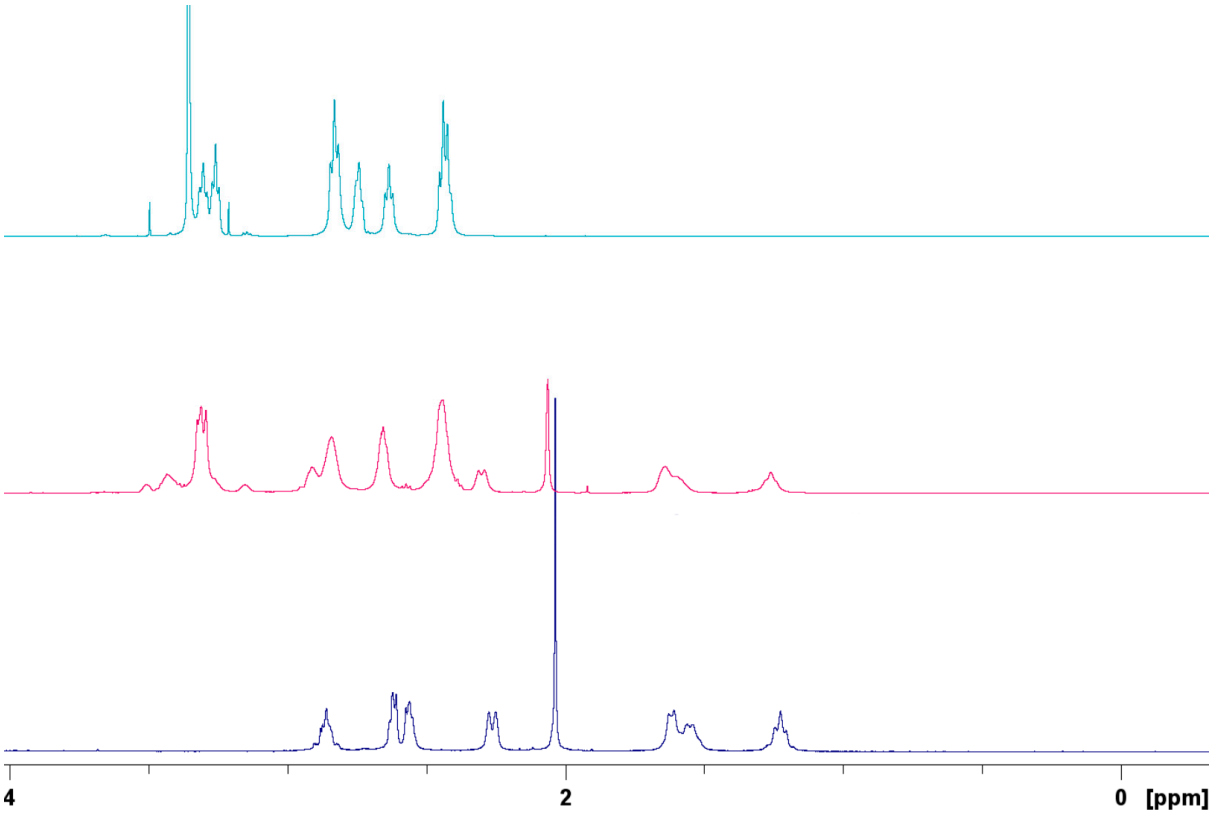

Figure S21. ^{1}H NMR spectra measured in D_2O of G4 PAMAM (top, turquoise), conjugate **C14** (middle, pink) and platinum(IV) complex **3** (bottom, dark blue).

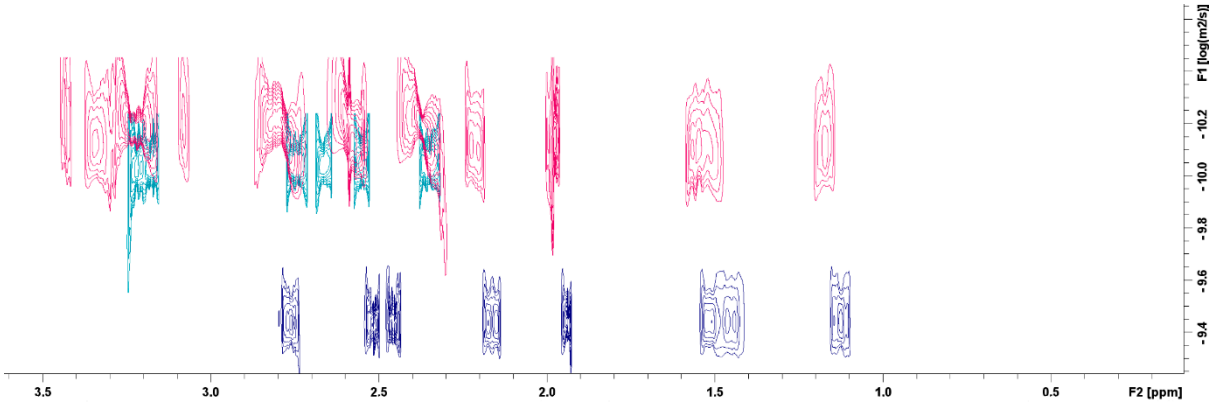

Figure S22. Overlay of DOSY spectra of conjugate **C14** (top, pink), G4 PAMAM (middle, turquoise) and platinum(IV) complex **3** (bottom, dark blue).

3. X-Ray Diffraction Analysis

X-ray intensity data was measured on Bruker D8 Venture diffractometer equipped with multilayer monochromator, Mo K/α INCOATEC micro focus sealed tube and Oxford cooling system. The structure was solved by Direct Methods. Non-hydrogen atoms were refined with anisotropic displacement parameters. Hydrogen atoms were inserted at calculated positions and refined with riding model. The following software was used: Bruker SAINT software package [1] using a narrow-frame algorithm for frame integration, SADABS [2] for absorption correction, OLEX2 [3] for structure solution, refinement, molecular diagrams and graphical user-interface, ShelXle [4] for refinement and graphical user-interface SHELXS-2015 [5] for structure solution, SHELXL-2015 [6] for refinement, Platon [7] for symmetry check. Crystallographic data have been deposited with the Cambridge Crystallographic Data Center with No. CSD 2252655. Copies of data can be obtained free of charge (available online: https://www.ccdc.cam.ac.uk/structures/).

Table S1. Overview of the sample and crystal data, data collection and structure refinement of platinum(IV) complex **3**.

Identification code	mo_KrYv410_P212121
Empirical formula	$C_{14}H_{26}N_2O_{12}Pt$
Formula weight	609.46
Temperature/K	100.0
Crystal system	orthorhombic
Space group	$P2_12_12_1$
a/Å	9.1152(2)
b/Å	11.2755(2)
c/Å	19.5809(4)
α/°	90
β/°	90
γ/°	90
Volume/Å^3	2012.49(7)
Z	4
ρ_{calc}g/cm^3	2.011
μ/mm^{-1}	7.037
F(000)	1192.0
Crystal size/mm^3	0.1 × 0.05 × 0.03
Radiation	MoKα (λ = 0.71073)
2Θ range for data collection/°	4.16 to 60.364
Index ranges	-12 ≤ h ≤ 12, -15 ≤ k ≤ 15, -27 ≤ l ≤ 23
Reflections collected	21714
Independent reflections	5890 [R_{int} = 0.0657, R_{sigma} = 0.0684]
Data/restraints/parameters	5890/12/280
Goodness-of-fit on F^2	1.023
Final R indexes [I>=2σ (I)]	R_1 = 0.0346, wR_2 = 0.0485
Final R indexes [all data]	R_1 = 0.0484, wR_2 = 0.0518
Largest diff. peak/hole / e Å^{-3}	0.85/-1.16
Flack parameter	-0.025(6)

Table S2. Overview of bond lengths of platinum(IV) complex **3**.

Atom	Atom	Length [Å]	Atom	Atom	Length [Å]

Pt1	O1	2.004(4)	N1	C1	1.490(8)
Pt1	O5	2.010(4)	N2	C2	1.499(8)
Pt1	O6	2.009(4)	C1	C2	1.489(9)
Pt1	O9	2.002(4)	C1	C6	1.531(9)
Pt1	N1	2.031(5)	C2	C3	1.539(9)
Pt1	N2	2.034(5)	C3	C4	1.530(9)
O1	C7	1.308(7)	C4	C5	1.510(10)
O2	C7	1.237(7)	C5	C6	1.527(9)
O3	C10	1.194(7)	C7	C8	1.508(8)
O5	C11	1.313(8)	C8	C9	1.510(8)
O6	C12	1.304(7)	C9	C10	1.498(9)
O7	C11	1.210(8)	C10	O4	1.353(14)
O8	C12	1.217(8)	C10	O4Z	1.362(13)
O9	C13	1.301(8)	C11	C12	1.543(9)
O10	C13	1.227(8)	C13	C14	1.494(9)

Table S3. Overview of angles of platinum(IV) complex **3**.

Atom	Atom	Atom	Angle [°]	Atom	Atom	Atom	Angle [°]
O1	Pt1	O5	95.13(18)	C1	C2	N2	106.3(5)
O1	Pt1	O6	94.81(18)	C1	C2	C3	112.0(5)
O1	Pt1	N1	84.0(2)	C4	C3	C2	108.9(6)
O1	Pt1	N2	86.5(2)	C5	C4	C3	111.8(6)
O5	Pt1	N1	97.0(2)	C4	C5	C6	111.1(6)
O5	Pt1	N2	178.3(2)	O1	C7	C8	113.6(5)
O6	Pt1	O5	84.74(16)	O2	C7	O1	125.0(5)
O6	Pt1	N1	177.9(2)	O2	C7	C8	121.4(5)
O6	Pt1	N2	94.7(2)	C7	C8	C9	114.8(5)
O9	Pt1	O1	177.1(2)	C10	C9	C8	115.8(5)
O9	Pt1	O5	86.66(19)	O3	C10	C9	124.4(6)
O9	Pt1	O6	83.11(18)	O3	C10	O4	119.6(8)
O9	Pt1	N1	98.1(2)	O3	C10	O4Z	121.5(8)
O9	Pt1	N2	91.7(2)	O4	C10	C9	112.1(8)
N1	Pt1	N2	83.59(19)	O4Z	C10	C9	111.4(7)
C7	O1	Pt1	124.4(4)	O5	C11	C12	116.2(7)
C11	O5	Pt1	111.2(4)	O7	C11	O5	123.8(7)
C12	O6	Pt1	111.2(4)	O7	C11	C12	120.0(7)
C13	O9	Pt1	123.3(5)	O6	C12	C11	116.7(7)
C1	N1	Pt1	108.8(4)	O8	C12	O6	122.1(7)
C2	N2	Pt1	108.4(4)	O8	C12	C11	121.2(7)
N1	C1	C6	113.1(6)	O9	C13	C14	112.4(7)
C2	C1	N1	108.2(5)	O10	C13	O9	125.4(7)
C2	C1	C6	111.3(6)	O10	C13	C14	122.1(7)
N2	C2	C3	112.3(6)	C5	C6	C1	109.8(6)

4. Concentration-Effect Curves

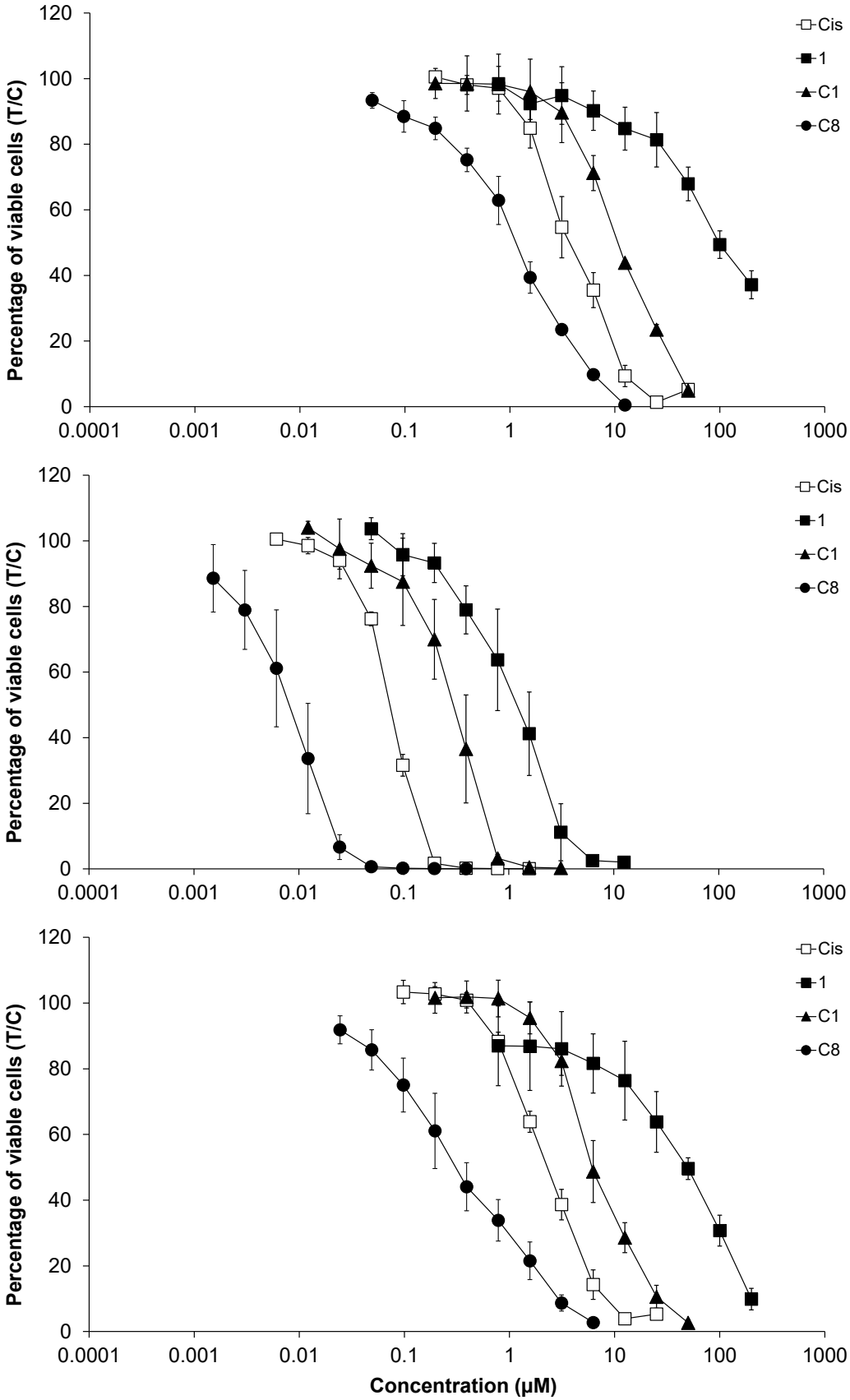

Figure S23. Concentration-effect curves of cisplatin, **1**, **C1** and **C8** in A549 (top), CH1/PA-1 (middle) and SW480 (bottom) cells, obtained by MTT assays with 96 h exposure time. Values are means ± standard deviations from at least three independent experiments.

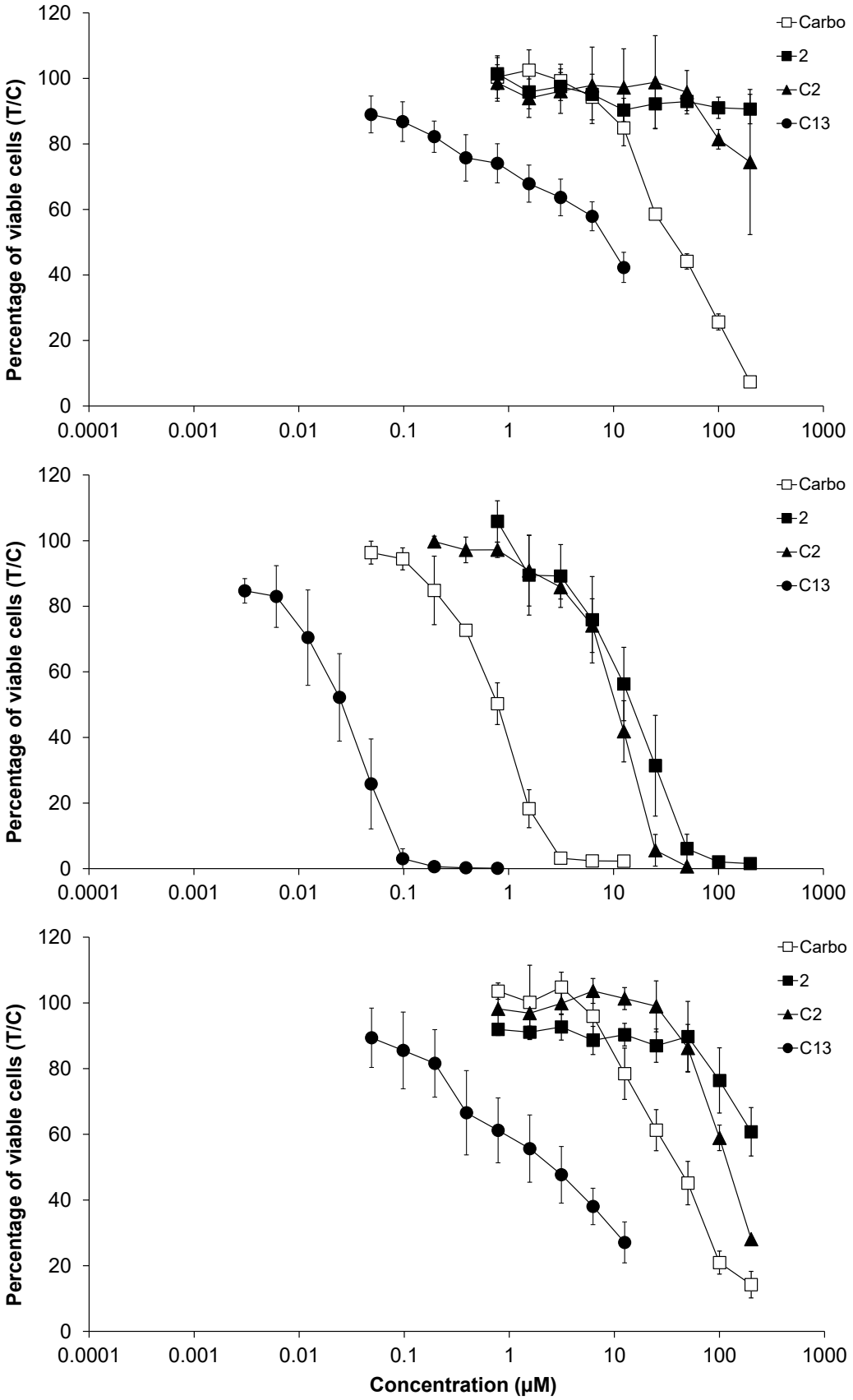

Figure S24. Concentration-effect curves of carboplatin, **2**, **C2** and **C13** in A549 (top), CH1/PA-1 (middle) and SW480 (bottom) cells, obtained by MTT assays with 96 h exposure time. Values are means ± standard deviations from at least three independent experiments.

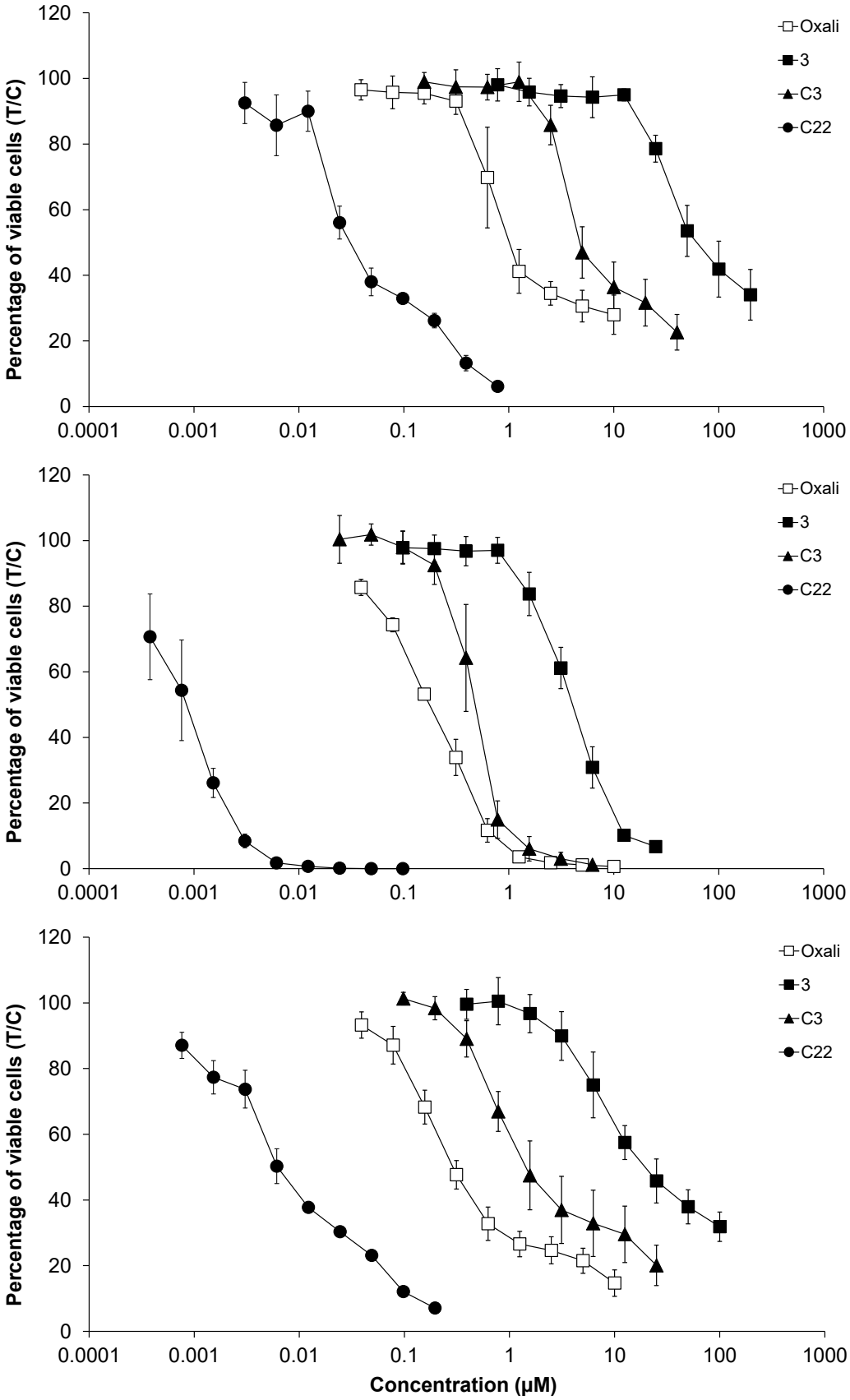

Figure S25. Concentration-effect curves of oxaliplatin, **3**, **C3** and **C22** in A549 (top), CH1/PA-1 (middle) and SW480 (bottom) cells, obtained by MTT assays with 96 h exposure time. Values are means ± standard deviations from at least three independent experiments.

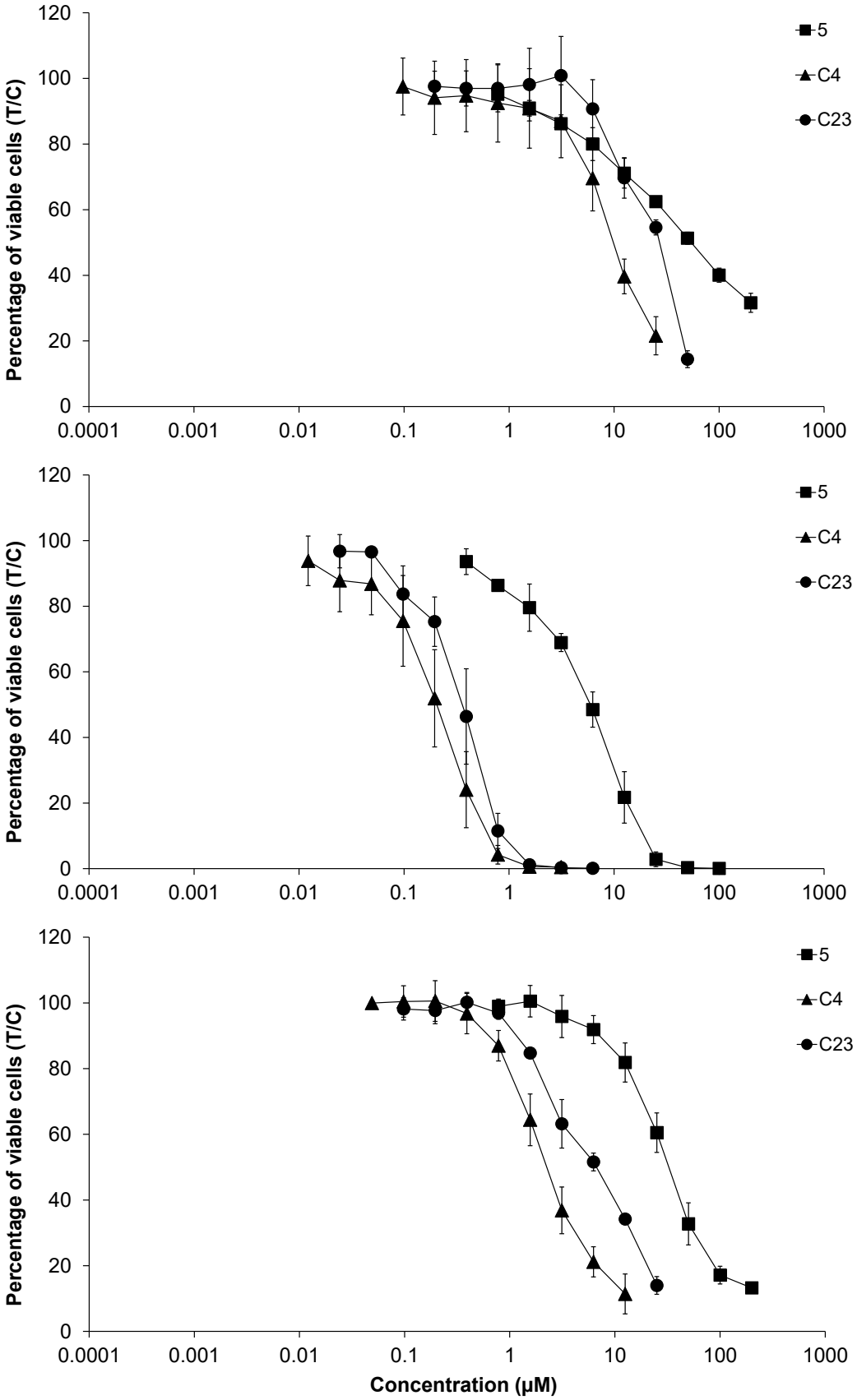

Figure S26. Concentration-effect curves of **5**, **C4** and **C23** in A549 (top), CH1/PA-1 (middle) and SW480 (bottom) cells, obtained by MTT assays with 96 h exposure time. Values are means ± standard deviations from at least three independent experiments.

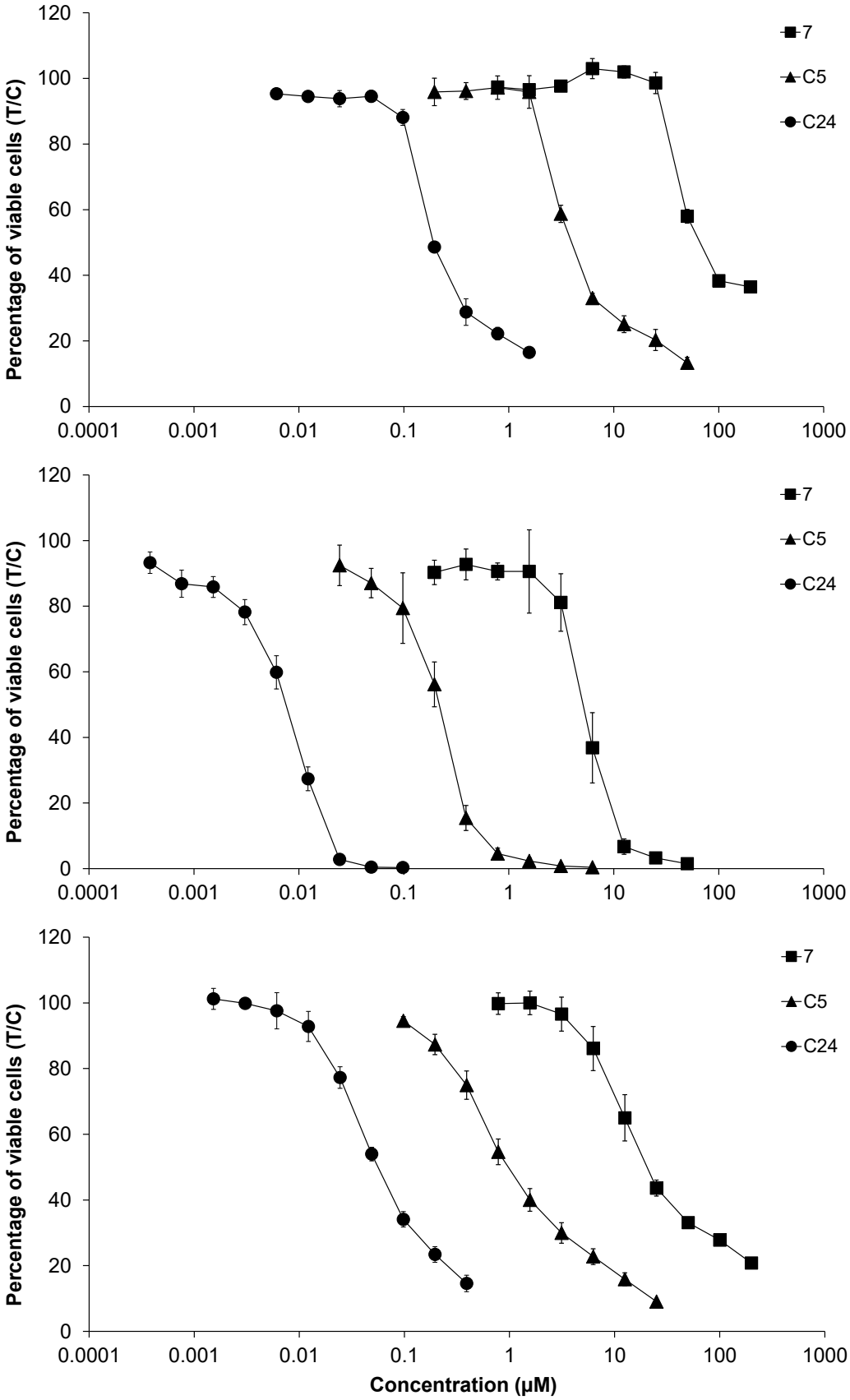

Figure S27. Concentration-effect curves of **7**, **C5** and **C24** in A549 (top), CH1/PA-1 (middle) and SW480 (bottom) cells, obtained by MTT assays with 96 h exposure time. Values are means ± standard deviations from at least three independent experiments.

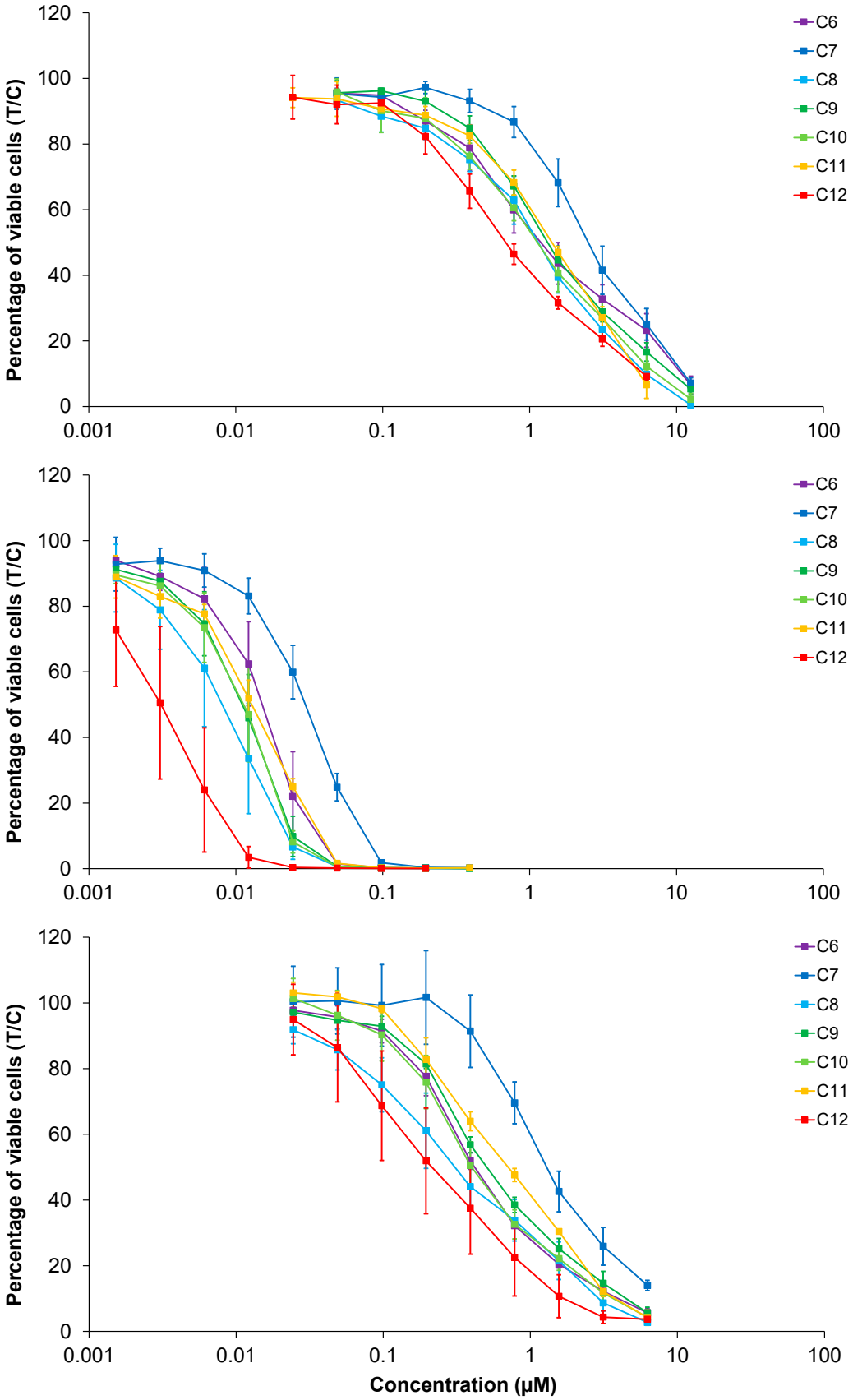

Figure S28. Concentration-effect curves of **C6**–**C12** in A549 (top), CH1/PA-1 (middle) and SW480 (bottom) cells, obtained by MTT assays with 96 h exposure time. Values are means ± standard deviations from at least three independent experiments. Compounds are color-coded according to their Pt loading from purple (lowest) to red (highest).

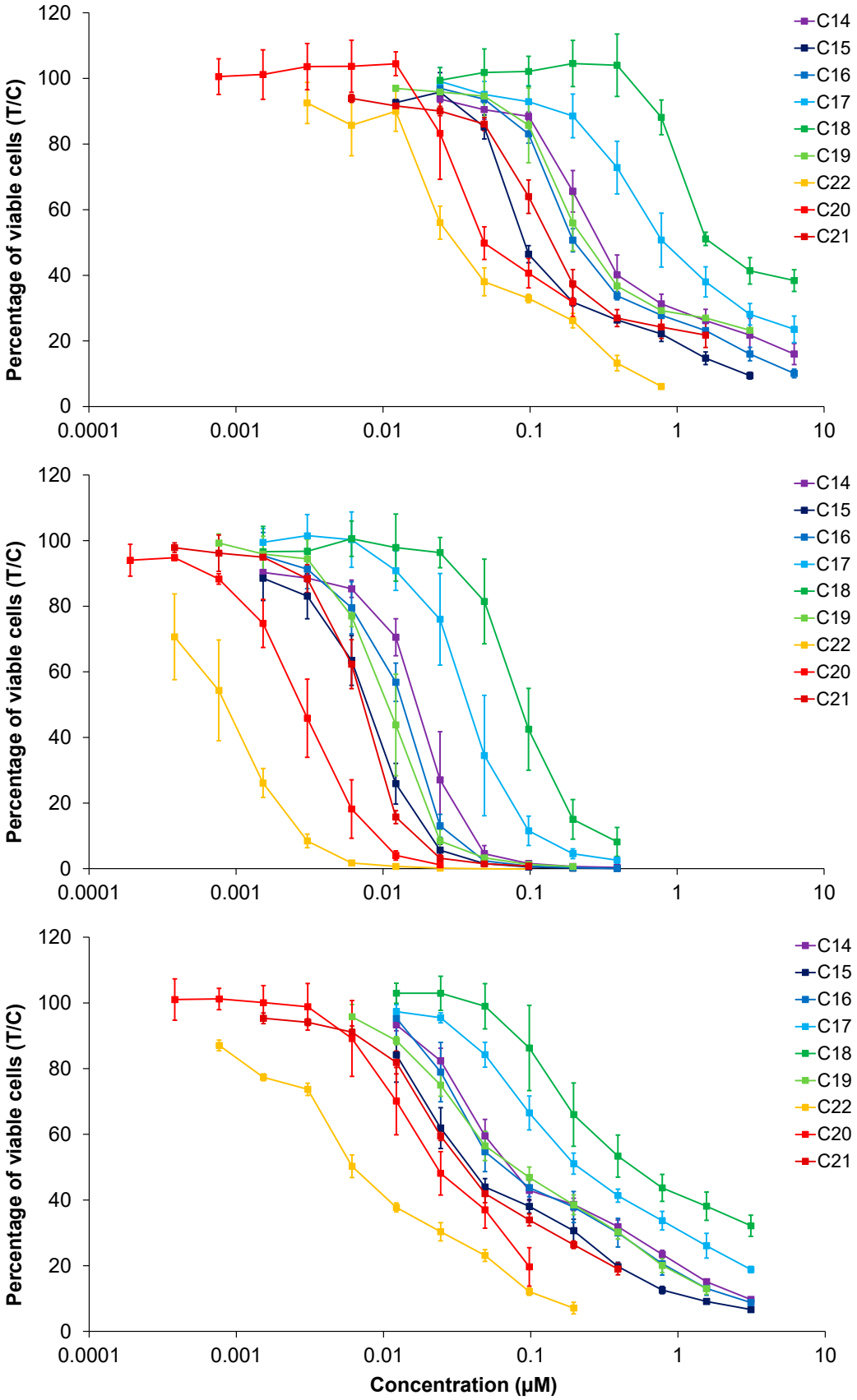

Figure S29. Concentration-effect curves of **C14**–**C21** in A549 (top), CH1/PA-1 (middle) and SW480 (bottom) cells, obtained by MTT assays with 96 h exposure time. Values are means ± standard deviations from at least three independent experiments. Compounds are color-coded according to their Pt loading from purple (lowest) to red (highest).

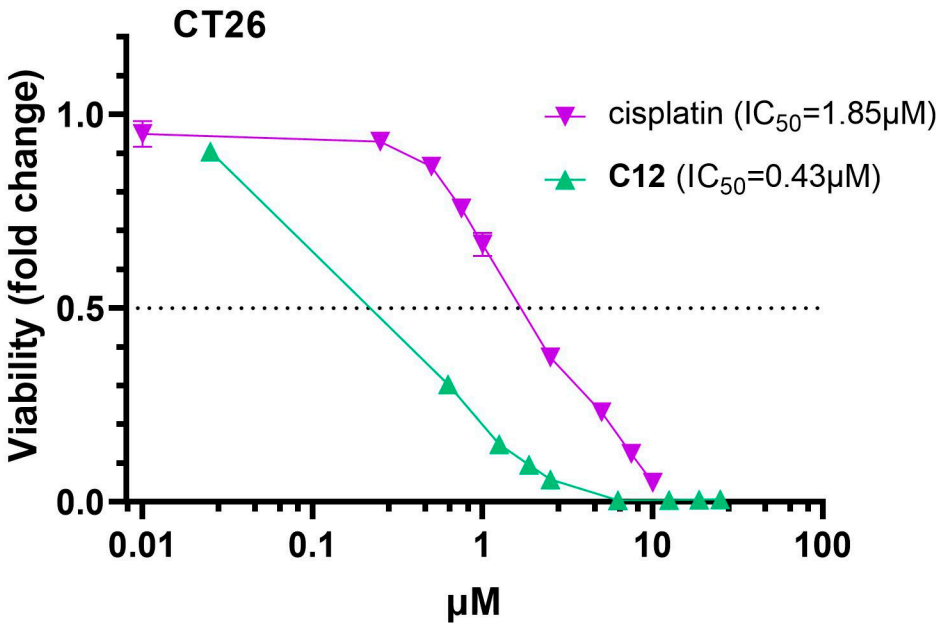

Figure S30. Concentration-effect curves of cisplatin and **C12** at the indicated doses (equimolar concerning cisplatin) in CT26 cells, obtained by MTT assays with 72 h exposure time.

5. In Vivo Data

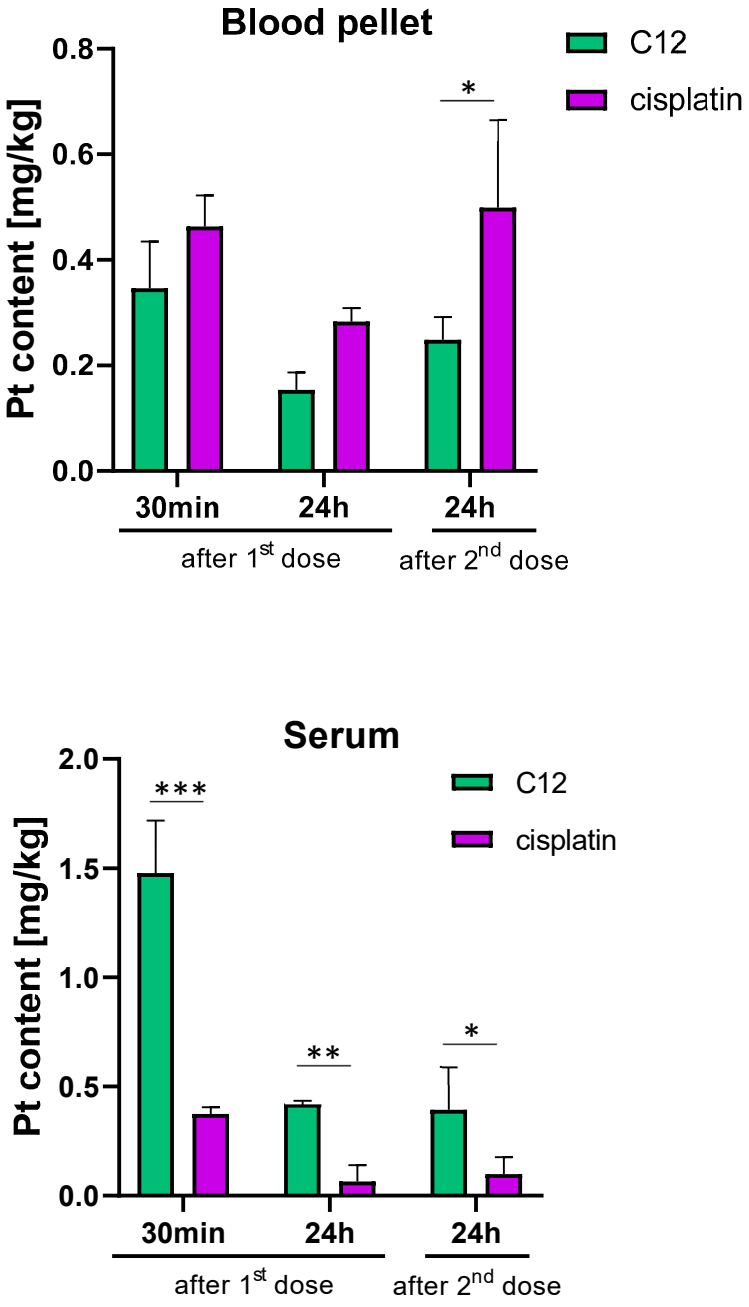

Figure S31. Comparison of platinum amount in the blood pellet and serum of conjugate **C12** and cisplatin. Significances were determined via Log-rank test (LRT) and Gehan-Breslow-Wilcoxon test (GBWT) with following abbreviations: ns = not significant, * $p < 0.05$, ** $p < 0.01$, *** $p < 0.001$, **** $p < 0.0001$.

6. References

1. Bruker SAINT v8.38B Copyright © 2005-2019 Bruker AXS.
2. Sheldrick, G. M. (1996). SADABS. University of Göttingen, Germany.
3. Dolomanov, O. V.; Bourhis, L.J.; Gildea, R.J.; Howard, J.A.K.; Puschmann, H. OLEX2: A Complete Structure Solution, Refinement and Analysis Program. *J Appl Crystallogr* **2009**, *42*, 339–341, doi:10.1107/S0021889808042726.
4. Hübschle, C.B.; Sheldrick, G.M.; Dittrich, B. ShelXle: A Qt Graphical User Interface for SHELXL. *J Appl Crystallogr* **2011**, *44*, 1281–1284, doi:10.1107/S0021889811043202.
5. Sheldrick, G. M. (2015). SHELXS v 2016/4 University of Göttingen, Germany.
6. Sheldrick, G. M. (2015). SHELXL v 2016/4 University of Göttingen, Germany.
7. Spek, A.L. Structure Validation in Chemical Crystallography. *Acta Crystallogr D Biol Crystallogr* **2009**, *65*, 148–155, doi:10.1107/S090744490804362X.

4. Conclusion

Despite severe adverse effects and occurrence of resistances, platinum-based chemotherapeutics are still an indispensable part in modern cancer treatment. However, low selectivity towards tumour tissue and dose-limiting toxicities such as nephrotoxicity and neurotoxicity, deteriorate their clinical efficiency. Consequently, the last decades were characterised by intensive research in order to develop novel (platinum-based) compounds and strategies to improve the current state of the art of cancer chemotherapy. Besides the promising platinum(IV) prodrug approach, macromolecules as drug delivery systems in the nanometre range, which are able to exploit the EPR effect for passive tumour targeting, attract more and more attention. Therefore, this thesis focused on the development of enhanced anticancer treatment approaches with increased selectivity towards cancer tissue by combining the cytotoxic activity of platinum(IV) complexes and the drug delivery properties of different polymers.

In the first project, platinum(IV) complexes of cisplatin, carboplatin and oxaliplatin were synthesised and characterised by multinuclear NMR spectroscopy (^{1}H, ^{13}C, ^{15}N, ^{195}Pt) and elemental analysis. As drug carrier, degraded glycol chitosan (dGC) polymers of different molecular weights (5, 10 and 18 kDa) were produced and subsequently loaded with platinum(IV) complexes. The 15 formed conjugates were analysed by ^{1}H and ^{195}Pt NMR spectroscopy as well as ICP-MS in order to determine the average amounts of platinum(IV) units per dGC molecule. The cytotoxicity was investigated in three human cancer cell lines (A549, CH1/PA-1, SW480) and the murine cancer cell line 4T1. All conjugates revealed significant increase of cytotoxic activity compared to their free platinum(IV) complexes and in case of a cisplatin-based conjugate also compared to cisplatin itself with IC_{50} values in the low micromolar to nanomolar range. Additionally, following observations were found: 1) Taking the respective platinum(IV) units per dGC polymer into account, conjugation of platinum(IV) complexes to dGC polymers led to increased cytotoxic activity. 2) Higher degree of platinum(IV) units per dGC polymer resulted in higher cytotoxicity. Finally, increased accumulation in the lung of healthy Balb/C mice treated with an oxaliplatin-based-dGC conjugate was detected in biodistribution studies compared to the unloaded oxaliplatin analogue.

In the second part of this thesis, quaternary ammonium palmitoyl glycol chitosan (GCPQ) polymers with different degrees of palmitoylation and quaternisation were synthesised and investigated as drug delivery system. Similar to the dGC-project, platinum(IV) complexes based on cisplatin, carboplatin and oxaliplatin were linked to the surface of GCPQ polymers *via* amide bond formation and characterised by ^{1}H and ^{195}Pt NMR spectroscopy as well as ICP-MS. MTT assays of 11 conjugates in three human cancer cell lines revealed increased cytotoxicity by factors of up to 286 times (compared to platinum(IV) complexes) and up to 9 times (compared to platinum(II) complexes),

respectively. Comparable with the oxaliplatin-based-dGC conjugate, biodistribution studies of an oxaliplatin-based-GCPQ conjugate displayed increased accumulation in the lung.

The last part of this thesis included the synthesis of several unsymmetrically carboxylated platinum(IV) complexes characterised by one- and two-dimensional NMR spectroscopy and elemental analysis. Additionally, the crystal structure of a platinum(IV) complex with an oxaliplatin core was analysed by X-Ray diffraction and deposited with the Cambridge Crystallographic Data Centre (CCDC). The platinum(IV) complexes were conjugated to PAMAM dendrimers of generation 2 (G2) and 4 (G4) resulting in 24 conjugates. Characterisation was performed by ^{1}H and ^{195}Pt as well as pseudo 2D diffusion ordered NMR spectroscopy and ICP-MS. Furthermore, investigation of the reduction behaviour revealed significantly increased reduction of the conjugates compared to the corresponding platinum(IV) complexes. The conjugates further displayed a tremendous increase of cytotoxicity compared to platinum(IV) and platinum(II) complexes with IC_{50} values in the low micromolar to high picomolar range. Finally, a cisplatin-based-G4-PAMAM conjugate was further investigated in activity studies with Balb/C mice. A significant tumour growth inhibition as well as a tendency of prolonged animal survival compared to cisplatin could be observed.

Based on these three projects of the thesis, the promising potential of the combination of platinum(IV) complexes and polymers could be demonstrated. In general, conjugation of platinum(IV) complexes to dGC, GCPQ and PAMAM dendrimers resulted in significant increase of cytotoxicity and even outperformed the respective platinum(II) complexes in case of the majority of GCPQ- and PAMAM-dendrimer-based conjugates. The increased accumulation in the lung tissue of dGC- and GCPQ-based conjugates opens up an auspicious cancer treatment approach particularly for different lung cancer types and metastases, which would need to be further investigated in activity studies. In contrast, PAMAM-dendrimer-based conjugates have already demonstrated their promising potential as a more selective anticancer therapy. Further fine-tuning in order to reduce the preferred kidney accumulation as well as deeper investigations with respect to optimize the therapeutic window could be interesting research topics for the future.

5. Abbreviations

CTR	Copper transporter
DA	Degree of acetylation
DACH	1,2-Diaminocyclohexane
dGC	degraded Glycol Chitosan
DNA	Deoxyribonucleic Acid
EPR	Enhanced Permeability and Retention
FDA	Food and Drug Administration
GCPQ	Quaternary ammonium Palmitoyl Glycol Chitosan
HMG	High Mobility Group
HSAB	Hard and Soft Acids and Bases
PAMAM	Poly(amidoamine)
RNA	Ribonucleic Acid

6. References

[1] World Health Organization, http://www.who.int (accessed 7th April **2023**)

[2] Nature, http://www.nature.com/articles (accessed 7th April **2023**)

[3] American Cancer Society, http://www.cancer.org (accessed 7th April **2023**)

[4] Global Cancer Observatory, http://gco.iarc.fr (accessed 7th April **2023**)

[5] Y. P. Ho, S. C. Au-Yeung, K. K. To, Medicinal Research Reviews **2003**, 23(5), 633-655, *Platinum-Based Anticancer Agents: Innovative Design Strategies and Biological Perspectives*

[6] M. Galanski, M. A. Jakupec, B. K. Keppler, Current Medicinal Chemistry **2005**, 12, 2075-2094, *Update of the Preclinical Situation of Anticancer Platinum Complexes: Novel Design Strategies and Innovative Analytical Approaches*

[7] H. P. Varbanov, S. Goschl, P. Heffeter, S. Theiner, A. Roller, F. Jensen, M. A. Jakupec, W. Berger, M. Galanski, B. K. Keppler, Journal of Medicinal Chemistry **2014**, 57, 6751−6764, *A Novel Class of Bis- and Tris-Chelate Diam(m)inebis(dicarboxylato)platinum(IV) Complexes as Potential Anticancer Prodrugs*

[8] B. Rosenberg, L. V. Camp, T. Krigas, Nature **1965**, 205, 698-99, *Inhibition of Cell Division in Eschericia coli by Electrolysis Products from a Platnium Electrode*

[9] J. J. Wilson, S. J. Lippard, Chemical Reviews **2014**, 114, 4470–4495, *Synthetic Methods for the Preparation of Platinum Anticancer Complexes*

[10] I. V. Tetko, I. Jaroszewicz, J. A. Platts, J. Kuduk-Jaworska, Journal of Inorganic Biochemistry **2008**, 102, 1424–1437, *Calculation of lipophilicity for Pt(II) complexes: Experimental comparison of several methods*

[11] G. B. Kauffman, R. Pentimalli, S. Doldi, M. D. Hall, Platinum Metals Review **2010,** 54 (4), 250-256, *Michele Peyrone (1813-1883), Discoverer of Cisplatin*

[12] L. Kelland, Nature Reviews Cancer **2007,** 7 (8), 573-584, *The resurgence of platinum-based cancer chemotherapy*

[13] B. Desoize, Anticancer Research **2004**, 24, 1529-1544, *Metals and Metal Compounds in Cancer Treatment*

[14] D. Wang, S. J. Lippard, Nature Reviews **2005**, 4, 307-320, *Cellular Processing of Platinum Anticancer Drugs*

[15] P. J. O'Dwyer, J. P. Stevenson, S. W. Johnson, Drugs **2000**, 59(4), 19-27, *Clinical Pharmacokinetics and Administration of Established Platinum Drugs*

[16] C. Bartel, A. K. Bytzek, Y. Y. Scaffidi-Domianello, G. Grabmann, M. A. Jakupec, C. G. Hartinger, M. Galanski, B. K. Keppler, Journal of Biological Inorganic Chemistry **2012**, 17, 465–474, *Cellular accumulation and DNA interaction studies of cytotoxic trans-platinum anticancer compounds*

[17] W. Voigt, A. Dietrich, H. J. Schmoll, Pharmzie in unserer Zeit **2006,** 35 (2), 134-143, *Cisplatin und seine Analoga*

[18] F. Muggia, Gynaecologic Oncology **2009**, 112, 275-81, *Platinum compounds 30 years after the introduction of cisplatin: Implications for the treatment of ovarian cancer*

[19] N. J. Wheate, S. Walker, G. E. Craig, R. Oun, Dalton Transactions **2010**, 39, 8113-8127, *The status of platinum anticancer drugs in the clinic and in clinical trials*

[20] T. C. Johnstone, K. Suntharalingam, S. J. Lippard, Chemical Reviews **2016**, 116, 3436-3486, *The Next Generation of Platinum Drugs: Targeted Pt(II) Agents, Nanoparticle Delivery, and Pt(IV) Prodrugs*

[21] R. C. Todd, S. J. Lippard, Metallomics **2009**, 1(4), 280–291, *Inhibition of transcription by platinum antitumor compounds*

[22] M. Galanski, B. K. Keppler, Anti-Cancer Agents in Medicinal Chemistry **2007**, 7, 55-73, *Searching for the Magic Bullet: Anticancer Platinum Drugs Which Can Be Accumulated or Activated in the Tumor Tissue*

[23] S. Amptoulach, N. Tsavaris, Chemotherapy Research and Practice **2011,** Article ID 843019, 1-5, *Neurotoxicity caused by the treatment with platinum analogues*

[24] T. J. Lehky, G. D. Leonard, R. H. Wilson, J. L. Grem, M. K. Floeter, Muscle Nerve **2004**, 29, 387–92, *Oxaliplatin-induced Neurotoxicity: Acute Hyperexcitability and Chronic Neuropathy*

[25] M. Kartalou, J. M. Essigmann, Mutation Research **2001**, 478, 1-21, *Recognition of cisplatin adducts by cellular proteins*

[26] S. Dasari, P. B. Tchounwou, European Journal of Pharmacology **2014**, 740, 364-378, *Cisplatin in cancer therapy: Molecular mechanisms of action*

[27] R. J. Browning, P. J. T. Reardon, M. Parhizkar, R. B. Pedley, M. Edirisinghe, J. C. Knowles, E. Stride, American Chemical Society Nano **2017**, 11 (9), 8560-8578, *Drug Delivery Strategies for Platinum-Based Chemotherapy*

[28] Z. Wang, G. Zhu, Reference Module in Chemistry, Molecular Sciences and Chemical Engineering **2018**, *DNA Damage Repair Pathways and Repair of Cisplatin-Induced DNA Damage*

[29] M. R. Reithofer, S. M. Valiahdi, M. A. Jakupec, V. B. Arion, A. Egger, M. Galanski, B. K. Keppler, Journal of Medicinal Chemistry **2007**, 50, 6692–6699, *Novel Di- and Tetracarboxylatoplatinum(IV) Complexes. Synthesis, Characterization, Cytotoxic Activity, and DNA Platination*

[30] E. Wexselblatt, E. Yavin, D. Gibson, Inorganica Chimica Acta **2012**, 393, 75-83, *Cellular interactions of platinum drugs*

[31] B. R. Hoffmeister, M. Hejl, M. S. Adib-Razavi, M. A. Jakupec, M. Galanski, B. K. Keppler, Chemistry & Biodiversity **2015**, 12, 559- 574, *Bis- and Tetrakis(carboxylato)platinum(IV) Complexes with Mixed Axial Ligands – Synthesis, Characterization, and Cytotoxicity*

[32] E. Wexselblatt, D. Gibson, Journal of Inorganic Biochemistry **2012**, 117, 220–229, *What do we know about the reduction of Pt(IV) pro-drugs?*

[33] P. Heffeter, U. Jungwirth, M. Jakupec, C. Hartinger, M. Galanski, L. Elbling, M. Micksche, B. Keppler, W. Berger, Drug Resistance Update **2008**, 11, 1-16, *Resistance against novel anticancer metal compounds: differences and similarities*

[34] M. D. Hall, T. W. Hambley, Coordination Chemistry Reviews **2002**, 232, 49-67, *Platinum(IV) antitumour compounds: their bioinorganic chemistry*

[35] D. Höfer, H. P. Varbanov, A. Legin, M. A. Jakupec, A. Roller, M. Galanski, B. K. Keppler, Journal of Inorganic Biochemistry **2015**, 153, 259–271, *Tetracarboxylatoplatinum(IV) complexes featuring monodentate leaving groups — A rational approach toward exploiting the platinum(IV) prodrug strategy*

[36] M. D. Hall, H. R. Mellor, R. Callaghan, T. W. Hambley, Journal of Medicinal Chemistry **2007**, 50(15), 3403-3411, *Basis for Design and Development of Platinum(IV) Anticancer Complexes*

[37] R. G. Kenny, S. W. Chuah, A. Crawford, C. J. Marmion, European Journal of Inorganic Chemistry **2017**, 1596–1612, *Platinum(IV) Prodrugs – A Step Closer to Ehrlich's Vision?*

[38] M. Galanski, B. K. Keppler, Inorganica Chimica Acta **2000**, 300-302, 783-789, *Is reduction required for antitumour activity of platinum(IV) compounds? Characterisation of a platinum(IV)–nucleotide adduct [enPt(OCOCH3)3(5%-GMP)] by NMR spectroscopy and ESI-MS*

[39] O. Vrana, V. Brabec, V. Kleinwachter, Anticancer Drug Design **1986**, 1, 95-109, *Polarographic Studies on the Conformation of Some Platinum Complexes: Relations to Anti-Tumour Activity*

[40] S. Choi, S. Delaney, L. Orbai, E. J. Padgett, A. S. Hakemian, Inorganic Chemistry **2001**, 40, 5481-5482, *A Platinum(IV) Complex Oxidizes Guanine to 8-Oxo-Guanine in DNA and RNA*

[41] V. Pichler, S. Göschl, E. Schreiber-Brynzak, Michael A. Jakupec, M. Galanski, B.K. Keppler, Metallomics **2015**, 7, 1078-1090, *Influence of reducing agents on the cytotoxic activity of platinum(IV) complexes: induction of G2/M arrest, apoptosis and oxidative stress in A2780 and cisplatin resistant A2780cis cell lines*

[42] D. Gibson, Dalton Transactions **2016**, 45, 12983-12983, *Platinum(IV) anticancer prodrugs – hypotheses and facs*

[43] T. W. Hambley, A. R. Battle, G. B. Deacon, E. T. Lawrenz, G. D. Fallon, B. M. Gatehouse, L. K. Webster, S. Rainone, Journal of Inorganic Biochemistry **1999**, 77, 3–12, *Modifying the properties of platinum(IV) complexes in order to increase biological effectiveness*

[44] M. D. Hall, R. Dolman, T. W. Hambley, Metal Ions in Biological Systems **2004**, 42, 297-322, *Platinum(IV) Anticancer Complexes*

[45] S. Choi, C. Filotto, M. Bisanzo, S. Delaney, D. Lagasee, J. L. Whitworth, A. Jusko, C. Li, N. A. Wood, J. Willingham, A. Schwenker, K. Spaulding, Inorganic Chemistry **1998**, 37, 2500-2504, *Reduction and Anticancer Activity of Platinum(IV) Complexes*

[46] J. Z. Zhang, E. Wexselblatt, T. W. Hambleya, D. Gibson, Chemical Communications **2012**, 48, 847-849, *Pt(IV) analogs of oxaliplatin that do not follow the expected correlation between electrochemical reduction potential and rate of reduction by ascorbate*

[47] Q. Mi, S. Shu, C. Yang, C. Gao, X. Zhang, X. Luo, C. Bao, X. Zhang, J. Niu, International Journal of Medical Physics, Clinical Engineering and Radiation Oncology **2018**, 7, 231-247, *Current Status for Oral Platinum (IV) Anticancer Drug Development*

[48] M. G. Apps, E. H. Y. Choi, N. J. Wheate, Endocrine-Related Cancer **2015**, 22(4), 219-233, *The state-of-play and future of platinum drugs*

[49] M. Reithofer, M. Galanski, A. Roller, B. K. Keppler, European Journal of Inorganic Chemistry **2006**, 2612–2617, *An Entry to Novel Platinum Complexes: Carboxylation of Dihydroxoplatinum(IV) Complexes with Succinic Anhydride and Subsequent Derivatization*

[50] L. R. Kelland, Expert Opinion on Investigational Drugs **2000**, 9, 1373-1382, *An update on satraplatin: the first orally available platinum anticancer drug*

[51] H. Choy, C. Park, M. Yao, Clinical Cancer Research **2008**, 14(6), 1633-1638, *Current Status and Future Prospects for Satraplatin, an Oral Platinum Analogue*

[52] C. N. Sternberg, D. P. Petrylak, O. Sartor, J. A. Witjes, T. Demkow, J. Ferrero, J. Eymard, S. Falcon, F. Calabrò, N. James, I. Bodrogi, P. Harper, M. Wirth, W. Berry, M. E. Petrone, T. J. McKearn, M. Noursalehi, M. George, M. Rozencweig, Journal of Clinical Oncology **2009**, 27, 5431-5438, *Multinational, Double-Blind, Phase III Study of Prednisone and Either Satraplatin or Placebo in Patients With Castrate-Refractory Prostate Cancer Progressing After Prior Chemotherapy: The SPARC Trial*

[53] S. Zhang, X. Wang, Z. Guo, Advances in Inorganic Chemistry **2020**, 75, 149-182, *Rational design of anticancer platinum(IV) prodrugs*

[54] I. Buß, D. Garmann, M. Galanski, G. Weber, G. V. Kalayda, B. K. Keppler, U. Jaehde, Journal of Inorganic Biochemistry **2011**, 105, 709–717, *Enhancing lipophilicity as a strategy to overcome resistance against platinum complexes?*

[55] M. R. Reithofer, A. K. Bytzek, S. M. Valiahdi, C. R. Kowol, M. Groessl, C. G. Hartinger, M. A. Jakupec, M. Galanski, B. K. Keppler, Journal of Inorganic Biochemistry **2011**, 105, 46–51, *Tuning of lipophilicity and cytotoxic potency by structural variation of anticancer platinum(IV) complexes*

[56] S. van Zutphen, J. Reedijk, Coordination Chemistry Reviews **2005**, 249, 2845–2853, *Targeting platinum anti-tumour drugs: Overview of strategies employed to reduce systemic toxicity*

[57] S.v. Zutphen, J. Reedijk, Coordination Chemistry Reviews **2005**, 249 (24), 2845-2853, *Targeting platinum antitumour drugs: overview of strategies employed to reduce systemic toxicity*

[58] M. Galanski, B.K. Keppler, *Drug Delivery in Oncology*, Wiley-VCH Verlag GmbH & Co. KGaA: **2011**, 1605-1629

[59] J. Fang, H. Nakamura, H. Maeda, Advanced Drug Delivery Reviews **2011**, 63, 136–151, *The EPR effect: Unique features of tumor blood vessels for drug delivery, factors involved, and limitations and augmentation of the effect*

[60] F. Danhier, O. Feron, V. Préat, Journal of Controlled Release **2010**, 148, 135–146, *To exploit the tumor microenvironment: Passive and active tumor targeting of nanocarriers for anti-cancer drug delivery*

[61] Y. Matsumura, H. Maeda, Cancer Research **1986**, 46, 6387–6392, *A new concept for macromolecular therapeutics in cancer chemotherapy: mechanism of tumoritropic accumulation of proteins and the antitumor agent SMANCS*

[62] F. Boateng, W. Ngwa, International Journal of Molecular Sciences **2020**, 21, 273-294, *Delivery of Nanoparticle-Based Radiosensitizers for Radiotherapy Applications*

[63] P. Antoni, Y. Hed, A. Nordberg, D. Nystrm, H. von Holst, A. Hult, M. Malkoch, Angewandte Chemie **2009**, 48, 2126-2130, *Bifunctional Dendrimers: From Robust Synthesis and Accelerated One-Pot Postfunctionalization Strategy to Potential Applications*

[64] O. Rolland, C. O. Turrin, A. M. Caminade, J. P. Majoral, New Journal of Chemistry **2009**, 33, 1793–1980, *Dendrimers and nanomedicine: multivalency in action*

[65] J. Grimma, M. Dolgushev, Physical Chemistry Chemical Physics **2016**, 18, 19050-19061, *Dynamics of internally functionalized dendrimers*

[66] E. Abbasi, S. F. Aval, A. Akbarzadeh, M. Milani, H. T. Nasrabadi, S. W. Joo, Y. Hanifehpour, K. Nejati-Koshki, R. Pashaei-Asl, Nanoscale Research Letters **2014**, 9, 247-257, *Dendrimers: synthesis, applications, and properties*

[67] S. Svenson, D. A. Tomalia, Advanced Drug Delivery Reviews **2012**, 64, 102–115, *Dendrimers in biomedical applications—reflections on the field*

[68] J. M. J. Fréchet, D. A. Tomalia, *Dendrimers and other Dendritic Polymers,* Chichester: Wiley: **2001**, 1-44

[69] D. A. Tomalia, H. Baker, J. Dewald, M. Hall, G. Kallos, S. Martin, J. Roeck, J. Ryder, P. Smith, Polymer Journal **1985**, 17 (1), 117-132, *A New Class of Polymers: Starburst-Dendritic Macromolecules*

[70] D. A. Tomalia, Progress in Polymer Science **2005**, 30, 294-324, *Birth of a new macromolecular architecture: dendrimers as quantized building blocks for nanoscale synthetic polymer chemistry*

[71] V. J. Venditto, C. A. S. Regino, M. W. Brechbiel, Molecular Pharmaceutics **2005**, 2(4), 302-311, *PAMAM Dendrimer Based Macromolecules as Improved Contrast Agents*

[72] P. M. R. Paulo, J. N. Canongia Lopes, S. M. B. Costa, The Journal of Physical Chemistry B **2007**, 111, 10651-10664, *Molecular Dynamics Simulations of Charged Dendrimers: Low-to-Intermediate Half-Generation PAMAMs*

[73] N. S. Sommerfeld, M. Hejl, M. H. M. Klose, E. Schreiber-Brynzak, A. Bileck, S. M. Meier, C. Gerner, M. A. Jakupec, M. Galanski, B. K. Keppler, European Journal of Inorganic Chemistry **2017**, 1713–1720, *Low-Generation Polyamidoamine Dendrimers as Drug Carriers for Platinum(IV) Complexes*

[74] A. Mecke, I. Lee, J. R. Baker jr., M. M. Banaszak Holl, B. G. Orr, The European Physical Journael E **2004**, 14, 7-16, *Deformability of poly(amidoamine) dendrimers*

[75] C. J. Morris, G. Aljayyoussi, O. Mansour, P. Griffiths, M. Gumbleton, Pharmaceutical Research **2017**, 34, 2517-2531, Endocytic Uptake, *Transport and Macromolecular Interactions of Anionic PAMAM Dendrimers within Lung Tissue*

[76] K.W. Chooi, M.I. Simão Carlos, R. Soundararajan, S. Gaisford, N. Arifin, A.G. Schätzlein, I.F. Uchegbu, Journal of Pharmaceutical Sciences **2014**, 103(8), 2296-2306, *Physical Characterisation and Long Term Stability Studies on Quaternary Ammonium Palmitoyl Glycol Chitosan (GCPQ) - A New Drug Delivery Polymer*

[77] I. Younes, M. Rinaudo, M., Marine Drugs **2015**, 13, 1133-1174, *Chitin and Chitosan Preparation from Marine Sources. Structure, Properties and Applications*

[78] A. Trapani, J. Sitterbergb, U. Bakowskyb, T. Kissel, International Journal of Pharmaceutics **2009**, 375, 97-106, *The potential of glycol chitosan nanoparticles as carrier for low water soluble drugs*

[79] I. F. Uchegbu, L. Sadiq, M. Arastoo, A. I. Gray, W. Wang, R. D. Waigh, A. G. Schätzlein, International Journal of Pharmaceutics **2001**, 224, 185–199, *Quaternary ammonium palmitoyl glycol chitosan—a new polysoap for drug delivery*

[80] M. N. V. Ravi Kumar, Reactive & Functional Polymers **2000**, 46, 1–27, *A review of chitin and chitosan applications*

[81] U. Odunze, F. O'Brien, L. Godfrey, A. Schätzlein, I. Uchegbu, Pharmaceutical Nanotechnology **2019**, 7, 57-71, *Unusual Enthalpy Driven Self Assembly at Room Temperature with Chitosan Amphiphiles*

[82] I. F. Uchegbu, M. Carlos, C. McKay, X. Hou, A. G. Schätzlein, Polymer international **2014**, 63, 1145-1153, *Chitosan amphiphiles provide new drug delivery opportunities*

[83] U. Kanwal, N. I. Bukhari, A. Raza, K. Hussain, N. Abbas, Importance & Applications of Nanotechnology **2019**, 2, 1-6, *Quaternary ammonium palmitoyl glycol chitosan-based nano-doxorubicin delivery system: Potential applications for cancer treatment and theranostic*

[84] V. López-Dávila, T. Magdeldin, H. Welch, M.V. Dwek, I.F. Uchegbu, M. Loizidou, Nanomedicine (Lond.) **2016**, 11(4), 331-344, *Efficacy of DOPE/DC-cholesterol liposomes and GCPQ micelles as AZD6244 nanocarriers in a 3D colorectal cancer in vitro model*

[85] R. Oun, Y.E. Moussa, N.J. Wheate, Dalton Transactions **2018**, 47, 6645–6653, *The Side Effects of Platinum-Based Chemotherapy Drugs: A Review for Chemists*

[86] N. Morin-Crini, E. Lichtfouse, G. Torri, G. Crini, Sustainable Agriculture Reviews 35; Springer International Publishing AG **2019**; Volume 35, ISBN 9783030165376**,** *Fundamentals and Applications of Chitosan*

[87] I.F. Uchegbu, L. Sadiq, M. Arastoo, A.I. Gray, W. Wang, R.D. Waigh, A.G. Schätzlein, International Journal of Pharmaceutics **2001**, 224, 185–199, *Quaternary Ammonium Palmitoyl Glycol Chitosan-a New Polysoap for Drug Delivery*

[88] U. Odunze, F. O'Brien, L. Godfrey, A. Schätzlein, I. Uchegbu, Pharmaceutical Nanotechnology **2019**, 7, 57–71, *Unusual Enthalpy Driven Self Assembly at Room Temperature with Chitosan Amphiphiles*